

STRUCTURE AND SUBSTRATE SPECIFICITY OF *TAXUS*
N-BENZOYLTRANSFERASE OF THE BAHD SUPERFAMILY

By

Danielle Marguerite Nevarez

A DISSERTATION

Submitted to
Michigan State University
in partial fulfillment of the requirements
for the degree of

DOCTOR OF PHILOSOPHY

Cell and Molecular Biology

2011

ABSTRACT

STRUCTURE AND SUBSTRATE SPECIFICITY OF *TAXUS* *N*-BENZOYLTRANSFERASE OF THE BAHD SUPERFAMILY

By

Danielle Marguerite Nevarez

The native *Taxus* *N*-debenzoyl-2-deoxypaclitaxel:*N*-benzoyltransferase (NDTBT) from the paclitaxel pathway transfers a benzoyl group from the corresponding CoA thioester to the amino group of the β -phenylalanine side chain of *N*-debenzoyl-2'-deoxypaclitaxel. To elucidate the substrate specificity NDTBT with a His₆-fusion epitope was overproduced in *Escherichia coli*. Purified enzyme was incubated with semisynthetically derived *N*-debenzoyltaxoid substrates and aroyl CoA donors (benzoyl; *ortho*-, *meta*-, and *para*-substituted benzoyls; various heterole carbonyls; alkanoyls; and butenoyl). Several unnatural *N*-aroyl-*N*-debenzoyl-2'-deoxypaclitaxel analogues were biocatalytically assembled with catalytic efficiencies (V_{\max}/K_M) ranging between 0.15 and 1.74 nmol/min/mM. In addition, several *N*-acyl-*N*-debenzoylpaclitaxel variants were biosynthesized when *N*-debenzoylpaclitaxel and *N*-de(*tert*-butoxycarbonyl) docetaxel (i.e., 10-deacetyl-*N*-debenzoylpaclitaxel) were used as substrates. The relative velocity (v_{rel}) for NDTBT with the latter two *N*-debenzoyl taxane substrates ranged between ~1% and 200% for the array of aroyl CoA thioesters compared to benzoyl CoA. Interestingly, NDTBT transferred hexanoyl, acetyl, and butyryl moieties more rapidly than butenoyl or benzoyl groups from the CoA donor to taxanes with isoserinoyl side chains, whereas *N*-debenzoyl-2'-deoxypaclitaxel was more rapidly converted to its *N*-benzoyl derivative than to its *N*-alkanoyl or *N*-butenoyl congeners. Biocatalytic *N*-acyl transfer of novel acyl groups to the amino functional group of *N*-debenzoylpaclitaxel and its 2'-deoxy precursor reveal the surprisingly indiscriminate

specificity of this transferase. This feature of NDTBT potentially provides a tool for alternative biocatalytic *N*-aroylation/alkanoylation to construct next generation taxanes or other novel bioactive diterpene compounds.

To elucidate the basis of the broad substrate specificity and to direct mutational analysis, the crystal structure for NDTBT was sought. Therefore, several chromatographic methods were applied to increase the purity of the protein from 70%, obtained in previous attempts, to >95%, without losing activity. This sequence of chromatographic steps was also used to purify 10-deacetylbaccatin III: 10 β -*O*-acetyltransferase (DBAT) and a modified taxane-2 α -*O*-benzoyltransferase (*m*TBT) to 90-95% purity. Preliminary screens for crystals of purified NDTBT (at 5 mg/mL) with and without benzoyl CoA in a matrix of crystallization buffers were negative. The histidine tag was hypothesized to inhibit crystallization and thus is currently being removed; attempts to cleavage of the His₆-tag from NDTBT by thrombin-catalyzed scission yields only ~10% of the liberated protein.

Meanwhile, a mutagenesis study was constructed to examine potential structural components of the *Taxus* acyltransferase family responsible for substrate selectivity. Regional and domain swapping between pairs of enzymes: NDTBT/DBAT and DBAT/*m*TBT were employed to evaluate these structural hypotheses. Vinorine synthase and anthocyanin malonyltransferase, homologous enzymes in the same BAHD family whose structures have been solved, were used as models to identify mutagenic sites for constructing the chimeras of the *Taxus* enzymes. The so-derived mutant chimeras were purified from a nickel affinity column at 0.24 mg/L yield. The mutants were incubated with the parent substrates and none of the mutants made products detectable by LC-ESI/MS analysis. The chimeras are potentially inactive because incorrect splicing sites were perhaps unexpectedly identified to construct the mutant enzymes.

Copyright by
DANIELLE MARGUERITE NEVAREZ
2011

Por mi familia

ACKNOWLEDGEMENTS

I would love to thank my husband Aaron J. McBride for putting up with me these past six years and actually marrying me. Special thanks to Dr. Kevin Walker for being my mentor and supporting my venture into the world of chemistry. I would like to recognize my guidance committee – Drs. Hausinger, Benning, Garavito, and Larkin – for providing guidance for my research and making me a better scientist. Special thanks to my family in Arizona for supporting my decision to attend graduate school in a snowy-laden state. I need to thank my former roomie "Dr. Julz" (Julie Bordowitz) for editing my papers, helping me adjust to graduate school, and sharing good times together at University of Arizona and at Michigan State University. To friends that made life enjoyable: Mike, Ruth, Siohban, Kramer, Eric, and Alec. To old and current lab members: Karin, Dr. Catherine Loncaric, Sanjit, Cliff, Sue, Dr. Washington Mutatu, Getrude, Ruth, Joshua, Udayanga, Dilini, Dennis, Dr. Brad Cox, Yemane, Chelsea, Dr. Irosha Nawarathne, and Dr. Mark Ondari. Special thanks to Irosha and Mark, because we started our graduate studies together, and formed a "team" and helped each other during our struggles in graduate school through several years. I could not have done it without you two. I thank Sanjit and Yemane for making the taxane substrates for my experiments, and Irosha for making the acyl CoA substrates. I extend my gratitude to the Cell & Molecular Biology program for admitting me as a graduate student, and to memorable people I met during my graduate career: Dr. Triezenberg, Dr. Conrad, Dr. Meeks, Christine, Becky, Jeanne, and Cheryl. The St. John's Cider group (Dr. Charlie Miller with Tracey and kids, Dr. Laura Lamb with Shannon (and now, Mitch), Dr. Eric Marrotte with Carol and Andrew), with whom I ate donuts and drank cider in the morning, deserve a special thanks for bringing childlike enthusiasm in the cornfield and at the apple smash. I wish to salute Dr. Dan Jones and Lijun Chen for educating me on how to use

the QToF mass spectrometer and evaluate the data from my experiments. I need to thank Dr. Lei Feng, Susan Strom, and Dr. James Geiger for their assistance in protein purification and crystal structure screening.

TABLE OF CONTENTS

LIST OF TABLES.....	x
LIST OF FIGURES.....	xi
LIST OF ABBREVIATIONS.....	xvi
CHAPTER 1: INTRODUCTION.....	1
1.1. Paclitaxel Background.....	1
1.2. Paclitaxel Production.....	3
1.3. <i>Taxus</i> Acyltransferases.....	11
1.4. Project Aims.....	12
References.....	16
CHAPTER 2: SUBSTRATE SPECIFICITY OF <i>TAXUS</i> <i>N</i> -BENZOYLTRANSFERASE.....	23
2.1. Introduction.....	24
2.2. Materials and Methods.....	27
2.2.1. Reagents and Solvents.....	27
2.2.2. Co-substrate Synthesis.....	28
2.2.3. Genetic Manipulation.....	34
2.2.4. Expression and Purification of <i>NDTBT</i>	39
2.2.5. Enzymatic Assays and Analysis.....	43
2.3. Results.....	48
2.3.1. Expression and Activity of <i>NDTBT</i>	48
2.3.2. Kinetic Evaluation with Competing CoA Substrate.....	49
2.3.3. Relative Velocities of Taxanes.....	50
2.3.4. Relative Velocities with Alkanoyl/Alkenoyl CoA Substrates.....	55
2.4. Discussion.....	57
Appendix A: Kinetic Parameters for <i>NDTBT</i>	62
Appendix B: Mass Spectra of Product Standards and Biosynthesized Products Made By <i>NDTBT</i>	64
References.....	89
CHAPTER 3: PROTEIN PURIFICATION OF <i>TAXUS</i> ACYLTRANSFERASES FOR PRELIMINARY CRYSTAL STRUCTURE ANALYSIS.....	92
3.1. Introduction.....	92
3.2. Materials and Methods.....	96
3.2.1. Substrates and Plasmids.....	96
3.2.2. Genetic Manipulations.....	96
3.2.3. Protein Expression and Purification.....	101
3.2.4. Enzymatic Assays and Analysis.....	104
3.2.5. Crystal Box Set-up.....	105
3.2.6. Thrombin Digestions.....	105
3.3. Results.....	105
3.3.1. Expression and Activity Assays for <i>NDTBT</i> , <i>DBAT</i> , and <i>mTBT</i>	105

3.3.2. Crystal Box Screening of NDTBT-CT	111
3.3.3. Thrombin Digestions of NT-NDTBT	112
3.4. Discussion	112
References	117
CHAPTER 4: ACYLTRANSFERASE SELECTIVITY OF REGION SWAPPED MUTANTS	120
4.1. Introduction	120
4.2. Materials and Methods	124
4.2.1. Reagents and Solvents	124
4.2.2. Genetic Manipulations	124
4.2.3. Expression and Purification of Chimeric Mutants	128
4.2.4. Enzymatic Assays and Analysis	131
4.3. Results	133
4.3.1. Regional NDTBT/DBAT Mutants	133
4.3.2. Regional DBAT/ <i>m</i> TBT Mutants	136
4.3.3. Domain Mutants	139
4.4. Discussion	141
Appendix C: Amino Acid Sequence Alignments of <i>Taxus</i> Acyltransferases with Anthocyanin Malonyltransferase and Vinorine Synthase	147
References	162
CHAPTER 5: FUTURE APPLICATIONS AND PERSPECTIVES	164
5.1. Summary	164
5.1.1. Substrate Specificity of NDTBT	164
5.1.2. Protein Purification for Crystal Structure	165
5.1.3. Mutagenesis Study to Analyze Substrate Selectivity	165
5.2. Future Goals	166
5.2.1. Re-evaluate and Survey the Substrate Specificity of NDTBT	166
5.2.2. Improving Protein Yield for Crystallography	167
5.3. Future Applications and Perspectives	168
5.3.1. Biocatalysis to Produce Paclitaxel	168
5.3.2. <i>In vivo</i> Studies	169
References	172

LIST OF TABLES

Table 1.1 – <i>Taxus</i> Acyltransferases Characteristics.....	12
Table 2.1 – Custom Primer Sequences.....	35
Table 2.2 – Relative Kinetics of NDTBT with Aroyl CoA Thioesters and <i>N</i> -Debenzoylpaclitaxel Analogues.....	51
Table 2.3 – Relative Kinetics of NDTBT with Short Hydrocarbon Chain CoA Thioesters and <i>N</i> -Debenzoylpaclitaxel Analogues.....	56
Table 3.1 – Custom Primer Sequences.....	98
Table 3.2 – Activity Assay for NDTBT, DBAT, and <i>m</i> TBT.....	104
Table 3.3 – Kinetic Parameters of N-terminal and C-terminal His ₆ -tagged NDTBT.....	114
Table 4.1 – Custom Primer Sequences.....	125
Table 4.2 – Activity Assay Composition for Chimeric Mutants.....	132
Table 4.3 – Domain Mutants.....	140

LIST OF FIGURES

Figure 1.1 – Structure of Paclitaxel.....	1
Figure 1.2 – Normal <i>versus</i> Paclitaxel-promoted Microtubule Assembly.....	2
Figure 1.3 – Crystal Structure of Paclitaxel in T-form.....	3
Figure 1.4 – Taxane Core Analogues: 10-Deacetylbaccatin III and Baccatin III.....	4
Figure 1.5 – Semi-Synthesis Beta-lactam Method.....	5
Figure 1.6 – Structure-Activity Relationships.....	6
Figure 1.7 – Semisynthetically-derived Docetaxel (Taxotere®).....	7
Figure 1.8 – Proposed Beginning Biosynthesis Pathway of Paclitaxel.....	8
Figure 1.9 – Acetylation at C10 and Biosynthesis Steps of the C13 Side-Chain.....	10
Figure 1.10 – Structures of Taxane Analogues: <i>N</i> -Debenzoylpaclitaxel and 10-Deacetyl- <i>N</i> -debenzoylpclitaxel.....	13
Figure 2.1 – Structures of Antineoplastic Taxanes: Paclitaxel, and Docetaxel.....	24
Figure 2.2 – A Route to <i>N</i> -Aroyl- <i>N</i> -debenzoylpaclitaxel Analogues.....	25
Figure 2.3 – Enzymatic Benzoylation of <i>N</i> -Debenzoyl-2'-deoxypaclitaxel.....	27
Figure 2.4 – Late-Occuring Steps on the Paclitaxel Biosynthetic Pathway.....	52
Figure 2.5 – Synthesis of <i>N</i> -Debenzoylisoserineoyltaxanes.....	53
Figure 2.6 – Typical Fragment Ions Observed in the MS/MS Profiles of Isoserinoyl Taxanes.....	54
Figure A.1 – Michaelis-Menten Curve for NDTBT.....	62
Figure A.2 – Synthesis of 3-Chlorobenzoyl CoA.....	63
Figure B.1 – Tandem Mass Spectrum of Paclitaxel Standard.....	64
Figure B.2 – Tandem Mass Spectrum of 2'-Deoxypaclitaxel Standard.....	65
Figure B.3 – Tandem Mass Spectrum of Docetaxel Standard.....	65

Figure B.4 – Tandem Mass Spectrum of Biosynthesized Paclitaxel	66
Figure B.5 – Tandem Mass Spectrum of Biosynthesized <i>N</i> -(2-Methylbenzoyl)- <i>N</i> -debenzoylpaclitaxel.....	66
Figure B.6 – Tandem Mass Spectrum of Biosynthesized <i>N</i> -(3-Methylbenzoyl)- <i>N</i> -debenzoylpaclitaxel.....	67
Figure B.7 – Tandem Mass Spectrum of Biosynthesized <i>N</i> -(4-Methylbenzoyl)- <i>N</i> -debenzoylpaclitaxel.....	67
Figure B.8 – Tandem Mass Spectrum of Biosynthesized <i>N</i> -(2-Fluorobenzoyl)- <i>N</i> -debenzoylpaclitaxel.....	68
Figure B.9 – Tandem Mass Spectrum of Biosynthesized <i>N</i> -(3-Fluorobenzoyl)- <i>N</i> -debenzoylpaclitaxel.....	68
Figure B.10 – Tandem Mass Spectrum of Biosynthesized <i>N</i> -(4-Fluorobenzoyl)- <i>N</i> -debenzoylpaclitaxel.....	69
Figure B.11 – Tandem Mass Spectrum of Biosynthesized <i>N</i> -(3-Cyanobenzoyl)- <i>N</i> -debenzoylpaclitaxel.....	69
Figure B.12 – Tandem Mass Spectrum of Biosynthesized <i>N</i> -(3-Methoxybenzoyl)- <i>N</i> -debenzoylpaclitaxel.....	70
Figure B.13 – Tandem Mass Spectrum of Biosynthesized <i>N</i> -(3-Chlorobenzoyl)- <i>N</i> -debenzoylpaclitaxel.....	70
Figure B.14 – Tandem Mass Spectrum of Biosynthesized <i>N</i> -(4-Chlorobenzoyl)- <i>N</i> -debenzoylpaclitaxel.....	71
Figure B.15 – Tandem Mass Spectrum of Biosynthesized <i>N</i> -(2-Furanoyl)- <i>N</i> -debenzoylpaclitaxel.....	71
Figure B.16 – Tandem Mass Spectrum of Biosynthesized <i>N</i> -(3-Furanoyl)- <i>N</i> -debenzoylpaclitaxel.....	72
Figure B.17 – Tandem Mass Spectrum of Biosynthesized <i>N</i> -(Thiophene-2-carbonyl)- <i>N</i> -debenzoylpaclitaxel.....	72
Figure B.18 – Tandem Mass Spectrum of Biosynthesized <i>N</i> -(Thiophene-3-carbonyl)- <i>N</i> -debenzoylpaclitaxel.....	73
Figure B.19 – Tandem Mass Spectrum of Biosynthesized <i>N</i> -(Thiazole)- <i>N</i> -debenzoylpaclitaxel.....	73

Figure B.20 – Tandem Mass Spectrum of Biosynthesized 10-deacetylpaclitaxel.....	74
Figure B.21 – Tandem Mass Spectrum of Biosynthesized <i>N</i> -(2-Methylbenzoyl)-10-deacetyl- <i>N</i> -debenzoylpaclitaxel.....	74
Figure B.22 – Tandem Mass Spectrum of Biosynthesized <i>N</i> -(3-Methylbenzoyl)-10-deacetyl- <i>N</i> -debenzoylpaclitaxel.....	75
Figure B.23 – Tandem Mass Spectrum of Biosynthesized <i>N</i> -(4-Methylbenzoyl)-10-deacetyl- <i>N</i> -debenzoylpaclitaxel.....	75
Figure B.24 – Tandem Mass Spectrum of Biosynthesized <i>N</i> -(2-Fluorobenzoyl)-10-deacetyl- <i>N</i> -debenzoylpaclitaxel.....	76
Figure B.25 – Tandem Mass Spectrum of Biosynthesized <i>N</i> -(3-Fluorobenzoyl)-10-deacetyl- <i>N</i> -debenzoylpaclitaxel.....	76
Figure B.26 – Tandem Mass Spectrum of Biosynthesized <i>N</i> -(4-Fluorobenzoyl)-10-deacetyl- <i>N</i> -debenzoylpaclitaxel.....	77
Figure B.27 – Tandem Mass Spectrum of Biosynthesized <i>N</i> -(3-Cyanobenzoyl)-10-deacetyl- <i>N</i> -debenzoylpaclitaxel.....	77
Figure B.28 – Tandem Mass Spectrum of Biosynthesized <i>N</i> -(3-Methoxybenzoyl)-10-deacetyl- <i>N</i> -debenzoylpaclitaxel.....	78
Figure B.29 – Tandem Mass Spectrum of Biosynthesized <i>N</i> -(3-Chlorobenzoyl)-10-deacetyl- <i>N</i> -debenzoylpaclitaxel.....	78
Figure B.30 – Tandem Mass Spectrum of Biosynthesized <i>N</i> -(4-Chlorobenzoyl)-10-deacetyl- <i>N</i> -debenzoylpaclitaxel.....	79
Figure B.31 – Tandem Mass Spectrum of Biosynthesized <i>N</i> -(2-Furanoyl)-10-deacetyl- <i>N</i> -debenzoylpaclitaxel.....	79
Figure B.32 – Tandem Mass Spectrum of Biosynthesized <i>N</i> -(3-Furanoyl)-10-deacetyl- <i>N</i> -debenzoylpaclitaxel.....	80
Figure B.33 – Tandem Mass Spectrum of Biosynthesized <i>N</i> -(Thiophene-2-carbonyl)-10-deacetyl- <i>N</i> -debenzoylpaclitaxel.....	80
Figure B.34 – Tandem Mass Spectrum of Biosynthesized <i>N</i> -(Thiophene-3-carbonyl)-10-deacetyl- <i>N</i> -debenzoylpaclitaxel.....	81

Figure B.35 – Tandem Mass Spectrum of Biosynthesized <i>N</i> -(Thiazole)-10-deacetyl- <i>N</i> -debenzoylpaclitaxel.....	81
Figure B.36 – Tandem Mass Spectrum of Biosynthesized <i>N</i> -Acetyl- <i>N</i> -debenzoyl-2'-deoxypaclitaxel.....	82
Figure B.37 – Tandem Mass Spectrum of Biosynthesized <i>N</i> -Butyryl- <i>N</i> -debenzoyl-2'-deoxypaclitaxel.....	82
Figure B.38 – Tandem Mass Spectrum of Biosynthesized <i>N</i> -(2-Butenoyl)- <i>N</i> -debenzoyl-2'-deoxypaclitaxel.....	83
Figure B.39 – Tandem Mass Spectrum of Biosynthesized <i>N</i> -Hexanoyl- <i>N</i> -debenzoyl-2'-deoxypaclitaxel.....	83
Figure B.40 – Tandem Mass Spectrum of Biosynthesized <i>N</i> -Acetyl- <i>N</i> -debenzoylpaclitaxel.....	84
Figure B.41 – Tandem Mass Spectrum of Biosynthesized <i>N</i> -Butyryl- <i>N</i> -debenzoylpaclitaxel....	84
Figure B.42 – Tandem Mass Spectrum of Biosynthesized <i>N</i> -(2-Butenoyl)- <i>N</i> -debenzoylpaclitaxel.....	85
Figure B.43 – Tandem Mass Spectrum of Biosynthesized <i>N</i> -Hexanoyl- <i>N</i> -debenzoylpaclitaxel.....	85
Figure B.44 – Tandem Mass Spectrum of Biosynthesized <i>N</i> -Acetyl-10-deacetyl- <i>N</i> -debenzoylpaclitaxel.....	86
Figure B.45 – Tandem Mass Spectrum of Biosynthesized <i>N</i> -Butyryl-10-deacetyl <i>N</i> -debenzoylpaclitaxel.....	86
Figure B.46 – Tandem Mass Spectrum of Biosynthesized <i>N</i> -(2-Butenoyl)-10-deacetyl <i>N</i> -debenzoylpaclitaxel.....	87
Figure B.47 – Tandem Mass Spectrum of Biosynthesized <i>N</i> -Hexanoyl-10-deacetyl <i>N</i> -debenzoylpaclitaxel.....	87
Figure 3.1 – NDTBT-CT Purification from Q-Sepharose Anion Exchange Column.....	106
Figure 3.2 – NDTBT-CT Purification from Superdex 200 Gel Filtration Column.....	107
Figure 3.3 – Enzymatic De-acetylation of Baccatin III by 10-Deacetylbaaccatin III:10- <i>O</i> -acetyltransferase.....	108
Figure 3.4 – DBAT-CT Purification from Q-Sepharose Anion Exchange Column.	109

Figure 3.5 – SDS-PAGE of <i>m</i> TBT Fractions from Nickel-Affinity Chromatography.....	110
Figure 3.6 – Enzymatic Benzoylation of 1,13- <i>O,O</i> -diacetyl-2- <i>O</i> -debenzoylbaccatin III by Modified Taxane-2 α - <i>O</i> -benzoyltransferase (<i>m</i> TBT).....	111
Figure 3.7 – Coupling Assay Scheme of Benzoate Ligase with <i>N</i> -Benzoyltransferase.....	115
Figure 4.1 – Crystal Structure of Vinorine Synthase.....	121
Figure 4.2 – Crystal Structure of the Anthocyanin Malonyltransferase.....	122
Figure 4.3 – Taxane Substrates Used by <i>Taxus</i> Acyltransferases.....	123
Figure 4.4 – Construction Scheme for Trimeric Mutants.....	126
Figure 4.5 – Sequence Alignment for Domain Swapping Between <i>Taxus</i> Acyltransferases and Schematic of Dimeric Mutants.....	128
Figure 4.6 – SDS-PAGE Gel of Region Mutant 611 and 661.....	130
Figure 4.7 – SDS-PAGE Gel of Dimeric Mutants A-6/2, A-2/6 and B-2/6.....	131
Figure 4.8 – Chromatogram from LC-ESI/MS of Controls from Reverse Reaction Assays with 7,13-Diacetylbaccatin.....	133
Figure 4.9 – Possible Products from NDTBT/DBAT Chimeric Mutants.....	135
Figure 4.10 – Scheme for DBAT with Natural Substrates and Possible Products from Chimeric Mutants.....	138
Figure 4.11 – Scheme for <i>m</i> TBT with Natural Substrates and Possible Products from Chimeric Mutants.....	139
Figure 4.12 – Homology Model of NDTBT Based on Dm3MaT3 with Conserved Residues Between NDTBT and DBAT.	142
Figure C.1 – Sequence Alignment of <i>Taxus</i> Acyltransferases.....	148
Figure C.2 – Sequence Alignment of NDTBT and DBAT with Dm3MaT3.....	151
Figure C.3 – Sequence Alignment of DBAT and <i>m</i> TBT with Vinorine Synthase.....	154
Figure C.4 – Sequence Alignment of Dm3MaT3 and Vinorine Synthase with <i>Taxus</i> Acyltransferases.....	157

ABBREVIATIONS

A ₂₂₈	absorption at 228 nm
AIDS	acquired immunodeficiency syndrome
Amp	ampicillin
<i>Amp^R</i>	ampicillin resistance gen
ATP	adenosine triphosphate
BAPT	baccatin III:3-amino-3-phenylpropanoyltransferase
bp	base pair
BMS	Bristol-Meyers Squibb
cDNA	complementary deoxyribonucleic acid
Cam	chloramphenicol
<i>Cam^R</i>	chloramphenicol resistance gene
CDCl ₃	Deuterated chloroform
CHCl ₃	Chloroform
CH ₃ CN	acetonitrile
CoA	coenzyme A
-CT	C-terminal His-tag
DAB	10-deacetylbaccatin III
DBAT	10-deacetylbaccatin III-10β- <i>O</i> -acetyltransferase
DFGWG	aspartate, phenylalanine, glycine, tryptophan, glycine motif
Dm3MaT1	anthocyanidin 3- <i>O</i> -glucoside-6''- <i>O</i> -malonyltransferase

Dm3MaT2	anthocyanidin 3- <i>O</i> -glucoside-3'',6''- <i>O</i> -dimalonyltransferase
DMAPP	dimethylallyl diphosphate
DNA	deoxyribonucleic acid
dNTPs	deoxyribonucleotide triphosphates
DTT	dithiothreitol
EB	elution buffer
ESI	electrospray ionization
EtOAc	ethyl acetate
FDA	Food and Drug Administration
FPLC	fast performance liquid chromatography
GGPPS	geranylgeranyl diphosphate synthase
GTP	guanosine-5'-triphosphate
HCl	hydrochloric acid
His ₆ -tag	hexa-histidine tag
HPLC	high pressure liquid chromatography
H ₃ PO ₄	phosphoric acid
IPP	isopentenyl diphosphate
IPTG	isopropyl β-D-thiogalactopyranoside
Kam	kanamycin
<i>Kam^R</i>	kanamycin resistance gene
kb	kilobase
<i>k_{cat}</i>	catalytic turnover

kDa	kilo-Daltons
K_M	Michaelis-Menten constant
LC-ESI	liquid chromatography ESI
LB	Luria-Bertani medium
MAPS	microtubule-associated proteins
MCOW	molecular cut off weight
MeOH	methanol
MgSO ₄	magnesium sulfate
MOPSO	3-(<i>N</i> -morpholine)-2-hydroxypropanesulfonic acid
MS	mass spectroscopy
MS/MS	tandem mass spectrometry
MSSSF	Macromolecular Structure, Sequencing and Synthesis Facility
MSU	Michigan State University
m/z	mass-to-charge ratio
<i>m</i> TBT	modified taxane-2 α - <i>O</i> -benzoyltransferase
NaCl	sodium chloride
NaHCO ₃	sodium bicarbonate
NCI	National Cancer Institute
NDTBT	<i>N</i> -debenzoyl-2'-deoxypaclitaxel: <i>N</i> -benzoyltransferase
NMR	nuclear magnetic resonance
NT-	N-terminal His-tag
OD ₆₀₀	optical density at 600 nm

ORF	open reading frame
PAM	phenylalanine aminomutase
PCR	polymerase chain reaction
QToF	quadrupole time of flight
RBS	ribosome binding site
R _f	retardation factor
rpm	revolutions per minute
rt	room temperature
SAR	structure activity relationships
SDS	sodium dodecyl sulfate
SDS-PAGE	SDS polyacrylamide gel electrophoresis
TAT	taxadien-5 α -ol- <i>O</i> -acetyltransferase
TBT	taxane-2 α - <i>O</i> -benzoyltransferase
TEMED	<i>N,N,N',N'</i> -tetramethylethylenediamine
TFA	trifluoroacetic acid
Tris-HCl	tris(hydromethyl)aminomethane hydrochloride
TS	taxadiene synthase
USDA	United States Department of Agriculture
UV	ultraviolet
V_{\max}	maximal velocity
v_{rel}	relative velocity
VS	vinorine synthase

CHAPTER 1

INTRODUCTION

1.1. Paclitaxel Background

Paclitaxel is a plant-derived tri-cyclic diterpenoid (Figure 1.1) with antimitotic properties that was originally isolated from the bark of the Pacific yew tree (*Taxus brevifolia*).¹ The National Cancer Institute (NCI) and the United States Department of Agriculture (USDA) identified this secondary metabolite in 1971 during a general screen of flora obtained in the Pacific Northwest for natural products with anticancer properties.²

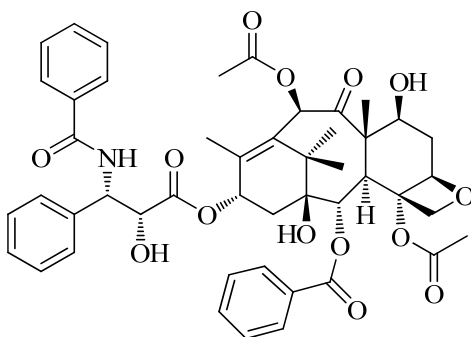


Figure 1.1 – Structure of Paclitaxel.

After clinical trials in the 1980s, the Food and Drug Administration (FDA) approved paclitaxel for use against ovarian cancer in 1992, and it has since been approved to treat a range of carcinomas.³ This pharmaceutical is applied in the treatment of breast cancer, non-small-cell lung cancer, head-and-neck cancer, AIDS-related Kaposi's sarcoma, and has recently been effective in regimens against Alzheimer's disease and tuberculosis.⁴⁻⁹ Paclitaxel has also been implemented as a preventative measure in heart disease by decreasing in-stent restenosis.¹⁰ These applications are possible due to unique characteristic of paclitaxel in regulating non-

functional, highly-reproducing tumor cells.

Unlike previous chemotherapeutic drugs (such as vinblastine, vincristine, and colchicine) that target tubulin and depolymerize microtubules, paclitaxel was the first anti-cancer agent to promote and stabilize microtubule assembly.¹¹⁻¹³ Both modes (microtubule depolymerization or stabilization) disrupt mitosis, leading to cell arrest and eventually apoptosis.¹⁴ Influenced by paclitaxel-promoted microtubules, essential, non-functional pathways associated with regulating apoptosis in cancerous cells are operational, i.e., the phosphorylation of Bcl2, activation of Raf-1, and activation of cJun kinase.¹⁵⁻¹⁷ Paclitaxel binds to the β -tubulin subunit in a stoichiometric ratio initiating polymerization and distorting the equilibrium between free-tubulin dimers and microtubules (Figure 1.2).^{18, 19} Although tubulin and paclitaxel interaction has been extensively

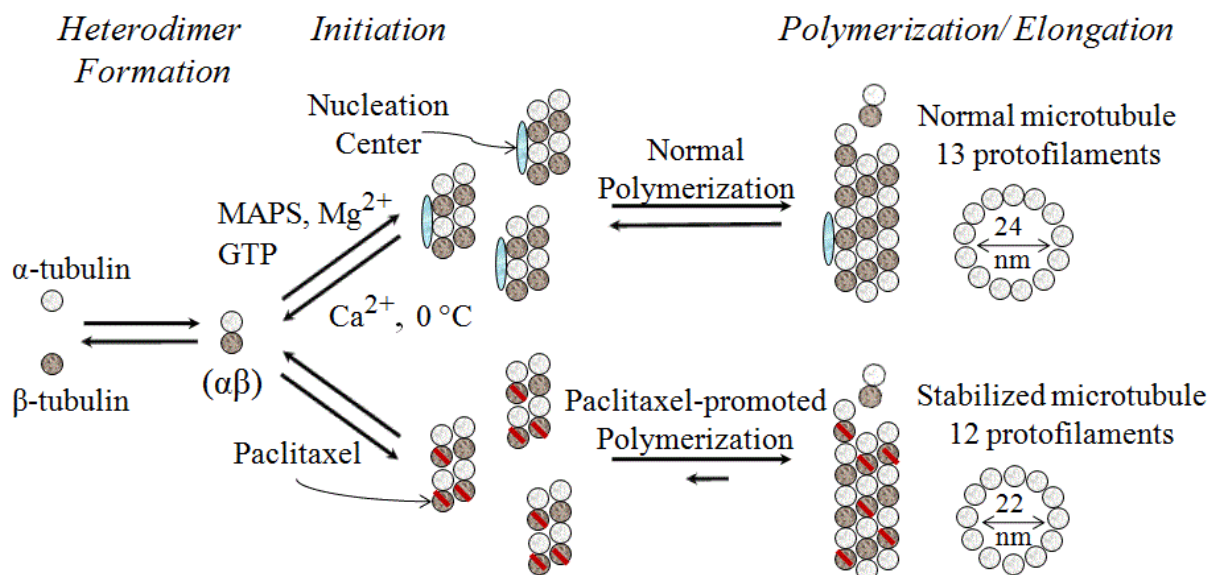


Figure 1.2 - Normal versus Paclitaxel –promoted Microtubule Assembly.

Adapted from Kingston, DGI (2001) *Chem. Comm.* 867-880.¹⁸ For interpretation of the references to color in this and all other figures, the reader is referred to the electronic version of this dissertation.

studied by photoaffinity labeling, fluorescence spectroscopy, and nuclear magnetic resonance measurement, the most compelling discovery was evidenced by x-ray crystallographic structural analysis.²⁰⁻²² Several research groups have provided experimental, theoretical, and molecular modeling evidence positing that paclitaxel adopts a T-shaped conformation when it binds tubulin, thus creating a stabilized paclitaxel-tubulin complex (Figure 1.3).^{23, 24}

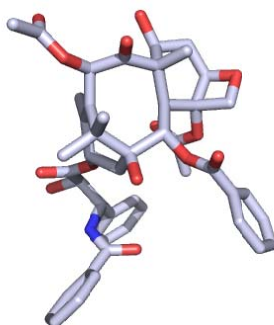


Figure 1.3 – Crystal Structure of Paclitaxel in T-Form.

Carbon is white, oxygen is red, and nitrogen is blue. Create by PyMol of PDB#1JFF.²³

This unique mode of tubulin binding has generated a high demand for paclitaxel in treating the aforementioned medical conditions. The supply from the natural source was not sustainable despite the prevalence of *Taxus sp.* in different parts of the world. Only a limited amount (140 mg per kg of bark) of paclitaxel could be isolated from the inner bark of the slow-growing and sparsely populated tree.² Consequently, other routes were explored as sustainable alternatives to mass-produce paclitaxel.² The pharmaceutical company Bristol-Myers Squibb (BMS) licensed a semi-synthesis technology for supplying the drug, which the company trademarked as Taxol. There were three approaches evaluated for the production of paclitaxel, including semi-synthesis, renewable *Taxus* cell cultures, and bioengineered heterologous hosts.

1.2. Paclitaxel Production

SEMI-SYNTHESIS

While the total synthesis of this complex diterpenoid structure was a major achievement by several research groups, the goal of these multistep processes (>80 steps) was not intended to address the supply chain (2% yield).²⁵⁻²⁸ Interesting chemistries and synthetic approaches, however, were elucidated while constructing the stereogenic centers, installing the oxy functional groups, acylating the various hydroxyls and amino groups towards the complex molecule.

A semi-synthetic approach developed at Florida State University (Tallahassee, FL) employed fewer steps (~37 steps) to mass-produce paclitaxel.²⁹ This technology was licensed by Bristol-Myers Squibb and involved isolating the advanced natural products 10-deacetylbaccatin III and baccatin III from the needles of *Taxus baccata* (English yew). These late-stage metabolites were present at 0.3% per dry weight compared to paclitaxel at 0.001-0.005% per dry weight in *T. baccata* (Figure 1.4).^{30, 31} These precursors were reacted with a β -lactam synthon to complete the semi-synthesis of paclitaxel (Figure 1-5). This method was easily employed to synthesize paclitaxel analogues to evaluate structure activity relationship (SAR) studies.^{31, 32}

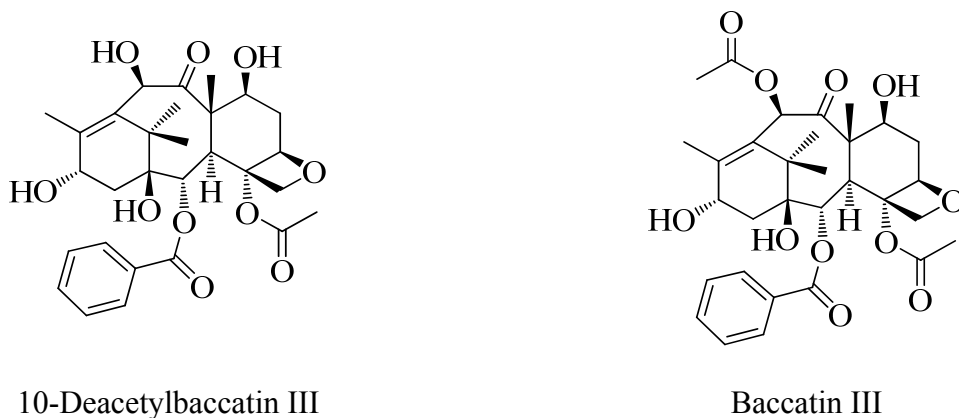


Figure 1.4 – Taxane Core Analogues: 10-Deacetylbaccatin III and Baccatin III.

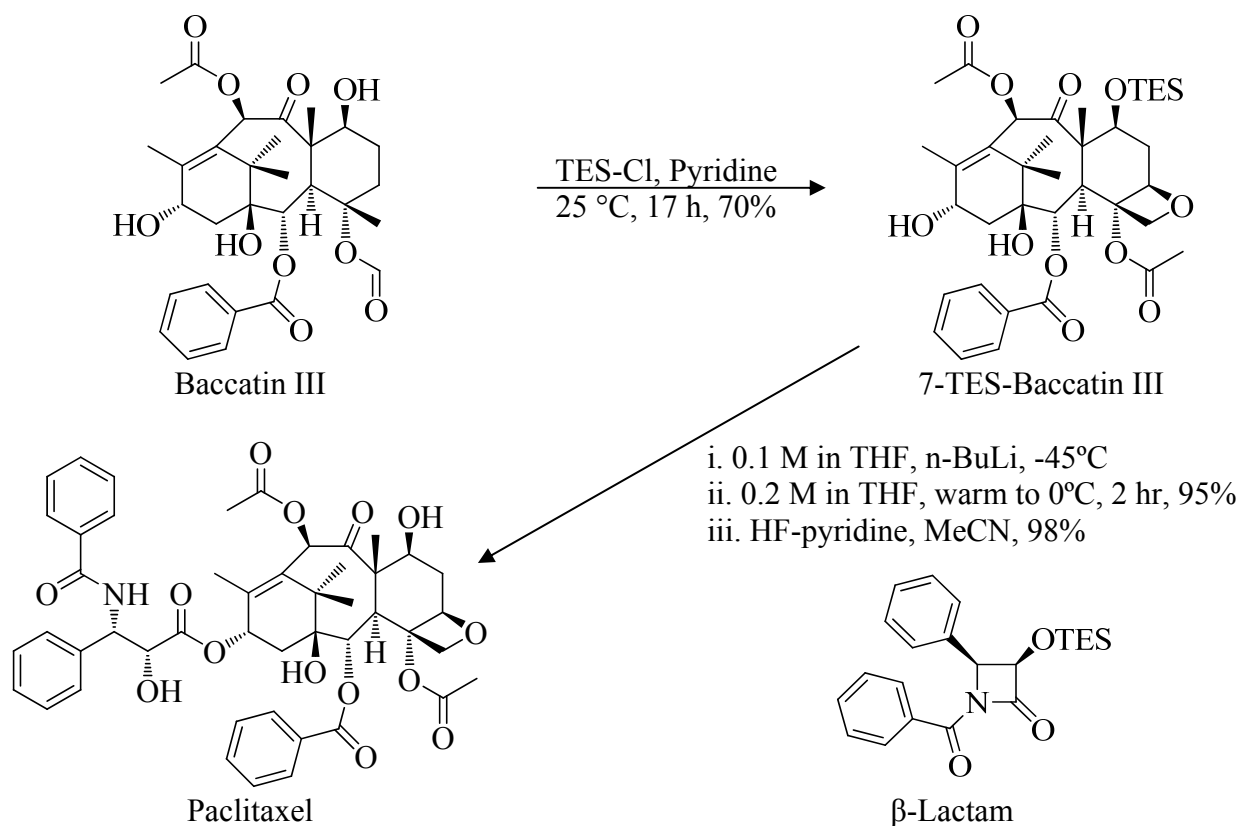


Figure 1.5 – Semi-synthesis Beta-lactam Method.

Paclitaxel analogues from combinational libraries were analyzed for potency, solubility, and cancer-type specificity.³³ Various SAR studies demonstrated that the acyl group side chains are responsible for cytotoxicity against cancer cells (Figure 1.6).³⁴ Antimitotic activity is achieved when there is an acyl group at the C2 hydroxyl (see Figure 1.6 for numbering) and the oxetane ring is intact.³⁵ In addition, the isoserinyl side chain at C13 is essential to anchor paclitaxel to β -tubulin.¹⁹ Furthermore, the most notable semisynthesized analogue identified in combinatorial chemical libraries from preliminary SAR studies is docetaxel, which entered the market as Taxotere by Rhone-Poulenc Rorer in 1996 (Figure 1.7),³⁶ and is used for breast, non-small cell lung, prostate, gastric adenocarcinoma, and head and neck cancers.³⁷

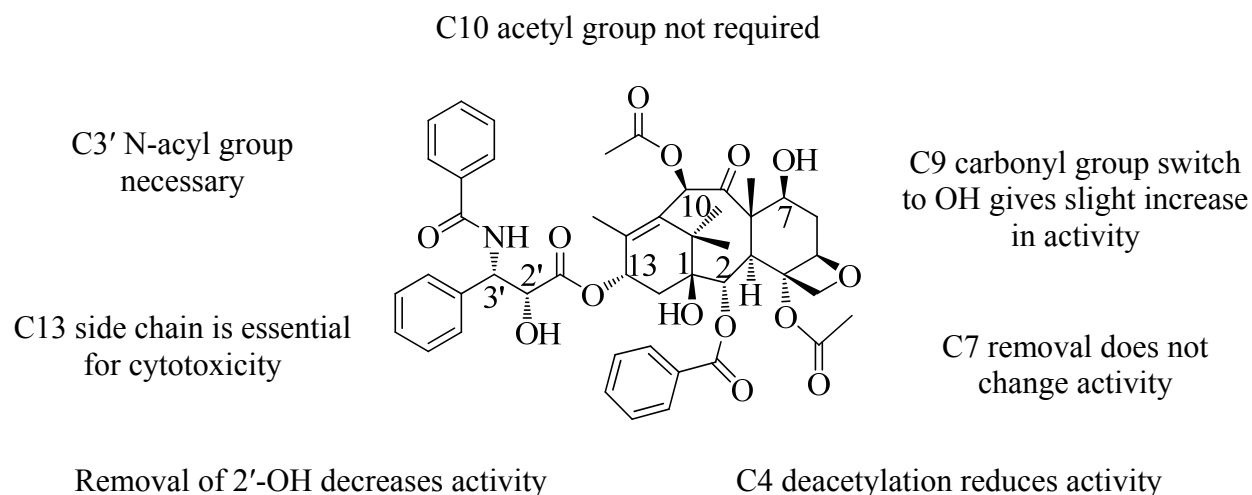


Figure 1.6 – Structure-Activity Relationships.

Adapted from Kingston, D. G. I. (2000) *J. Nat. Prod.* 63, 726-734.³⁴

CELL CULTURES

Despite the deployment of the semi-synthetic method, the large-scale production required exorbitant volumes of organic solvents, redundant protecting group manipulations, heavy metal catalysts, and large volume disposal.¹⁸ In addition, BMS realized that extracting the natural products from renewable *Taxus* needles needed for the semisynthesis was costly and laborious. Thus, to reduce their environmental footprint and cut back on the processing workload, the pharmaceutical company licensed a *Taxus* plant cell fermentation technology from Phyton.³⁸ This technology is the current resource to supply paclitaxel; unfortunately, this technology also has challenges pertaining to cell maintenance costs, and requires obligatory isolation and purification steps.³⁸ Along with Taxol, Taxotere is currently being produced by the semisynthesis approach using baccatin III isolated from the cell cultures. Incidentally, besides cultivating paclitaxel and related taxanes exclusively from the *Taxus* species, several endophytic fungi have been identified which also produce taxanes.³⁹⁻⁴³

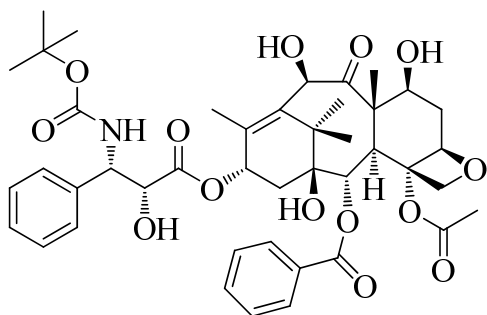


Figure 1.7 – Semisynthetically-derived Docetaxel (Taxotere[®]).

PACLITAXEL BIOSYNTHESIS

The biosynthesis of paclitaxel purportedly involves 19 enzymatic steps including a cyclase, several hydroxylases, an aminomutase, and several acyltransferases.⁴⁴ Like most diterpenes found in plants, the carbon skeleton of paclitaxel is derived from the 1-deoxy-D-xylulose-5-phosphate pathway to form the terpene building blocks isopentenyl diphosphate (IDP) and dimethylallyl diphosphate (DMADP).^{45, 46} The committed step towards paclitaxel biosynthesis is the cyclization of the universal diterpenoid precursor geranylgeranyl diphosphate to taxa-4(5),11(12)-diene by taxadiene synthase. Taxadiene is oxidized to taxadien-5 α -ol by a cytochrome P450-dependent taxadiene 5 α -hydroxylase followed by double-bond rearrangement and hydroxylation.^{47, 48} Next, the C5 hydroxyl group is likely acetylated by taxadien-5 α -ol-*O*-acetyltransferase (TAT), followed by hydroxylation at C10 by a taxane 10 β -hydroxylase (Figure 1.8).^{49, 50}

The order of the next steps in the pathway has not yet been determined, and the timing of the taxane-2 α -*O*-benzoyltransferase (TBT) catalysis on the pathway is currently being explored by *in vitro* experiments to identify alternative natural substrates. Compared to hypothetical pathways drawn for paclitaxel biosynthesis, TBT favors taxane substrates that are acylated at the

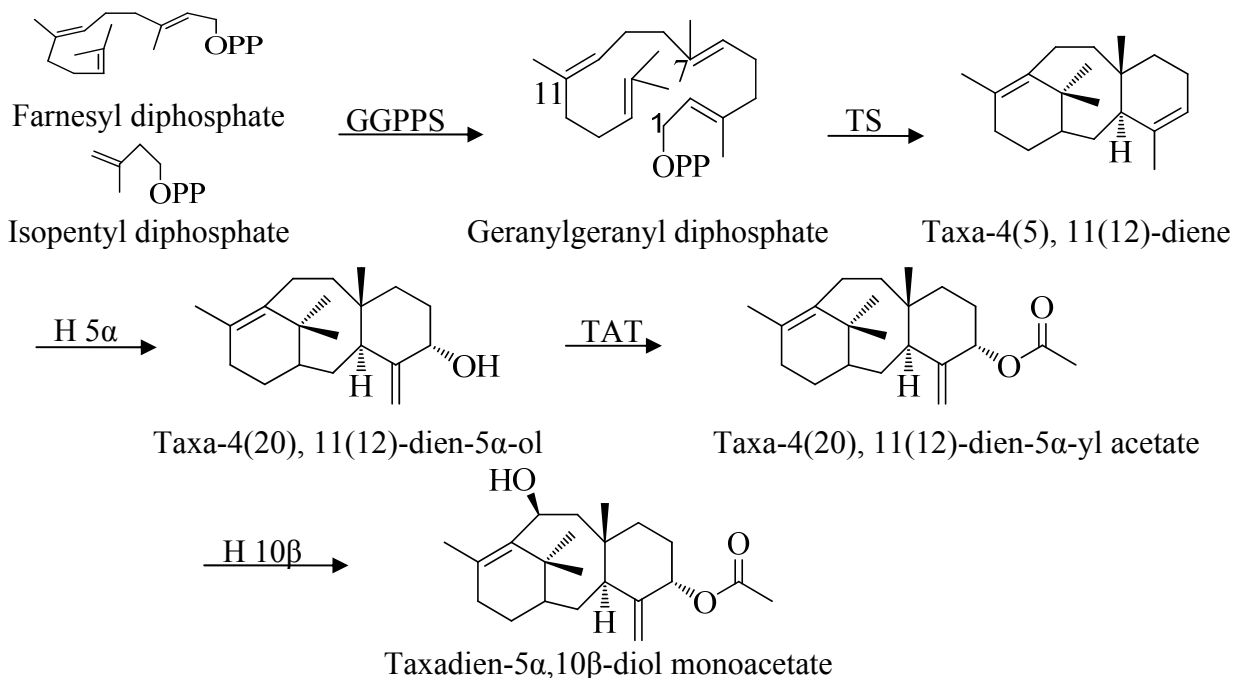


Figure 1.8 – Proposed Beginning Biosynthesis Pathway of Paclitaxel.

GGPPS: geranylgeranyl diphosphate synthase; TS: taxadiene synthase; H 5 α : cytochrome P450 taxadiene 5 α -hydroxylase; TAT: taxadien-5 α -ol-*O*-acetyltransferase; H 10 β : cytochrome P450 taxadiene 10 β -hydroxylase.

C7 hydroxyl.^{51, 52} The regioselectivity of other hydroxylases, besides the 5 α - and 10 β -

hydroxylase, are known, but their timing on the paclitaxel pathway is not established.⁵³⁻⁵⁵

Nonetheless, as with the very early steps, the order of the later-occurring steps on the pathway can be delineated with more certainty. The last steps on the pathway continue with acetylation at the C10 hydroxyl by 10-deacetylbaccatin III-10 β -*O*-acetyltransferase (DBAT) to make baccatin III (Figure 1.9), the taxane core of paclitaxel.⁵⁶ A β -phenylalanyl moiety is then transferred to the C13 hydroxyl of baccatin III by an acyl CoA-dependent baccatin III:3-amino-3-phenylpropanoyltransferase (BAPT). Subsequent C2'-hydroxylation of the β -amino phenylpropanoid by a P450-dependent hydroxylase, and final *N*-benzoylation of the amino group by *N*-debenzoyl-2'-deoxypaclitaxel:*N*-benzoyltransferase (NDTBT) completes the biosynthesis

of paclitaxel (Figure 1.9).⁵⁷⁻⁵⁹ β -Phenylalanine is isomerized from α -phenylalanine via a phenylalanine aminomutase (PAM) that is connected to the paclitaxel pathway; however, the ligase needed to biosynthesize the β -phenylalanine CoA substrate for BAPT so far remains unidentified.⁶⁰ This missing catalyst is necessary to completely semi-biosynthesize paclitaxel from baccatin III in a heterologous host bioengineered with the necessary genes.

BIOENGINEERING

Over the last two decades, several genes on the paclitaxel pathway were isolated from a cDNA library, and the encoded enzymes were expressed and biochemically characterized *in vitro* and assayed in heterologous systems (e.g. *Escherichia coli* and *Saccharomyces cerevisiae*) by analyzing their activity *in vitro* and *in vivo*.^{44, 61-63} A current goal is to produce paclitaxel from primary metabolites in organisms bioengineered with *Taxus* enzymes and by manipulating the endogenous *Taxus* pathways to increase flux to the final product. There have been recent achievements in this endeavor, pertaining to isoprenoids in microbes and taxadiene biosynthesis in yeast and *Arabidopsis thaliana*.⁶⁴⁻⁶⁶ Very recently, *E. coli* was successfully engineered to over-produce the building blocks of the taxane skeleton that ultimately yielded taxa-4(20),11(2)-diene-5 α -ol in the host bacteria engineered to co-express of a soluble P450 hydroxylase.⁶⁷ In another bacterial-based system, *E. coli* was engineered to express 10-deacetylbaccatin III-10 β -O-acetyltransferase (DBAT) and a small/medium chain acid:CoA ligase. Baccatin III and its C10 analogues were semi-biosynthesized from 10-deacetylbaccatin III and cosubstrates acetic-, propionic-, or butyric acid fed to the bacteria.^{56, 68}

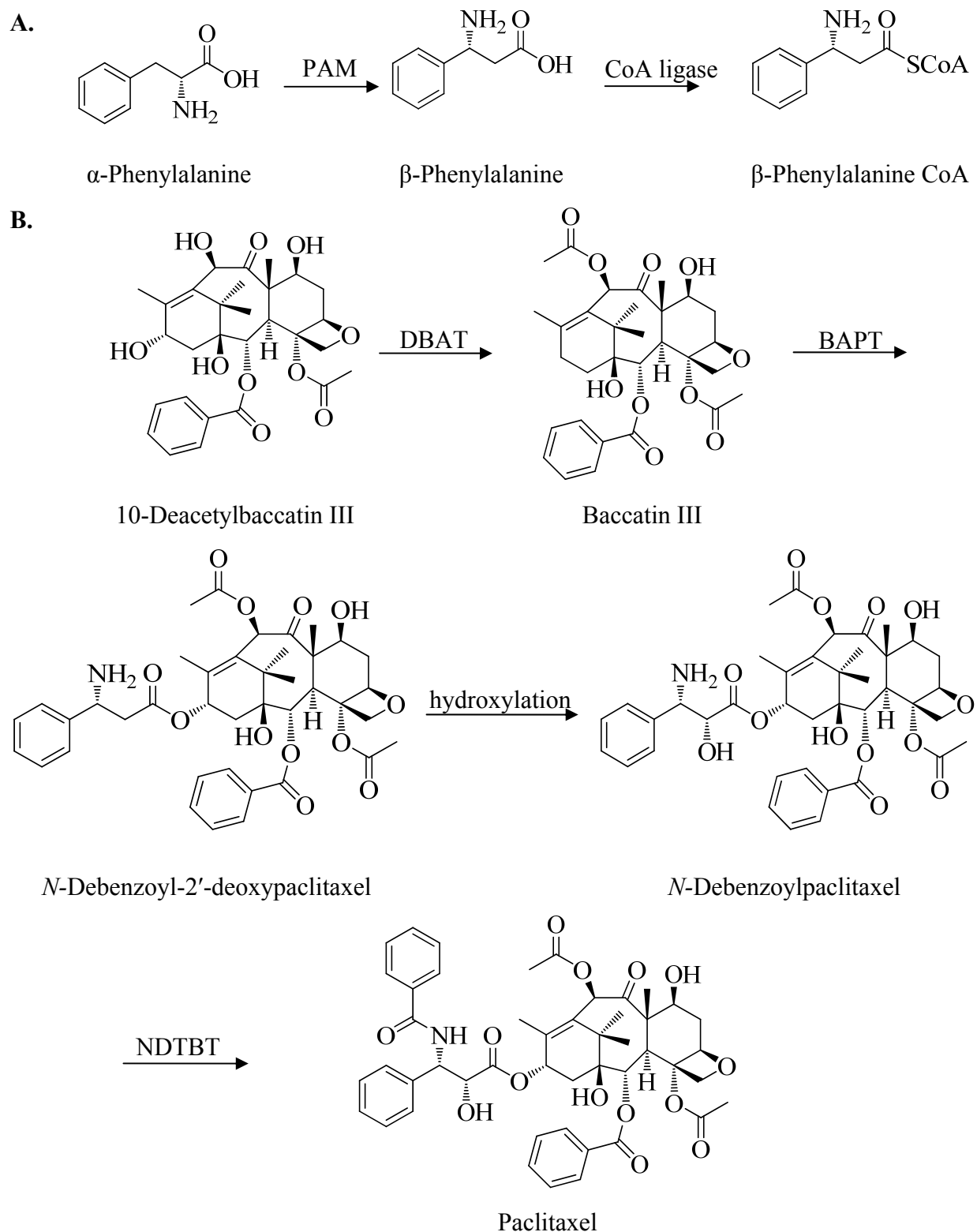


Figure 1.9 - Acetylation at C10 and Biosynthesis Steps of the C13 Side-Chain.

A. Biosynthesis of β -phenylalanine coenzyme A substrate, PAM: phenylalanine aminomutase. B. DBAT: 10-deacetylpaclitaxel:10-*O*-acetyltransferase; BAPT: 13-*O*-phenylpropanoyltransferase; NDTBT: *N*-debenzoyl-2'-deoxypaclitaxel:*N*-benzoyltransferase.

In vitro production of paclitaxel is a tractable alternative that would employ enzymes as biocatalysts in one-pot reactions. This approach is commonly used in academia and in industry to produce novel compounds or alter the structure of existing lead compounds for commercial use. Since several enzymes on the paclitaxel pathway are characterized with their presumed natural cosubstrates, it is foreseeable that an *in vitro* approach can potentially be used for paclitaxel synthesis. Thus, the substrate specificity and mechanisms of the *Taxus*-derived enzymes need to be explored. This information will be valuable when designing biocatalytic routes to produce paclitaxel analogues. Further, directed mutagenesis within the active site of these catalysts could either expand or hone substrate selectivity and increase turnover.

1.3. *Taxus* Acyltransferases

Of the 19 enzymatic steps in the pathway, five steps are catalyzed by functionally-defined acyltransferases, which belong to a super-family of acyltransferases designated BAHD [benzylalcohol acetyl-, anthocyanin-O-hydroxy-cinnamoyl-, anthranilate-N-hydroxy-cinnamoyl/benzoyl-, deacetylvindoline acetyltransferase] (Table 1.1).⁶⁹ Each family member requires a coenzyme A-dependent acyl group donor and contains a conserved HXXXD sequence motif presumed to be involved in the transfer mechanism of various acyl groups [alkyl, aroyl, or phenylpropanoyl] to the acceptor molecule.⁵⁹ As mentioned above, these acyl side chains are responsible for the pharmacophore of paclitaxel and its analogues; some of the latter have demonstrated increased potency and solubility compared to the parent molecule.

The native DBAT from *Taxus* has modest promiscuity for non-natural acyl groups (propionyl and butyryl) from CoA donors to its corresponding diterpene co-substrate, 10-deacetylbaccatin III.^{62, 68} Recently, a modified TBT (Table 1.1) with increased protein solubility was found productive with 7,13-*O,O*-diacetyl-2-*O*-debenzoylbaccatin III and a broad range of acyl coenzyme A cosubstrates (benzoyl; *ortho*-, *meta*-, and *para*-substituted benzoyls; various heteroaromatic carbonyls; alkanoyls; and butenoyl).⁵²

Table 1.1 - *Taxus* Acyltransferases Characteristics

Name	Accession Number	Amino Acids	Reference
Taxadien-5 α -ol- <i>O</i> -acetyltransferase (TAT)	AF190130	439	44
Taxane-2 α - <i>O</i> -benzoyltransferase (TBT)	AF297618	440	46
10-Deacetylbaccatin III-10 β - <i>O</i> -acetyltransferase (DBAT)	AF193765	440	51
Baccatin III:3-amino-3-phenylpropanoyltransferase (BAPT).	AY082804	445	52
<i>N</i> -Debenzoyl-2'-deoxypaclitaxel: <i>N</i> -benzoyltransferase (NDTBT)	AF466397	441	65

1.4. Project Outline

In the foregoing discussion, it is apparent that *Taxus* acyltransferases can transfer a range of natural acyl groups from CoA thioester donors to a hydroxytaxoid acceptor. Therefore, it seems the *Taxus* family of acyltransferases can generally transfer similar non-natural acyl groups of slightly altered form. This hypothesis was tested by challenging an *N*-debenzoylpaclitaxel-*N*-benzoyltransferase (designated NDTBT) on the paclitaxel pathway with a broad array of cosubstrates.

In Chapter 2, the relative substrate-specificity was examined and the kinetics constants were calculated for native NDTBT, using benzoyl CoA and non-natural aroyl/alkyl CoA thioesters with *N*-debenzoyl-2'-deoxypaclitaxel. A variety of non-natural acyl CoA thioesters

obtained from commercial sources or synthesized were incubated with enzyme, and each product mixture was examined by HPLC, MS, and NMR to identify *de novo* biosynthetic products. In addition, the substrate specificity study on NDTBT was examined with two other taxane acceptors *N*-debenzoyl-paclitaxel and 10-deacetyl-*N*-debenzoyl-paclitaxel, which lacked or possessed an acetyl group at C10, respectively (Figure 1.10). Together, the taxane substrates examined whether the C10-acetyl group and the 2'-hydroxyl group of the side chain would preclude catalysis.

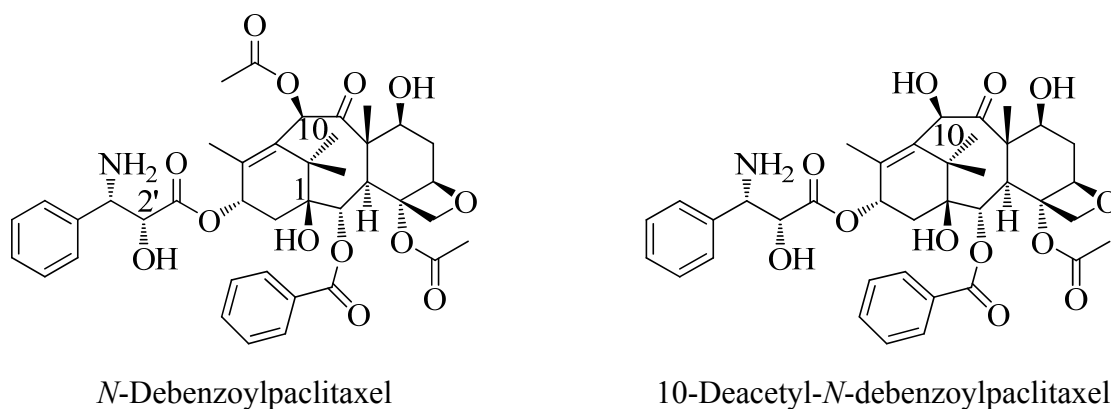


Figure 1.10 - Structures of Taxane Analogues: *N*-Debenzoylpaclitaxel and 10-Deacetyl-*N*-debenzoylpaclitaxel.

Chapter 3 details the improvements made towards purifying three *Taxus* acyltransferases for future crystallographic analysis. A series of nickel affinity, anion exchange, and gel filtration column chromatography steps was used to extend an original purification strategy employing only nickel affinity chromatography. The additional purification steps yielded protein at 95-99% purity 1 mg/L cell culture, compared to the 70% purity enzyme outlined previously in Chapter 2. These purified enzymes will also be employed in coupled enzyme assays containing coenzyme A ligases to optimize the turnover of acylated taxanes as well as to recycle the CoA by-product back into the reaction stream as an acyl CoA.

In Chapter 4, a mutagenesis screen was conducted among three *Taxus* acyltransferases *N*-debenzoyl-2'-deoxypaclitaxel:*N*-benzoyltransferase (NDTBT), 10-deacetylbaaccatin III-10 β -*O*-acetyltransferase (DBAT), and taxane-2 α -*O*-benzoyltransferase (TBT) by domain and regional swaps to create chimeric mutants for crystal structure analysis. A homology-modeled structure of the *Taxus* DBAT (10-deacetyl-baccatin III:10-*O*-acetyltransferase) was constructed based on the structure of acetyltransferase vinorine synthase in the same family, and the conserved active site residues were identified.⁷⁰ These residues established a basis for site-directed mutagenesis and domain swapping. These changes were be assessed by assays that compared kinetic parameters between the wild-type and mutant enzymes.^{52, 70, 71} Also, based on regional swaps of a homologous anthocyanin malonyltransferase in an earlier study, similar regions were swapped to make chimeric proteins between pair 1: NDTBT and DBAT and pair 2: DBAT and TBT.^{52, 72} These alterations were anticipated to reveal, at least in part, the dependence of certain regions or domains on substrate specificity by converting aroyltransferases NDTBT or TBT into alkyl transferases, and reciprocally changing alkyltransferase DBAT to an aroyltransferase.

Chapter 5 provides an overview of future applications of *Taxus* acyltransferases as biocatalysts and describes a possible direction for paclitaxel synthesis in heterologous organisms. Also described are some insights based on preliminary experiments involving *in vivo* biosynthetic turnover and evaluating the properties of the transferases to optimize crystallization conditions for structural analysis.

REFERENCES

REFERENCES

1. Wani, M. C., Taylor, H. L., Wall, M. E., Coggon, P., and Mcphail, A. T. (1971) Plant antitumor agents .6. Isolation and structure of Taxol, a novel antileukemic and antitumor agent from *Taxus brevifolia*, *J. Am. Chem., Soc.* *93*, 2325-2327.
2. Suffness, M., and Wall, M. E. (1995) Discovery and Development of Taxol, In *Taxol: Science and Applications* (Suffness, Matthew, Ed.), pp 3-25, CRC Press, New York.
3. McGuire, W. P., Rowinsky, E. K., Rosenshein, N. B., Grumbine, F. C., Ettinger, D. S., Armstrong, D. K., and Donehower, R. C. (1989) Taxol: A unique antineoplastic agent with significant activity in advanced ovarian epithelial neoplasms, *Ann. Intern. Med.* *111*, 273.
4. Sgadari, C., Toschi, E., Palladino, C., Barillari, G., Carlei, D., Cereseto, A., Ciccolella, C., Yarchoan, R., Monini, P., Sturzl, M., and Ensoli, B. (2000) Mechanism of paclitaxel activity in Kaposi's sarcoma, *J. Immunol.* *165*, 509-517.
5. Oshige, M., Takenouchi, M., Kato, Y., Kamisuki, S., Takeuchi, T., Kuramochi, K., Shiina, I., Suenaga, Y., Kawakita, Y.-i., and Kuroda, K. (2004) Taxol derivatives are selective inhibitors of DNA polymerase α , *Bioorg. Med. Chem.* *12*, 2597-2601.
6. Garber, K. (2004) Improved Paclitaxel formulation hints at new chemotherapy approach, *J. Natl. Cancer Inst.* *96*, 90-91.
7. Rouzier, R., Perou, C. M., Symmans, W. F., Ibrahim, N., Cristofanilli, M., Anderson, K., Hess, K. R., Stec, J., Ayers, M., Wagner, P., Morandi, P., Fan, C., Rabiul, I., Ross, J. S., Hortobagyi, G. N., and Puztai, L. (2005) Breast cancer molecular subtypes respond differently to preoperative chemotherapy, *Clin. Cancer Res.* *11*, 5678-5685.
8. Cheung, M. C., Pantanowitz, L., and Dezube, B. J. (2005) AIDS-related malignancies: Emerging challenges in the era of highly active antiretroviral therapy, *Oncologist* *10*, 412-426.
9. Eisenhauer, E. A., and Vermorken, J. B. (1998) The taxoids. Comparative clinical pharmacology and therapeutic potential, *Drugs* *55*, 5-30.
10. Raja, S. G. (2006) Drug-eluting stents and the future of coronary artery bypass surgery: Facts and fiction, *Ann. Thorac. Surg.* *81*, 1162-1171.
11. Schiff, P. B., Fant, J., and Horwitz, S. B. (1979) Promotion of microtubule assembly *in vitro* by Taxol, *Nature* *277*, 665-667.
12. Wilson, L., and Jordan, M. A. (1995) Microtubule dynamics: Taking aim at a moving target, *Chem. Biol.* *2*, 569-573.

13. Manfredi, J. J., and Horwitz, S. B. (1984) Taxol: an antimitotic agent with a new mechanism of action, *Pharmacol. Ther.* 25, 83-125.
14. Yeung, T. K., Germond, C., Chen, X., and Wang, Z. (1999) The mode of action of Taxol: Apoptosis at low concentration and necrosis at high concentration, *Biochem. Biophys. Res. Commun.* 263, 398-404.
15. Scatena, C. D., Stewart, Z. A., Mays, D., Tang, L. J., Keefer, C. J., Leach, S. D., and Pietenpol, J. A. (1998) Mitotic phosphorylation of Bcl-2 during normal cell cycle progression and Taxol-induced growth arrest, *J. Biol. Chem.* 273, 30777-30784.
16. Tonini, T., Gabellini, C., Bagella, L., D'Andrilli, G., Masciullo, V., Romano, G., Scambia, G., Zupi, G., and Giordano, A. (2004) PRb2/p130 decreases sensitivity to apoptosis induced by camptothecin and doxorubicin but not by Taxol, *Clin. Cancer Res.* 10, 8085-8093.
17. Blagosklonny, M. V., Giannakakou, P., el-Deiry, W. S., Kingston, D. G., Higgs, P. I., Neckers, L., and Fojo, T. (1997) Raf-1/bcl-2 phosphorylation: a step from microtubule damage to cell death, *Cancer Res.* 57, 130-135.
18. Kingston, D. G. I. (2001) Taxol, a molecule for all seasons, *Chem. Commun.* 867-880.
19. Horwitz, S. B. (1992) Mechanism of action of taxol, *Trends Pharmacol. Sci.* 13, 134-136.
20. Rao, S., Krauss, N. E., Heerding, J. M., Swindell, C. S., Ringel, I., Orr, G. A., and Horwitz, S. B. (1994) 3'-(p-azidobenzamido)taxol photolabels the N-terminal 31 amino acids of β -tubulin, *J. Biol. Chem.* 269, 3132-3134.
21. Li, Y., Poliks, B., Cegelski, L., Poliks, M., Gryczynski, Z., Piszczek, G., Jagtap, P. G., Studelska, D. R., Kingston, D. G. I., Schaefer, J., and Bane, S. (2000) Conformation of microtubule-bound paclitaxel determined by fluorescence spectroscopy and REDOR NMR, *Biochemistry* 39, 281-291.
22. Nogales, E., Wolf, S. G., and Downing, K. H. (1998) Structure of the α , β -tubulin dimer by electron crystallography, *Nature* 391, 199-203.
23. Löwe, J., Li, H., Downing, K., and Nogales, E. (2001) Refined structure of α β -tubulin at 3.5 Å resolution., *J. Mol. Biol.* 313, 1045-1057.
24. Ganesh, T., Norris, A., Sharma, S., Bane, S., Alcaraz, A. A., Snyder, J. P., and Kingston, D. G. I. (2006) Design, synthesis, and bioactivity of simplified paclitaxel analogs based on the T-Taxol bioactive conformation, *Bioorg. Med. Chem.* 14, 3447-3454.

25. Nicolaou, K. C., Yang, Z., Liu, J. J., Ueno, H., Nantermet, P. G., Guy, R. K., Claiborne, C. F., Renaud, J., Couladouros, E. A., Paulvannan, K., and Sorensen, E. J. (1994) Total synthesis of Taxol, *Nature* **367**, 630-634.
26. Ojima, I., Habus, I., Zhao, M., Zucco, M., Park, Y. H., Sun, C. M., and Brigaud, T. (1992) New and efficient approaches to the semisynthesis of Taxol and Its C-13 side-chain analogs by means of beta-Lactam synthon method, *Tetrahedron* **48**, 6985-7012.
27. Holton, R. A., Somoza, C., Kim, H. B., Liang, F., Biediger, R. J., Boatman, P. D., Shindo, M., Smith, C. C., Kim, S. C., Nadizadeh, H., Suzuki, Y., Tao, C. L., Vu, P., Tang, S. H., Zhang, P. S., Murthi, K. K., Gentile, L. N., and Liu, J. H. (1994) First total synthesis of Taxol .1. Functionalization of the B-Ring, *J. Am. Chem. Soc.* **116**, 1597-1598.
28. Holton, R. A., Kim, H. B., Somoza, C., Liang, F., Biediger, R. J., Boatman, P. D., Shindo, M., Smith, C. C., Kim, S. C., Nadizadeh, H., Suzuki, Y., Tao, C. L., Vu, P., Tang, S. H., Zhang, P. S., Murthi, K. K., Gentile, L. N., and Liu, J. H. (1994) First total synthesis of Taxol .2. Completion of the C-Ring and D-Ring, *J. Am. Chem. Soc.* **116**, 1599-1600.
29. Holton, R. A., Somoza, C., and Chai, K. B. (1994) A simple synthesis of 10-deacetoxytaxol derivatives, *Tetrahedron Lett.* **35**, 1665-1668.
30. Denis, J. N., Greene, A. E., Guenard, D., Gueritte-Voegelein, F., Mangatal, L., and Potier, P. (1988) Highly efficient, practical approach to natural taxol, *J. Am. Chem. Soc.* **110**, 5917-5919.
31. Exposito, O., Bonfill, M., Moyano, E., Onrubia, M., Mirjalili, M., Cusido, R., and Palazon, J. (2009) Biotechnological production of Taxol and related taxoids: Current state and prospects, *Anticancer Agents Med. Chem.* **9**, 109-121.
32. Xue, M., Long, B. H., Fairchild, C., Johnston, K., Rose, W. C., Kadow, J. F., Vyas, D. M., and Chen, S. H. (2000) Structure-activity relationships study at the 3'-N position of paclitaxel. Part 2: Synthesis and biological evaluation of 3'-N-thiourea- and 3'-N-thiocarbamate-bearing paclitaxel analogues, *Bioorg. Med. Chem. Lett.* **10**, 1327-1331.
33. Amato, I. (1992) Chemists vie to make a better Taxol, *Science* **256**, 311.
34. Kingston, D. G. I. (2000) Recent advances in the chemistry of Taxol, *J. Nat. Prod.* **63**, 726-734.
35. Georg, G., Boge, T., Cheruvallath, Z., Clowers, J., Harriman, G., Hepperle, M., and Park, H. (1995) The medicinal chemistry of Taxol., In *Taxol – Science and Applications* (M. Suffness, Ed.), pp 71-95, CRC Press, Boca Raton, FL, USA.

36. Bissery, M. C., Nohynek, G., Sanderink, G. J., and Lavelle, F. (1995) Docetaxel (Taxotere): a review of preclinical and clinical experience. Part I: Preclinical experience, *Anticancer Drugs* 6, 339-355, 363-338.
37. Taxotere Official FDA Information, S. e. a. U. <http://www.drugs.com/pro/taxotere.html>.
38. Patel, R. N. (1998) Tour de paclitaxel: biocatalysis for semisynthesis, *Annu. Rev. Microbiol.* 52, 361-395.
39. Stierle, A., Strobel, G., and Stierle, D. (1993) Taxol and taxane production by *Taxomyces-Andreanae*, an endophytic fungus of Pacific Yew, *Science* 260, 214-216.
40. Strobel, G., Yang, X., Sears, J., Kramer, R., Sidhu, R. S., and Hess, W. M. (1996) Taxol from *Pestalotiopsis microspora*, an endophytic fungus of *Taxus wallachiana*, *Microbiology* 142 (Pt 2), 435-440.
41. Li, J., Stroble, G., Sidhu, R., Hess, W., and Ford, E. (1996) Endophytic Taxol-producing fungi from bald cypress, *Taxodium distichum*, *Microbiology* 142, 2223-2226.
42. Kim, S., Strobel, G., and Ford, E. (1999) Screening of Taxol-producing endophytic fungi from *Ginko biloba* and *Taxus cuspidata* in Korea, *Agric. Chem. Biotechnol.* 42, 97-99.
43. Wang, J., Li, G., Lu, H., Zheng, Z., Huang, Y., and Su, W. (2000) Taxol from *Tubercularia* sp.strain TF5, an endophytic fungus of *Taxus mairei*, *FEMS Microbiol. Lett.* 193, 249-253.
44. DeJong, J., Liu, Y., Bollon, A., Long, R., Jennewein, S., Williams, D., and Croteau, R. (2005) Genetic engineering of Taxol biosynthetic genes in *Saccharomyces cerevisiae*, *Biotechnol. Bioeng.* 93, 212-224.
45. Eisenreich, W., Menhard, B., Hylands, P. J., Zenk, M. H., and Bacher, A. (1996) Studies on the biosynthesis of taxol: The taxane carbon skeleton is not of mevalonoid origin, *Proc. Natl. Acad. Sci.U. S. A.* 93, 6431-6436.
46. Lichtenthaler, H. K. (1999) The 1-deoxy-D-xylulose-5-phosphate pathway of isoprenoid biosynthesis in plants, *Annu. Rev. Plant Physiol.Plant Mol. Biol.* 50, 47-65.
47. Wildung, M. R., and Croteau, R. (1996) A cDNA clone for taxadiene synthase, the diterpene cyclase that catalyzes the committed step of Taxol biosynthesis, *J. Biol. Chem.* 271, 9201-9204.
48. Jennewein, S., Long, R. M., Williams, R. M., and Croteau, R. (2004) Cytochrome P450 taxadiene 5 α -hydroxylase, a mechanistically unusual monooxygenase catalyzing the first oxygenation step of Taxol biosynthesis, *Chem. Biol.* 11, 379-387.

49. Walker, K., Schoendorf, A., and Croteau, R. (2000) Molecular cloning of a taxane 4(20),11(12)-dien-5 α -ol-*O*-acetyl transferase cDNA from *Taxus* and functional expression in *Escherichia coli*, *Arch. Biochem. Biophys.* 374, 371-380.
50. Schoendorf, A., Rithner, C., Williams, R., and Croteau, R. (2001) Molecular cloning of a cytochrome P450 taxane 10 β -hydroxylase cDNA from *Taxus* and functional expression in yeast, *Proc. Natl. Acad. Sci. U. S. A.* 98, 1501-1506.
51. Walker, K., and Croteau, R. (2000) Taxol biosynthesis: Molecular cloning of a benzoyl-CoA:taxane 2 α -*O*-benzoyltransferase cDNA from *Taxus* and functional expression in *Escherichia coli*, *Proc. Natl. Acad. Sci. U. S. A.* 97, 13591-13596.
52. Nawarathne, I. N., and Walker, K. D. (2010) Point mutations (Q19P and N23K) increase the operational solubility of a 2 α -*O*-benzoyltransferase that conveys various acyl groups from CoA to a taxane acceptor, *J. Nat. Prod.* 73, 151-159.
53. Jennewein, S., Rithner, C. D., Williams, R. M., and Croteau, R. B. (2001) Taxol biosynthesis: Taxane 13-hydroxylase is a cytochrome P450-dependent monooxygenase, *Proc. Natl. Acad. Sci. U. S. A.* 98, 13595-13600.
54. Chau, M., and Croteau, R. (2004) Molecular cloning and characterization of a cytochrome P450 taxoid 2 α -hydroxylase involved in Taxol biosynthesis, *Arch. Biochem. Biophys.* 427, 48-57.
55. Chau, M., Jennewein, S., Walker, K., and Croteau, R. (2004) Taxol biosynthesis: Molecular cloning and characterization of a cytochrome P450 taxoid 7 β -hydroxylase, *Chem. Biol.* 11, 663-672.
56. Walker, K., and Croteau, R. (2000) Molecular cloning of a 10-deacetylbaccatin III-10-*O*-acetyl transferase cDNA from *Taxus* and functional expression in *Escherichia coli*, *Proc. Natl. Acad. Sci. U. S. A.* 97, 583-587.
57. Walker, K., Fujisaki, S., Long, R., and Croteau, R. (2002) Molecular cloning and heterologous expression of the C-13 phenylpropanoid side chain-CoA acyltransferase that functions in Taxol biosynthesis, *Proc. Natl. Acad. Sci. U. S. A.* 99, 12715-12720.
58. Long, R. M., and Croteau, R. (2005) Preliminary assessment of the C13-side chain 2'-hydroxylase involved in Taxol biosynthesis, *Biochem. Biophys. Res. Commun.* 338, 410-417.
59. Walker, K., Long, R., and Croteau, R. (2002) The final acylation step in Taxol biosynthesis: cloning of the taxoid C13-side chain *N*-benzoyltransferase from *Taxus*, *Proc. Natl. Acad. Sci. U. S. A.* 99, 9166-9171.

60. Walker, K. D., Klettke, K., Akiyama, T., and Croteau, R. (2004) Cloning, heterologous expression, and characterization of a phenylalanine aminomutase involved in Taxol biosynthesis, *J. Biol. Chem.* 279, 53947-53954.
61. Jennewein, S., Wildung, M. R., Chau, M., Walker, K., and Croteau, R. (2004) Random sequencing of an induced *Taxus* cell cDNA library for identification of clones involved in Taxol biosynthesis, *Proc. Natl. Acad. Sci. U. S. A.* 101, 9149-9154.
62. Loncaric, C., Ward, A. F., and Kevin D. Walker. (2007) Expression of an acetyl-CoA synthase and a CoA-transferase in *Escherichia coli* to produce modified taxanes *in vivo*, *Biotechnol.* 2, 266-274.
63. Jennewein, S., Park, H., DeJong, J. M., Long, R. M., Bollon, A. P., and Croteau, R. B. (2005) Coexpression in yeast of *Taxus* cytochrome P450 reductase with cytochrome P450 oxygenases involved in Taxol biosynthesis, *Biotechnol. Bioeng.* 89, 588-598.
64. Engels, B., Dahm, P., and Jennewein, S. (2008) Metabolic engineering of taxadiene biosynthesis in yeast as a first step towards Taxol (Paclitaxel) production, *Metab. Eng.* 10, 201-206.
65. Chang, M. C., and Keasling, J. D. (2006) Production of isoprenoid pharmaceuticals by engineered microbes, *Nat. Chem. Biol.* 2, 674-681.
66. Besumbes, O., Sauret-Gueto, S., Phillips, M. A., Imperial, S., Rodriguez-Concepcion, M., and Boronat, A. (2004) Metabolic engineering of isoprenoid biosynthesis in *Arabidopsis* for the production of taxadiene, the first committed precursor of Taxol, *Biotechnol. Bioeng.* 88, 168-175.
67. Ajikumar, P. K., Xiao, W. H., Tyo, K. E., Wang, Y., Simeon, F., Leonard, E., Mucha, O., Phon, T. H., Pfeifer, B., and Stephanopoulos, G. (2010) Isoprenoid pathway optimization for Taxol precursor overproduction in *Escherichia coli*, *Science* 330, 70-74.
68. Loncaric, C., Merriweather, E., and Walker, K. D. (2006) Profiling a Taxol pathway 10 β -acetyltransferase: Assessment of the specificity and the production of baccatin III by *in vivo* acetylation in *E. coli*, *Chem. Biol.* 13, 1-9.
69. St-Pierre, B., and De Luca, V. (2000) Evolution of acyltransferase genes: Origin and diversification of the BAHD superfamily of acyltransferases involved in secondary metabolism, *Recent Adv. Phytochem.* 34, 285-315.
70. Ma, X. Y., Koepke, J., Panjikar, S., Fritzsche, G., and Stockigt, J. (2005) Crystal structure of vinorine synthase, the first representative of the BAHD superfamily, *J. Biol. Chem.* 280, 13576-13583.

71. Ondari, M. E., and Walker, K. D. (2008) The Taxol pathway 10-*O*-acetyltransferase shows regioselective promiscuity with the oxetane hydroxyl of 4-deacetyltaxanes, *J. Am. Chem. Soc.* *130*, 17187-17194.
72. Unno, H., Ichimaida, F., Suzuki, H., Takahashi, S., Tanaka, Y., Saito, A., Nishino, T., Kusunoki, M., and Nakayama, T. (2007) Structural and mutational studies of anthocyanin malonyltransferases establish the features of BAHD enzyme catalysis, *J. Biol. Chem.* *282*, 15812-15822.

CHAPTER 2

SUBSTRATE SPECIFICITY OF A *TAXUS* N-BENZOYLTRANSFERASE

Reproduced by permission from Danielle M. Nevarez, Yemane A. Mengistu, Irosha N.

Nawarathne, and Kevin D. Walker.

“An *N*-Aroyltransferase of the BAHD Superfamily Has Broad Aroyl CoA Specificity *in Vitro* with Analogues of *N*-Dearoylpaclitaxel”. Journal of the American Chemical Society, 131, 5994-6002. Copyright 2009 American Chemical Society.

Yemane A. Mengistu synthesized the paclitaxel core substrates and standards.

Irosha N. Nawarathne synthesized the CoA substrates.

2.1. Introduction

The antineoplastic agent paclitaxel (Taxol) and docetaxel (Taxotere) (Figure 2.1) promote and stabilize microtubule assembly and, consequently, disrupt mitosis. This aberration ultimately leads to cell cycle arrest and apoptosis.¹ Application of these drugs remains prominent in the treatment of various cancer types and in the management of heart disease. The pharmaceuticals are also receiving interest in newly developed regimens against Alzheimer's disease and tuberculosis.²⁻⁵ Structure-activity relationship studies demonstrated that the various acyl group types and their distinct regiochemistry partially define the potency of the active pharmacophore that causes the drugs to bind tubulin and stabilize microtubules.⁶ Analysis of the biological activity of paclitaxel analogues derived from various combinatorial chemistry libraries has identified several lead compounds with greater efficacy than the parent drug, with regards to better water solubility, tissue-specific targeting, and enhanced blood-brain barrier permeability.⁷⁻¹³ Several components of the isoserinyl side chain are required for activity, including the 2'-hydroxyl, 2-aryl, and a 3'-*N*-arylamide.¹⁴ Presently, each derivative is principally obtained by

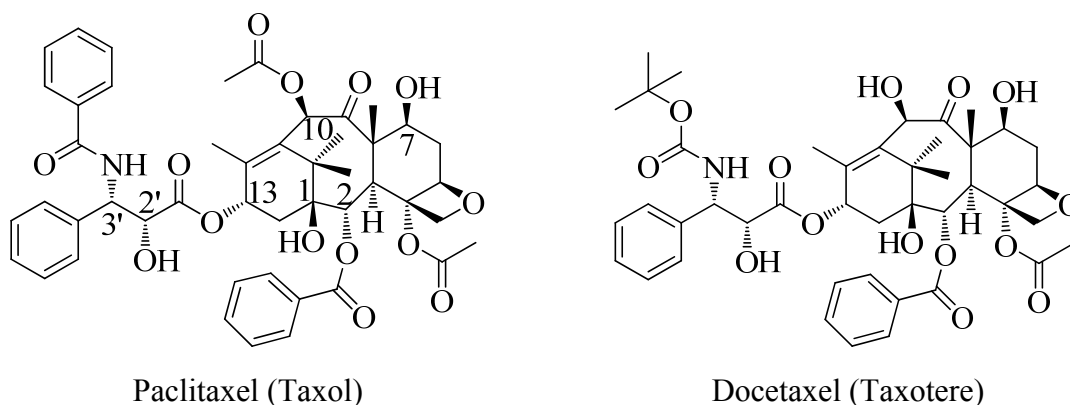


Figure 2.1 - Structures of Antineoplastic Taxanes: Paclitaxel, and Docetaxel.

semisynthetic methods that require protecting group management, which generally affects overall product yield.¹⁵ At least 10 steps are necessary to install a 3'-(4-*O*-methylbenzamide) in place of the naturally occurring 3'-benzamide in the molecule, five of which include protection/deprotection manipulation of competing reactive centers. Briefly, the semisynthesis of arylamide analogues of paclitaxel includes selective hydroxyl group protection at C7, selective acylation at the C13 hydroxyl with either a *N,O*-acetal-*N*-aroylphenylisoserine, activated as a mixed anhydride or a *N*-aroyllactam precursor of *N*-aroylphenylisoserine, and finally deprotection to construct the target product (Figure 2.2).^{9, 16}

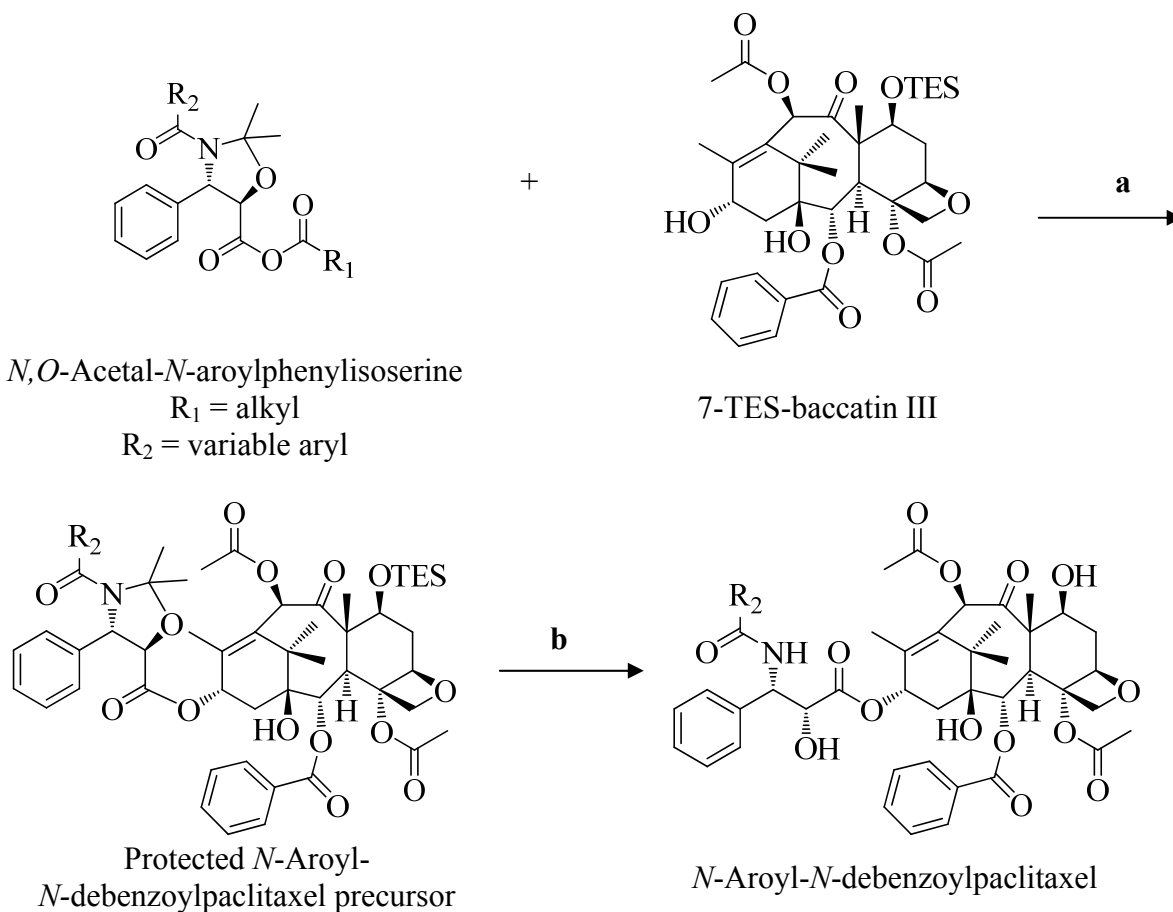


Figure 2.2 - A Route to *N*-Aroyl-*N*-debenzoylpaclitaxel Analogues.

a. Base, THF. b. Deprotection.

Conceivably, the application of biocatalytic acylation in the described semi-synthetic methods could potentially reduce the number of protection steps in the assembly of these next generation compounds. *Taxus*-derived acyltransferases belong to a superfamily of plant-derived acyltransferases designated BAHD, the acronym being derived from the abbreviations of the names (BEAT, AHCT, HCBT, and DAT) of the first four enzymes identified and characterized in this family.¹⁷⁻¹⁹ In general terms, each member of this family requires a coenzyme A-dependent acyl group donor and contains a conserved HXXXD amino acid sequence diad that is presumably involved in the transfer of various acyl groups [alkyl, aroyl, or phenylpropanoyl] to a corresponding hydroxylated and/or aminated substrate.¹⁹ Generally, the specificity of individual members of the BAHD superfamily varies from restricted to broad substrate access *in vitro* and *in vivo*.^{20, 21} The paclitaxel biosynthetic pathway in *Taxus* spp. contains five such acyltransferases that transfer alkanoyl/aroyl groups to different taxane structures. The *N*-debenzoyl-2'-deoxypaclitaxel:*N*-benzoyltransferase (designated herein as NDTBT) is unique among the pathway catalysts in terms of recognizing an amine acceptor group of the diterpene co-substrate; the other *Taxus* acyltransferases convey an alkanoyl or aroyl group to variously positioned hydroxyls. In particular, the monomeric NDTBT catalyzes the formation of a benzamide functional group from cosubstrates benzoyl CoA and *N*-debenzoyl-2'-deoxypaclitaxel (Figure 2.3).²² A previous, limited study revealed that the product derived from NDTBT in assays containing acetyl CoA and the diterpene substrate was below detection limits.²² In addition, the substrate specificity of NDTBT was recently assessed with the aim of dissecting the function of the catalyst in the biosynthesis of naturally occurring advanced taxanes found in *Taxus* spp.²³ The results from this previous work demonstrated that NDTBT was limited to

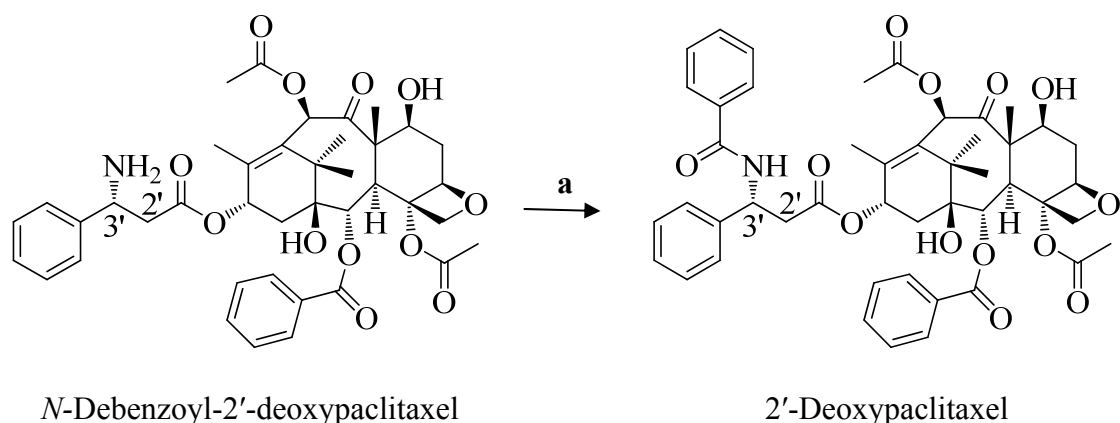


Figure 2.3 – Enzymatic Benzoylation of *N*-Debenzoyl-2'-deoxypaclitaxel.
a. NDTBT, benzoyl CoA.

benzoyl CoA as the acyl donor; whereas, tigloyl, hexanoyl, or butenoyl was not transferred to the *N*-debenzoyl taxanes as assessed by UV-HPLC monitoring of the biosynthetic products.

In this chapter, the products isolated from *in vitro* assays with mixtures of NDTBT, *N*-debenzoylpaclitaxel precursors, and acyl CoA thioesters were either analyzed by UV-HPLC in mixed substrate assays to calculate specificity constants or separated by HPLC with the effluent directed toward a tandem mass spectrometer (MS/MS) for selected molecular ion fragmentation analysis. The high sensitivity of this MS/MS method enabled us to reveal the extremely broad substrate specificity of the *N*-benzoyltransferase. Relative kinetic constants are reported for the enzyme with the various combinations of taxane and acyl CoA substrates.

2.2 Materials and Methods

2.2.1. Reagents and Solvents

N-*tert*-Butoxycarbonyl-(3*R*)- β -phenylalanine was obtained from Acros Organics (Morris Plains, NJ), docetaxel was obtained from OChem (Des Plaines, IL), coenzyme A was acquired from ARC (St. Louis, MO), and benzoyl CoA and all other reagents were obtained from Sigma-

Aldrich (St. Louis, MO) and used without further purification, unless indicated otherwise. Baccatin III was purchased from Natland (Research Triangle Park, NC). *N*-Debenzoyl-(3'*R*)-2'-deoxypaclitaxel was synthesized as described, except that the enantiomeric *N*-*tert*-butoxycarbonyl-(3*R*)- β -phenylalanine, instead of the racemate, was coupled to 7-TES-baccatin III; deprotection by described methods yielded the desired product.²⁴⁻²⁶

2.2.2. Co-substrate Synthesis

2.2.2.1. Synthesis of Coenzyme A Thioesters

The following synthesis was conducted by Irosha Nawarathne. Several aroyl CoA donors (heteroaroyls and variously substituted benzoyls) were synthesized *via* a previously described method that proceeds through a mixed ethyl carbonate anhydride.²⁷ Briefly, triethylamine (3.0 μ L, 30 μ mol) was added to a solution of the corresponding carboxylic acid (27 μ mol) in 5:2 CH₂Cl₂/THF (v/v, 1.4 mL) under N₂ gas. The mixture was stirred for 10 min at 23 °C, ethyl chloroformate (2.9 μ L, 30 μ mol) was added in one portion, and the reaction was stirred for 1 h at 23 °C. The solvents were evaporated under reduced pressure, and the residue was dissolved in 0.5 mL of *tert*-butyl alcohol. Coenzyme A as the sodium salt (23 mg, 30 μ mol dissolved in 0.5 mL of 0.4 M NaHCO₃) was added to the solution, and the mixture was stirred for 0.5 h at 23 °C, then quenched with dropwise addition of 1 M HCl, and adjusted to pH 3-5. The solvents were evaporated under vacuum, and the residue was dissolved in water (5 mL, pH 5) and loaded onto a C18 silica gel column (10% capped with TMS) that was washed with 100% MeOH (50 mL) and pre-equilibrated with distilled water (100 mL, pH 5). The sample was washed with water (100 mL, pH 5) and then eluted with 15% MeOH in water (50 mL, pH 5).

The fractions containing aroyl CoA, as determined by TLC, were combined, and the solvent was evaporated to yield product (95-99% yield at 95-99% purity, assessed by ^1H NMR). A Varian Inova-300 or a Varian UnityPlus500 instrument was used to acquire proton nuclear magnetic resonance (^1H NMR) spectra.

2.2.2.2. Synthesis of *N*-debenzoylpaclitaxel Analogues

The following synthesis was conducted by Yemane Mengistu.

2.2.2.2.1. *Synthesis of 2'-TBDMS-docetaxel.*

The following synthesis is based on a similar procedure reported previously.²⁸ In brief, to a solution of docetaxel (220 mg, 0.27 mmol) dissolved in DMF (2.4 mL) were added imidazole (92 mg, 1.32 mmol, 5 equiv) and *tert*-butyldimethylsilyl chloride (TBDMS-Cl) (204 mg, 1.32 mmol, 5 equiv). The solution was stirred at 23 °C, and then after 18 h, the mixture was diluted with ethyl acetate and extracted with water (2 × 30 mL) and brine (1 × 30 mL). The organic layer was dried (MgSO₄), concentrated *in vacuo*, and purified by silica gel column chromatography (1:2 EtOAc/hexane, v/v) to yield 2'-TBDMS-docetaxel as a white powder (246 mg, 0.267 mmol, 99% yield at 99% purity as judged by ^1H NMR). ESI-MS (positive ion mode) 944.6 $[\text{M} + \text{Na}]^+$. ^1H NMR (CDCl₃, 300 MHz) δ : 8.09 (d, 2H, *J* 7.5 Hz, *ortho*-ArH of C2 benzoyl), 7.56 (t, 1H, *J* 7.5, 7.2 Hz, *para*-ArH of C2 benzoyl), 7.46 (t, 2H, *J* 7.8, 7.2 Hz, *meta*-ArH of C2 benzoyl), 7.36 (m, 4H, ArH of C3' phenyl), 7.28 (m, 1H, ArH of C3' phenyl), 6.31 (t, 1H, *J* 8.7 Hz, H-13), 5.66 (d, 1H, *J* 7.2 Hz, H-2), 5.43 (br d, 1H, *J* 9.3 Hz, H-3'), 5.30 (br d, 1H, *J* 9.0 Hz,

NH), 5.18 (s, 1H, H-10), 4.95 (d, 1H, J) 8.1 Hz, H-5), 4.5 (d, 1H, J) 2.6 Hz, H-2'), 4.32-4.17 (m, 1H, H-7), 4.17 (dd, 2H, J) 7.2 Hz, H-20), 3.93 (d, 1H, J) 6.6 Hz, H-3), 2.61-2.58 (m, 1H, H-6), 2.53 (s, 3H, C(O)OCH₃ at C4), 2.38-2.39 (m, 3H, H-6 α , H-14), 2.02 (s, 4H, H-18, H-6 β) 1.73 (s, 3H, H-19), 1.28 (s, 9H, OC(CH₃)₃), 1.28 (s, 3H, H-17), 0.72 (s, 9H, SiC(CH₃)₃), -0.13 (s, 3H, SiCH₃), -0.34 (s, 3H, SiCH₃).

2.2.2.2.2. Synthesis of 10-Acetyl-2'-TBDMS-docetaxel.

To a solution of 2'-TBDMS-docetaxel (240 mg, 0.26 mmol) and anhydrous cerium chloride (6.3 mg, 0.1 equiv) dissolved in THF (5 mL) was added excess acetic anhydride (10 mL, dropwise). The reaction progress was checked by TLC for the formation of product. After 1 h, the reaction mixture was diluted with EtOAc (100 mL) and washed with saturated aqueous NaHCO₃ solution (3 \times 40 mL) and then brine (20 mL). The organic layer was dried (Na₂SO₄) and concentrated under reduced pressure. The residue was purified by silica gel flash column chromatography (1:1 EtOAc/Hexane, v/v), and the isolated product was concentrated *in vacuo* to give 10-acetyl-2'-TBDMS-docetaxel (231 mg, 0.24 mmol, 93% yield at 95% purity as determined by ¹H NMR). ESI-MS (positive ion mode) 986.4 [M + Na]⁺. ¹H NMR (CDCl₃, 300 MHz) δ : 8.09 (d, 2H, J) 6.9 Hz, *ortho*-ArH of C2 benzoyl), 7.56 (t, 1H, J) 7.5 Hz, *para*-ArH of C2 benzoyl), 7.45 (t, 2H, J) 7.5 Hz, *meta*-ArH of C2 benzoyl), 7.36 (m, 4H, ArH of C3' phenyl), 7.28 (m, 1H, ArH of C3' phenyl), 6.30 (s and br t, 2H, H-10, H-13), 5.66 (d, 1H, J) 7.2 Hz, H-2), 5.44 (d, 1H, J) 9.6 Hz, H-3'), 5.30 (br d, 1H, J) 9.2 Hz, NH), 4.95 (d, 1H, J) 7.8 Hz, H-5), 4.5 (d, 1H, J) 1.8 Hz, H-2'), 4.42 (dd, J) 6.6, 4.5 Hz, 1H, H-7), 4.30 (d, 1H, J) 8.4 Hz, H-20 α), 4.17 (d, 1H, J) 8.1 Hz, H-20 β), 3.81 (d, 1H, J) 7.2 Hz, H-3), 2.53 (s, 3H, C(O)OCH₃ at C-4), 2.41-

2.33 (m, 3H, H-6R, H-14), 2.20 (s, 3H, C(O)OCH₃ at C-10), 2.04 (s, 4H, H-18, H-6 β) 1.83 (s, 3H, H-19), 1.28 (s, 12H, H-16, OC(CH₃)₃), 1.13 (s, 3H, H-17), 0.724 (s, 9H, SiC(CH₃)₃), -0.14 (s, 3H, SiCH₃), -0.32 (s, 3H, SiCH₃).

2.2.2.2.3. *Synthesis of 10-Acetyldocetaxel.*

To a solution of 10-acetyl-2'-TBDMS-docetaxel (231 mg, 0.24 mmol) dissolved in THF (5 mL) at 0 °C were added pyridine (0.75 mL) and a solution of 70% HF dissolved in pyridine (0.75 mL). The reaction was stirred at 0 °C and then gradually warmed to room temperature (25 °C). The progress of the reaction was monitored by TLC, showing ~40% conversion of the starting material. Additional pyridine (0.5 mL) and HF/pyridine solution (0.5 mL) were added at 0 °C, and the mixture was warmed to 25 °C and stirred for 10 h to complete the reaction. The solution was diluted with EtOAc (100 mL), and the organic layer was washed successively with a 5% (w/v) solution of NaHCO₃ (2 \times 10 mL), a 5% (v/v) solution of HCl (2 \times 10 mL), water (10 mL), and brine (15 mL). The organic fraction was dried (MgSO₄) and concentrated under vacuum, the crude mixture was purified by silica gel column chromatography (1:1 EtOAc/hexane, v/v), and the fractions containing product were concentrated *in vacuo* to provide 10-acetyldocetaxel (193 mg, 0.22 mmol, 89% yield at 95% purity as judged by ¹H NMR). ESI-MS (positive ion mode) 872.3 [M + Na]⁺. ¹H NMR (CDCl₃, 500 MHz) δ : 8.12 (d, 2H, *J*) 7.5 Hz, *ortho*-ArH of C2 benzoyl), 7.62 (t, 1H, *J*) 7.5, 7.0 Hz, *para*-ArH of C2 benzoyl), 7.51 (t, 2H, *J*) 7.5 Hz, *meta*-ArH of C2 benzoyl), 7.40 (m, 4H, ArH of C3' phenyl), 7.33 (m, 1H, ArH of C3' phenyl), 6.31 (s, 1H, H-10), 6.25 (t, 1H, *J*) 9.0 Hz, H-13), 5.68 (d, 1H, *J*) 7.0 Hz, H-2), 5.45

(br d, 1H, J) 9.3 Hz, H-3'), 5.30 (br d, 1H, J) 9.3 Hz, NH), 4.95 (d, 1H, J) 8.0 Hz, H-5), 4.64 (d, 1H, J) 2.3 Hz, H-2'), 4.42 (dd, J) 9.0, 8 Hz, 1H, H-7), 4.30 (d, 1H, J) 8.5 Hz, H-20 α), 4.17 (d, 1H, J) 8.5 Hz, H-20 β), 3.81 (d, 1H, J) 7.5 Hz, H-3), 3.4 (br d, 1H, 2'-OH), 2.61-2.57 (m, 1H, H-6 α), 2.38 (s, 3H, C(O)OCH₃ at C-4), 2.33 (m, 3H, H-14), 2.25 (s, 3H, C(O)OCH₃ at C-10), 1.91-1.89 (m, 1H, H-6 β), 1.86 (s, 3H, H-18), 1.70 (s, 3H, H-19), 1.35 (s, 9H, OC(CH₃)₃), 1.27 (s, 3H, H-16), 1.16 (s, 3H, H-17).

2.2.2.2.4. Synthesis of *N*-Debenzoylpaclitaxel.

To a solution of 10-acetyldocetaxel (170 mg, 0.20 mmol) dissolved in acetonitrile (1 mL) was added (dropwise) 88% formic acid solution (2 mL) at 0 °C, and the reaction was slowly warmed to 25 °C. After 4 h, the reaction was judged to be ~50% complete according to TLC (90:10 chloroform/methanol, v/v, R_f = 0.3) and was quenched by partitioning between NaHCO₃ solution and chloroform. The aqueous fraction was removed, and the organic layer was extracted with 5% (w/v) NaHCO₃ solution (40 mL). The aqueous fractions were combined and back-extracted with chloroform (2 \times 25 mL). The organic fractions were combined, dried (MgSO₄), and concentrated *in vacuo*, and the resultant residue was purified by silica gel column chromatography (8% MeOH in CHCl₃) to provide *N*-debenzoylpaclitaxel (105 mg, 0.14 mmol, 70% yield) as a pale yellow solid. ESI-MS (positive ion mode) 750.2 [M + H]⁺, 768 [M + Na]⁺.

¹H NMR (CDCl₃, 300 MHz) δ : 8.07-8.04 (m, 2H, *ortho*-ArH of C2 benzoyl), 7.65 (t, 1H, J) 8.3 Hz, *para*-ArH of C2 benzoyl), 7.51 (t, 2H, J) 8.1, 6.9 Hz, *meta*-ArH of C2 benzoyl), 7.38 (m, 4H, ArH of C3' phenyl), 7.28 (m, 1H, ArH of C3' phenyl), 6.27 (s, 1H, H-10), 6.14 (t, 1H, J) 8.0

Hz, H-13), 5.63 (d, 1H, *J* 7.2 Hz, H-2), 4.93 (d, 1H, *J* 8.1 Hz, H-5), 4.42-4.34 (m, 1H, H-7), 4.32-4.27 (m, 3H, H-20 α , β and H-2'), 4.13 (d, 1H, *J* 8.7 Hz, H-3'), 3.75 (d, 1H, *J* 6.9 Hz, H-3), 2.56-2.48 (m, 1H, H-6R), 2.24 (s, 3H, C(O)OCH₃ at C10 or C4), 2.23 (s, 3H, C(O)OCH₃ at C10 or C4), 1.98-2.10 (m, 3H, H-14 and H-6 β), 1.88 (br s, 3H, H-18), 1.65 (s, 3H, H-19), 1.24 (s, 3H, H-16), 1.12 (s, 3H, H-17).

2.2.2.2.5. Synthesis of 10-Deacetyl-*N*-debenzoypaclitaxel.

A solution of docetaxel (100 mg, 0.124 mmol) in concentrated formic acid (25 mL) was stirred for 4 h at 25 °C. The mixture was concentrated, and the residual acid was removed as an azeotrope with toluene. The residue was partitioned against 5% (w/v) NaHCO₃ solution and ethyl acetate. The aqueous fraction was removed, and the organic layer was again extracted with 5% (w/v) NaHCO₃ solution (40 mL). The aqueous fractions were combined and back extracted with ethyl acetate (3 \times 25 mL). The organic layer was dried (MgSO₄) and concentrated under vacuum. The resulting crude product was purified by silica gel column chromatography (95:5 EtOAc/MeOH, v/v) to obtain 10-deacetyl-*N*-debenzoypaclitaxel as a white powder (54 mg, 0.075 mmol, 60% yield). ESI-MS (positive ion mode) 708.2 [M + H]⁺. ¹H NMR (CDCl₃, 300 MHz) δ : 8.06 (d, 2H, *J* 7.8 Hz, *ortho*-ArH of C2 benzoyl), 7.62 (t, 1H, *J* 7.5, 7.2 Hz, *para*-ArH of C2 benzoyl), 7.51 (t, 2H, *J* 7.5 Hz, *meta*-ArH of C2 benzoyl), 7.39 (m, 4H, ArH of C3' phenyl), 7.30 (m, 1H, ArH of C3' phenyl), 6.13 (t, 1H, *J* 9.0 Hz, 13-H), 5.64 (d, 1H, *J* 7.2 Hz, H-2), 5.20 (s, 1H, H-10), 4.93 (d, 1H, *J* 7.8 Hz, H-5), 4.35-4.28 (m, 3H, H-2', H-3', H-20 α), 4.26 (m, 1H, H-7), 4.15 (d, 1H, *J* 8.4 Hz, H-20 β), 3.88 (d, 1H, *J* 7.2 Hz, H-3), 2.62-2.52 (m,

1H, H-6R), 2.25 (s, 3H, C(O)OCH₃ at C-4), 2.07-2.02 (m, 1H, 2H, H-14), 1.90 (s, 3H, H-18), 1.82 (m, 1H, H-6β), 1.75 (s, 3H, H-19), 1.21 (s, 3H, H-16), 1.11 (s, 3H, H-17).

2.2.3. Genetic Manipulations

2.2.3.1. Storage of *E. coli* Strains and Plasmids

The *ndtbt* cDNA (accession AF466397) in pSBET vector was given by Washington State Research Foundation (Pullman, WA). This was originally transformed into JM109 *E. coli* cells and DH5α cells for long-term storage. Glycerol samples were prepared by adding 0.75 mL of an overnight culture to a sterile vial containing 0.25 mL of 80% (v/v) glycerol. The solution was mixed, flash frozen in liquid N₂, and then stored at -78 °C.

2.2.3.2. Small-scale Purification of Plasmid DNA

Overnight 5 mL cultures were used as the start culture for the QIAprep Spin Kit (Qiagen, Valencia, CA). Instead of their Elution Buffer (EB), 30-40 μL of deionized water at pH 8.0 was used to elute plasmid from the column.

2.2.3.3. Customized Primers

Primers were created to amplify *ndtbt* with the addition of restriction enzyme cut-sites flanking the gene for subcloning into other expression vectors. Other primers were made for incorporating mutations and a sequencing set was necessary for DNA sequencing. Custom primers (Table 2.1) were ordered from MSU's Macromolecular Structure, Sequencing and Synthesis Facility (MSSSF) using the Applied Biosystems 3948 DNA Synthesis and Purification System.

Table 2.1 Custom Primer Sequences

Name	KDW	5' → 3' Sequence	Apply
F10-1	77	ATGGAGAAGGCAGGCTCAAC	Seq
F10-2	78	TTGGCATCCATTGGACACTGC	Seq
F10-3	79	TGGATAGCACGGACAAAGGC	Seq
F10-4	80	CTTTTCTATACCTACTACCTGCC	Seq
R10-A	81	CAACACCTTGGAGAGAGCC	Seq
R10-B	82	AGATGTAGAGGGTCTTCAGG	Seq
R10-C	83	GGGTTTGTAACCTACCCTTGACC	Seq
R10-D	84	TCACACTTTACTTACATATTTCTCTATC	Seq
NdeIKOFor	121	GCCATTGGTACTGCATACGCAATGGATAATGTC	Mut
NdeIKORev	122	GGACATTATCCATTGCGTATGCAGTACCAATGG	Mut
T7 promoter	155	TAATACGACTCACTATAGGG	Sub/Seq
T7 terminator	156	GCTAGTTATTGCTCAGCGG	Sub/Seq
Sub – subcloning; Seq – sequencing; Mut – mutations			

2.2.3.4. Polymerase Chain Reaction Protocol

A general subcloning procedure was conducted as follows: in a 50-μL reaction were added 10X buffer (5 μL), 10 mM dNTP mixture (1 μL), forward primer (20 pmol/μL, 1 μL), reverse primer (20 pmol/μL, 1 μL), 100 ng DNA/plasmid, Turbo *Pfu* DNA polymerase (1 μL), and ddH₂O to bring the volume to 50 μL. A PTC-100 Programmable Thermal Controller (MJ Research, Inc.) was used with this program: dwell at 94 °C for 2 min, and then cycle at 94 °C for 45 s, between 48-54 °C (exact temperature determined empirically) for 30 s, 72 °C for 1 min/kb of template sequence, cycled 25-35 times (determined empirically), with an extension temperature of 72 °C for 5 min and a final 4 °C hold.

To facilitate subcloning a site-specific mutagenesis protocol was used to remove an internal *NdeI* restriction site with the following oligonucleotide sets:

pair 1: T7 promoter primer (5'-TAATACGACTCACTATAGGG-3')

NdeIKORev primer (5'-GACATTATCCATTGCGTATGCAGTACCAATGG-3')

pair 2: NdeIKOFor primer (5'-GCCATTGGTACTGCATACGCAATGGATAATGTC-3')

T7 terminator primer (5'-GCTAGTTATTGCTCAGCGG-3')

The nucleotide mutation is bold text and underlined.

2.2.3.5. Agarose Gel Electrophoresis and Isolation, Purification, and Quantification of DNA

Agarose gels are comprised of 1% Ultra Pure Agarose (w/v) (Sigma, St. Louis, MO) in TAE buffer (40 mM Tris base, 40 mM glacial acetic acid, 1 mM EDTA, pH 8.3). Ethidium bromide (0.5 $\mu\text{g/mL}$) was added to the agarose to allow visualization of DNA fragments under a UV lamp. Agarose gels were run in the TAE buffer at 89-109 volts, depending on gel size. The size of the DNA fragments was determined by comparison to a 1-kb DNA Ladder (New England Biolabs, Ipswich, MA). The DNA band of interest was excised from the gel using a razor while visualizing by UV light. DNA was isolated from the agarose by using the QIAquick Gel Extraction Kit (Qiagen, Valencia, CA). 30-40 μL of deionized water at pH 8.0 was used to elute a plasmid from the column. The purity and concentration of DNA was calculated from taking the spectrophotometer measurement at 260 nm and 280 nm.

2.2.3.6. Subcloning Procedures

2.2.3.6.1. *Restriction Enzyme Digestions of DNA.*

The derived blunt-end cDNA amplicons of *ndtbt* and empty pET28a (Novagen) were digested with *NdeI* and *BamHI* (New England Biolabs, Ipswich, MA). Usually about 1 μg of DNA/plasmid was incubated for 1 h at 37 °C with 2-5 units of each restriction enzyme with appropriate buffer. Digestions were cleaned by separation and size detection on agarose gel before excising band from gel for purification.

2.2.3.6.2. Ligation of DNA.

Molar ratios of insert to vector were typically maintained at 3 to 1 for DNA ligations with sticky over-hanging ends. Most reactions contained 3 µg of DNA along with 5X T4 ligation buffer (2 µL) and T4 DNA ligase (1 µL) (New England Biolabs, Ipswich, MA) in a total volume of 20 µL. The reaction was incubated at 16 °C for 10 h and then used to transform competent *E. coli* cells.

2.2.3.6.3. Preparation of Competent *E. coli* Cells.

Competent cells were prepared according to a modified procedure reported by Sambrook *et al.*²⁹ Luria-Bertani (LB) medium (5 mL) containing antibiotics, when appropriate, was inoculated with a single colony from an LB plate containing the appropriate antibiotics. The culture was grown at 37 °C with shaking at 250 rpm for 10-12 h. An aliquot (1 mL) from the culture (5 mL) was used to inoculate LB (100 mL) containing the appropriate antibiotics. The culture was grown at 37 °C with shaking at 250 rpm until the cells reached OD₆₀₀ between 0.4 and 0.6. The culture was transferred to a centrifuge bottle that had been sterilized with a 25% (v/v) bleach solution and rinsed four times with sterile, deionized water. The cells were harvested by centrifugation (4000g, 5 min, 4 °C) and the culture medium was decanted. All subsequent manipulations were carried out on ice. The harvested cells were resuspended in ice-cold 0.9% NaCl (100 mL), and the cells were collected by centrifugation (4000g, 5 min, 4 °C). The 0.9% NaCl solution was decanted, the cells were resuspended in ice-cold 100 mM CaCl₂ (50 mL) and stored on ice for 30 min. After centrifugation (4000g, 5 min, 4 °C), the cells were resuspended in 4 mL of ice-cold 100 mM CaCl₂ containing 15% glycerol (v/v). Aliquots (100 µL) of competent

cells were added to 500 μ L microfuge tubes, immediately frozen in liquid nitrogen, and stored at -78 °C.

2.2.3.6.4. *Transformation of Competent E. coli Cells.*

Frozen competent cells were thawed on ice for 5 min before transformation. A small aliquot (1 to 10 μ L) of plasmid DNA or a ligation reaction was added to the thawed competent cells (0.1 mL). The solution was gently mixed by tapping and stored on ice for 30 min. The cells were then heat-shocked at 42 °C for 30 seconds and returned to ice briefly (1 min). LB (0.5 mL, no antibiotics) was added to the cells, and the sample was incubated at 37 °C (with agitation) for 1 h. If the transformation was plated onto LB plates, 0.1 mL of the culture was spread onto plates containing the appropriate antibiotics. An aliquot of competent cells with no DNA added was also carried through the transformation protocol as a control. These cells were used to check the viability of the competent cells and to verify the absence of growth on selective medium.

2.2.3.6.5. *Verifying cDNA Insertion*

Transformation colonies were individually selected and transferred to a new agar plate with appropriate antibiotics. Some cells were resuspended in water (20 μ L), boiled for 5 min, and centrifuged at 16 000g for 1 min to clear cell debris. 5 μ L of colony sample was added to ddH₂O (13.6 μ L), 10X *Taq* buffer (2.5 μ L), 50 mM MgCl₂ (0.75 μ L), 10 mM dNTP mixture (1 μ L), T7 promoter primer (1 μ L), T7 terminator primer (1 μ L), and *Taq* DNA polymerase (0.2 μ L) (Invitrogen) for (see 2.2.3.4.). Samples were loaded onto an agarose gel and viewed by UV for a positive amplicon size ~1.3 kb. Plasmid from positive colonies was collected as previously described (see 2.2.3.2.). Sequencing was completed by MSU's Research Technology Support

Facility using ABI PRISM® 3730 Genetic Analyzer. Primers are listed on Table 2.3 for forward and reverse sequencing and analysis was conducted by aligning sequences with known DNA sequence (accession AF466397).

2.2.4. Expression and Purification of *NDTBT*

2.2.4.1. Culture Medium and Solutions

All solutions were prepared in deionized water. LB medium contained Bacto tryptone (10 g), Bacto yeast extracts (5 g), and NaCl (10 g) or 25 g of LB Miller mixture per 1 L was autoclaved. Solid medium was prepared by addition of 1.5% (w/v) Bacto agar to the LB medium before autoclaving and cooled before appropriate antibiotics were added.

Antibiotics were added where appropriate to the following final concentrations unless noted otherwise: ampicillin, 50 µg/mL; kanamycin, 50 µg/mL; and chloramphenicol 34 µg/mL. Stock solutions of antibiotics were prepared in water with the exceptions of chloramphenicol, which was prepared in 100% aqueous ethanol. Antibiotics and isopropyl β-D-thioglucopyranoside (IPTG) were sterilized through 0.22-µm membrane filters.

2.2.4.2. Heterologous Expression of *ndtbt*, Protein Isolation, and Purification

2.2.4.2.1. *Expresson of ndtbt cDNA.*

Recombinant *ndtbt* was expressed in the described bacterial expression system and harvested according to a previously reported protocol, with slight modifications.²⁹ Cultures were grown overnight at 37 °C in 5 mL of LB medium supplemented with 50 µg/mL kanamycin and 35 µg/mL chloramphenicol. Bacteria transformed with empty vector were processed analogously. The 5-mL inoculum was added and grown at 37 °C to OD₆₀₀ = 0.5-0.7 in 1 L of

LB medium supplemented with the appropriate antibiotics, and then gene expression was induced with 100 μ M IPTG, and the culture was incubated at 20 °C. After 18 h, the cells were harvested by centrifugation at 2000g for 20 min at 4 °C, the supernatant was discarded, and the pellet transferred to a pre-weighed 50-mL Corning Tube for storage at -20 °C.

2.2.4.2.2. *Protein Harvest*

The pellet was resuspended in lysis buffer (50 mM sodium phosphate, 300 mM sodium chloride, and 10 mM imidazole, pH 8.0 at 3 mL/g cells) at 4 °C. The cells were lysed at 4 °C by sonication (6 \times 20 s bursts at 60% power at 1 min intervals) with a Misonix XL-2020 sonicator (Misonix Inc., Farmingdale, NY), and the cell-lysate was clarified by ultracentrifugation at 46 000g for 1 h at 4 °C.

2.2.4.2.3. *Determination of Protein Concentration*

Protein concentrations were assessed by the Bradford method (Coomassie (Bradford) Protein Assay Kit (Pierce, Rockford, IL)) and compared against a series of bovine serum albumin protein standards of varying concentrations.

2.2.4.2.4. *Protein SDS-PAGE Analysis*

SDS-PAGE (sodium dodecyl sulfate polyacrylamide gel electrophoresis) analysis followed the standard Laemmli protocol. Preparation of a 12% separating gel started from mixing 4 mL of 30% (w/v) aqueous acrylamide stock solution containing *N,N'*-methylene-bisacrylamide (0.8% (w/v)), 1.5 M Tris-HCl (pH 8.8) (2.5 mL), 3.4 mL of distilled de-ionized water, 20% (w/v) aqueous SDS solution (50 μ L), 10% (w/v) aqueous ammonium persulfate

solution (50 μ L), and *N,N,N,N*-tetramethylethylenediamine (TEMED) (5 μ L). The solution was mixed thoroughly and poured into a 0.75 mm-width gel cassette to about 1.5 cm below the top of the gel cassette. *t*-Amyl alcohol was overlaid on top of the solution and the gel was allowed to polymerize for 1 h at room temperature (25 °C). The stacking gel was prepared by mixing 0.67 mL 30% acrylamide stock solution containing *N,N*-methylene-bisacrylamide (0.8% (w/v)), 1.25 mL of 0.5 M Tris-HCl (pH 6.8), and 3.075 mL of distilled de-ionized water, 50 μ L of 20% (w/v) aqueous SDS solution, 25 μ L of 10% (w/v) aqueous ammonium persulfate solution, and 5 μ L of *N,N,N',N'*-tetramethylethylenediamine (TEMED). *t*-Amyl alcohol was removed from the top of the gel cassette, which was subsequently rinsed with water and wiped dry. After insertion of the comb, the gel cassette was filled with stacking gel solution, and was allowed to polymerize for 1 h at 25 °C.

The comb was removed and the gel cassette was installed into the electrophoresis apparatus PROTEAN (Bio-Rad, Hercules, CA). The apparatus was then filled with buffer containing 192 mM glycine, 25 mM Tris-base, and 0.1% SDS (w/v). Each protein sample (10 μ L) was diluted with 5X Laemmli sample buffer consisting of 62.5 mM Tris-HCl, 10% glycerol, 4% SDS, 5% β -mercaptoethanol, and 0.002% bromophenol blue; then heated at 100 °C for 5 min and centrifuged. Samples and 8 μ L of protein ladder marker (ProSieve) were loaded into the sample wells and were run at 180 volts for 1.5 hours.

The gel was removed from the cassette and submerged in 45% (v/v) methanol, 10% (v/v) glacial acetic acid in water for 3 min. Then protein gel was transferred into staining solution containing 0.1% (w/v) Coomassie Brilliant Blue R, 45% (v/v) methanol, and 10% (v/v) glacial acetic acid in water for 1 h. Destaining was carried out in a solution containing 45% (v/v) methanol, 10% (v/v) glacial acetic acid in water for 30-60 min. The recombinant protein

migrated to an R_f consistent with the calculated molecular weight of NDTBT (~49 kDa) on SDS-PAGE. For long-term storage, SDS-PAGE gels were dried following Promega's Gel Drying Kit (Madison, WI).

KODAK 1D Image Analysis Software (Version 3.6.3) was used to integrate the relative intensity of the enzyme band against BSA standards ranging from 2 to 10 mg/mL, and overexpression was verified by immunoblot analysis. By comparison, NDTBT was not detectable in soluble extracts isolated from bacteria transformed with empty vector.

The protein was recognized in a Western blot analysis according to a method based on the 1-Step TMB-Blotting Kit (Pierce, Rockford, IL) with the following antibodies: Monoclonal Anti-polyHistidine and Anti-Mouse IgG Peroxidase Conjugate (Sigma, St. Louis, MO).

2.2.4.2.5. Protein Purification

The supernatant of the lysed bacterial cells was incubated with 1 mL of HIS-Select Nickel Affinity Gel (Sigma, St. Louis, MO) per 8 g of wet pellet in batch mode at 4 °C. After 2 h, the mixture was poured into an Econo column (BioRad, 20 cm × 2.5 cm), the lysis buffer was drained. The resin was washed with five column volumes of wash buffer (50 mM sodium phosphate and 300 mM sodium chloride, pH 8.0) containing 20 mM imidazole, and the bound protein was eluted with one column volume of wash buffer containing 250 mM imidazole. The imidazole was removed from the eluent by consecutive concentration by centrifugation (30 000 MWCO, YM30 membrane, Millipore, Billerica, MA) and dilution in assay buffer (50 mM sodium phosphate, 5% glycerol, pH 8.0) until the imidazole was 1.5 μM. After the concentration and purity of the NDTBT were determined, aliquots containing NDTBT at 2-10 mg/mL were flash frozen in liquid nitrogen, and stored at -78 °C.

2.2.5. Enzymatic Assays and Analysis

2.2.5.1. Crude Lysate Activity Assay

To verify functional expression of the NDTBT, total protein (5 mg) from the clarified lysate was withdrawn from the supernatant of lysed bacteria that expressed *ndtbt* and from the supernatant of similarly processed cells that were transformed with empty vector. Each soluble enzyme fraction (1 mL) was separately assayed with benzoyl CoA and *N*-debenzoyl-2'-deoxypaclitaxel (each at 1 mM) at 31 °C. After 2 h, the assays were quenched with 0.1 N HCl until pH 4-5 to partition the amine substrate to the aqueous fraction.

The assays were then separately extracted with ethyl acetate (2 × 1 mL), the respective organic fractions were combined, the solvent was evaporated, and the residue was redissolved in 50 µL of acetonitrile. A 25-µL aliquot was loaded onto a reversed-phase column (Allsphere ODS-25 µm, 250 mm × 4.6 mm, Alltech, Mentor, OH) and eluted isocratically with 50:50 (v/v) solvent A/solvent B [97.99% H₂O with 2% CH₃CN and 0.01% H₃PO₄ (v/v); 99.99% CH₃CN with 0.01% H₃PO₄ (v/v); flow rate of 1 mL/min; *A*₂₂₈ monitoring of the effluent for 20 min] on an Agilent 1100 HPLC system (Agilent Technologies, Wilmington, DE) connected to a UV detector. UV-absorbance profiles of the biosynthetic product isolated from the assay containing crude enzyme extract of *ndtbt*-expressing cells were compared to absorbance profiles of the products identically isolated from control assays containing extracts of cells transformed with empty vector.

Products eluting from the HPLC column corresponding to a *de novo* UV-absorbance peak were collected and further analyzed by direct injection-electrospray ionization mass spectrometry, in positive ion mode. A Q-ToF Ultima Global electrospray ionization tandem mass

spectrometer (ESI-MS/MS, Waters, Milford, MA) with a Waters CapLC capillary HPLC was used for mass spectral analysis. The isolated product had a molecular weight and ionization pattern that were identical to those of authentic 2'-deoxypaclitaxel when analyzed by similar methods.

2.2.5.2. Kinetic Evaluation of NDTBT with *N*-Debenzoyl-(3'*R*)-2'-deoxypaclitaxel

To establish linearity with respect to time and enzyme concentration, varying amounts of NDTBT were incubated with benzoyl CoA (the natural acyl group donor, at 50 μ M), and *N*-debenzoyl-(3'*R*)-2'-deoxypaclitaxel was maintained at saturation (1 mM) in 2 mL of assay buffer. Aliquots (200 μ L) from each assay were collected, quenched with 0.1 M HCl at 30 min intervals over 2.5 h, and extracted with ethyl acetate. The organic solvent was removed, and the products in the resultant residue were dissolved in 50 μ L of acetonitrile and were analyzed by UV-HPLC with A_{228} monitoring of the effluent, as before. The peak area corresponding to the biosynthetic 2'-deoxypaclitaxel was converted to concentration by comparison to the peak area obtained with authentic 2'-deoxypaclitaxel (0 to 30 μ M at 5 μ M intervals). Kinetic parameters were determined under steady state parameters using 0.5 mg/mL of protein and a 20-min incubation time. The concentration of benzoyl CoA was independently varied (0-1000 μ M) in separate assays while *N*-debenzoyl-(3'*R*)-2'-deoxypaclitaxel was maintained at apparent saturation (1 mM). The initial velocity (v_0) was plotted against substrate concentration for each data set, and the equation of the best-fit line ($R^2 = 0.96$) was determined (Microsoft Excel 2003, Microsoft Corporation, Redmond, WA) to calculate the V_{\max} and K_M parameters (see Appendix A).

2.2.5.3. Kinetic Evaluation of NDTBT with Competing CoA Substrates

The general NDTBT assay to identify productive aroyl CoA substrates contained purified enzyme (~100 µg) in 500 µL of assay buffer, *N*-debenzoyl-2'-deoxypaclitaxel, and an aroyl CoA, each at 500 µM. The reaction was incubated for 3 h at 31 °C, quenched by the addition of 0.1 M HCl, and extracted with ethyl acetate (1 × 2 mL). The solvent was evaporated *in vacuo*, and the remaining residue was dissolved in 50 µL of acetonitrile and analyzed by HPLC, as described above. UV-Absorbance profiles of isolated crude product derived from these assays were compared to absorbance profiles of a sample identically isolated from control assays, in which one cosubstrate and/or enzyme was omitted. Eluent from the HPLC column that correlated with a *de novo* UV-absorbance peak was further analyzed by ESI-MS (positive ion mode) to confirm product identity.

After productive CoA thioester substrates were identified, the procedure to calculate the relative kinetic constants of NDTBT for multiple competing CoA substrates was adapted from a method used to study the kinetics of a *Taxus* acyltransferase with multiple substrates. This relative kinetics evaluation method was advantageous toward conserving the dearth of semisynthetically derived *N*-debenzoyl-2'-deoxypaclitaxel and acyl CoA cosubstrates by reducing the number of replicate assays needed to construct plots to evaluate the kinetics of the transferase with each acyl CoA substrate. The substrate specificity of NDTBT for the productive acyl CoA thioesters, identified above, was assessed by incubating each CoA thioester (500 µM) separately with 100 µM benzoyl CoA, 100 µg of NDTBT enzyme, and 500 µM *N*-debenzoylpaclitaxel, in a 200 µL assay.

After 20 min, the samples were acidified, and the biosynthetic products were isolated by extraction with ethyl acetate as described previously. The products were loaded onto the

reversed-phase HPLC column and eluted by a gradient of solvent A/solvent B [99.99% H₂O with 0.1% TFA (v/v); 99.99% CH₃CN with 0.1% TFA (v/v); gradient: 0-5 min at 80% (A), 5-11 min at 80-50% (A), 11-21 min at 50-20% (A), 21-23 min at 20-0% (A), 23-25 min at 0% (A), 25-33 min at 0-80% (A)] at a flow rate of 1.5 mL/min and A_{228} monitoring of the effluent.

The following calculations were used to correct the variance in the molar absorptivity of the different aromatic chromophores of the various biosynthetically *N*-aroylated products. The area under the absorbance peak corresponding to 2 nmol of each aroyl free acid (A_{acid}) was independently calculated. The A_{acid} values were each added to the peak area for the absorbance of the substrate *N*-debenzoyl-2'-deoxypaclitaxel (A_{taxane}) monitored at the same wavelength and concentration as the free acids to approximate the total absorbance peak area ($A_{\text{total}} = A_{\text{acid}} + A_{\text{taxane}}$). The quotient derived by dividing A_{total} for the benzoic acid/taxane pair by A_{total} for each free acid/taxane pair was used to calculate the relative molar absorptivity. This ratio was multiplied by the area under the UV absorbance (A_{228}) peak for each biosynthetic *N*-aroyl product, eluting from the HPLC; this normalized peak area was directly compared to the absorbance peak corresponding to the 2'-deoxypaclitaxel (made biosynthetically in the same mixed-substrate assay). The acquired absorbance ratios were each multiplied by the specificity constant ($V_{\text{max}}/K_{\text{M}}$) of NDTBT calculated for benzoyl CoA and *N*-debenzoyl-2'-deoxypaclitaxel as substrates, and the resultant values are reported as specificity constants relative to that of NDTBT for each surrogate acyl CoA substrate.

2.2.5.4. Relative Velocities of NDTBT with *N*-Debenzoylpaclitaxel Analogues

In general, the conversion rate of each *N*-debenzoyl isoserinoyl taxane substrate to its *N*-benzoyl isoserine derivative by NDTBT catalysis was estimated to be 10-20-fold less compared to the conversion rate for the *N*-debenzoyl-2'-*deoxy*paclitaxel substrate. Therefore, to optimize the amount of biosynthetic product for detection by LC-ESI/MS/MS analysis, *N*-debenzoylpaclitaxel or 10-deacetyl-*N*-debenzoylpaclitaxel (derived from docetaxel) and several different acyl CoA thioesters, all substrates at apparent saturation (1 mM), were incubated for 2 h with NDTBT (100 μ g in 200 μ L of assay buffer, as described previously) to calculate the relative velocity (v_{rel}) of each set of diterpene and acyl CoA substrate. The isoserinoyl taxanes and CoA thioester substrates at 1 mM were judged to be at steady state (<10% conversion of substrate) at the termination of the reactions.

Each assay was extracted with ethyl acetate (2×1 mL), the solvent was removed *in vacuo*, the remaining residue was dissolved in 50 μ L of acetonitrile, and a 20- μ L aliquot of the sample was analyzed by LC-ESI tandem mass spectrometry. The abundance of the selected molecular ion (MH^+), derived in the first-stage MS, of the authentic standard was linearly proportional to a concentration below 25 μ M, and the ion abundance profiles in the MS/MS spectra of authentic compounds were comparable to those observed for each biosynthetic product that was structurally similar (see Appendix B). Based on these correlations, the relative amounts of *N*-aroylated biosynthetic product (paclitaxel, its *N*-acyl-, or 10-deacetyl-*N*-acyl derivatives) made by the NDTBT was assessed by comparing the area under the corresponding ion abundance peak for each of the selected molecular ions (MH^+).

2.3. Results

2.3.1. Expression and Activity of *NDTBT*

To obtain a sufficient quantity of functional catalyst needed for this investigation, where several activity screens and kinetic assays were conducted, methods used previously to express *ndtbt* in bacteria were modified to scale up the production of enzyme.²² Briefly, the *ndtbt* cDNA was subcloned into expression vector pET28a to incorporate an N-terminal His₆-tag epitope for immunoblot analysis and purification by nickel-affinity resin chromatography. To optimize the enzyme expression level, the resulting plasmid was transferred into *E. coli* BL21-CodonPlus (DE3)-RIPL cells. These cells were used to express tRNA adapter molecules (rare in wild-type *E. coli*) that recognize codons present in the recombinant *ndtbt* cDNA derived from *Taxus* plants. The NDTBT-His₆ fusion (1 mg) was used at 70% purity.

The function of the benzoyltransferase was assessed similarly to a previously described method.²² To produce sufficient *de novo* biosynthetic product for characterization, larger amounts of NDTBT (0.5 mg/mL) were used in 200 μ L assays in the present investigation compared to the 0.5 μ g/mL used in a previous study.²² The co-substrate concentrations of the donor and acceptor substrates (0.40 and 0.42 mM, respectively) were approximately 2.5 times their reported K_M values.²² After reacting under these conditions, the biosynthetic product was isolated as described previously and was characterized by ¹H NMR and direct injection LC-ESI/MS to confirm its identity as 2'-deoxypaclitaxel, thus verifying that the isolated enzyme was functional.²²

2.3.2. Kinetic Evaluation with Competing CoA Substrates

N-Debenzoyl-2'-deoxypaclitaxel at 1 mM and the benzoyltransferase were assayed separately with different aroyl CoA substrates that were synthesized by a previously described process, which involved coupling a mixed anhydride carboxylic acid with coenzyme A under mildly basic aqueous conditions.²⁷ Acidifying the aqueous assay solutions to pH 4, to terminate the assays prior to extraction of the assay buffer with organic solvent, ensured that the amine substrate persisted as the ammonium ion and thus partitioned to the water fraction, while the *N*-aroylated products partitioned to the organic phase. The extracted products were further authenticated as *N*-acyl analogues by mass spectrometry. Analogous assays conducted with enzyme isolated from *E. coli* harboring the empty vector did not show a detectable product.

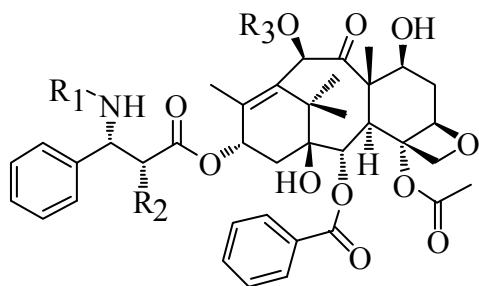
All of the aroyl CoA thioesters examined, except for 2-methylbenzoyl CoA, in this study were productive with NDTBT and *N*-debenzoyl-2'-deoxypaclitaxel. The specificity constant (V_{\max}/K_M) of NDTBT for each aroyl CoA was estimated from the amount of *N*-aroylated taxane made from the corresponding thioester in a competitive substrate reaction under typical assay conditions. The resulting product mixture was analyzed by reversed phase HPLC with UV monitoring (A_{228}) of the effluent. To assess the relative molar absorptivity for quantifying each biosynthetic *N*-aroyl product would require the synthesis of several different *N*-aroylated authentic standards *via* the *N*-debenzoyl substrate. This route would quickly exhaust our supply of this costly diterpene substrate. Therefore, instead of using a linear regression correlation of concentration and absorbance to quantify the biosynthetic products in the competitive assays, the absorbance (A_{228}) of each *N*-acyl-*N*-debenzoyl-2'-deoxypaclitaxel derivative was approximated by first individually determining the A_{228} of each free acid corresponding to the *N*-acyl group of

a biosynthetic product. This absorbance value was then added to that of the *N*-debenzoyl-2'-deoxypaclitaxel substrate at the same concentration and wavelength used with the free acids to calculate the molar absorptivity. From these values, the relative specificity constants (Table 2.2) were calculated based on that of NDTBT for benzoyl coenzyme A (V_{\max}/K_M) $1.6 \text{ nmol} \cdot \text{min}^{-1} \cdot \text{mM}^{-1}$ (Entry 1A); the catalytic efficiency for 4-methylbenzoyl CoA ($1.7 \text{ nmol} \cdot \text{min}^{-1} \cdot \text{mM}^{-1}$, Entry 4A) was nearly equal to that of the natural substrate. The efficiencies of NDTBT for the other coenzyme A thioesters of substituted-aroyls or heterole carbonyls ranged from 0.15 to $1.1 \text{ nmol} \cdot \text{min}^{-1} \cdot \text{mM}^{-1}$. The *para*-substituted aroyls displayed the highest efficiency compared to their *meta*- and/or *ortho*-regioisomers (Table 2.2).

2.3.3. Relative Velocities of NDTBT with Taxanes

In a previous survey, cytochrome P450 hydroxylase activity in microsome preparations derived from *Taxus* cell cultures was found to hydroxylate at C2' of *N*-debenzoyl-2'-deoxypaclitaxel to produce *N*-debenzoylpaclitaxel.³⁰ These data suggested that *N*-benzoylation occurs as the last step in the paclitaxel biosynthetic pathway and hinted that the benzoyltransferase could transfer an acyl group to the substrate amino group located vicinal to a hydroxyl group (Figure 2.4). In contrast, a nontaxane acyltransferase, anthranilate *N*-benzoyltransferase, has narrow substrate specificity for the amine acceptor substrate; intriguingly, 3- or 4-hydroxyanthranilate substrates were not productive substrates of the anthranilate benzoyltransferase.³¹ These results prompted us to examine the effect of the hydroxyl group vicinal to the amine acceptor group of isoserinoyl taxanes on NDTBT catalysis

Table 2.2 – Relative Kinetics of NDTBT with Aroyl CoA Thioesters and *N*-Debenzoylpaclitaxel Analogues



A. *N*-Debenzoyl-2'-deoxypaclitaxel

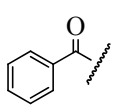
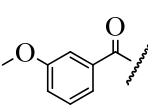
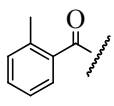
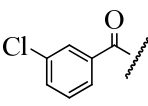
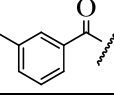
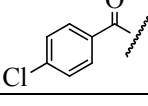
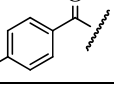
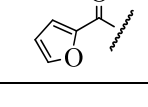
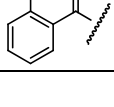
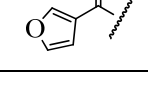
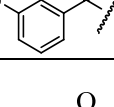
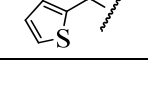
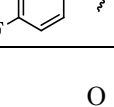
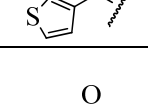
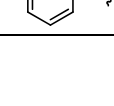
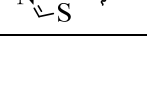
$R_1=H$, $R_2=H$, $R_3=Acetyl$

B. *N*-Debenzoylpaclitaxel

$R_1=H$, $R_2=OH$, $R_3=Acetyl$

C. 10-*O*-Deacetyl-*N*-debenzoylpaclitaxel

$R_1=H$, $R_2=OH$, $R_3=H$

R_1 (from CoA)		A (V_{max}/K_M)	B v_{rel}	C v_{rel}	R_1 (from CoA)		A (V_{max}/K_M)	B v_{rel}	C v_{rel}
	1	1.6 (nmol/min/mM)	100%	100%		9	0.38	85%	11%
	2	Not Detectable (ND)	ND	3%		10	0.37	<1%	8%
	3	0.27	27%	33%		11	1.1	<1%	40%
	4	1.7	33%	ND		12	0.31	200%	36%
	5	0.85	8%	38%		13	0.15	19%	43%
	6	0.34	11%	19%		14	0.39	19%	5%
	7	0.97	11%	68%		15	0.37	22%	3%
	8	0.15	9%	17%		16	0.16	22%	29%

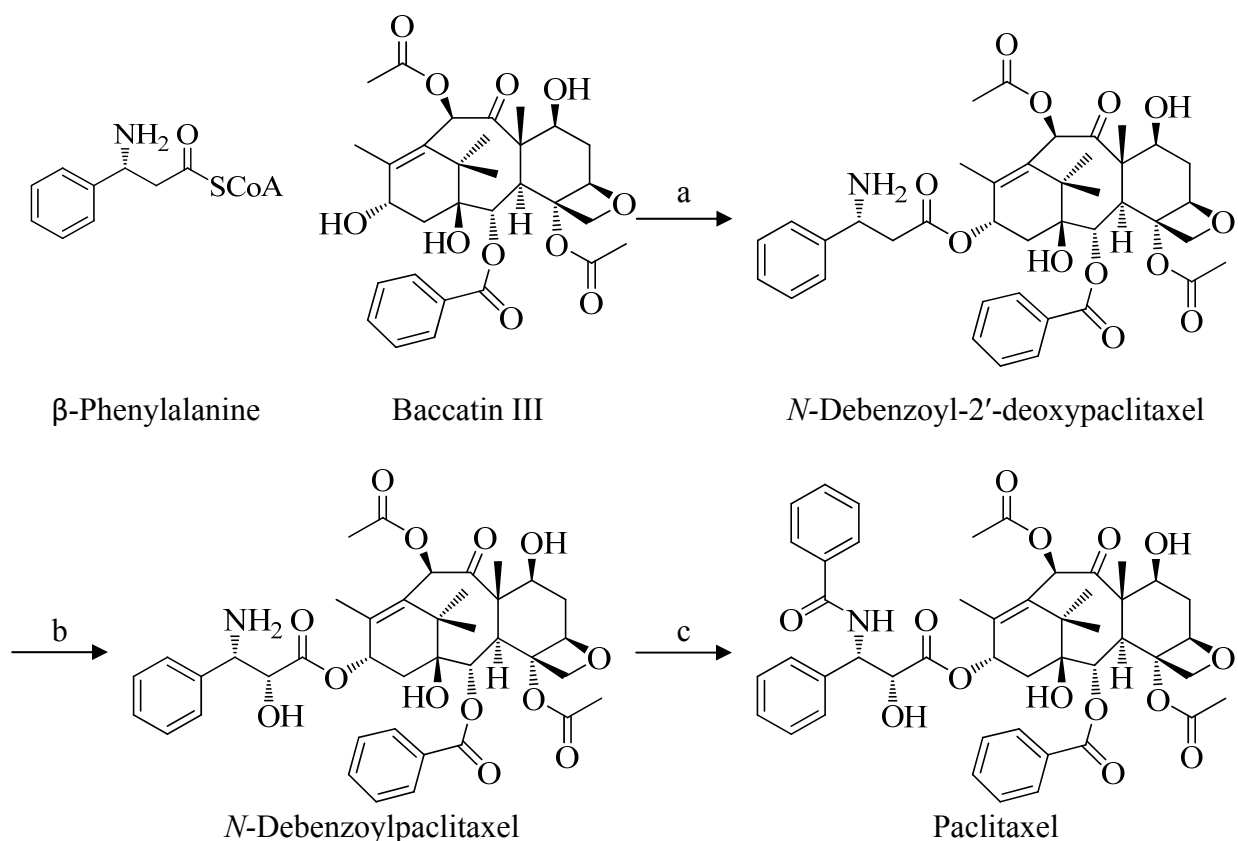


Figure 2.4 – Late-Occurring Steps on the Paclitaxel Biosynthesis Pathway.

a. Phenylpropanoyltransferase, b. C2' P450 hydroxylase, c. NDTBT, benzoyl CoA.

with a broad range of non-natural aroyl CoA substrates. *N*-Debenzoylpaclitaxel and *N*-de(*tert*-butoxycarbonyl)docetaxel (i.e., 10-deacetyl-*N*-debenzoylpaclitaxel) substrates required for this investigation were both prepared from docetaxel (Figure 2.5).

Because of the prohibitive expense of docetaxel to semisynthesize adequate *N*-debenzoylpaclitaxel analogues, the use of these analogues needed to be rationed, in the present study. Therefore, to conserve the supply of these derivatives, the substrates were incubated at a single concentration (1 mM) with each of the 16 aroyl CoA thioesters (at 1 mM) for 2 h, in duplicate runs. Each sample was analyzed by ESI-MS/MS to verify *N*-aroylated product identity and to quantify the relative rate at which the biosynthesized products were formed. The first

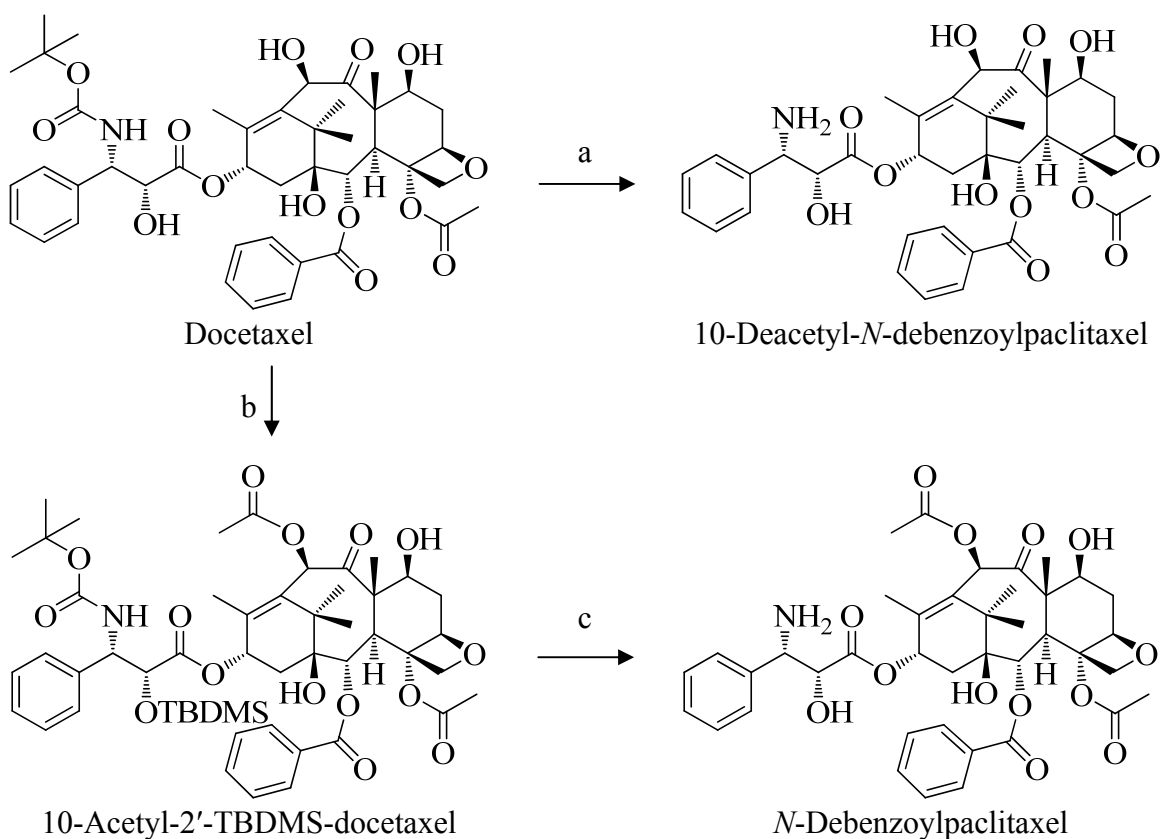


Figure 2.5 - Synthesis of *N*-Debenzoylisoserineoyltaxanes.

a. i. Formic acid, ii. NaHCO₃, 60% yield. b. i. TBDMS-Cl, imid., 99% yield, ii. Ac₂O, CeCl₃, 93% yield. c. i. HF/pyridine, ii. Formic acid, iii. NaHCO₃, 62% yield.

stage mass spectrometer was set to select for the MH⁺ ion of the product, which was directed into a fragmentation chamber, and the resulting fragment ions were analyzed by the second-stage mass spectrometer set to scan mode. Typical diagnostic fragment ions were *m/z* 509 (for the 10-acetyl and 10-deacetyl taxane substrates), 569 (for the 10-acetyl taxane substrates), and the distinct side chain fragment ion for product characterization (Figure 2.6 and see Appendix B). In these assays, the kinetic parameters of NDTBT were unknown, regarding whether the non-natural aroyl CoA thioesters were first-order or at saturation at 1 mM; however, to provide a rough approximation of the relative velocities (*v*_{rel}) of NDTBT (100 μg) for each CoA thioester (Table 2.2), the rates were estimated to be at steady state and first-order.

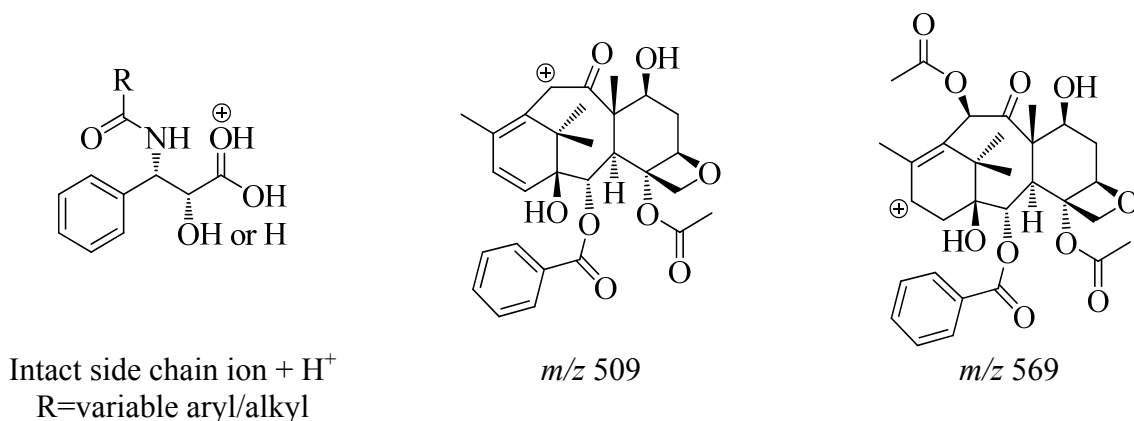


Figure 2.6 - Typical Fragment Ions Observed in the MS/MS Profiles of Isoserinoyl Taxanes.

The rate (~10 pmol/h) at which benzoyl CoA and *N*-debenzoylpaclitaxel was converted to paclitaxel by NDTBT was set at 100% and compared to the rates of NDTBT with each of various aroyl CoA thioesters and the same taxane substrate (Table 2.2 for the following entries). Surprisingly, the v_{rel} of 2-furanoyl CoA was 200% (Entry 12B) relative to benzoyl CoA, whereas 3-furanoyl CoA was 19% (Entry 13B). The v_{rel} values for the other 2- and 3-heteroaromatic carbonyl CoA thioesters displayed similar kinetics to that of the 3-furanoyl thioester, ranging between 19% and 22% (Entries 14-16B). NDTBT was productive with 3-methoxybenzoyl CoA, which was utilized at 85% (Entry 9B) of the rate for benzoyl CoA. The relative rates of the catalyst for the methyl-, fluoro-, and cyano-substituted benzoyl CoA thioesters were modest (Entries 3-8B), with the exception of 2- and 3-chlorobenzoyl CoA (Entries 10-11B); the products derived from the latter were only marginally detectable, at $v_{\text{rel}} < 1\%$ (data not shown).

In a parallel study, we assessed whether the absence of the acetyl group at C10 of the *N*-debenzoylpaclitaxel affected the specificity of the NDTBT with the array of aroyl CoA thioesters. The rate (~20 pmol/h) at which benzoyl CoA and 10-deacetyl-*N*-debenzoylpaclitaxel

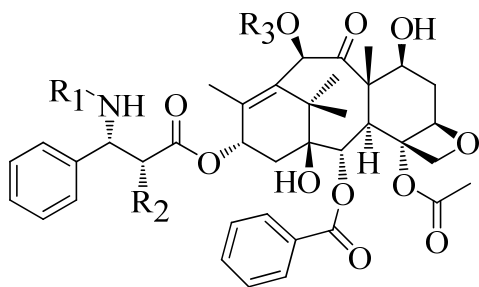
was converted to 10-deacetylpaclitaxel (Entry 1C) by NDTBT was set at 100% and compared to the rates at which the enzyme converted each of various aroyl CoA thioesters and the taxane substrate to a respective product. 4-Fluorobenzoyl CoA (v_{rel}) 68%, Entry 7C) and 3-furanoyl CoA (v_{rel}) 43%, Entry 13C) were used at a rate most comparable to that at which NDTBT used benzoyl CoA. Interestingly, all of the other aroyl CoA thioesters tested were productive (with relative conversion rates between 3% and 38%), except for 4-methylbenzoyl CoA (Entry 4C), which did not produce detectable product.

2.3.4. Relative Velocities with Alkanoyl/Alkenoyl CoA Substrates

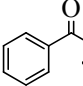
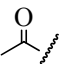
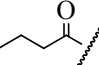
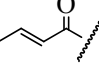
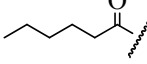
Four non-aromatic CoA thioesters (acetyl CoA, butyryl CoA, butenoyl CoA, and hexanoyl CoA) were assayed with the three *N*-debenzoyl taxoids, described herein. None of the isolated biosynthetic products were detectable by HPLC with UV monitoring (A_{228}), likely due to low abundance and/or co-elution of the biosynthetic products from the HPLC column with other unknown compounds extracted from the assay mixture. As an alternative, the samples were analyzed by the more selective LC-ESI-MS/MS procedure utilized earlier in this study. As before, typical diagnostic fragment ions were m/z 509, 569, and the side chain fragment ion (ordinarily the base peak) that confirmed the identity of the *N*-alkanoyl/alkenoyl taxane (Figure 2.6 and see Appendix B). The relative rates of product formation were calculated from the mass spectrometry data by a method analogous to that used for the *N*-aroylation products (Table 2.3).

N-Debenzoyl-2'-deoxypaclitaxel was incubated with NDTBT and benzoyl CoA, and the relative rate (~200 nmol/h) of the benzoyl group transfer to the *N*-debenzoyl taxane was compared to the rate of acyclic carbonyls. The v_{rel} for the transfer of acetyl (shortest chain) and

Table 2.3 – Relative Kinetics of NDTBT with Short Hydrocarbon Chain CoA Thioesters and *N*-Debenzoylpaclitaxel Analogues



- A.** *N*-Debenzoyl-2'-deoxypaclitaxel
 $R_1=H$, $R_2=H$, $R_3=Acetyl$
B. *N*-Debenzoylpaclitaxel
 $R_1=H$, $R_2=OH$, $R_3=Acetyl$
C. 10-*O*-Deacetyl-*N*-debenzoylpaclitaxel
 $R_1=H$, $R_2=OH$, $R_3=H$

R_1 (from CoA)		A V_{rel}	B V_{rel}	C V_{rel}
	1	100%	13%	12%
	17	47%	85%	35%
	18	3%	100%	92%
	19	2%	2%	3%
	20	36%	68%	100%

hexanoyl (longest chain) groups were 47% and 36%, respectively (Entries 17D and 20D), relative to the transfer rate for the benzoyl group. The v_{rel} for the C4 chains, butenoyl and butanoyl, were only at 2% and 3%, respectively. For *N*-de(*tert*-butoxycarbonyl)docetaxel and *N*-debenzoylpaclitaxel (i.e., 2'-hydroxylated substrates), the relative velocity of the most productive acyclic CoA substrate was set to 100%. In contrast to *N*-debenzoyl-2'-deoxypaclitaxel, the alkanoyl CoA thioesters (Entries 17E/F, 18E/F, and 20E/F) gave superior turnover with the 2'-hydroxylated taxoids, compared to benzoyl CoA (~10 and ~20 pmol/h, Entries 1E/F, respectively). The 2-butenoyl group was transferred the slowest by NDTBT to all of the taxoid

cosubstrates (Entries 19D/E/F), which may be a consequence of the extended, fixed geometry of the *trans*-double bond.

2.4. Discussion

Broad substrate specificity of enzymes on secondary metabolic pathways has been suggested as important for the evolution of metabolite diversity.³² The results of this study demonstrated the extraordinarily broad substrate specificity of the recombinantly expressed NDTBT enzyme in purified form when incubated with several acyl CoA donor substrates and three *N*-debenzoylpaclitaxel derivatives, *N*-debenzoyl-2'-deoxypaclitaxel, *N*-debenzoylpaclitaxel, or 10-deacetyl-*N*-debenzoylpaclitaxel. Other BAHD family acyltransferases, benzoyl CoA:benzoyl alcohol benzoyl transferase (*Clarkia breweri* plant), and alcohol acyltransferases from wild strawberry (*Fragaria Vesca*), cultivated strawberry (*Fragaria* × *ananassa*), and banana (*Musa sapientum*) also have broad substrate specificity with varying acyl CoA donors and a range of alcohol acceptor substrates.^{33, 34} As structural information becomes available for these BAHD acyltransferases, including NDTBT, the rationale for their broad substrate specificity can likely be understood, and the mechanism defining the variable substrate access can be systematically compared.

A prior seminal description of NDTBT primarily focused within the context of paclitaxel biosynthesis and thus screened the function of the catalyst with benzoyl CoA and a single diterpene substrate, *N*-debenzoyl-2'-deoxypaclitaxel.²² Substrate specificity analysis was limited to acetyl CoA and phenylacetyl CoA, neither of which was found to be productive in this earlier study.²² In a more recent biosynthesis investigation, the assembly of the isoserinoyl side chain of

paclitaxel was investigated.²³ The superior catalytic transfer of benzoyl to *N*-debenzoylpaclitaxel compared to *N*-debenzoyl-2'-deoxypaclitaxel (Figure 2.4) supported an earlier claim that 2'-hydroxylation precedes *N*-benzoylation.³⁰ This prior study also concluded that NDTBT did not transfer other naturally occurring short chain alkanoyl/alkenoyl groups to the amino group of the *N*-debenzoylpaclitaxel substrate as assessed by UV-HPLC analysis alone.²³

In contrast, the current investigation was formulated by consideration of the several described next-generation paclitaxel molecules derived by synthetic replacement of the *N*-benzoyl of the natural product with several different kinds of non-natural *N*-aroyl groups.^{10, 15} The hypothesis developed herein was that NDTBT could feasibly transfer non-natural aroyl moieties in addition to transferring a benzoyl to the amino functional group of various derivatives of *N*-debenzoylpaclitaxel. To evaluate this theory, the paclitaxel pathway *N*-benzoyltransferase was examined for its utility to *N*-aroylate analogues of advanced taxane metabolites. NDTBT was shown to indiscriminately transfer aroyl groups, including heteroles, 2-, 3-, and 4-substituted benzoyls, alkanoyl, and alkenoyl (cf. Tables 2.2 and 2.3) to any tested *N*-debenzoylated taxane used as a cosubstrate. More importantly, these results indicate that the *N*-benzoyltransferase is not limited to *N*-debenzoyl-2'-deoxypaclitaxel as a substrate that contains the β -phenylalanine side chain. The diverse specificity for *N*-aroylation was largely unaffected by the presence of the vicinal hydroxyl group at C2' of the phenylisoserinoyl diterpenes and thus supports the observation described in a previous study.²³ In addition, the lack of a C10-acetyl group on the taxane substrate did not affect the function of the enzyme, and therefore, conceivably, C10-acetylation could occur as a last step in the biosynthesis of paclitaxel. Furthermore, *ortho*-, *para*-, or *meta*-substitution on the benzoyl group transferred from CoA

generally did not affect NDTBT activity, although the *para*-regioisomers within a homologous series were typically transferred faster.

It was very apparent that the scale of the assays used in this investigation produced a paucity of isoserinoyl taxane products, on the order of pmol/h, and thus precluded their detection by UV-HPLC. The application of a selective and more sensitive HPLC electrospray ionization tandem mass spectrometric analysis enabled the detection of the array of biosynthetic products made by NDTBT catalysis, described herein; moreover, this mode of analysis enabled categorical identification of the fragment ion of the intact side chain for each of the biosynthetically acquired *N*-acyl derivatives.

In conclusion, we demonstrated that the wild-type *Taxus* *N*-benzoyltransferase functions as a general *acyl*/transferase. The broad substrate specificity of NDTBT for a variety of acyl CoA thioesters provides momentum for the eventual application of this biocatalyst toward the production of modified paclitaxel compounds and likely accounts for the variety of *N*-acyl derivatives of paclitaxel analogues found in *Taxus* plants and derived cell cultures.³⁵ In addition, the described substrate specificity will expand the current knowledge of the selectivity of enzymes that belong to the BAHD acyltransferase superfamily. It is still premature nonetheless, particularly without enzyme structural data, to speculate why NDTBT displays the unique kinetic parameters in terms of substituent regiochemistry in the aroyl CoA substrate, with regards to sterics and inductive effects. Furthermore, it was anticipated that NDTBT, a benzoyltransferase, would primarily aroylate the *N*-debenzoyl substrates; thus, it was intriguing to see alkanoyl and butenoyl groups transferred by the catalyst to the acceptor substrate. Moreover, the presence of a 2'-hydroxy group on the phenylpropanoyl side chain of the taxane substrate increased the rate of *N*-alkanoylation/alkenoylation over *N*-benzoylation. At the early stages of defining the scope of

NDTBT specificity, the underlying effect of the 2'-hydroxyl on preferential alkanoyl CoA binding remains a mystery. Conceivably, when structural data become available for NDTBT, valuable insight into the mechanism of substrate specificity can be dissected, and directed mutational analysis can be employed to potentially produce new catalyst derivatives that are able to transfer a greater or refined scope of novel acyl groups to the taxane core or other diterpene scaffolds. The production of efficacious paclitaxel analogues through biocatalytic means *in vitro* or *in vivo* in a suitable host system will facilitate semi-biosynthetic methods that interface synthetic chemistry and molecular biology.

APPENDICES

APPENDIX A

KINETIC PARAMETERS FOR NDTBT

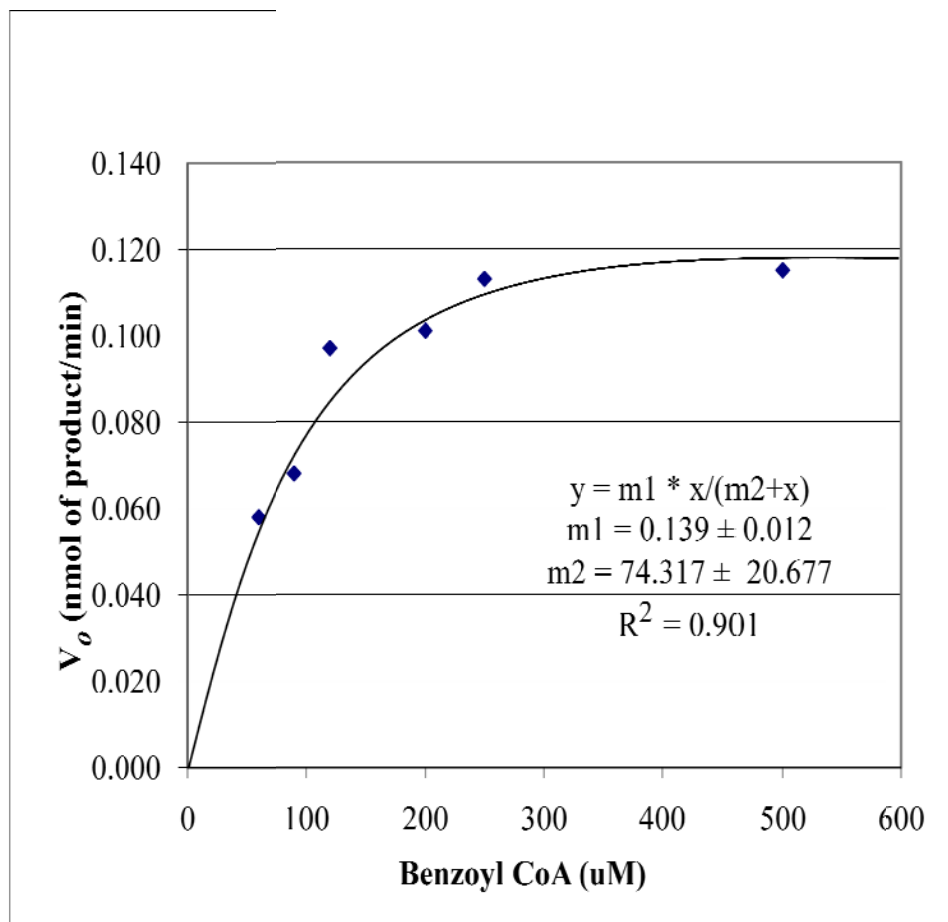


Figure A.1 – Michaelis-Menten Curve for NDTBT.

$V_{\max} = m1 = 0.139 \text{ nmol/min}$; $K_M = m2 = 74.31 \text{ } \mu\text{M}$

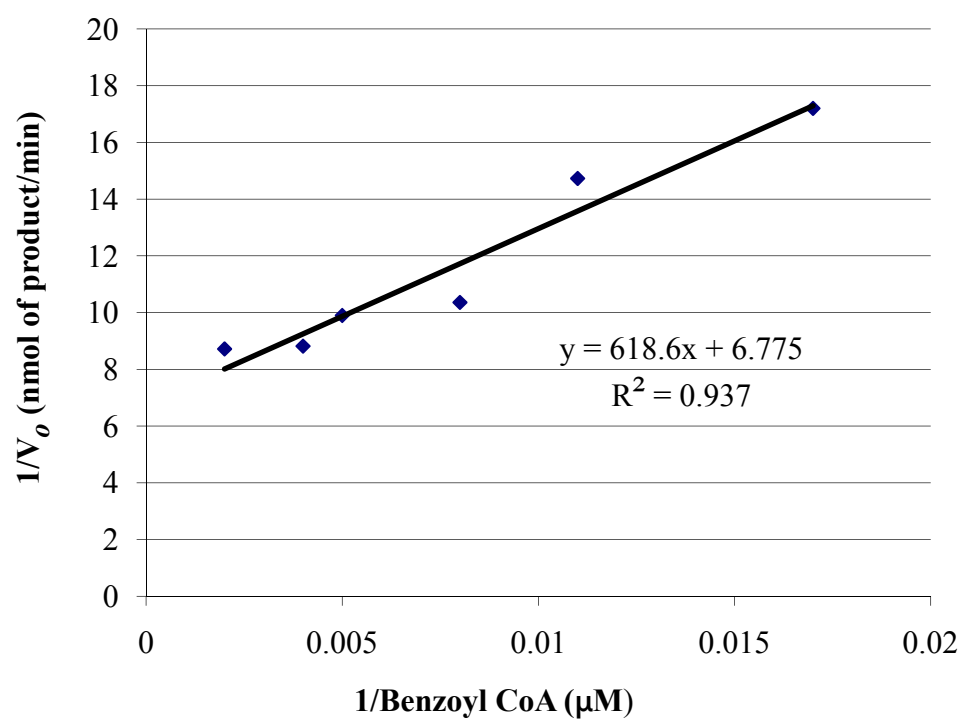


Figure A.2 – Double-Reciprocal Plot for NDTBT.

$$V_{\max} = 0.147 \text{ nmol/min}; K_M = 93 \mu\text{M}$$

APPENDIX B

MASS SPECTRA OF PRODUCT STANDARDS AND BIOSYNTHESIZED PRODUCTS MADE BY *NDTBT*

I, Danielle M. Nevarez, obtained the following mass spectra data. Standards were either commercially available or synthetically made by either Yemane A. Mengistu or Irosha N. Nawarathne (See Chapter 2). A Q-ToF Ultima Global electrospray ionization tandem mass spectrometer, (ESI-MS/MS, Waters, Milford, MA) was used for mass spectral analysis.

ESI-MS/MS Analysis of Authentic Taxanes Analogs. ESI-MS/MS of authentic *N*-benzoylated taxane standards (paclitaxel, 2'-deoxypaclitaxel, and docetaxel) are shown in Figures B.1, B.2, and B.3.

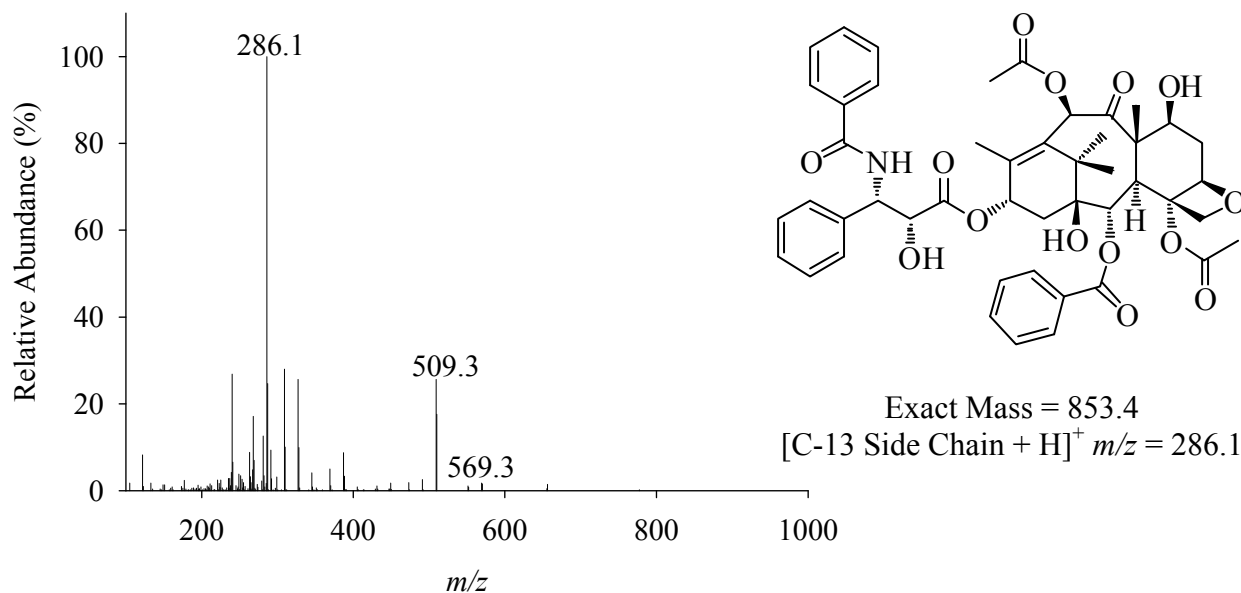


Figure B.1 – Tandem Mass Spectrum of Paclitaxel Standard.

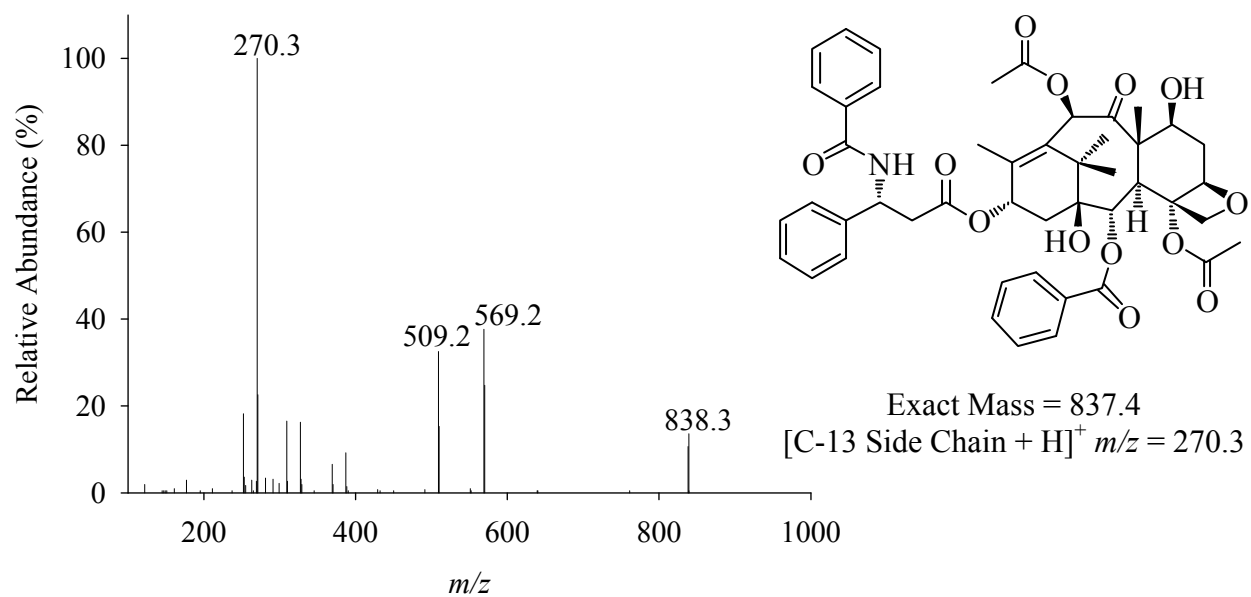


Figure B.2 – Tandem Mass Spectrum of 2'-Deoxypaclitaxel Standard.

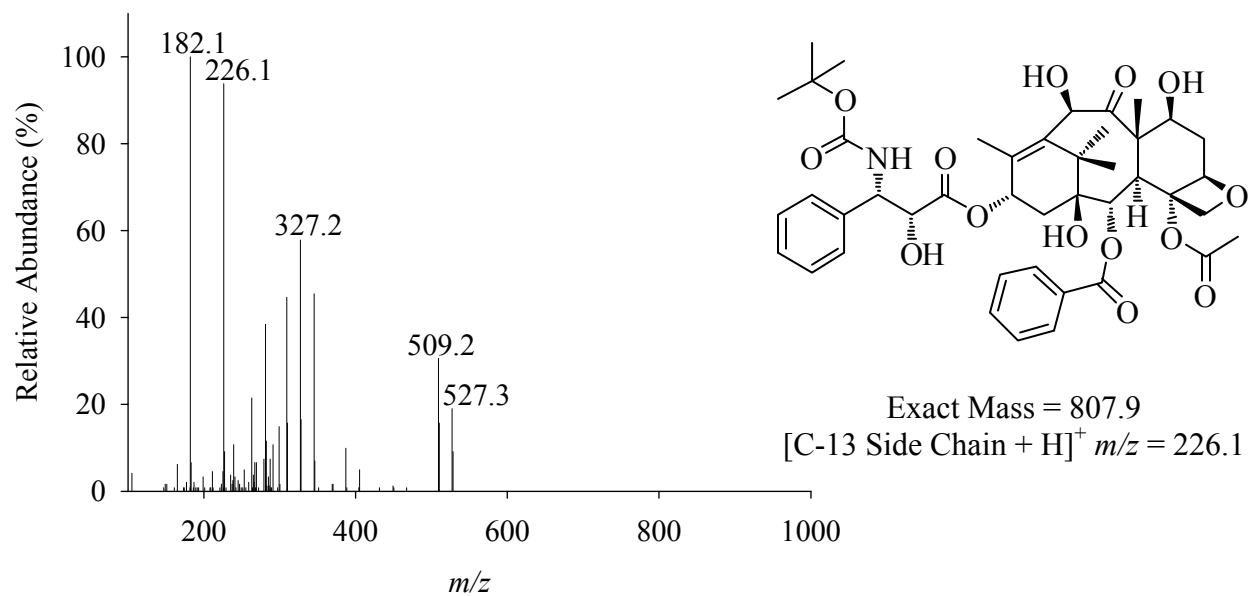


Figure B.3 – Tandem Mass Spectrum of Docetaxel Standard.

ESI-MS/MS Analysis of Biosynthetic Products Catalyzed by NDTBT. Spectra of the various biosynthetically derived *N*-aroyl- and *N*-alkyl-*N*-debenzoylpaclitaxel analogs and the spectra are labeled by structure (below).

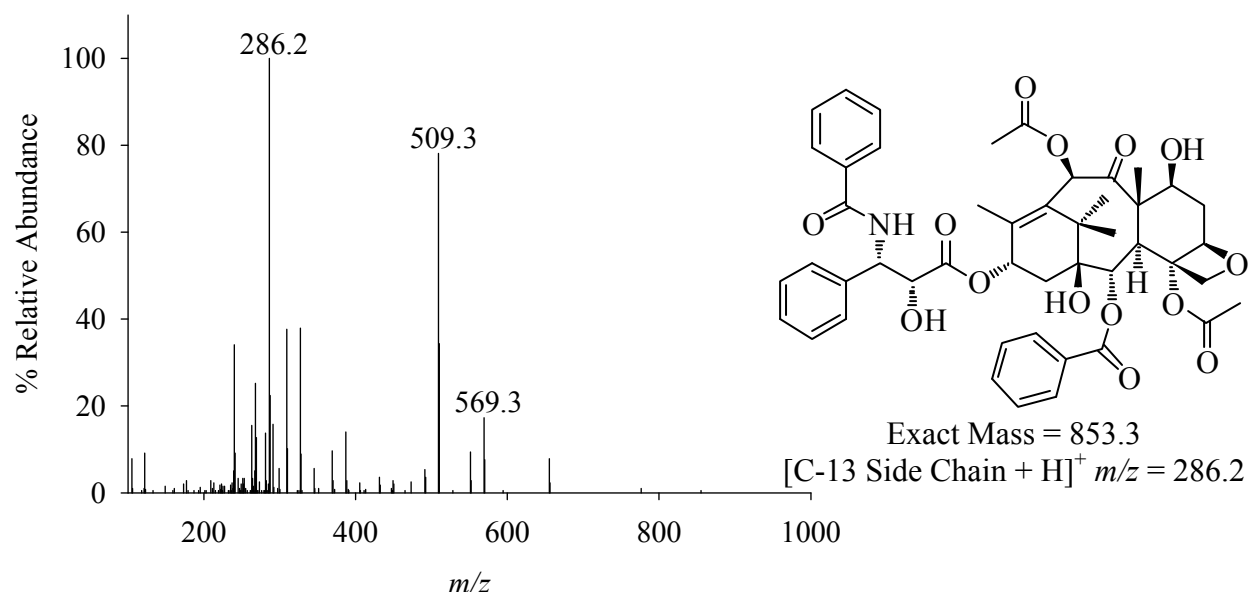


Figure B.4 – Tandem Mass Spectrum of Biosynthesized Paclitaxel.

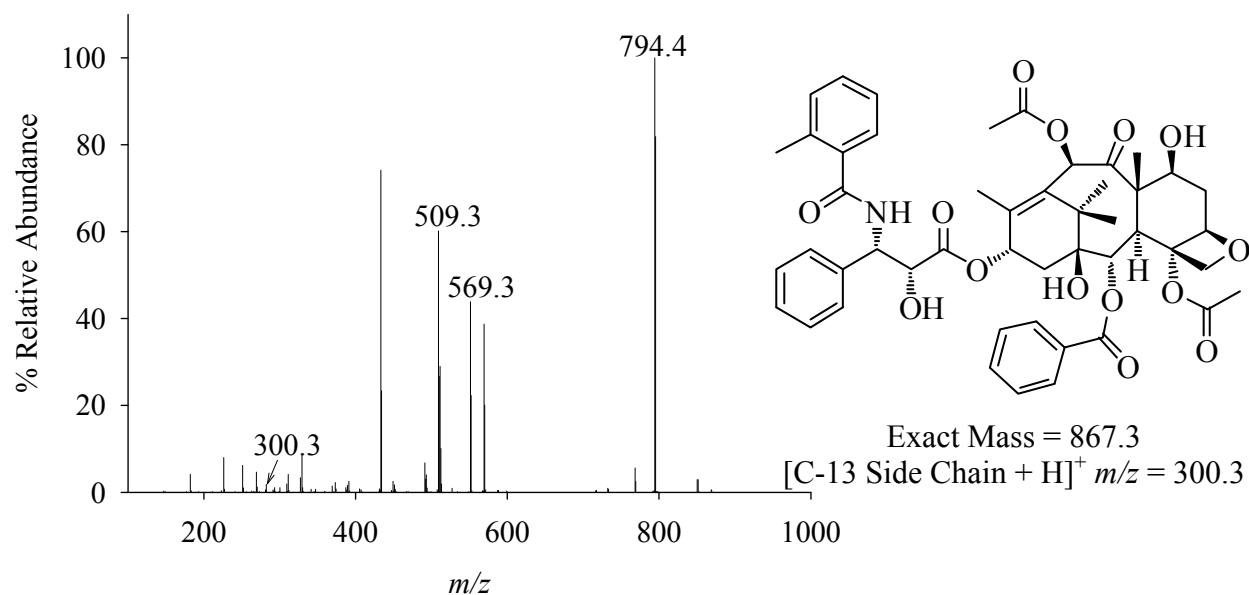


Figure B.5 – Tandem Mass Spectrum of Biosynthesized *N*-(2-Methylbenzoyl)-*N*-debenzoylpaclitaxel.

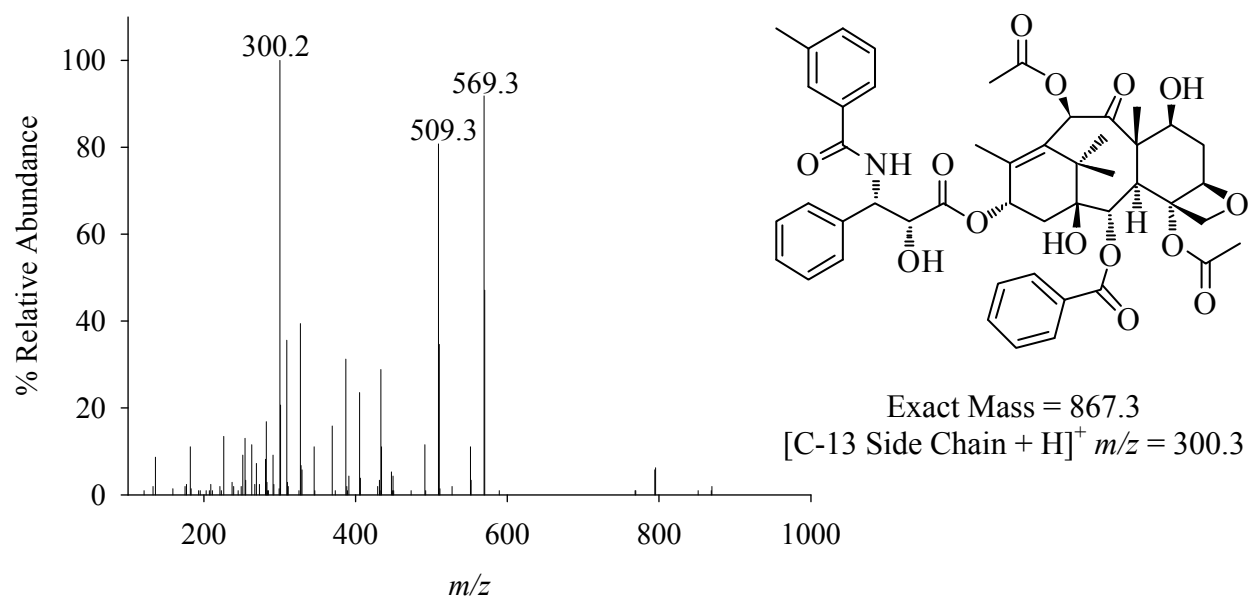


Figure B.6 – Tandem Mass Spectrum of Biosynthesized *N*-(3-Methylbenzoyl)-*N*-debenzoylpaclitaxel.

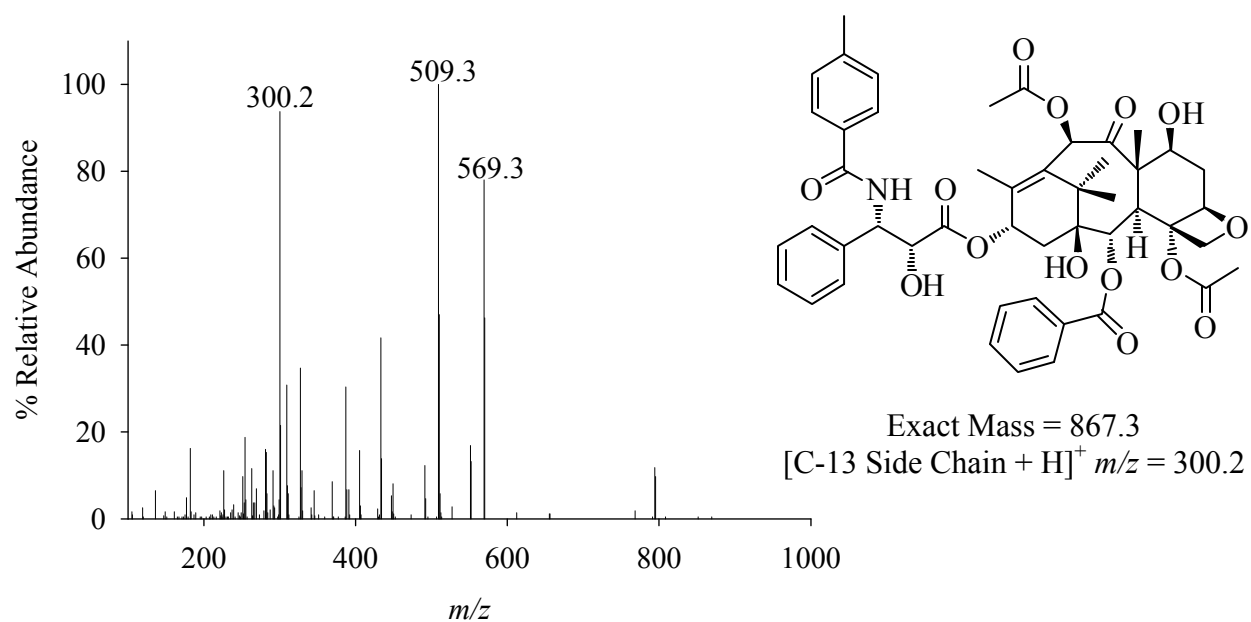


Figure B.7 – Tandem Mass Spectrum of Biosynthesized *N*-(4-Methylbenzoyl)-*N*-debenzoylpaclitaxel.

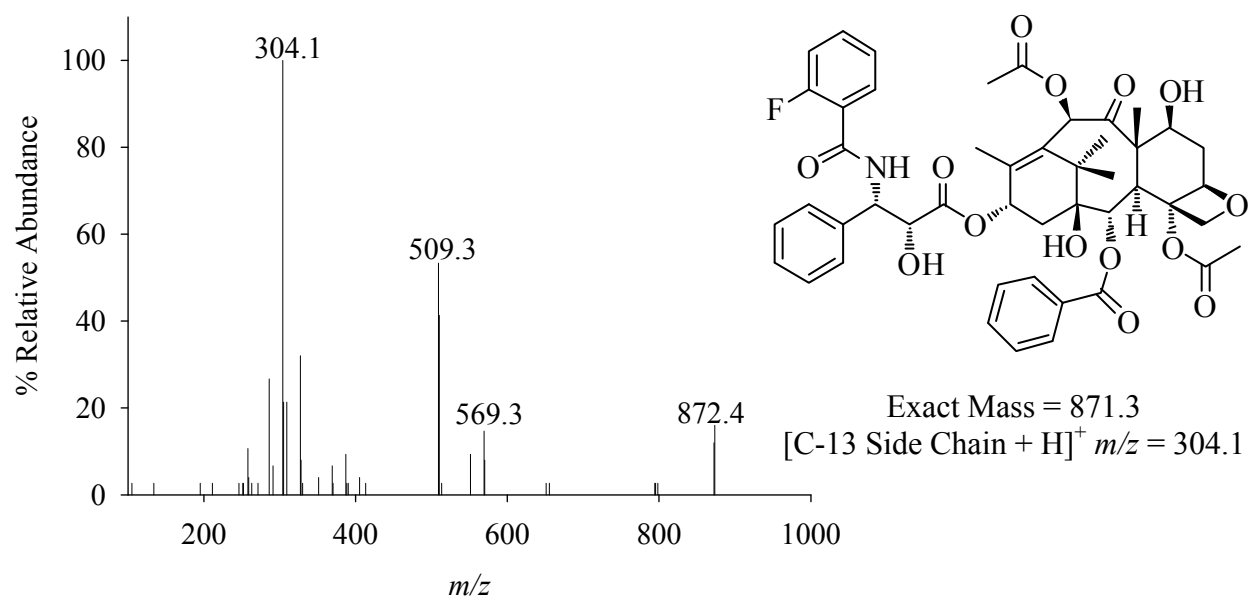


Figure B.8 – Tandem Mass Spectrum of Biosynthesized *N*-(2-Fluorobenzoyl)-*N*-debenzoypaclitaxel.

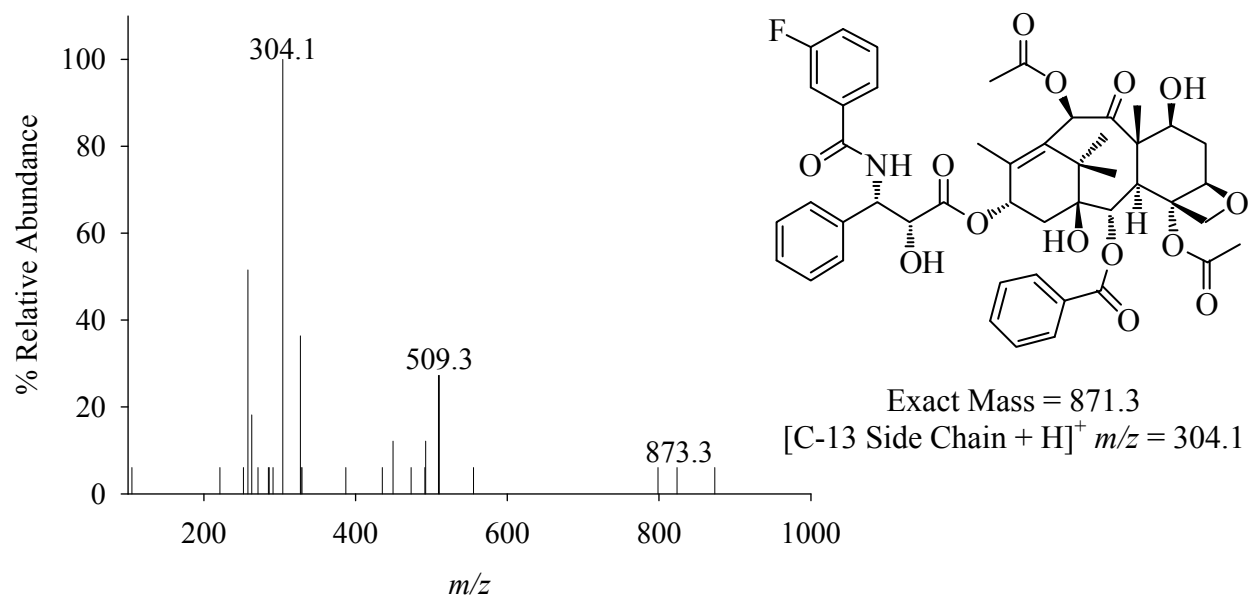


Figure B.9 – Tandem Mass Spectrum of Biosynthesized *N*-(3-Fluorobenzoyl)-*N*-debenzoypaclitaxel.

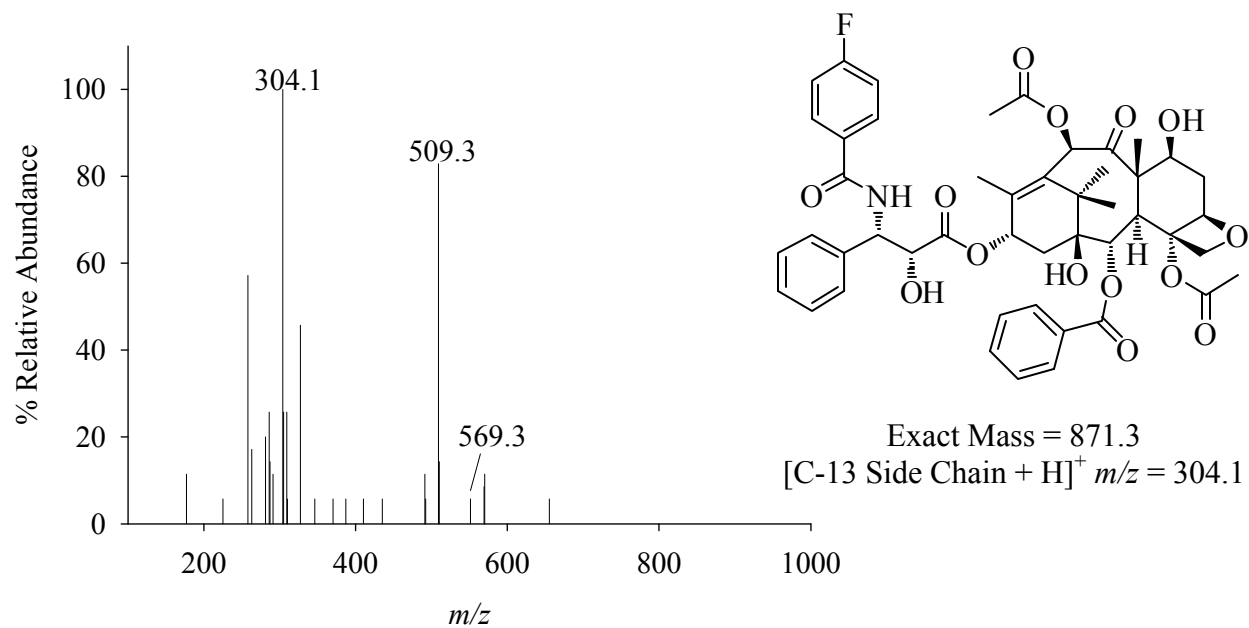


Figure B.10 – Tandem Mass Spectrum of Biosynthesized *N*-(4-Fluorobenzoyl)-*N*-debenzoylpaclitaxel.

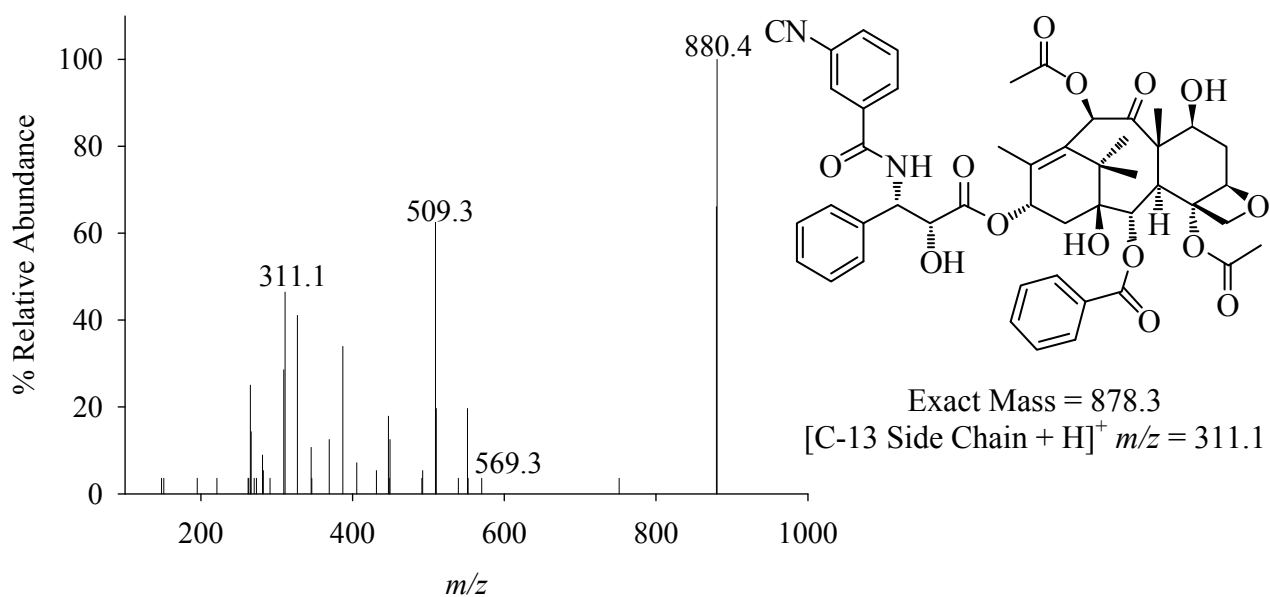


Figure B.11 – Tandem Mass Spectrum of Biosynthesized *N*-(3-Cyanobenzoyl)-*N*-debenzoylpaclitaxel.

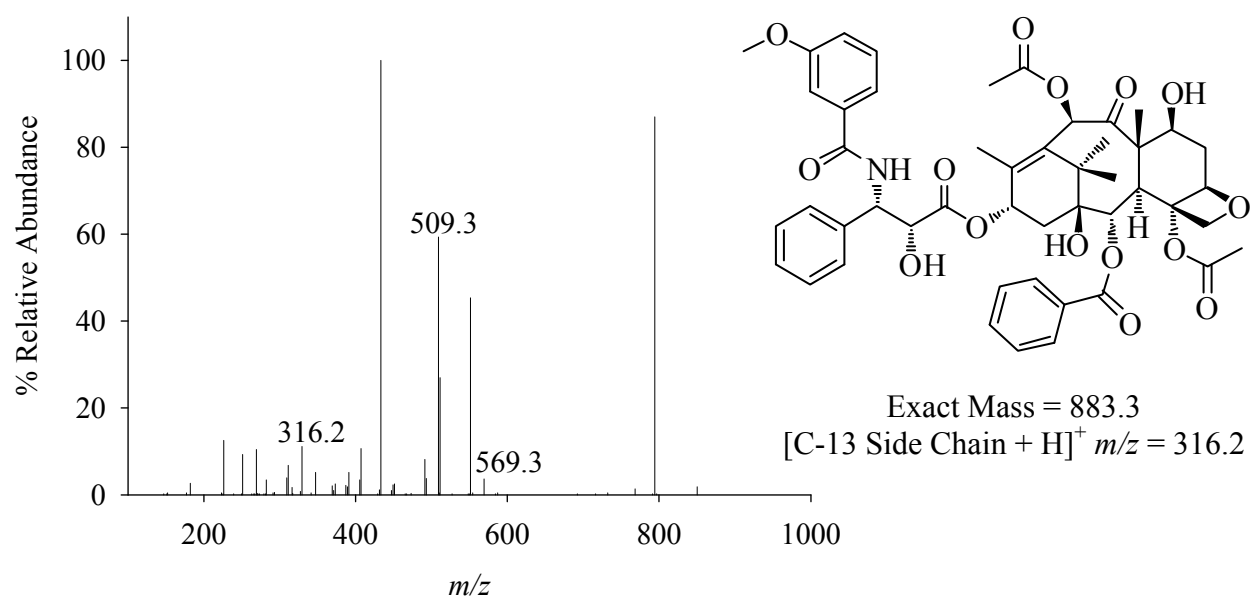


Figure B.12 – Tandem Mass Spectrum of Biosynthesized *N*-(3-Methoxybenzoyl)-*N*-debenzoylpaclitaxel.

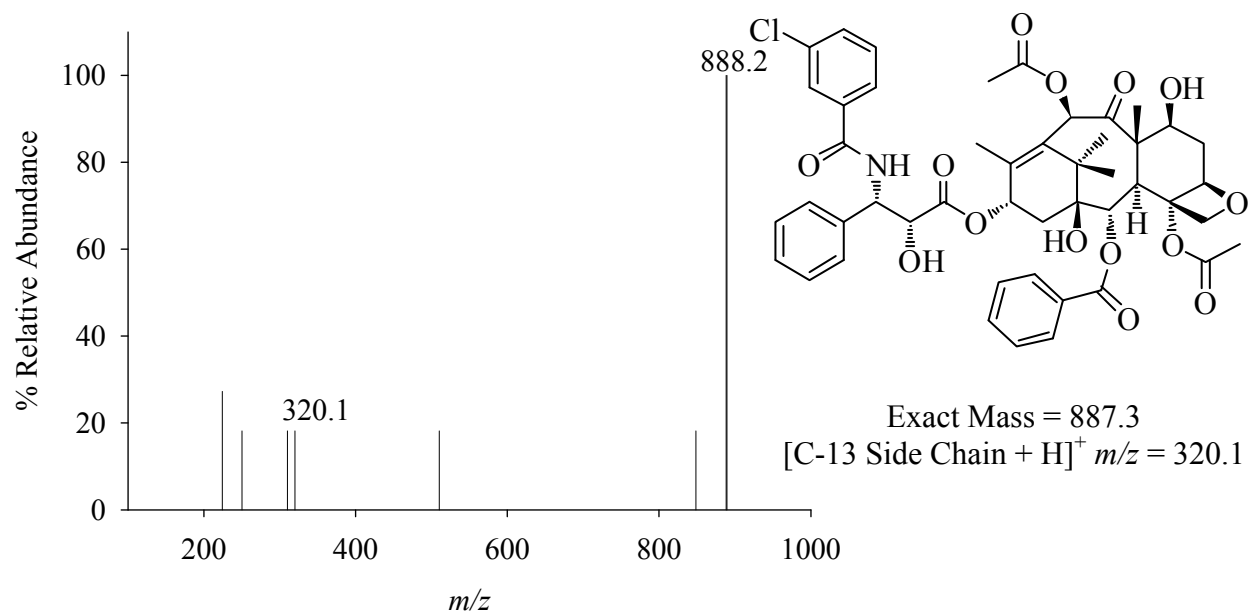


Figure B.13 – Tandem Mass Spectrum of Biosynthesized *N*-(3-Chlorobenzoyl)-*N*-debenzoylpaclitaxel.

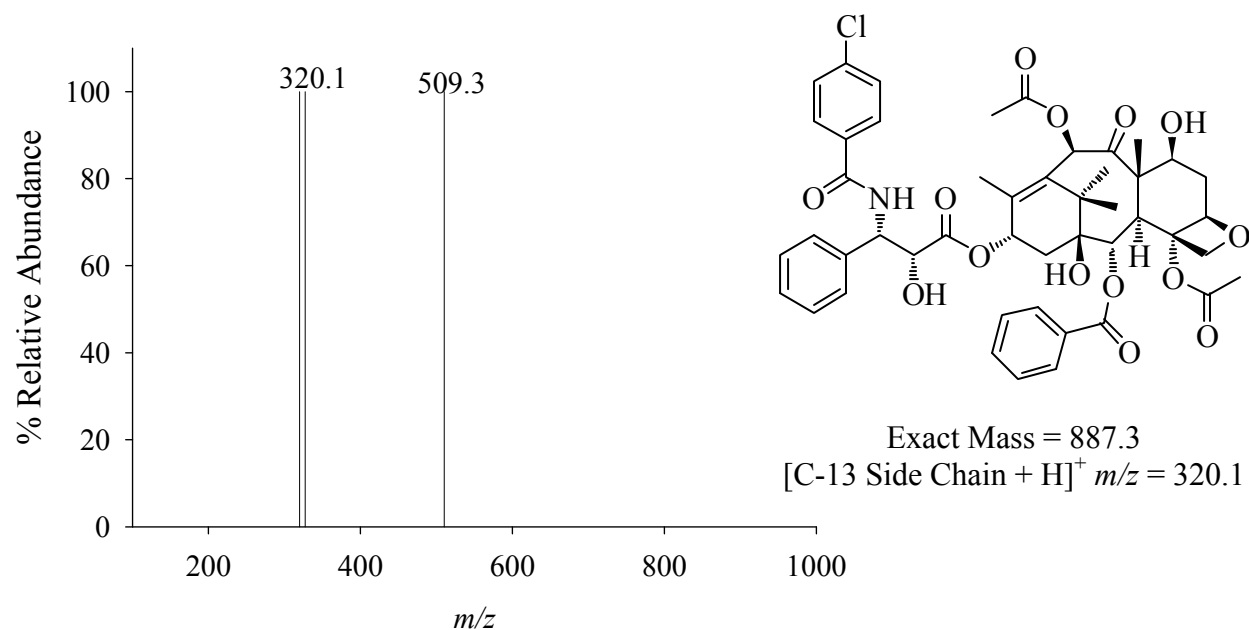


Figure B.14 – Tandem Mass Spectrum of Biosynthesized *N*-(4-Chlorobenzoyl)-*N*-debenzoylpaclitaxel.

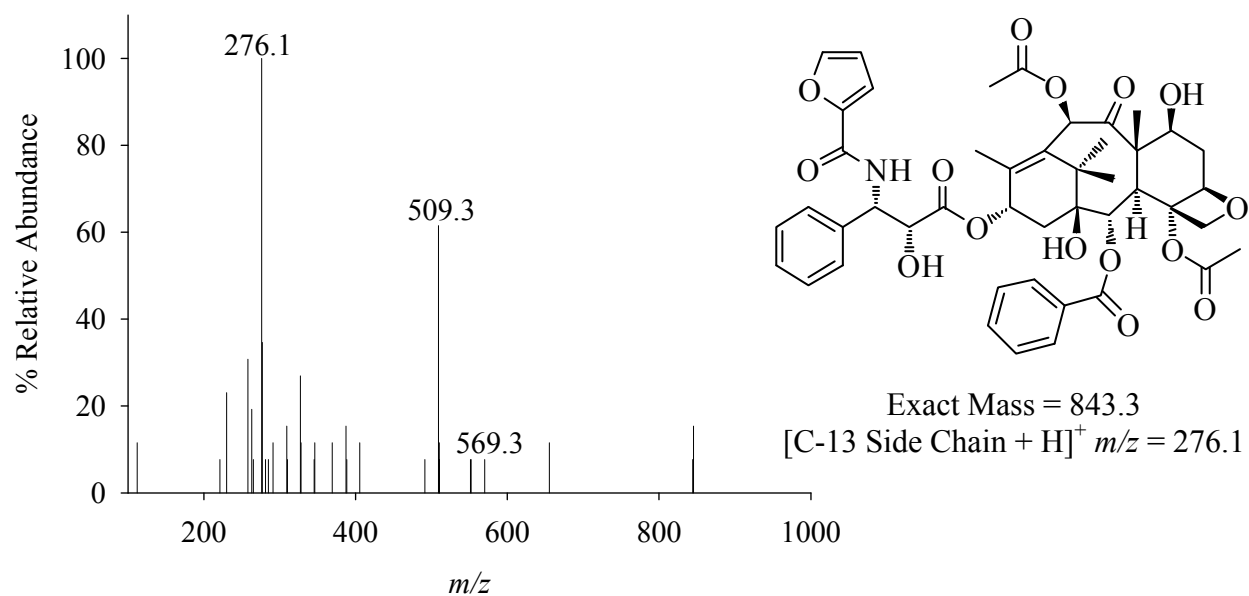


Figure B.15 – Tandem Mass Spectrum of Biosynthesized *N*-(2-Furanoyl)-*N*-debenzoylpaclitaxel.

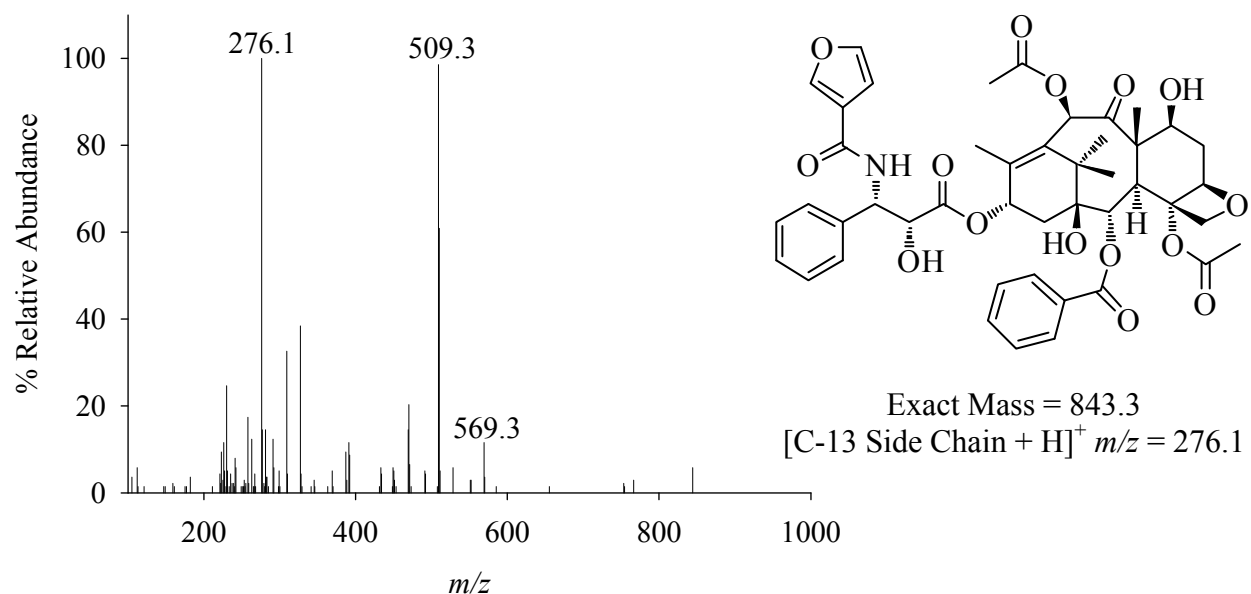


Figure B.16 – Tandem Mass Spectrum of Biosynthesized *N*-(3-Furanoyl)-*N*-debenzoylpaclitaxel.

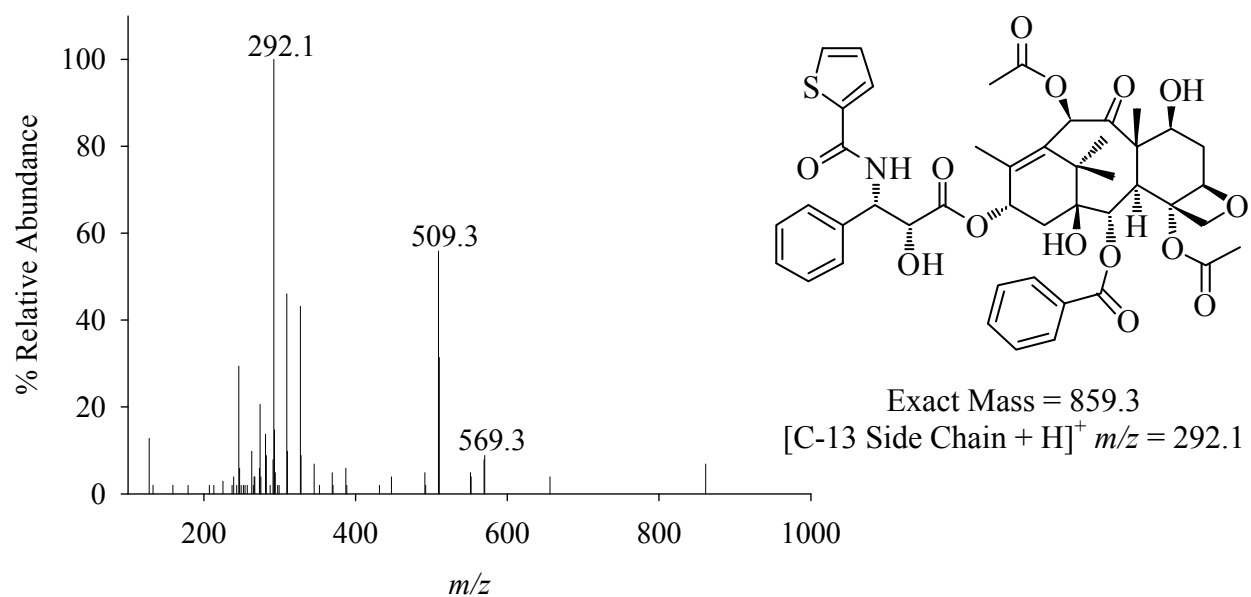


Figure B.17 – Tandem Mass Spectrum of Biosynthesized *N*-(Thiophene-2-carbonyl)-*N*-debenzoylpaclitaxel.

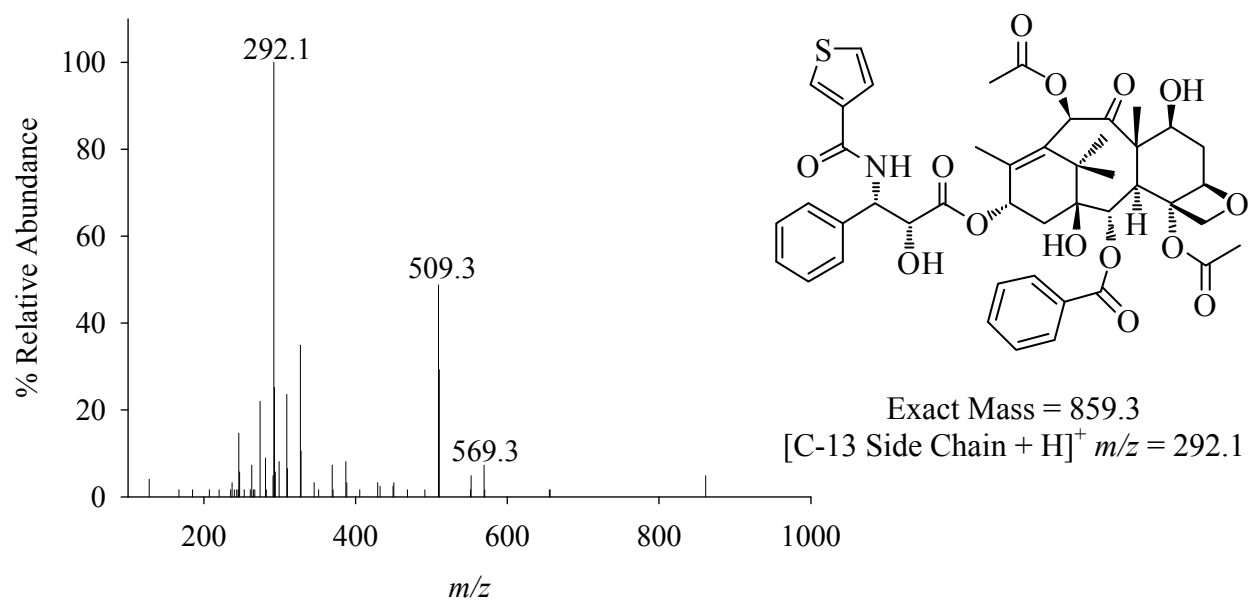


Figure B.18 – Tandem Mass Spectrum of Biosynthesized *N*-(Thiophene-3-carbonyl)-*N*-debenzoylpaclitaxel.

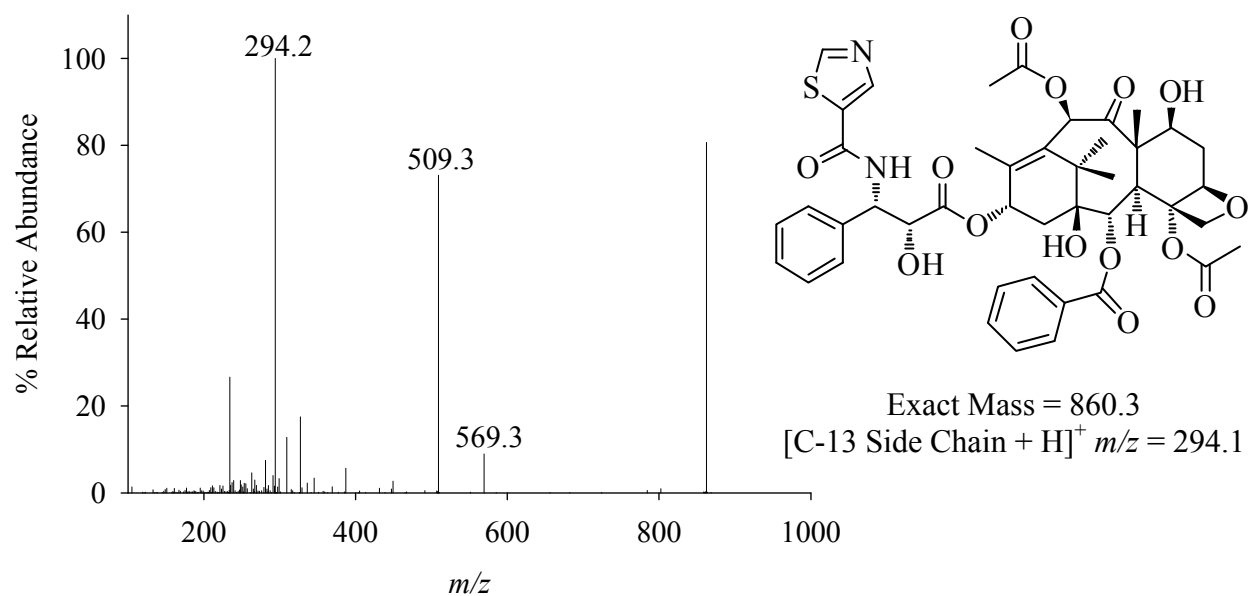


Figure B.19 – Tandem Mass Spectrum of Biosynthesized *N*-(Thiazole)-*N*-debenzoylpaclitaxel.

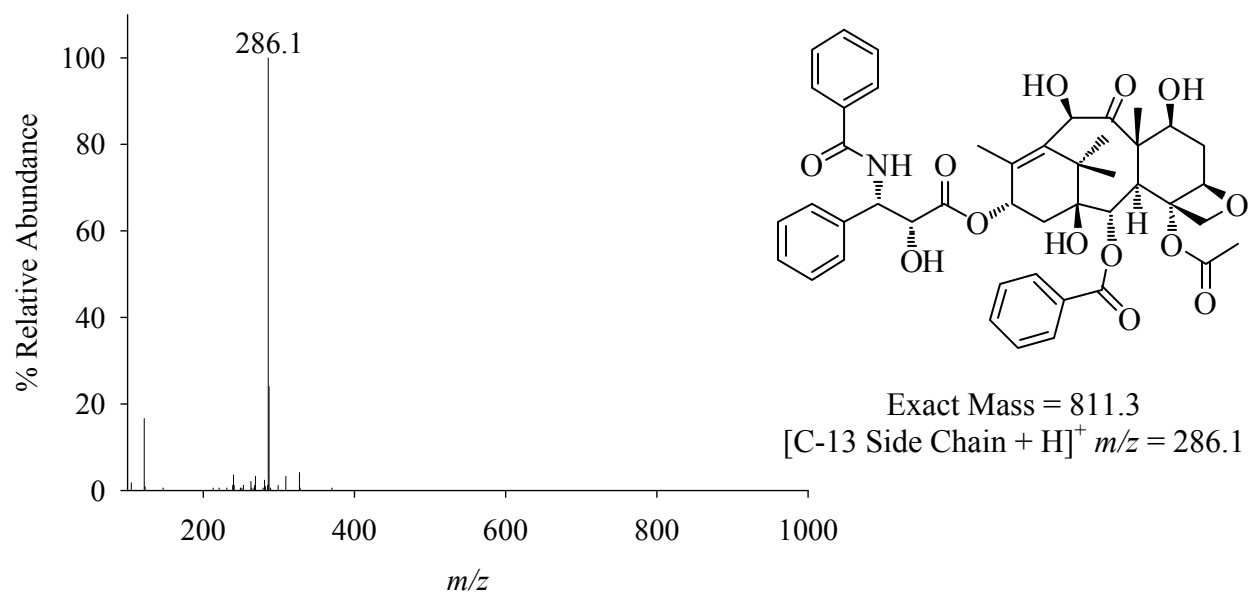


Figure B.20 – Tandem Mass Spectrum of Biosynthesized 10-deacetylpaclitaxel.

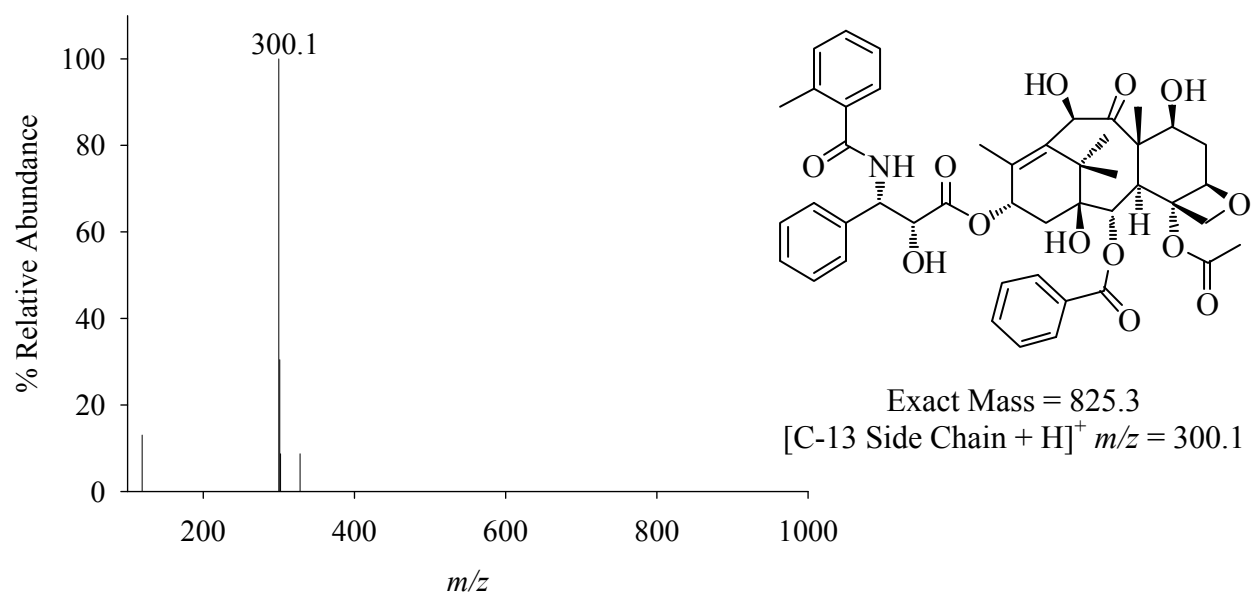


Figure B.21 – Tandem Mass Spectrum of Biosynthesized *N*-(2-Methylbenzoyl)-10-deacetyl-*N*-debenzoylpaclitaxel.

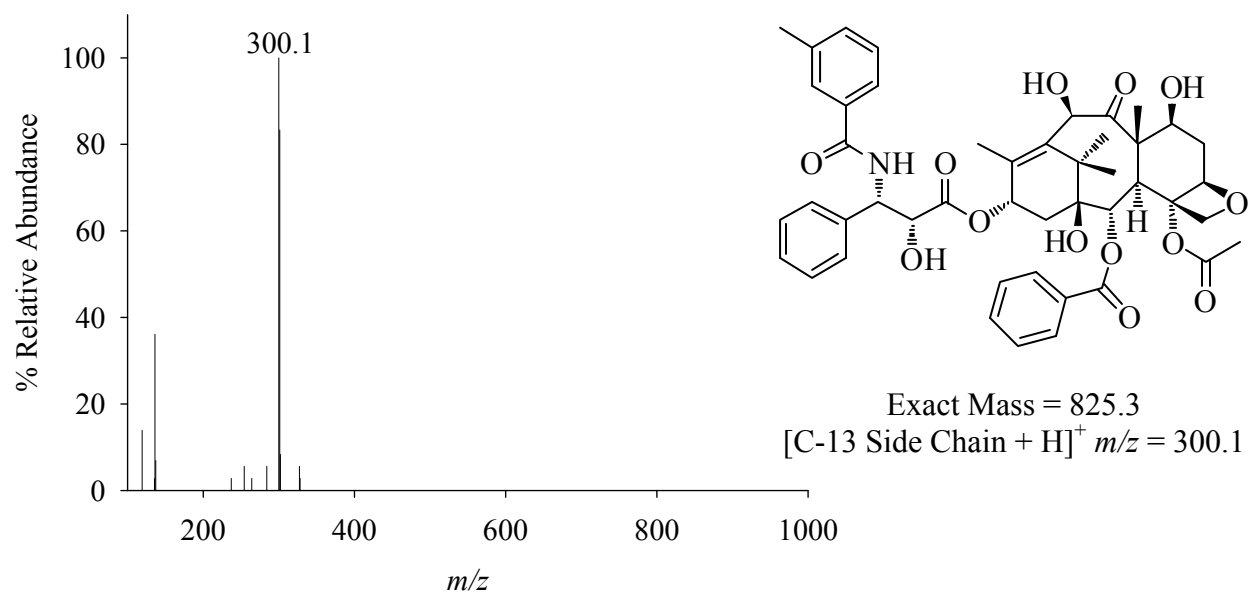


Figure B.22 – Tandem Mass Spectrum of Biosynthesized *N*-(3-Methylbenzoyl)-10-deacetyl-*N*-debenzoylpaclitaxel.

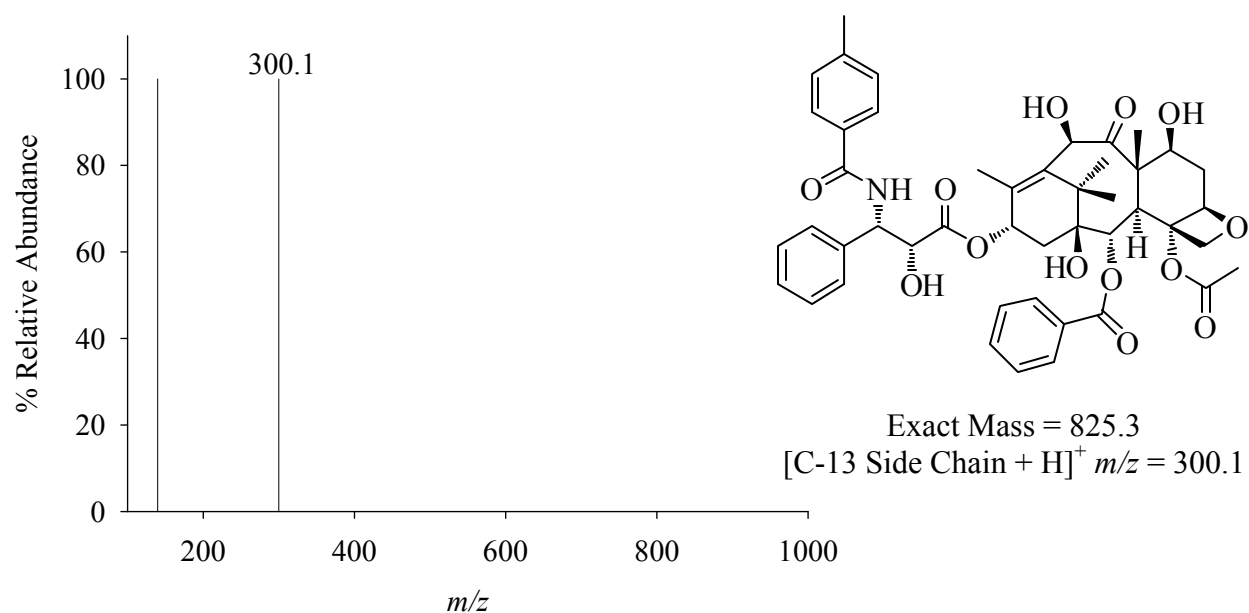


Figure B.23 – Tandem Mass Spectrum of Biosynthesized *N*-(4-Methylbenzoyl)-10-deacetyl-*N*-debenzoylpaclitaxel.

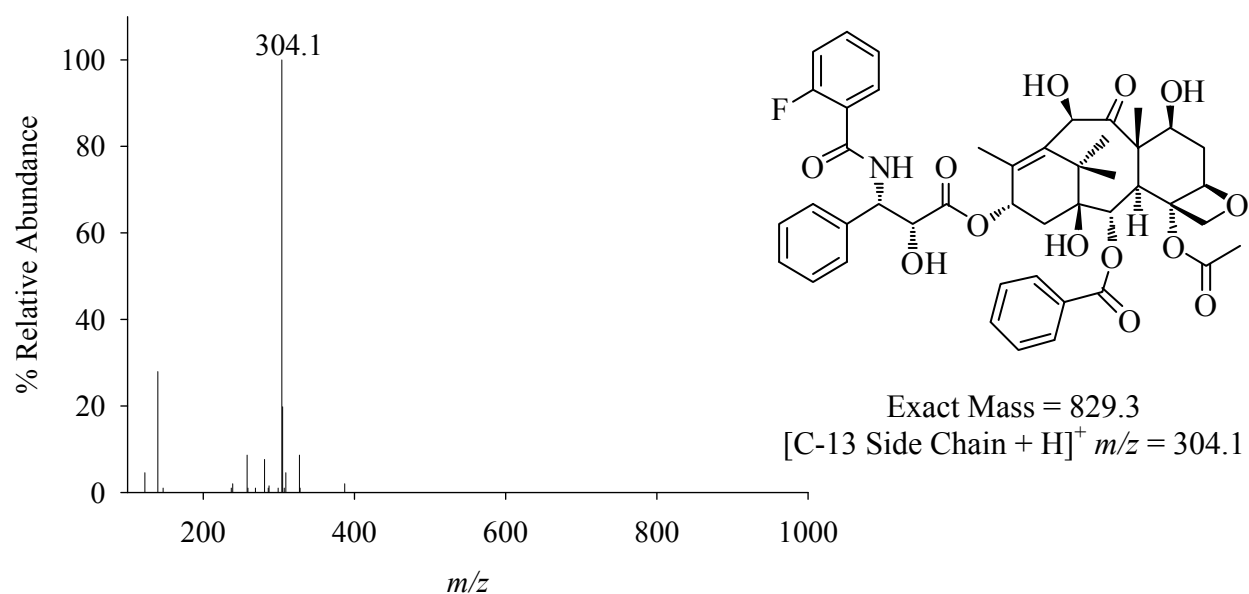


Figure B.24 – Tandem Mass Spectrum of Biosynthesized *N*-(2-Fluorobenzoyl)-10-deacetyl-*N*-debenzoylpaclitaxel.

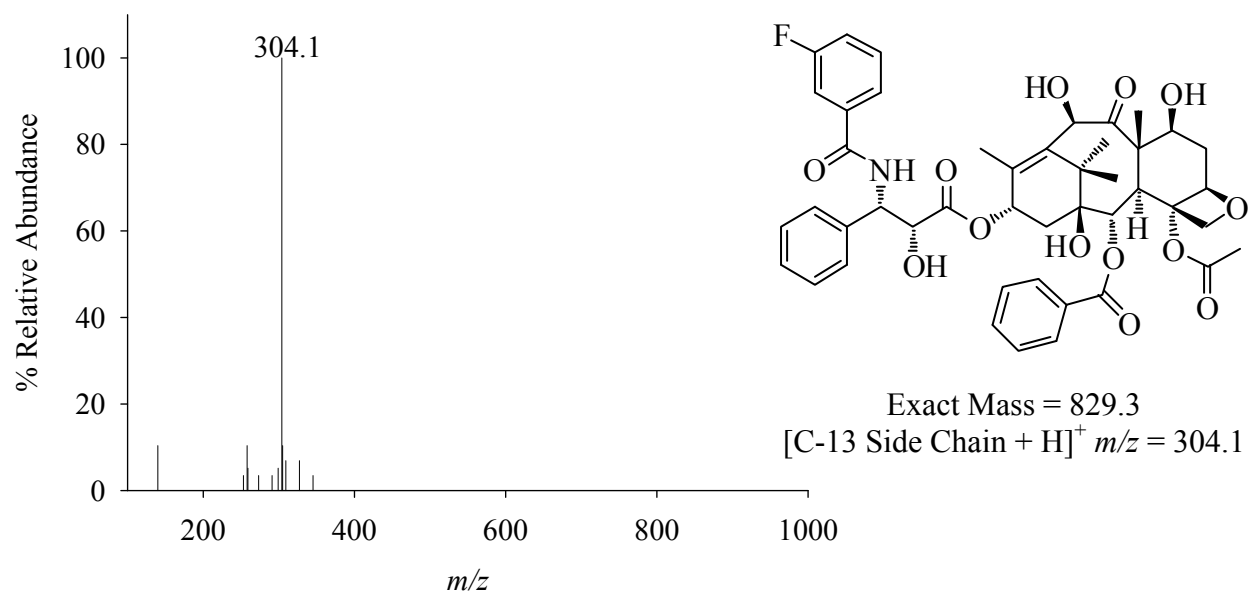


Figure B.25 – Tandem Mass Spectrum of Biosynthesized *N*-(3-Fluorobenzoyl)-10-deacetyl-*N*-debenzoylpaclitaxel.

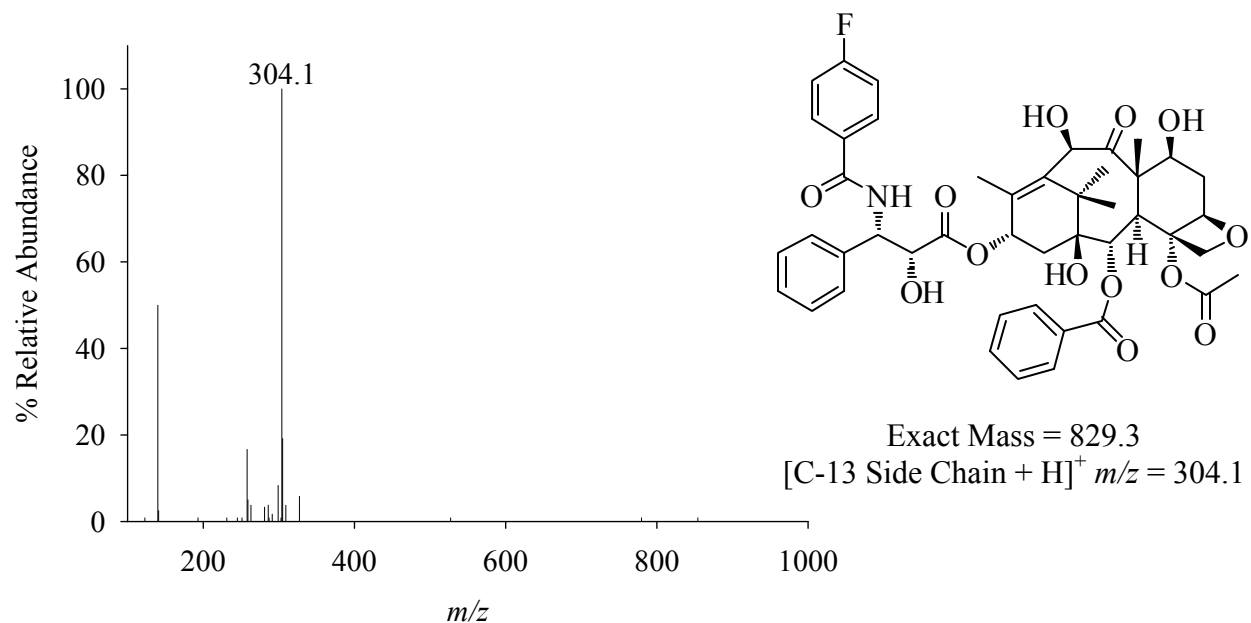


Figure B.26 – Tandem Mass Spectrum of Biosynthesized *N*-(4-Fluorobenzoyl)-10-deacetyl-*N*-debenzoylpaclitaxel.

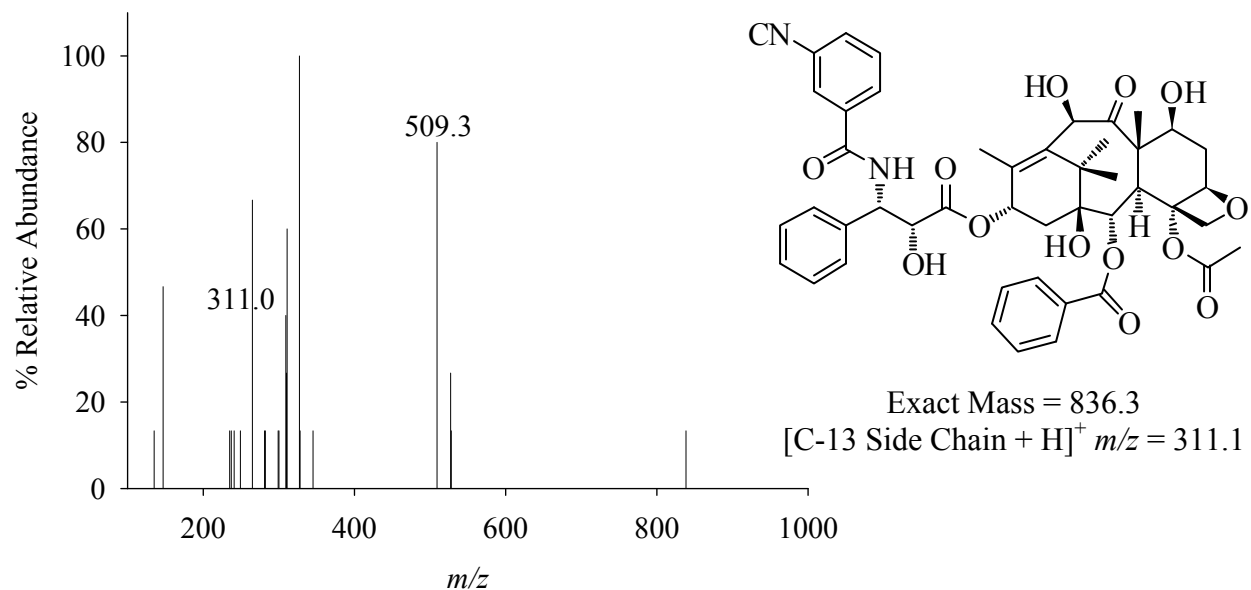


Figure B.27 – Tandem Mass Spectrum of Biosynthesized *N*-(3-Cyanobenzoyl)-10-deacetyl-*N*-debenzoylpaclitaxel.

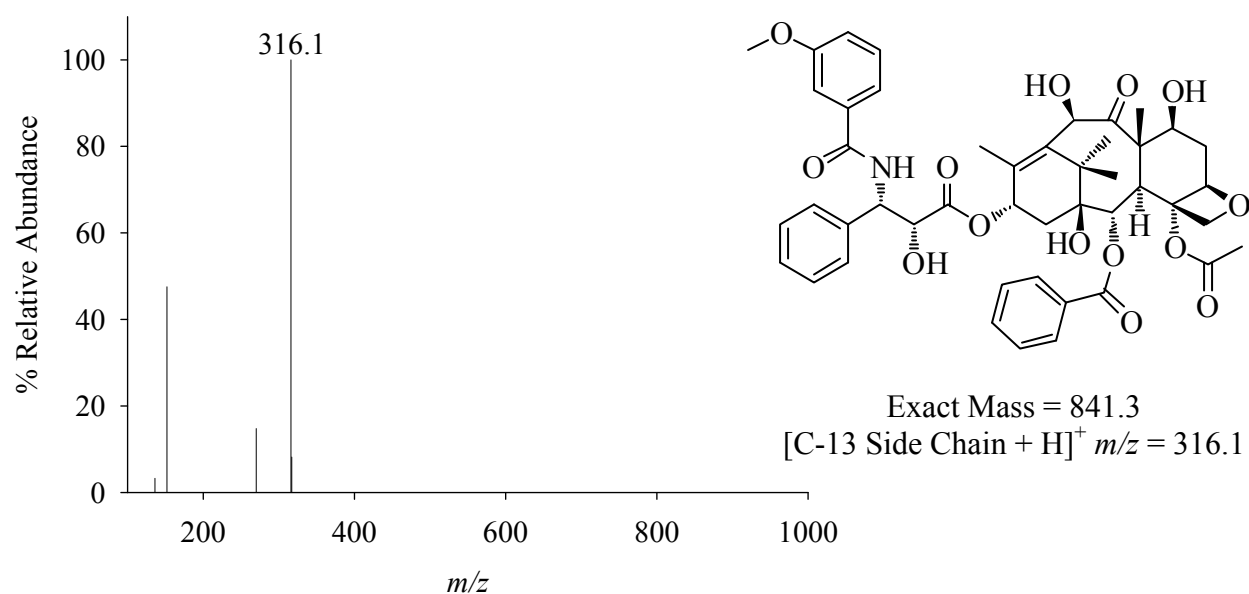


Figure B.28 – Tandem Mass Spectrum of Biosynthesized *N*-(3-Methoxybenzoyl)-10-deacetyl-*N*-debenzoylpaclitaxel.

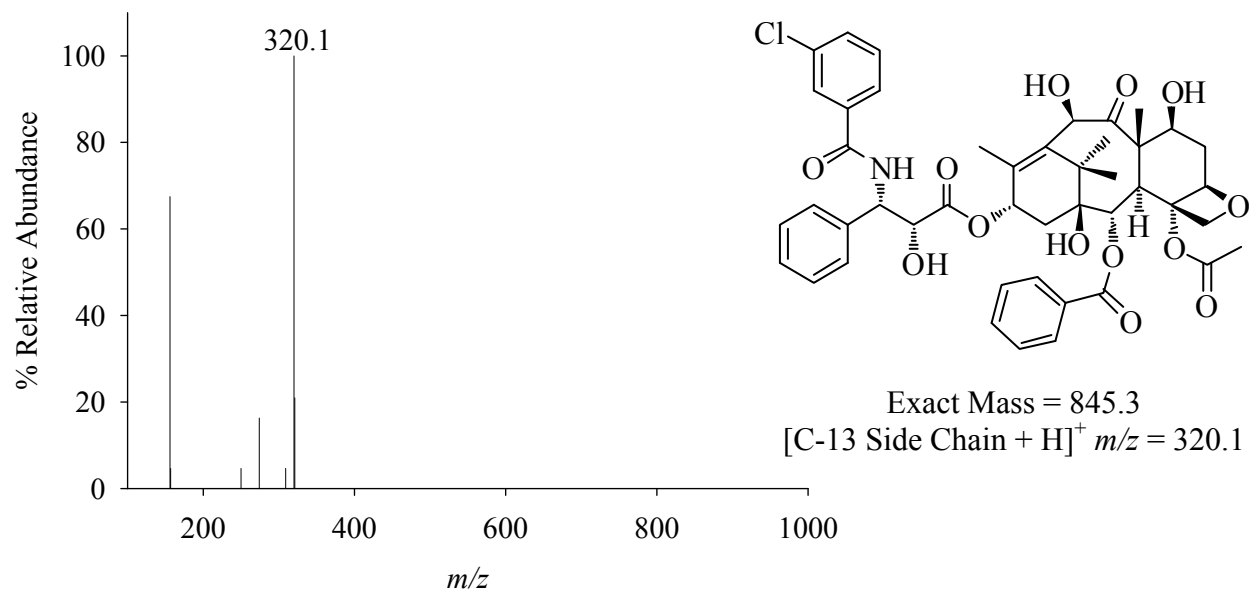


Figure B.29 – Tandem Mass Spectrum of Biosynthesized *N*-(3-Chlorobenzoyl)-10-deacetyl-*N*-debenzoylpaclitaxel.

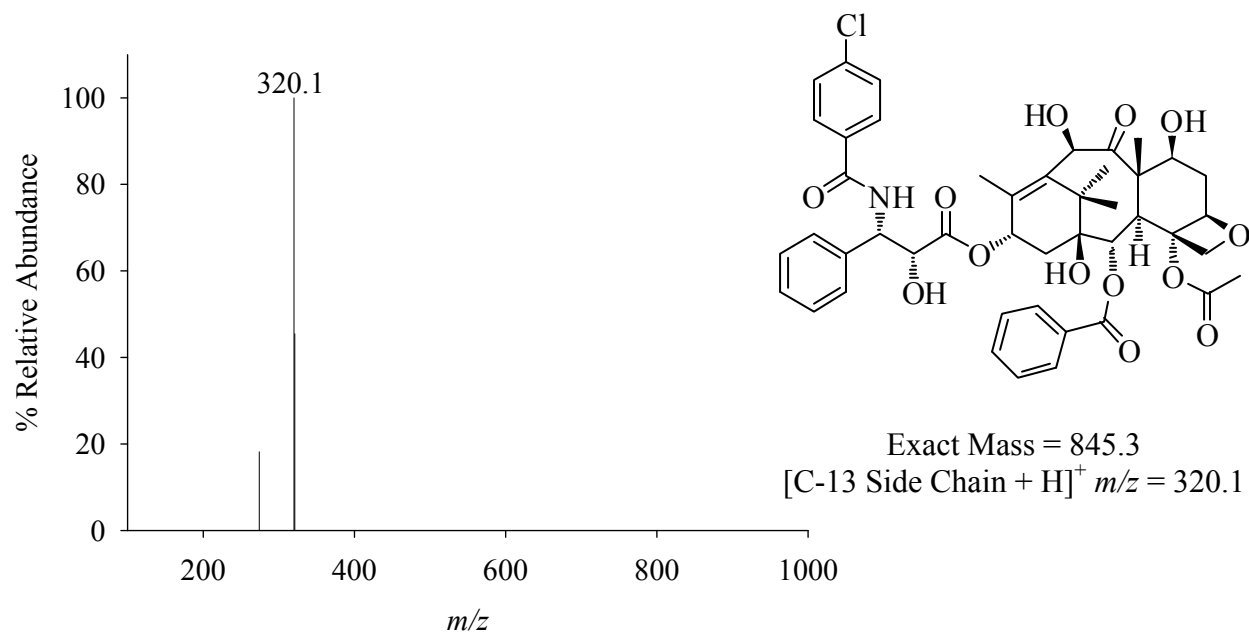


Figure B.30 – Tandem Mass Spectrum of Biosynthesized *N*-(4-Chlorobenzoyl)-10-deacetyl-*N*-debenzoylpaclitaxel.

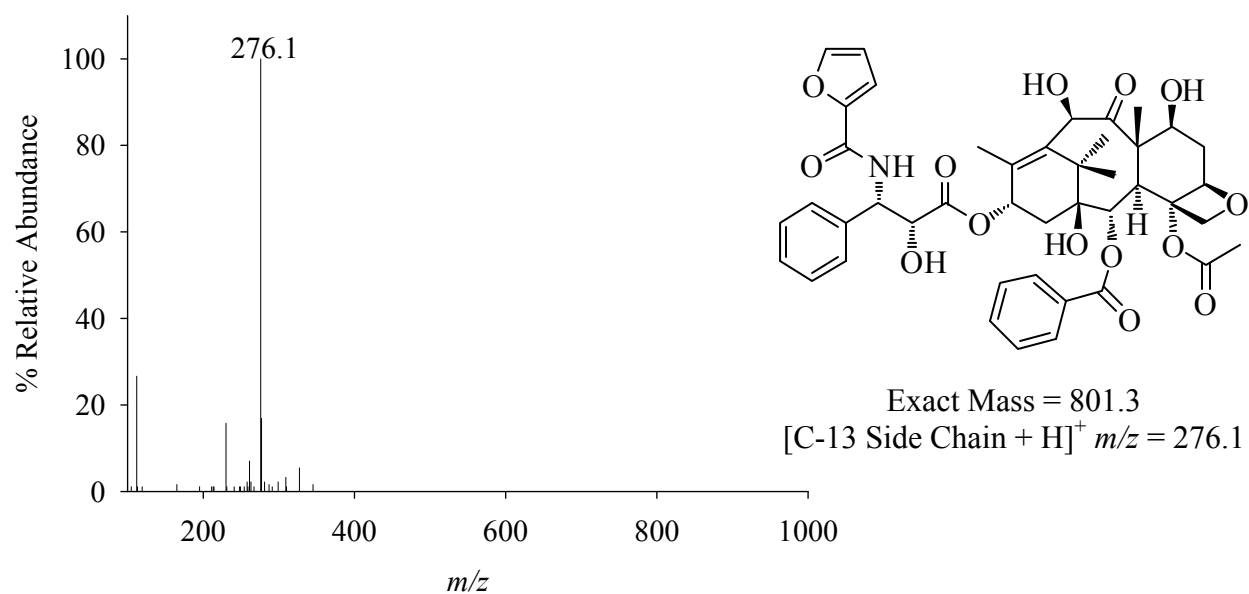


Figure B.31 – Tandem Mass Spectrum of Biosynthesized *N*-(2-Furanoyl)-10-deacetyl-*N*-debenzoylpaclitaxel.

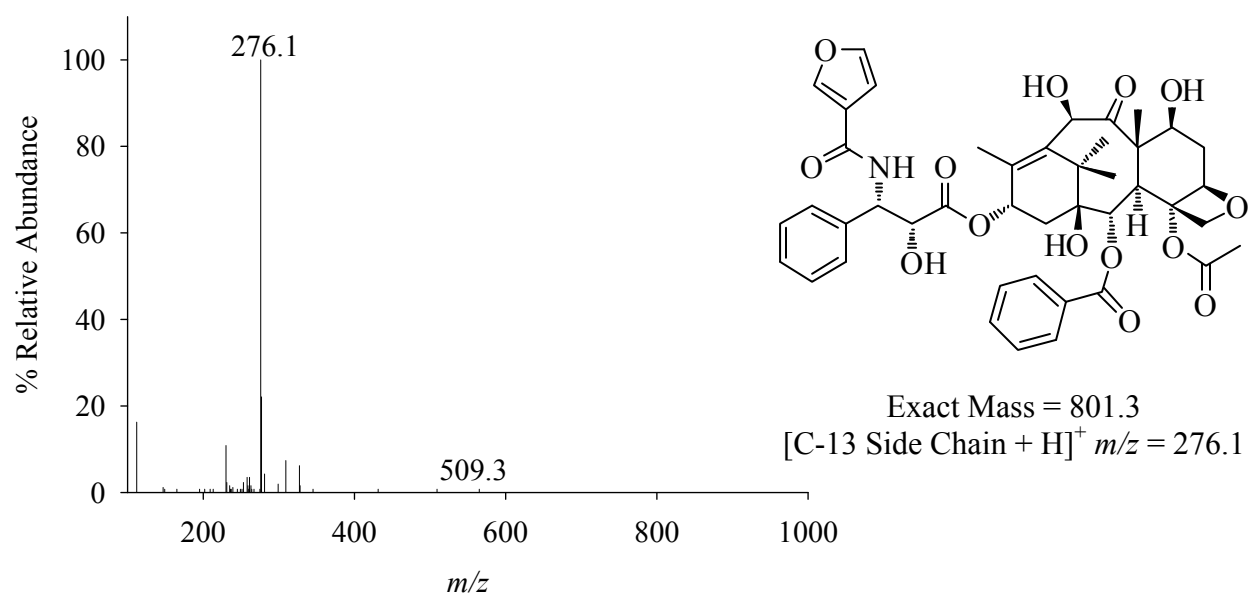


Figure B.32 – Tandem Mass Spectrum of Biosynthesized *N*-(3-Furanoyl)-10-deacetyl-*N*-debenzoylpaclitaxel.

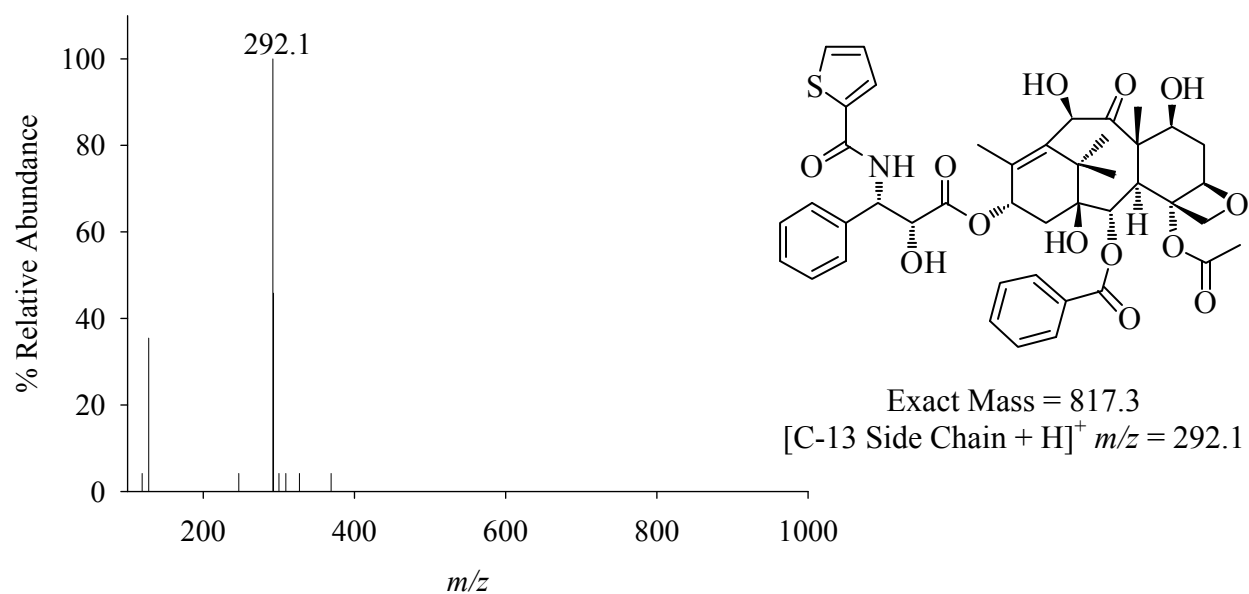


Figure B.33 – Tandem Mass Spectrum of Biosynthesized *N*-(Thiophene-2-carbonyl)-10-deacetyl-*N*-debenzoylpaclitaxel.

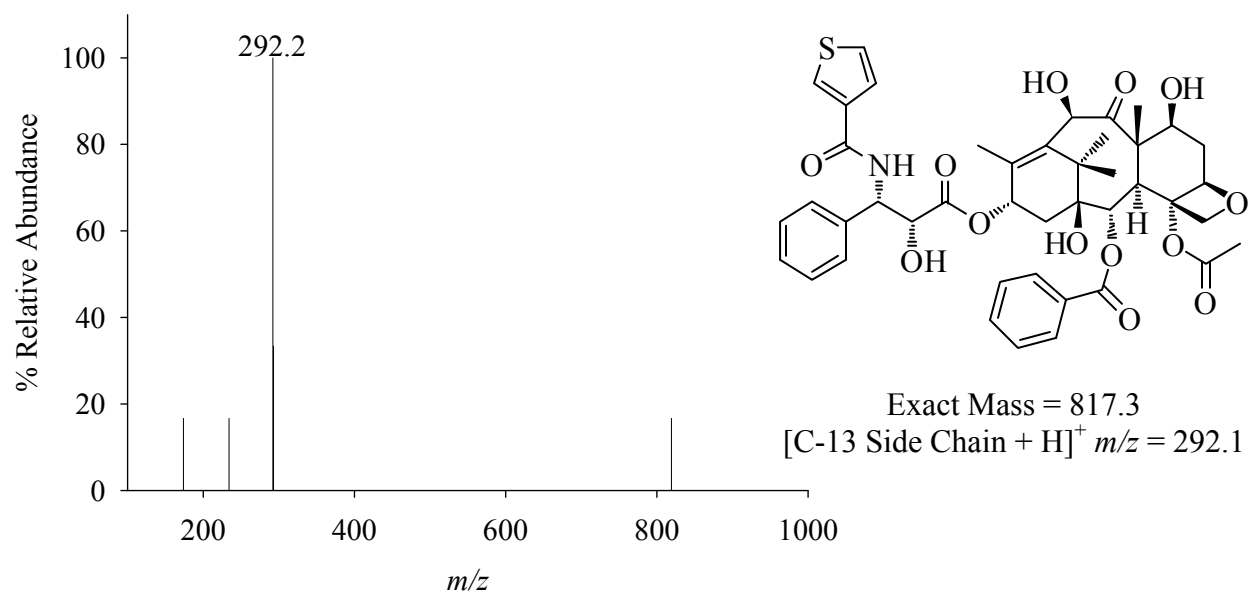


Figure B.34 – Tandem Mass Spectrum of Biosynthesized *N*-(Thiophene-3-carbonyl)-10-deacetyl-*N*-debenzoylpaclitaxel.

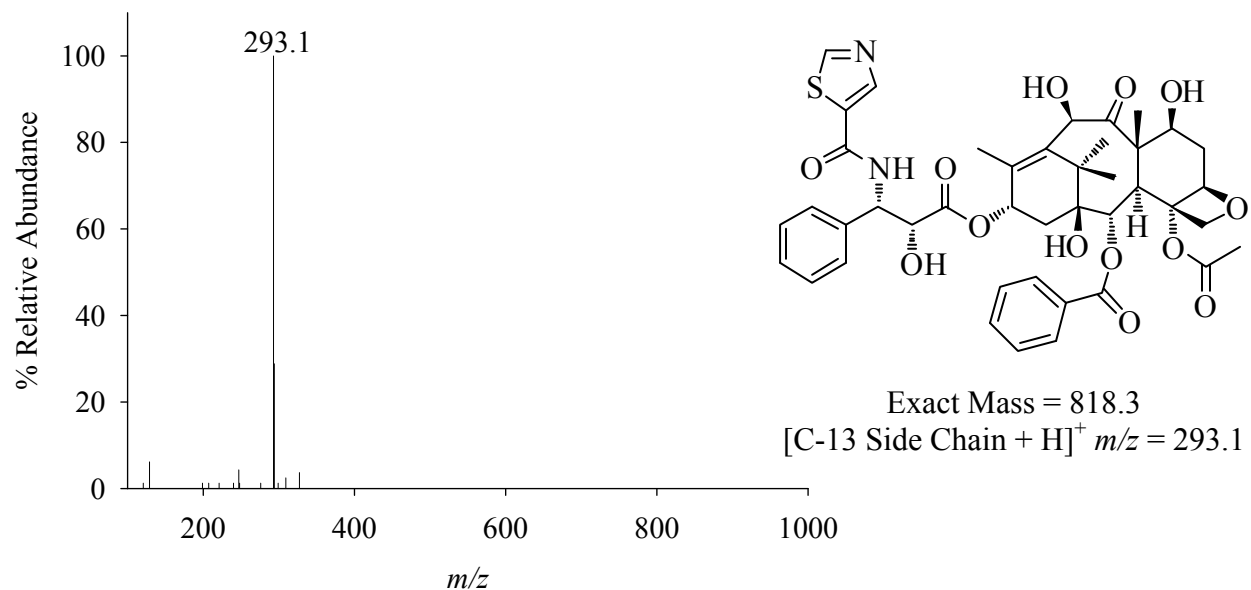


Figure B.35 – Tandem Mass Spectrum of Biosynthesized *N*-(Thiazole)-10-deacetyl-*N*-debenzoylpaclitaxel.

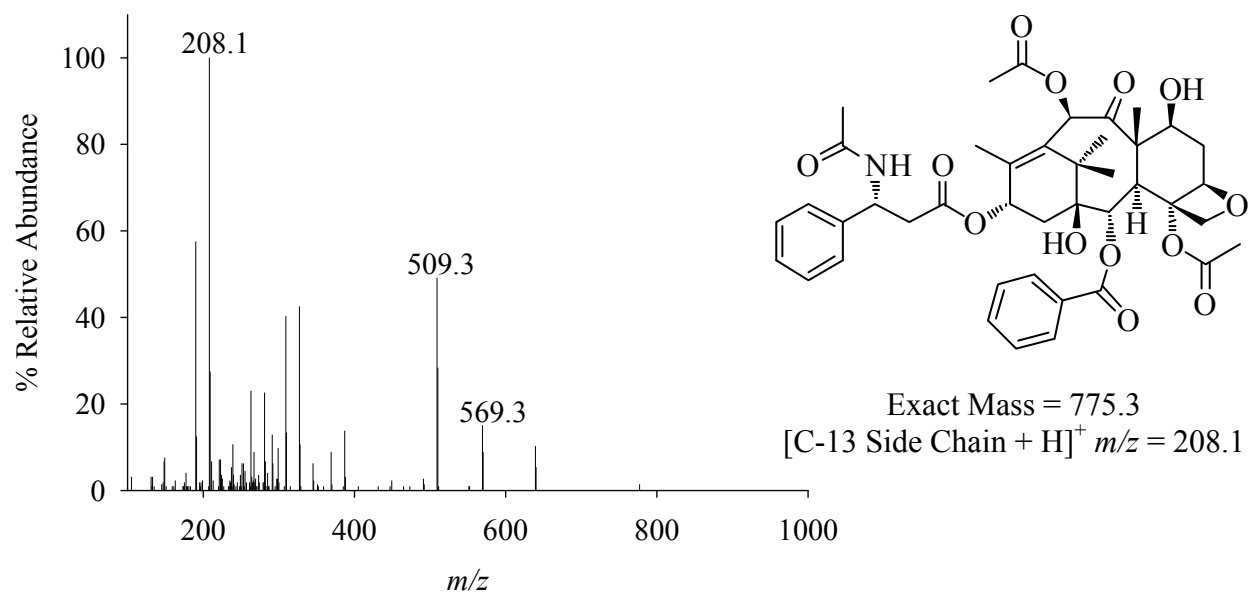


Figure B.36 – Tandem Mass Spectrum of Biosynthesized *N*-Acetyl-*N*-debenzoyl-2'-deoxypaclitaxel.

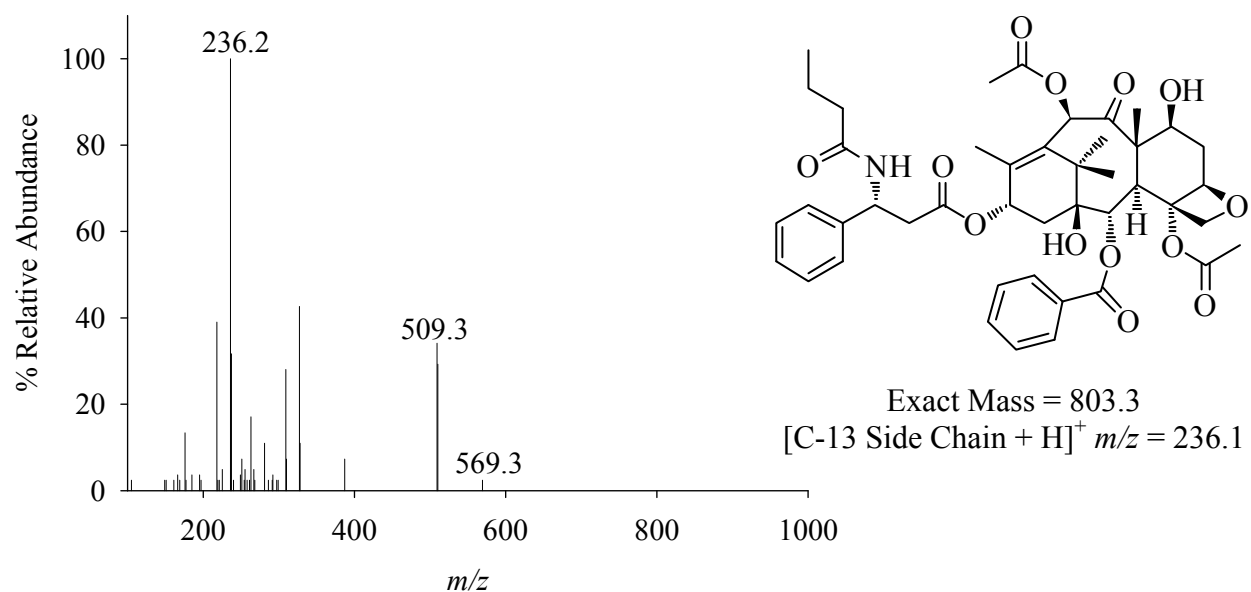


Figure B.37 – Tandem Mass Spectrum of Biosynthesized *N*-Butyryl-*N*-debenzoyl-2'-deoxypaclitaxel

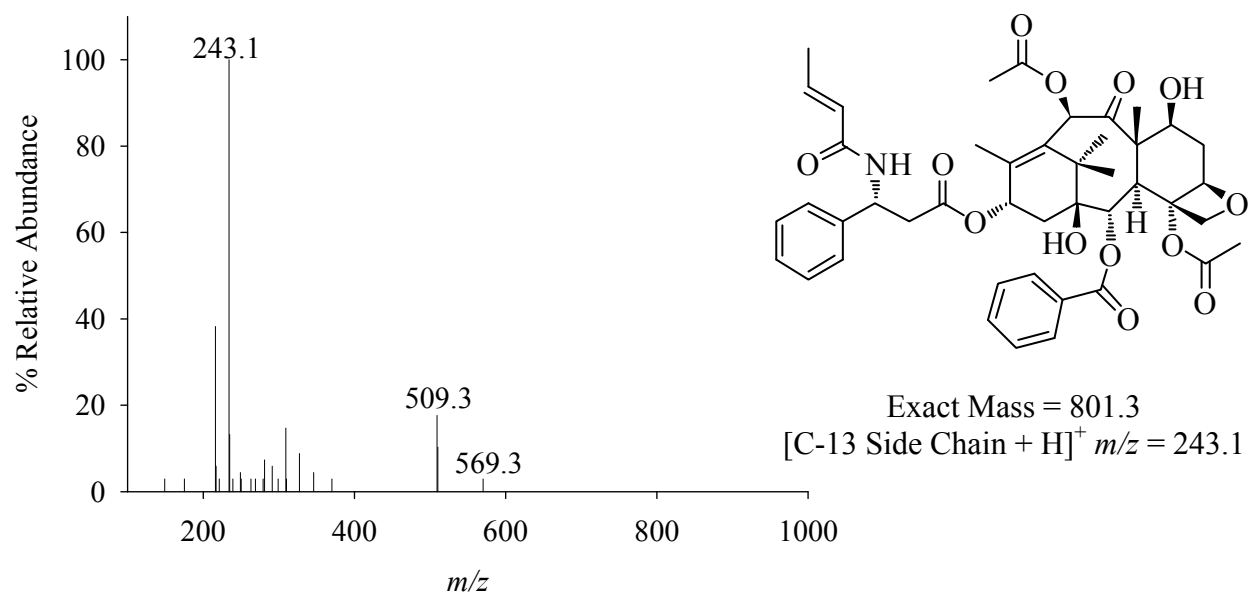


Figure B.38 – Tandem Mass Spectrum of Biosynthesized *N*-(2-Butenoyl)-*N*-debenzoyl-2'-deoxypaclitaxel

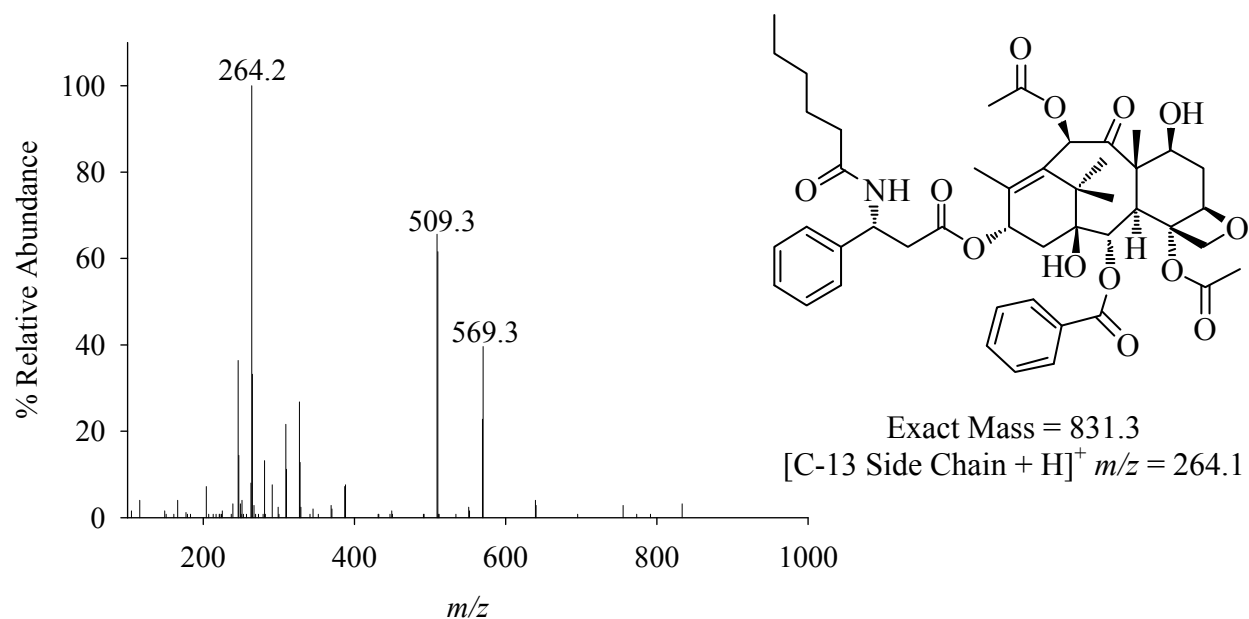


Figure B.39 – Tandem Mass Spectrum of Biosynthesized *N*-Hexanoyl-*N*-debenzoyl-2'-deoxypaclitaxel

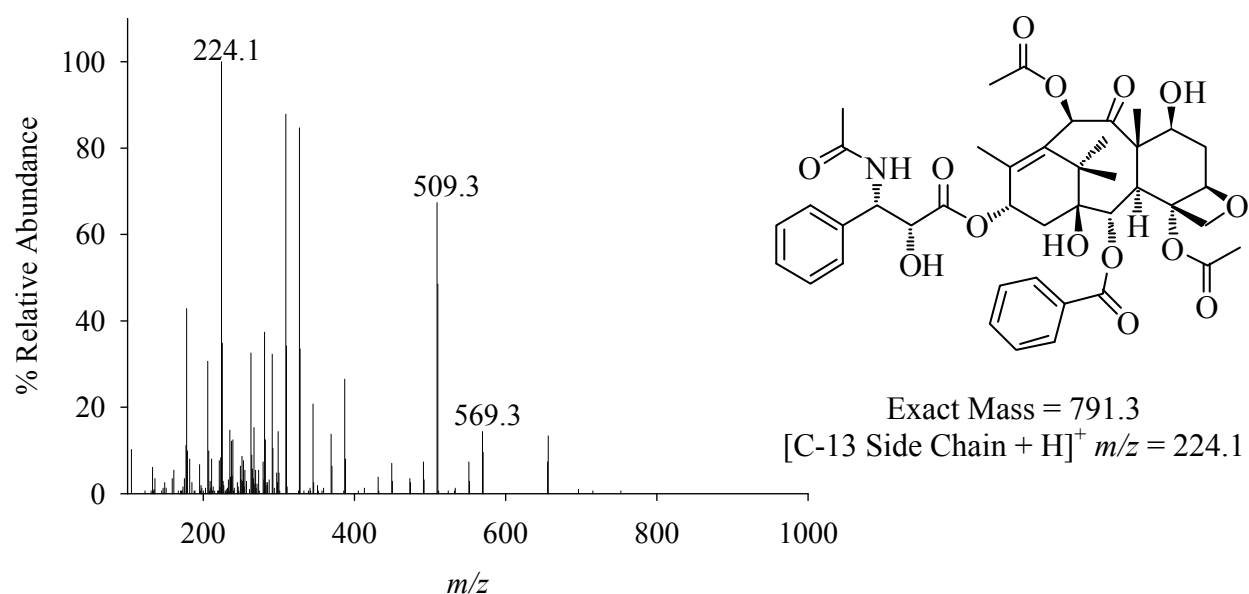


Figure B.40 – Tandem Mass Spectrum of Biosynthesized *N*-Acetyl-*N*-debenzoylpaclitaxel.

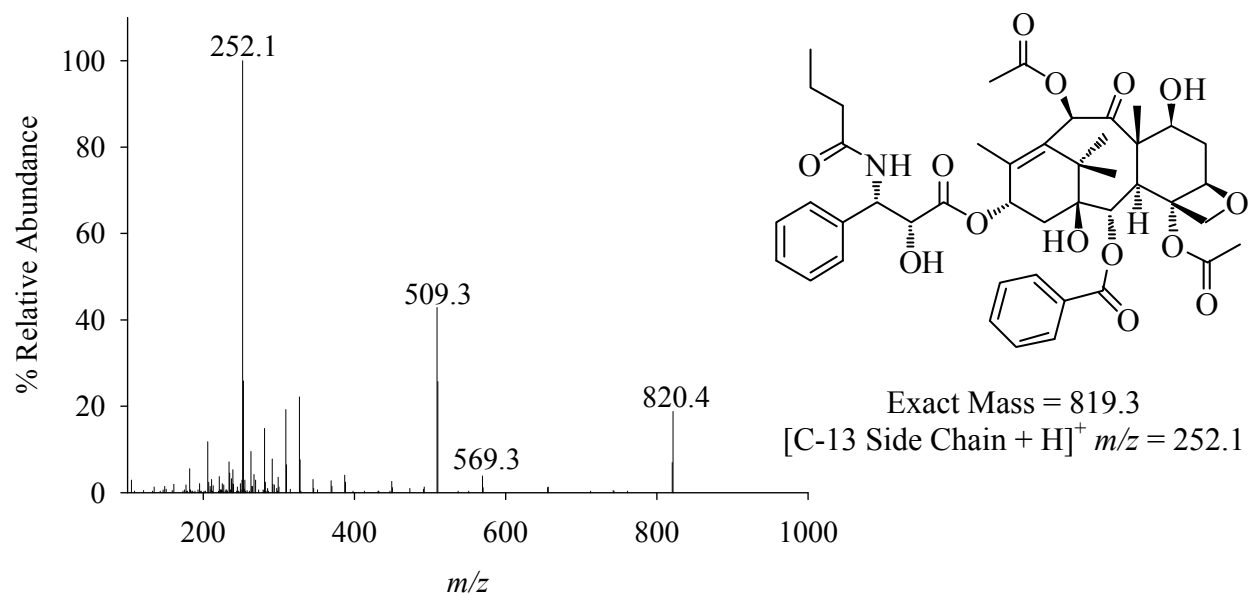


Figure B.41 – Tandem Mass Spectrum of Biosynthesized *N*-Butyryl-*N*-debenzoylpaclitaxel

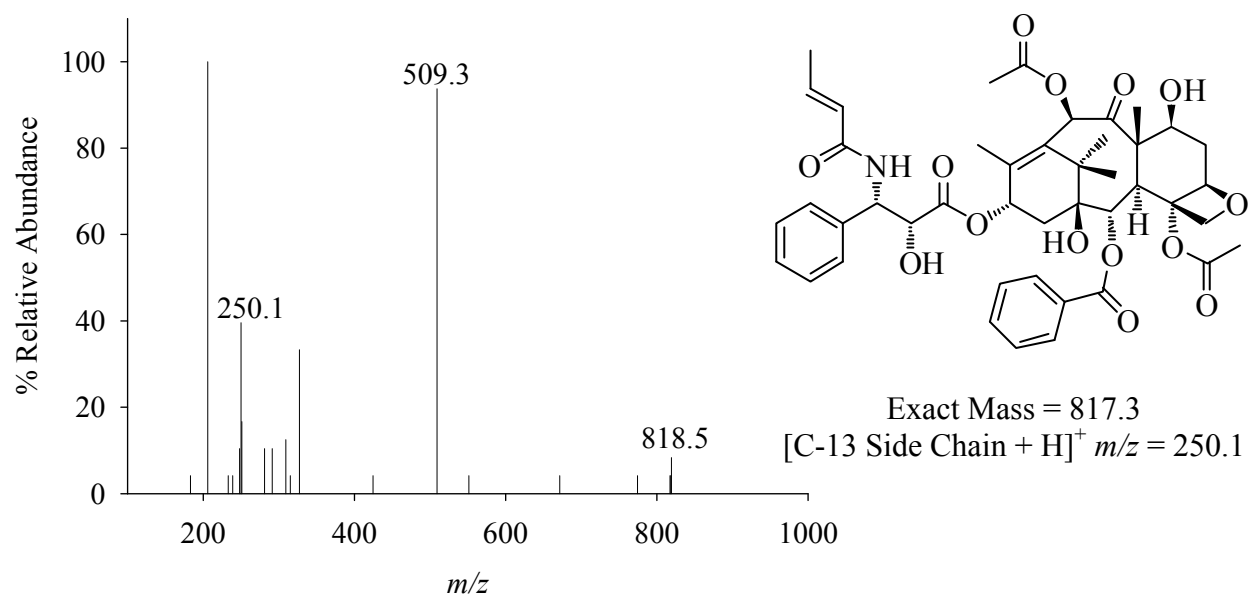


Figure B.42 – Tandem Mass Spectrum of Biosynthesized *N*-(2-Butenoyl)-*N*-debenzoylpaclitaxel

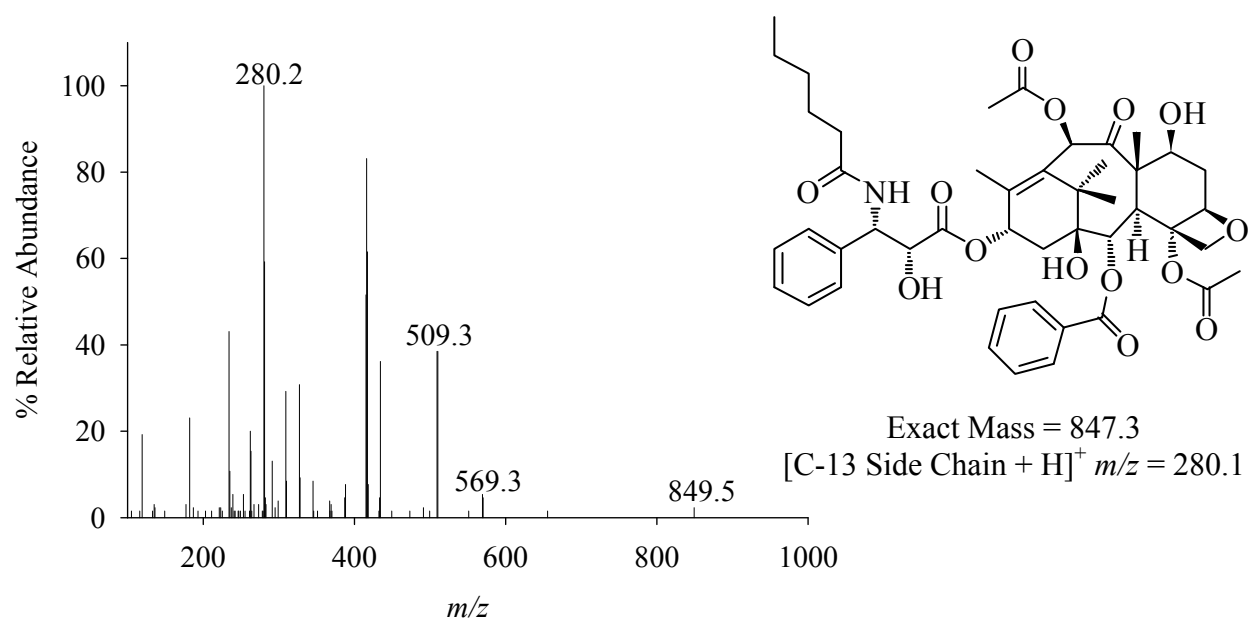


Figure B.43 – Tandem Mass Spectrum of Biosynthesized *N*-Hexanoyl-*N*-debenzoylpaclitaxel

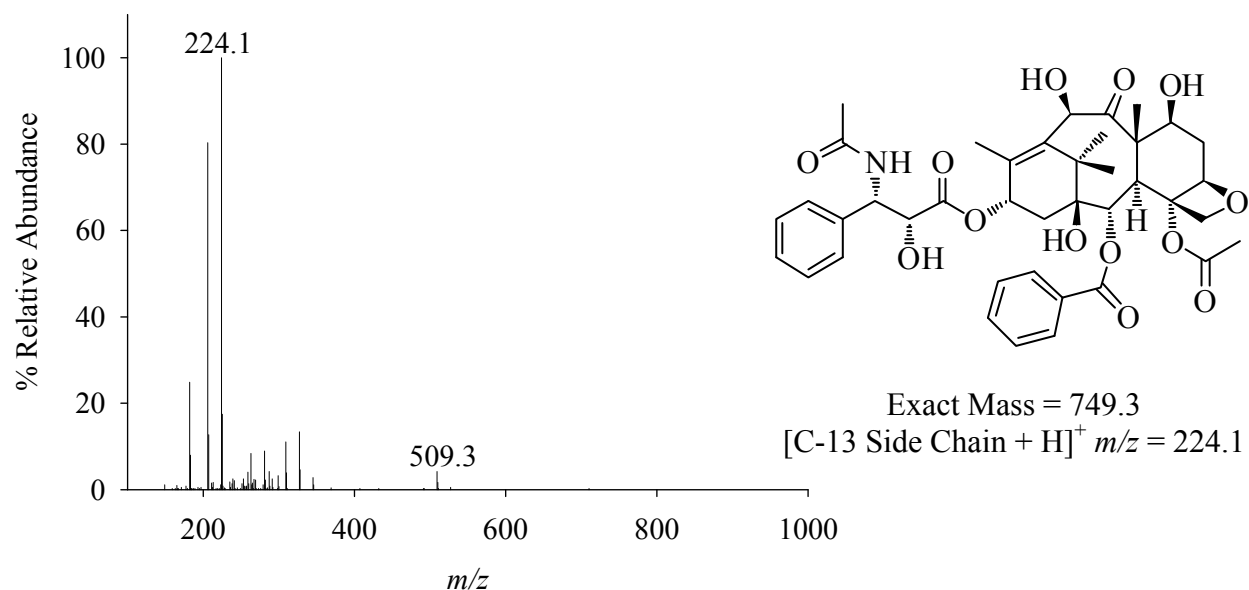


Figure B.44 – Tandem Mass Spectrum of Biosynthesized *N*-Acetyl-10-deacetyl-*N*-debenzoylpaclitaxel.

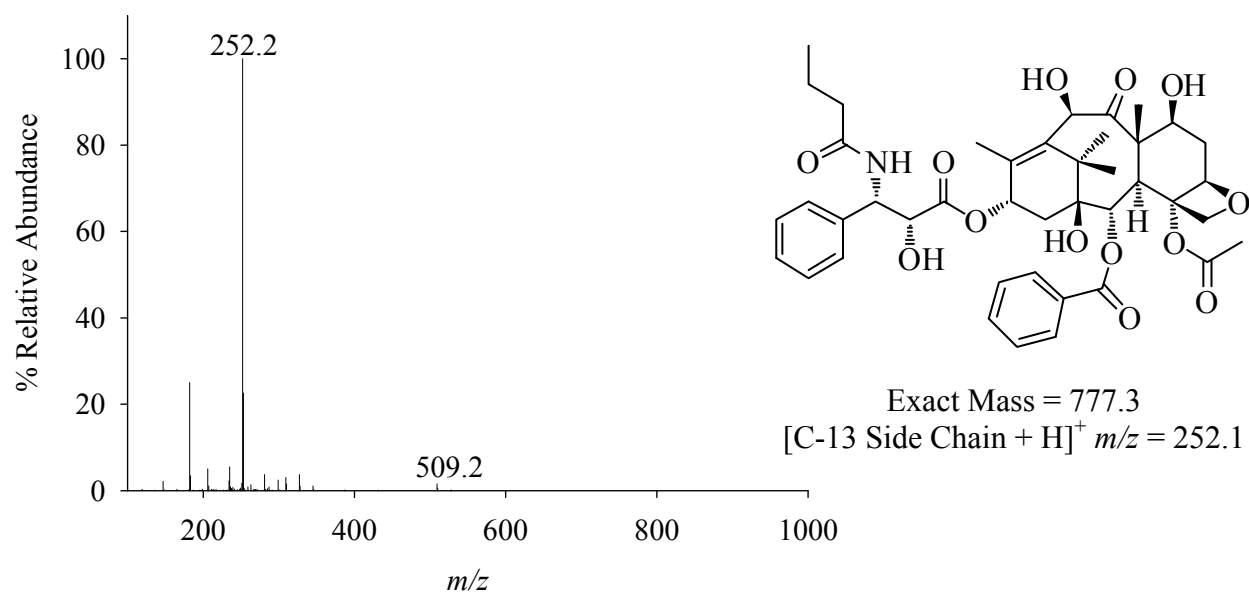


Figure B.45 – Tandem Mass Spectrum of Biosynthesized *N*-Butyryl-10-deacetyl-*N*-debenzoylpaclitaxel.

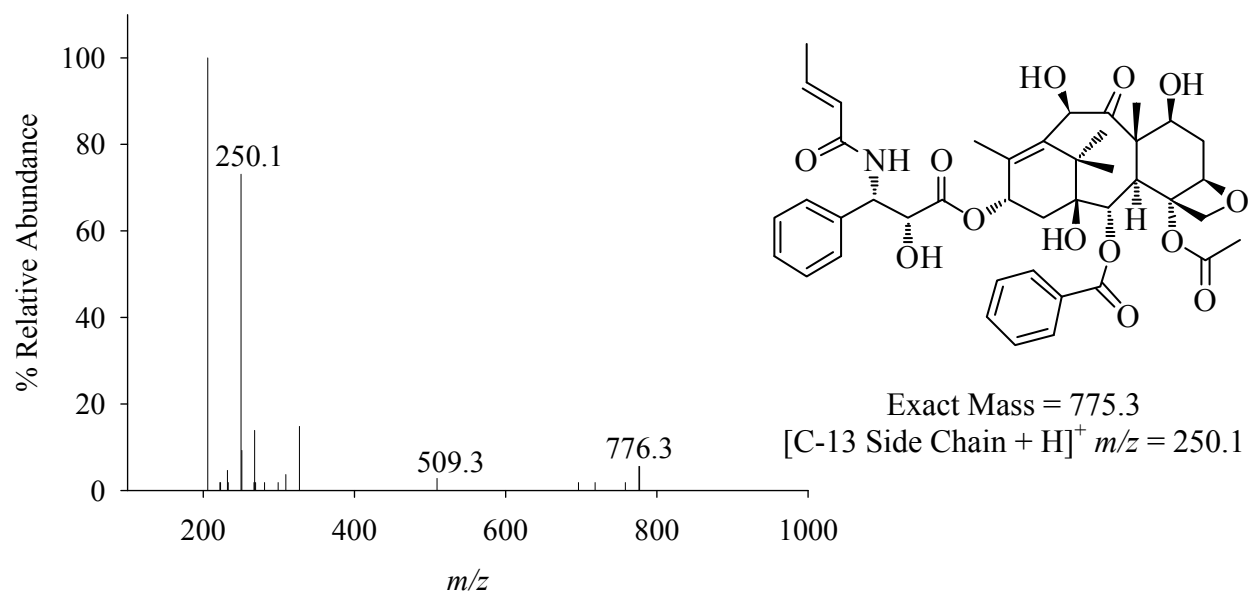


Figure B.46 – Tandem Mass Spectrum of Biosynthesized *N*-(2-Butenoyl)-10-deacetyl *N*-debenzoylpaclitaxel

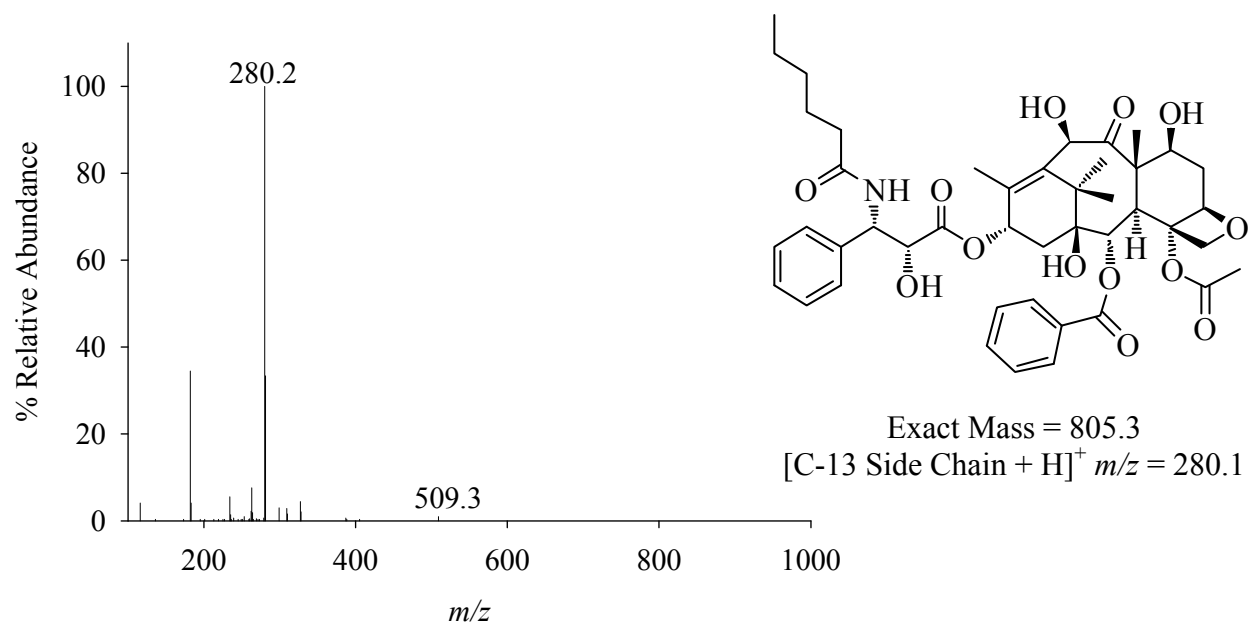


Figure B.47 – Tandem Mass Spectrum of Biosynthesized *N*-Hexanoyl-10-deacetyl *N*-debenzoylpaclitaxel

REFERENCES

REFERENCES

1. Schiff, P. B., Fant, J., and Horwitz, S. B. (1979) Promotion of microtubule assembly *in vitro* by Taxol, *Nature* 277, 665-667.
2. Hayes, D. F., Thor, A. D., Dressler, L. G., Weaver, D., Edgerton, S., Cowan, D., Broadwater, G., Goldstein, L. J., Martino, S., Ingle, J. N., Henderson, I. C., Norton, L., Winer, E. P., Hudis, C. A., Ellis, M. J., Berry, D. A., and Investigators, C. (2007) HER2 and response to paclitaxel in node-positive breast cancer, *N. Engl. J. Med.* 357, 1496-1506.
3. Weissman, N. J., Ellis, S. G., Grube, E., Dawkins, K. D., Greenberg, J. D., Mann, T., Cannon, L. A., Cambier, P. A., Fernandez, S., Mintz, G. S., Mandinov, L., Koglin, J., and Stone, G. W. (2007) Effect of the polymer-based, paclitaxel-eluting TAXUS Express stent on vascular tissue responses: a volumetric intravascular ultrasound integrated analysis from the TAXUS IV, V, and VI trials, *Eur. Heart J.* 28, 1574-1582.
4. Seyb, K. I., Ansar, S., Bean, J., and Michaelis, M. L. (2006) P-amyloid and endoplasmic reticulum stress responses in primary neurons - Effects of drugs that interact with the cytoskeleton, *J. Mol. Neurosci.* 28, 111-123.
5. Huang, Q., Kirikae, F., Kirikae, T., Pepe, A., Amin, A., Respicio, L., Slayden, R. A., Tonge, P. J., and Ojima, I. (2006) Targeting FtsZ for antituberculosis drug discovery: Noncytotoxic taxanes as novel antituberculosis agents, *J. Med. Chem.* 49, 463-466.
6. Kingston, D. G. I. (2000) Recent advances in the chemistry of Taxol, *J. Nat. Prod.* 63, 726-734.
7. Ganesh, T., Norris, A., Sharma, S., Bane, S., Alcaraz, A. A., Snyder, J. P., and Kingston, D. G. I. (2006) Design, synthesis, and bioactivity of simplified paclitaxel analogs based on the T-Taxol bioactive conformation, *Bioorg. Med. Chem.* 14, 3447-3454.
8. Kingston, D. G. I., Bane, S., and Snyder, J. P. (2004) The taxol pharmacophore and the T-taxol bridging principle, *Cell Cycle* 4, 279-289.
9. Ojima, I., Fumero-Oderda, C. L., Kuduk, S. D., Ma, Z., Kirikae, F., and Kirikae, T. (2003) Structure-activity relationship study of taxoids for their ability to activate murine macrophages as well as inhibit the growth of macrophage-like cells, *Bioorg. Med. Chem.* 11, 2867-2888.
10. Baloglu, E., Hoch, J. M., Chatterjee, S. K., Ravindra, R., Bane, S., and Kingston, D. G. I. (2003) Synthesis and biological evaluation of C-3'NH/C-10 and C-2/C-10 modified paclitaxel analogues, *Bioorg. Med. Chem.* 11, 1557-1568.

11. Kingston, D. G. I., Jagtap, P. G., Yuan, H., and Samala, L. (2002) The Chemistry of Taxol and Related Taxoids, In *Progress in the Chemistry of Organic Natural Products* (Herz, W., Falk, H., and Kirby, G. W., Eds.), pp 53-225, Springer-Verlag Wien, New York.
12. Roh, E. J., Song, C. E., Kim, D., Pae, H. O., Chung, H. T., Lee, K. S., Chai, K., Lee, C. O., and Un Choi, S. (1999) Synthesis and biology of 3'-N-acyl-N-debenzoylpaclitaxel analogues, *Bioorg. Med. Chem.* 7, 2115-2119.
13. Xue, M., Long, B. H., Fairchild, C., Johnston, K., Rose, W. C., Kadow, J. F., Vyas, D. M., and Chen, S. H. (2000) Structure-activity relationships study at the 3'-N position of paclitaxel. Part 2: Synthesis and biological evaluation of 3'-N-thiourea- and 3'-N-thiocarbamate-bearing paclitaxel analogues, *Bioorg. Med. Chem. Lett.* 10, 1327-1331.
14. Ganesh, T., Yang, C., Norris, A., Glass, T., Bane, S., Ravindra, R., Banerjee, A., Metaferia, B., Thomas, S. L., Giannakakou, P., Alcaraz, A. A., Lakdawala, A. S., Snyder, J. P., and Kingston, D. G. I. (2007) Evaluation of the tubulin-bound paclitaxel conformation: Synthesis, biology, and SAR studies of C-4 to C-3 ' bridged paclitaxel analogues, *J. Med. Chem.* 50, 713-725.
15. Kingston, D. G. I., Ganesh, T., Snyder, J. P., Lakdawala, A. S., and Bane, S. (2005) Preparation of conformationally constrained paclitaxel analogs as anticancer and anti-Alzheimer's agents, p pp. 78, Virginia Tech Intellectual Properties, Inc., USA.
16. McChesney, J. D., Venkataraman, S. K., and Henri, J. T. (2007) Plant natural products: Back to the future or into extinction?, *Phytochemistry* 68, 2015-2022.
17. Jennewein, S., Wildung, M. R., Chau, M., Walker, K., and Croteau, R. (2004) Random sequencing of an induced *Taxus* cell cDNA library for identification of clones involved in Taxol biosynthesis, *Proc. Natl. Acad. Sci. U. S. A.* 101, 9149-9154.
18. D'Auria, J. C. (2006) Acyltransferases in plants: A good time to be BAHD, *Curr. Opin. Plant Biol.* 9, 331-340.
19. St-Pierre, B., and De Luca, V. (2000) Evolution of acyltransferase genes: Origin and diversification of the BAHD superfamily of acyltransferases involved in secondary metabolism, *Recent Adv. Phytochem.* 34, 285-315.
20. Souleyre, E. J. F., Greenwood, D. R., Friel, E. N., Karunairetnam, S., and Newcomb, R. D. (2005) An alcohol acyl transferase from apple (cv. Royal Gala), MpAAT1, produces esters involved in apple fruit flavor, *FEBS J.* 272, 3132-3144.
21. Loncaric, C., Ward, A. F., and Kevin D. Walker. (2007) Expression of an acetyl-CoA synthase and a CoA-transferase in *Escherichia coli* to produce modified taxanes *in vivo*, *Biotechnol. J.* 2, 266-274.

22. Walker, K., Long, R., and Croteau, R. (2002) The final acylation step in Taxol biosynthesis: Cloning of the taxoid C13-side-chain *N*-benzoyltransferase from *Taxus*, *Proc. Natl. Acad. Sci. U. S. A.* 99, 9166-9171.
23. Long, R. M., Lagisetti, C., Coates, R. M., and Croteau, R. B. (2008) Specificity of the *N*-benzoyl transferase responsible for the last step of Taxol biosynthesis, *Arch. Biochem. Biophys.* 477, 384-389.
24. Shiina, I., Suenaga, Y., Nakano, M., and Mukaiyama, T. (2000) A convenient method for the preparations of carboxamides and peptides by using di(2-pyridyl) carbonate and *O,O'*-di(2-pyridyl) thiocarbonate as dehydrating reagents, *Bull. Chem. Soc. Japan* 73, 2811-2818.
25. Georg, G. I., Boge, T. C., Cheruvallath, Z. S., Harriman, G. C. B., Hepperle, M., Park, H., and Himes, R. H. (1994) Schotten-Baumann acylation of *N*-debenzoyltaxol; an efficient route to *N*-acyl Taxol analogs and their biological evaluation, *Bioorg. Med. Chem. Lett.* 4, 335-338.
26. Saitoh, K., Shiina, I., and Mukaiyama, T. (1998) *O,O'*-Di-2-pyridyl thiocarbonate as an efficient reagent for the preparation of carboxylic esters from highly hindered alcohols, *Chem. Lett.* 679-680.
27. Loncaric, C., Merriweather, E., and Walker, K. D. (2006) Profiling a Taxol pathway 10 β -acetyltransferase: Assessment of the specificity and the production of baccatin III by *in vivo* acetylation in *E. coli*, *Chem. Biol.* 13, 1-9.
28. Tilburg, E. W. v., Franssen, E. J. F., Hoeven, J. J. M. v. d., Meij, M. v. d., Elshove, D., Lammertsma, A. A., and Windhorst, A. D. (2004) Radiosynthesis of [¹¹C]docetaxel *J. Labelled Comp. Rad.* 47, 763-777.
29. Sambrook, J. R., D. (2001) *Molecular Cloning: A Laboratory Manual*, Cold Spring Harbor Laboratory Press.
30. Long, R. M., and Croteau, R. (2005) Preliminary assessment of the C13-side chain 2'-hydroxylase involved in Taxol biosynthesis, *Biochem. Biophys. Res. Commun.* 338, 410-417.
31. Yang, Q., Reinhard, K., Schiltz, E., and Matern, U. (1997) Characterization and heterologous expression of hydroxycinnamoyl/benzoyl- CoA:anthranilate *N*-hydroxycinnamoyl/benzoyltransferase from elicited cell cultures of carnation, *Dianthus caryophyllus* L, *Plant Mol. Biol.* 35, 777-789.
32. Firn, R. D., and Jones, C. G. (2003) Natural products - a simple model to explain chemical diversity, *Nat. Prod. Rep.* 20, 382-391.

33. D'Auria, J. C., Chen, F., and Pichersky, E. (2002) Characterization of an acyltransferase capable of synthesizing benzylbenzoate and other volatile esters in flowers and damaged leaves of *Clarkia breweri*, *Plant Physiol.* *130*, 466-476.
34. Beekwilder, J., Alvarez-Huerta, M., Neef, E., Verstappen, F. W. A., Bouwmeester, H. J., and Aharoni, A. (2004) Functional characterization of enzymes forming volatile esters from strawberry and banana, *Plant Physiol.* *135*, 1865-1878.
35. Kingston, D. (1995) In *Taxol: Science and Applications* (Suffness, M., Ed.), pp 287-315, CRC Press, Boca Raton, FL.

CHAPTER 3

PROTEIN PURIFICATION OF *TAXUS* ACYLTRANSFERASES FOR PRELIMINARY CRYSTAL STRUCTURE ANALYSIS

3.1. Introduction

As mentioned previously in Chapter 1, *Taxus* acyltransferases belong to an enzyme superfamily called BAHD, which is the acronym for the first four plant-derived members, including BEAT: benzylalcohol *O*-acetyltransferase from *Clarkia breweri*; AHCT: anthocyanin *O*-hydroxycinnamoyltransferases from *Petunia*; HCBT: anthranilate *N*-hydroxycinnamoyl/benzoyltransferase from *Dianthus caryophyllus*; DAT: deacetylvindoline 4-*O*-acetyltransferase from *Catharanthus roseus*).¹ These members use an acyl coenzyme A as a substrate to transfer the alkyl/aroyl group to an acceptor hydroxyl or amino group of a co-substrate. Although these enzymes participate in secondary metabolite biosynthesis in plants, their products can provide functions ranging from phenotypic advantages for reproduction to defense mechanisms.²⁻⁴

The first identified member of this family is a benzylalcohol acetyltransferase, designated BEAT, produces acetylated precursors that are responsible for floral scent in *C. breweri*.⁵ A malonyltransferase, found in the anthocyanin biosynthetic pathway in scarlet sage (*Salvia splendens*) flowers, gives rise to compounds responsible for floral pigmentation whose colors range from red to blue.³ BAHD members were also identified to catalyze steps on the pathway to phytoalexins used to defend the plant against specific pathogens.⁴ Other members are characterized as catalyzing important steps leading to precursors or end products identified

fortuitously as medicinal compounds, such as vincleucoblastine and vincristine from *Catharanthus roseus* and morphine from *Papaver somniferum*.⁶⁻⁸

Most members of the BAHD family contain conserved amino acids, a catalytic diad HXXXD and a DFGWG sequence near the C-terminus thought to join in preserving the enzyme structure.⁹ Earlier mutagenesis studies demonstrated that the catalytic histidine is essential for function and that alteration of the structural motif resulted in decreased activity.¹⁰⁻¹² The BAHD family sorts into clades according to phylogenetic analysis, which reveals other conserved secondary motifs.^{9, 13} Of the 5 distinct clades, the *Taxus* acyltransferases belong to clade 5, which is the only clade that contains benzoyl transferases, and whose sequences share a GYYGN motif.⁹ The benzoyltransferases from *Taxus* *N*-debenzoyl-2'-deoxypaclitaxel:*N*-benzoyltransferase (NDTBT) (described in this dissertation) and a modified taxane-2 α -*O*-benzoyltransferase (described elsewhere¹⁴) use an array of aroyl- and alkyl CoA substrates with three *N*-debenzoylated taxane analogues (cf. Chapter 2) and several different 2-debenzoyl taxanes, respectively, indicating their broad substrate specificity.^{14, 15} The *Taxus* 10-deacetylbaccatin III: 10 β -*O*-acetyltransferase (DBAT) was able to catalyze the transfer of acetyl, propionyl, and *n*-butyryl to the C10 hydroxyl group of 10-deacetylbaccatin III and docetaxel (cf. Chapter 1, Figures – 1.4 and 1.7 for structure).¹⁶ Surprisingly, DBAT could also transfer an acetyl group to the C4 hydroxyl of 4-deacetylbaccatin III.¹⁷

Homology-based structural analysis is one strategy used to model an enzyme active site and identify crucial residues or structural motifs responsible for substrate binding, catalytic

activity, and substrate specificity. However, the accuracy of a homology model is dependent on the sequence identity between the reference-template sequence and the sequence whose structure is unknown. Alignment errors are more prevalent when the identity is below 30% due to mis- or non-aligned stretches of sequence that results in unguided folding assignments.¹⁸ These errors include distortions of core segments as well as side-chain packing. Therefore, a bona fide crystal structure of NDTBT would better inform about the active site topology over that of a modeled structure and, moreover, would provide a solid basis for rational mutation strategies.

Vinorine synthase from *Rauvolfia serpentina* (VS) and anthocyanin malonyltransferase from *Dendranthema morifolium* (Dm3MaT) are the only acyltransferases from the BAHD family with crystal structure data.^{10, 19} Their structures show they are comprised of two domains connected by a loop region, and a substrate-access channel connecting the binding site of the acceptor substrate to that of the acyl CoA donor.¹⁹ Additional mutagenesis studies on the malonyltransferase identified key residues responsible for substrate selectivity.¹⁰ Successful crystallization of NDTBT would provide another candidate to compare with the known structures in the BAHD family.

The art of crystallizing an enzyme is dependent on the size of the protein, its solubility, its tertiary and quaternary structure, and its purity.²⁰ Protein at greater than 90% purity is essential for success in crystallographic studies, although crystallization has been observed for protein at between 80% to 90% purity. The purity of NDTBT was obtained at 70% in previous attempts for the study described herein. Alternatively, several chromatographic methods were applied to obtain NDTBT at >95% purity, without losing activity. Once the purification

milestone was achieved, NDTBT was added to screening boxes containing a matrix of variable crystallization conditions.

3.2. Materials and Methods

3.2.1. Substrates and Plasmids

Baccatin III and 10-deacetylbaccatin III (10-DAB) were purchased from Natland Corp. (Research Triangle Park, NC). Acetyl- and benzoyl-coenzyme A thioesters were obtained from Sigma-Aldrich. The 7,13-diacetylbaccatin III and 7,13-deacetyl-10-debenzoylbaccatin III were synthesized by Irosha Nawarathne and obtained from laboratory stocks. N-Terminal DBAT and N-terminal *m*TBT were available from laboratory stock.

3.2.2. Genetic Manipulations

All protocols pertaining to genetic manipulation can be found in Chapter 2 Materials and Methods section. Any variations to previously described methods are listed in this section.

3.2.2.1. Customized Primers

Primers were created to amplify the *ndtbt*, *dbat*, and *mtbt* cDNAs an insert restriction enzyme cut-sites flanking the genes for sub-cloning into pET28a vector (Novagen). The *Nco*I cut site (5'-CCATGG-3') was at the 5'-terminus, while the *Bam*HI cut site (5'-GGATCC-3') was at the 3'-terminus of the full-length cDNA. Other primers were made for incorporating internal mutations and a generic set was designed for DNA sequence applications. Custom primers were ordered from the Macromolecular Structure, Sequencing and Synthesis Facility (MSSSF)

(Michigan State University, East Lansing, MI) using the Applied Biosystems 3948 DNA Synthesis and Purification System. All the primers used in this section are listed in Table 3.1.

3.2.2.2. Polymerase Chain Reaction Protocol

A general subcloning procedure was conducted as follows: in a 50- μ L reaction were added 10X buffer (5 μ L), 10 mM dNTP mixture (1 μ L), forward primer (1 μ L of a 20 pmol/ μ L solution), reverse primer (1 μ L of a 20 pmol/ μ L solution), 100 ng plasmid DNA, Turbo *Pfu* DNA polymerase (1 μ L), and ddH₂O to bring the volume to 50 μ L. A PTC-100 Programmable Thermal Controller (MJ Research, Inc.) was used with this program: dwell at 94 °C for 2 min, and then cycle at 94 °C for 45 s, between 48-54 °C (exact temperature determined empirically) for 30 s, 72 °C for 1 min/kb of template sequence, cycled 25-35 times (determined empirically), with an extension temperature of 72 °C for 5 min and a final 4 °C hold. The annealing temperature was 4 °C less than the melting temperature (T_m) of the primers used, and the elongation rate (1 min/kilobase) was dependent upon amplicon size.

3.2.2.2. Sub-cloning for C-terminal His₆-tag Inserts

All the following constructs were sequence verified and the primer sequences can be found in Table 3.1.

3.2.2.2.1. *Construction of NDTBT-CT Insert*

To facilitate sub-cloning, an internal *Nco*I restriction site was altered with the following primer sets – pair 1: For*Nco*I (RED) and RevKON*Nco*I primers were used to insert a *Nco*I site

Table 3.1 – Custom Primer Sequences

Name	5' → 3' Sequence	Application
F10-1	ATGGAGAAGGCAGGCTCAAC	Seq
F10-2	TTGGCATCCATTGGACACTGC	Seq
F10-3	TGGATAGCACGGACAAAGGC	Seq
F10-4	CTTTTCTATACCTACTACCTGCC	Seq
R10-A	CAACACCTTGGAGAGAGCC	Seq
R10-B	AGATGTAGAGGGTCTTCAGG	Seq
R10-C	GGGTTTGTAACCTACCCTTGACC	Seq
R10-D	TCACACTTTACTTACATATTTCTCTATC	Seq
<i>Bam</i> HI-NS	CTCGAGCGGATCCACTTTACTTAC	Sub
T7 promoter	TAATACGACTCACTATAGGG	Sub/Seq
T7 terminator	GCTAGTTATTGCTCAGCGG	Sub/Seq
For <i>Nco</i> I (RED)	GCAGATATACCATGGAGAAGGC	Sub
ForKO- <i>Nco</i> I	GTTTGTGGAAGCTATGGTGAAG	Mut
RevKO- <i>Nco</i> I	CTTCCACCATAGCTTCCACAAAC	Mut
R06-A	AGTCATCCAAATCTCCTAAGACTG	Seq
R06-B	CGGTATAAAGGGTCTTCCGG	Seq
R06-C	TATCCATTGCACATACGGTACC	Seq
R06-D	CACGAGACTTACATTATCTGCATG	Seq
F06-1	TGCCTCAGACAGAGTTTCCG	Seq
F06-2	CAGGTAACCTCGTTTTACATGTGG	Seq
F06-3	GCTCTGCGTTCGAAGTTGTATC	Seq
F06-4	CATAGTTGGATTTGGTGATCGAAG	Seq
T6NCO-311F	GTGGAAGCAATGGCTGACAC	Mut
T6NCO-311R	GTGTCAGCCATTGCTTCCAC	Mut
T6NCO-483F	GAGTTTCTGCCACGGTATATGTG	Mut
T6NCO-483R	CACATATACCGTGGCAGAACTC	Mut
T6NCO-527F	CTTATAGCTATGGGAGAGATGGC	Mut
T6NCO-527R	GCCATCTCTCCCATAGCTATAAG	Mut
RBNST6	AATTAACGGATCCCCAGGCTTAGTTAC	Sub
FNCOT6	TATAGCACCATGGCAGGCTCAAC	Sub
R02-A	CTG AAA TGC TGG ATC GTA CTC ATT G	Seq
R02-B	GCT ACT ACA ACT TCG AAC GCA G	Seq
R02-C	GCA TGG GGC TTA CAT TCA CTG	Seq
F02-1	GGC AGG TTC AAT GTA GAT ATG ATT G	Seq
F02-2	GGA ATC GGC CAG TTA CTT AAA G	Seq
F02-3	GCA ATG GAT AAT GTC AAA GAC CTC	Seq
FN <i>Nco</i> I-2	TATAGCACCATGGGCAGGTTC	Sub
F2-A/B	TTTGTGGAAGCAATGGCTGAC	Mut
R2-A/B	GTCAGCCATTGCTTCCACAAA	Mut
RBHNS-2	AATTAAAGGATCCCCTAACTTAGAGTT	Sub
Sub – sub-cloning; Seq – sequencing; Mut – mutations		

upstream of the *ndtbt* cDNA and remove the internal *NcoI* site, respectively; pair 2: ForKO-*NcoI* and *BamHI*-NS primer were used to remove the wild-type stop codon yet kept the cDNA in-frame with the C-terminal polyhistidine tag and terminal stop codon encoded on the vector. Primer pairs 1 and 2 were used separately to amplify the *ndtbt* cDNA, and then equal amounts were mixed in a PCR reaction with the For*NcoI* (RED) primer and *BamHI*-NS primer creating a full length insert for directional ligation using *NcoI* and *BamHI*.

3.2.2.2.2. Construction of DBAT-CT Insert

To facilitate sub-cloning of the *dbat* cDNA, install a 5'-terminal *NcoI* site and remove three internal *NcoI* restriction sites (311, 483, and 527 base pair from the beginning) the following primer sets were used. To install the 5'-terminal *NcoI* site and remove the *NcoI* site beginning at base pair 311 from the start codon – pair 1: FNCOT6 primer (inserted a *NcoI* site upstream of the *dbat* cDNA) and T6NCO-311R primer (removed the internal *NcoI* site); pair 2: T6NCO-311F primer and RBNST6 primer, removed the wild-type stop codon yet kept the cDNA in-frame with the C-terminal polyhistidine tag and terminal stop codon encoded on the vector. Primer pairs 1 and 2 were used separately to amplify the *ndtbt* cDNA, and then equal amounts were mixed in a PCR reaction with the FNCOT6 primer and RBNST6 primer creating a full length insert for the next mutation.

NcoI 483 Site (located 483 base pairs from the start codon) was removed with the following primer pairs – pair 1: FNCOT6 primer and T6NCO-483R primer; pair 2: T6NCO-483F primer and RBNST6 primer. Primer pairs 1 and 2 were used separately to amplify the *ndtbt* cDNA, and then equal amounts were mixed in a PCR reaction with the FNCOT6 primer and RBNST6 primer creating a full length insert for the next mutation.

NcoI 527 Site (located 527 base pairs from the start codon) – pair 1: FNCOT6 primer and T6NCO-527R primer; pair 2: T6NCO-527F primer and RBNST6 primer. Primer pairs 1 and 2 were used separately to amplify the *ndtbt* cDNA, and then equal amounts were mixed in a PCR reaction with the FNCOT6 primer and RBNST6 primer creating a full length insert for directional ligation using *NcoI* and *BamHI*.

3.2.2.2.3. Construction of *mTBT-CT* Insert

To facilitate sub-cloning, an internal *NcoI* restriction site was altered with the following primer sets - pair 1: F*NcoI*-2 primer (inserted a *NcoI* site upstream of the *mtbt* cDNA) and R2-A/B primer, pair 2: F2-A/B primer and RBHNS-2 primer, used to remove the wild-type stop codon yet kept the cDNA in-frame with the C-terminal polyhistidine tag and terminal stop codon encoded on the vector. Each set was separately amplified, and then equal amounts were mixed in a PCR reaction with F*NcoI*-2 primer and RBHNS-2 primer creating a full length insert for directional ligation using *NcoI* and *BamHI*.

3.2.2.3. Preparation of Competent *E. coli* Cells

Competent cells were prepared according to a procedure adapted from Sambrook et al.²¹ In general, Luria-Bertani (LB) medium (5 mL) containing antibiotics when appropriate was inoculated with a single colony from an LB agarose plate containing the appropriate antibiotics. The culture was grown at 37 °C with shaking at 250 rpm for 10-12 h, and eight 500-μL aliquots of the overnight culture were used to inoculate separate 5-mL portions of LB containing the appropriate antibiotics. These cultures were grown at 37 °C with shaking at 250 rpm until OD₆₀₀ = 0.4 – 0.6. These cultures were transferred to a 50 mL conical centrifuge tube, harvested by

centrifugation (4000g, 5 min, 4 °C) and the culture medium was decanted. All subsequent manipulations were carried out on ice. The harvested cells were resuspended in ice-cold 100 mM CaCl₂ (50 mL), incubated for 30 min, centrifuged (4000g, 5 min, 4 °C), the supernatant was decanted, the cells were resuspended in ice-cold 100 mM CaCl₂ (50 mL), and incubated for 10 min. The samples were decanted, and the cells were centrifuged (4000g, 5 min, 4 °C) and resuspended in 4 mL of ice-cold 100 mM CaCl₂ containing 15% glycerol (v/v). Aliquots (100 µL) of competent cells were added to 500-µL microfuge tubes, immediately frozen in liquid nitrogen, and stored at -78 °C.

3.2.3. Protein Expression and Purification

All proteins, wild type and mutants, were subjected to the following procedures, unless otherwise stated.

3.2.3.1. *E. coli* Cell Culture

All N- or C-terminal His₆-tagged recombinant proteins were overproduced in the described bacterial expression system and harvested according to a previously reported protocol, with slight modifications.¹⁵ Cultures were grown overnight at 37 °C in 100 mL of LB medium supplemented with 50 µg/mL kanamycin and 35 µg/mL chloramphenicol for *nt-ndtbt* and *ndtbt-ct* (the *nt*-prefix or *ct*-suffix designate a cDNA encoding either the N- or C-terminal His₆ epitope, respectively) expressed in *E. coli* BL21-CodonPlus (DE3)-RIPL cells. Since

recombinants *nt-dbat*, *dbat-ct*, *nt-mtbt*, and *mtbt-ct* were expressed in BL21 (DE3) *E. coli* cell lines, the growth media was supplemented with 50 µg/mL kanamycin.

To six flasks containing LB medium (850 mL), supplemented with the appropriate antibiotics, was added 16 mL of the 100-mL inoculum, and the cultures were grown at 37 °C to $OD_{600} = 0.5 - 0.7$. Gene expression was induced with isopropyl-β-D-1-thiogalactopyranoside (500 µM), and the culture was incubated at 20 °C for 18 h. The cells were harvested by centrifugation (4000g, 10 min, 4 °C), the supernatant was discarded, and the pellet was transferred to a pre-weighed 50 mL Corning Tube for storage at -20 °C.

3.2.3.2. Protein Harvest

The pellet was resuspended in lysis buffer (50 mM Tris-HCl, 300 mM sodium chloride, 10% glycerol, pH 8.0 at 3 mL/g cells) at 4 °C. The cells were lysed at 4 °C by sonication (6 × 15 sec bursts at 60% power at 45 sec intervals) with a Misonix XL-2020 sonicator (Misonix Inc., Farmingdale, NY), and the cell-lysate was clarified by ultracentrifugation at 46,000g for 1 h at 4 °C.

3.2.3.3. Protein Purification

The supernatant of the lysed bacterial cells was incubated with 1 mL of Ni-NTA agarose (Qiagen, Valencia, CA) per 8 g of wet pellet in batch mode at 4 °C. After 1 h, the mixture was poured into an Econo column (BioRad, 20 cm × 2.5 cm), and the lysis buffer was drained. The resin was washed with five column volumes of wash buffer (50 mM Tris-HCl, 300 mM sodium chloride, 10% glycerol, pH 8.0), and the bound protein was eluted with 1.5 column volumes each of a step-gradient of wash buffer containing a 10, 50, 100, 150, 200 mM imidazole.

To determine which fraction of imidazole contained the target enzyme, an SDS-PAGE gel was run. An aliquot (5 μ L) of enzyme fraction eluting from the column was combined with 10 μ L of SDS-PAGE dye, and the mixture was boiled, centrifuged, decanted and the supernatant was loaded onto the gel. Usually the recombinant protein eluted from the column in the 100 mM and 150 mM imidazole. These fractions were combined, and the imidazole was removed from the eluent by repeated cycles of concentration by centrifugation (30,000 MWCO, YM30 membrane, Millipore, Billerica, MA) and dilution in storage buffer (50 mM Tris-HCl, 10% glycerol, pH 8.0) until the imidazole was 1.5 μ M.

The protein was diluted with storage buffer (50 mL) before loading onto a column packed with Q-Sepharose Fast Flow anion exchange resin (Amersham) (40 mL) that was previously equilibrated with storage buffer. Proteins were eluted with a linear gradient NaCl (0 – 400 mM in storage buffer) at 5 mL/min over 33 min. The target enzyme principally eluted from the column in 90 – 150 mM NaCl. These fractions were pooled and the NaCl was removed by repeated cycles of concentration by centrifugation and dilution in gel buffer (50 mM Tris-HCl, 20 mM NaCl, 10% glycerol, pH 8.0). The isolated protein (~10 mg) was loaded onto a gel filtration column (150 mL, Superdex 200 Prep grade in a XK16/70 column (GE Healthcare, Piscataway, NJ)) and eluted with gel buffer at 1 mL/min over 2.5 h. Generally, the enzyme eluted between 75 – 90 min. Fractions containing the protein were pooled and the NaCl was removed from the eluent by repeated cycles of concentration by centrifugation (30,000 MWCO, YM30 membrane, Millipore, Billerica, MA) and dilution in storage buffer (50 mM Tris-HCl, 10% glycerol, pH 8.0).

3.2.3.4. Enzyme Storage

After enzyme concentration and purity is determined, aliquots (100 μ L) at 2 mg/mL were flash frozen in liquid nitrogen and stored at -78 $^{\circ}$ C.

3.2.4. Enzymatic Assays and Analysis

3.2.4.1. Activity Assay

In general, the function of the expressed target purified protein (20 – 100 μ g) was assayed (200 μ L reaction volume) with appropriate cosubstrates (each at 200 μ M) at 31 $^{\circ}$ C. Briefly, NDTBT was incubated with benzoyl CoA and *N*-debenzoyl-2'-deoxypaclitaxel, DBAT with free CoA and baccatin III, and *m*TBT with benzoyl CoA and 7,13-diacetyl-2-debenzoylbaccatin III. After 20 min, each assay was separately quenched and extracted with ethyl acetate (3 \times 1 mL), the organic fractions were combined, the solvent was evaporated, and the residue was re-dissolved in 100 μ L of acetonitrile. Aliquots (10 μ L) were analyzed by direct injection-electrospray ionization mass spectrometry, in positive ion mode. A Q-ToF Ultima Global electrospray ionization tandem mass spectrometer (ESI-MS/MS, Waters, Milford, MA) with a Waters CapLC capillary HPLC was used for mass spectral analysis. The molecular ions ($[M + H]^+$) of the isolated products and their fragment ion profiles were identical to those of authentic 2'-deoxypaclitaxel, baccatin III, and 7,13-diacetylbaccatin III, respectively, when analyzed by identical methods (Table 3.2).

Table 3.2 – Activity Assay for NDTBT, DBAT, and *m*TBT

Enzyme	Reaction	Taxane (200 μ M)	Coenzyme A Substrate (200 μ M)	Product, $[M + H]^+$ <i>m/z</i>
NDTBT	Forward	<i>N</i> -debenzoyl-2'- deoxypaclitaxel	Benzoyl CoA	2'-deoxypaclitaxel, 838
DBAT	Reverse	baccatin III	Free CoA	10-deacetylbaccatin, 545
<i>m</i> TBT	Forward	7,13-diacetyl-2- debenzoylbaccatin	Benzoyl CoA	7,13-diacetylbaccatin, 671

3.2.5. Crystal Box Set-up

Crystallization screens were set up using the Crystal Gryphon (Art Robbins Instrument) for the sitting-drop method in a 96-well plate format. Purified enzyme (0.3 μ L of a 5 mg/mL stock) was mixed with 0.3 μ L of buffer solutions. The matrices used were Index, SaltRx-1, SaltRx-2, PEG/Ion Screen 1, PEG/Ion Screen 2, Crystal Screen 1, Crystal Screen 2 (Hampton Research Corp., Aliso Viejo, CA), Wizard I, Wizard 2, Wizard 3, and Wizard 4 (Emerald BioSystems, Inc, Bainbridge Island, WA). Each screen was conducted in duplicate; one batch was incubated at room temperature (25 °C), the other at 4 °C. Boxes were observed under a compound light microscope every day for two weeks, then every other week for 2 months at ambient temperature.

3.2.6. Thrombin Digestions

Thrombin digestions were conducted using Novagen's Thrombin Kit with purified protein (1 mg) and biotinylated thrombin (1 unit) with the mixture incubated for 16 h at 25 °C. Thrombin was removed after running the sample over streptavidin agarose, and eluents containing protein were detected by immunoblot analysis. The fractions containing protein were combined, concentrated during the buffer exchange into storage buffer (50 mM Tris-HCl, 10% glycerol, pH 8.0) by centrifugation (30,000 MWCO, YM30 membrane, Millipore, Billerica, MA) and stored at -80 °C.

3.3. Results

3.3.1. Expression and Activity Assays for NDTBT, DBAT, and *m*TBT

3.3.1.1. *N*-Debenzoyl-2'-deoxypaclitaxel:*N*-benzoyltransferase (NDTBT)

NDTBT was expressed in *E. coli* as described in Chapter 2, with slight modifications as follows. The N-terminal and C-terminal His₆-tag epitopes of NDTBT (designated NT-NDTBT and NDTBT-CT, respectively) were expressed from the vector pET28 in *E. coli* BL21-CodonPlus (DE3)-RIPL cells. The expressed epitopes were separately loaded onto nickel affinity resin. The column was eluted with a step gradient of imidazole and NDTBT-CT was obtained at 75% purity, after concentrating and desalting.

The sample was then loaded onto and eluted from an anion exchange column (Q-Sepharose). The NDTBT-CT (~50 kDa) partitioned into 3 'Pools' with other proteins in the sample as indicated by the peaks detected by UV-monitoring of the effluent from the FPLC

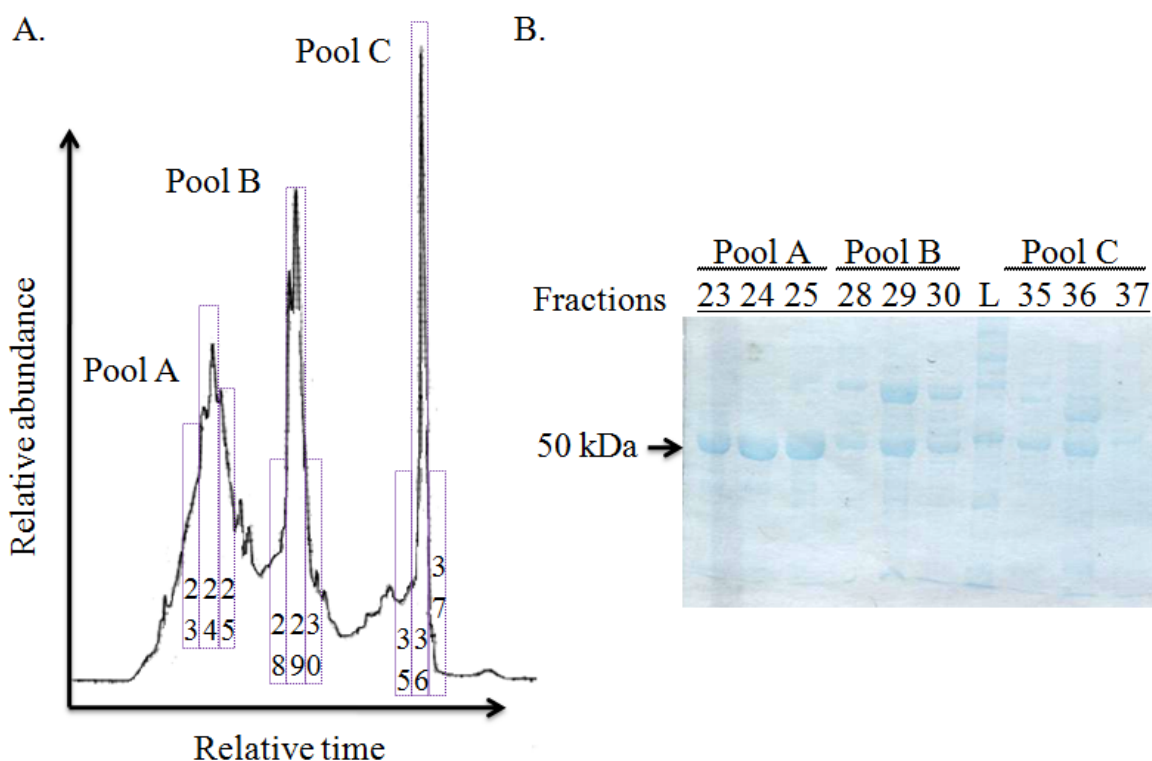


Figure 3.1 - NDTBT-CT Purification from Q-Sepharose Anion Exchange Column.

A. Chromatogram of protein elution from FPLC with 5-mL fractions (5 mL/min) indicated in purple boxes. B. Stained SDS-PAGE of 10 µL of each fraction listed, and L is the protein ladder (225, 150, 100, 75, 50, 35, 25, 15, 10, 5 kDa).

chromatogram (Figure 3.1.A). 'Pool' A was partitioned into three 5-mL fractions 23, 24, and 25, 'Pool' B into fractions 28, 29, and 30, and 'Pool' C into fractions 35, 36, and 37. 'Pool' A eluted in 270 – 310 mM salt, concentrated, and desalted before testing positive for activity. 'Pools' B and C were not investigated further since additional protein bands, not related to NDTBT-CT, were observed by SDS-PAGE analysis with Coomassie Blue staining (Figure 3.1.B).

The 'Pool' A fractions were combined and loaded onto a gel-filtration column of Superdex 200 prep from which the majority of NDTBT-CT eluted four 3-mL fractions (25, 26, 27, and 28) (Figure 3.2.A). The elution volume of the target protein (in 9 mL of gel buffer) matched that of a ~40 kDa standard (evaluated earlier), providing evidence that NDTBT-CT was monomeric (Figure 3.2.B). This gel permeation step yielded protein at >95% purity with an isolated yield from *E. coli* at about 1.2 mg/L culture.

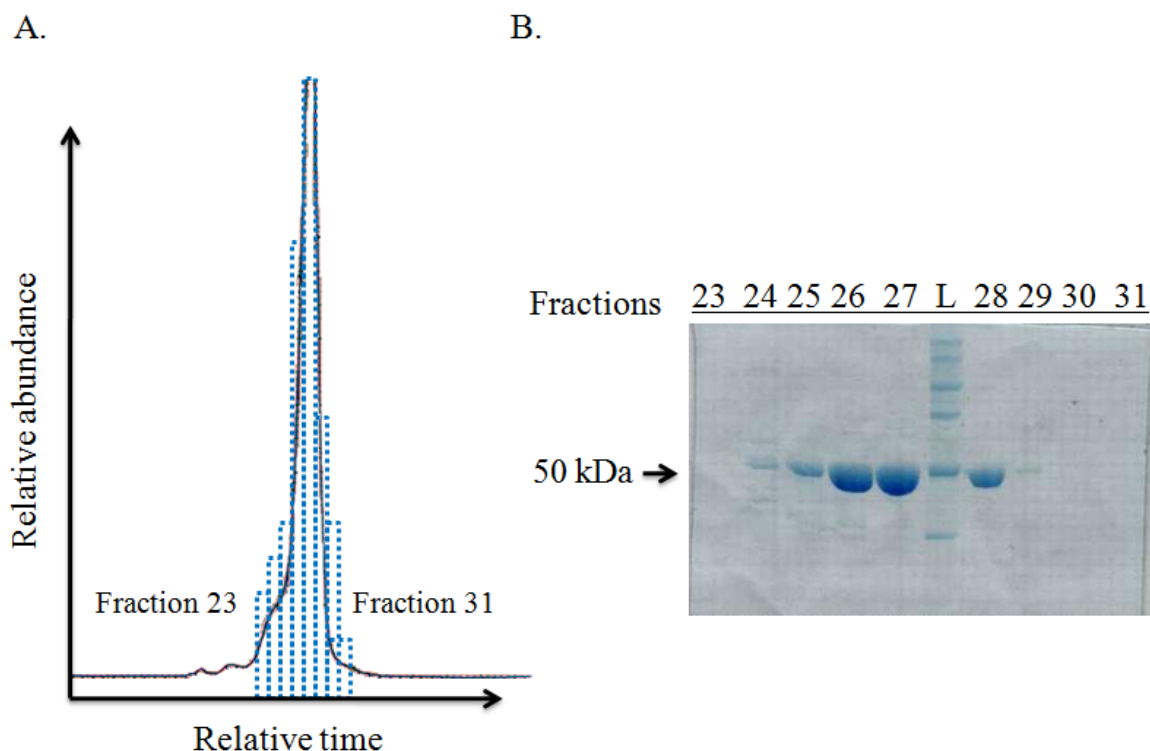


Figure 3.2 - NDTBT-CT Purification from Superdex 200 Gel Filtration Column.
A. Chromatogram of protein elution from FPLC with 3-mL fractions (1 mL/min) indicated in blue boxes. B. Stained SDS-PAGE of 10 µL of each fraction listed, and L is the protein ladder (225, 150, 100, 75, 50, 35, 25, 15, 10, 5 kDa).

The activity of the benzoyltransferase was assessed by incubating it with *N*-debenzoyl-2'-deoxypaclitaxel and benzoyl CoA cosubstrates, and the product was analyzed by LC-ESI/MS in positive-ion mode. The retention time ($R_t = 8.7$ min) and molecular ion ($[M + H]^+$ (m/z 838)) and the diagnostic fragment ion (m/z 270, derived from *N*-benzoylated 13-side chain) of the biosynthetic product 2'-deoxypaclitaxel were identical to those of the authentic standard.

3.3.1.2. 10-Deacetyl-baccatin III:10-*O*-acetyltransferase (DBAT)

The N-terminal His₆-tag fusion of DBAT (10-deacetylbaccatin III:10-*O*-acetyltransferase), designated NT-DBAT, was purified by nickel affinity column chromatography to provide NT-DBAT at 60% purity from fractions eluting between 100 mM and 150 mM imidazole. After desalting and concentrating, the activity was tested in the reverse DBAT reaction by employing substrates baccatin III and free CoA, and analyzed by LC-ESI/MS in positive-ion mode (Figure 3.3). The retention time ($R_t = 5.4$ min) and molecular ion ($[M + H]^+$ (m/z 545)) of the product 10-deacetylbaccatin were identical to that of the authentic standard.

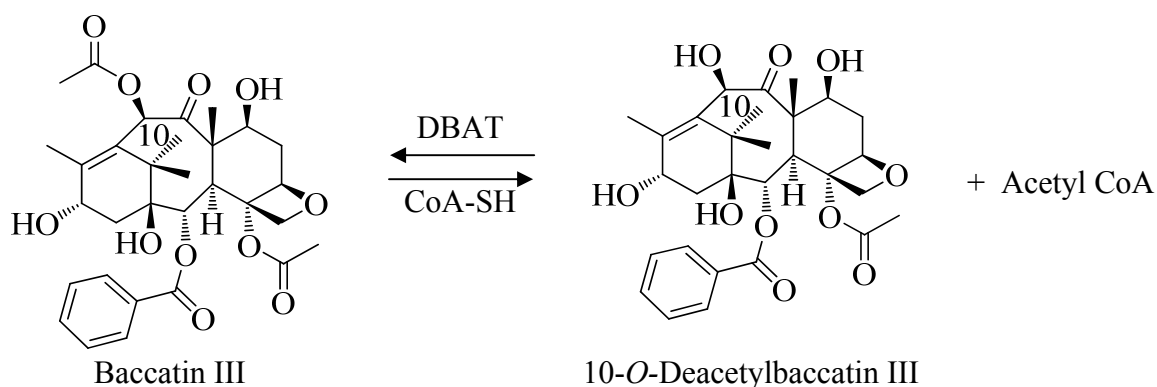


Figure 3.3 - Enzymatic De-acetylation of Baccatin III by 10-Deacetylbaccatin III: 10-*O*-acetyltransferase.

To increase the yield of full-length DBAT protein isolated from the expression host, *dbat* cDNA was modified so it would express as a C-terminal His₆-tag fusion (designated DBAT-CT). The *dbat* cDNA was mutated to remove three internal *Nco*I restriction sites. This allowed directional ligation of the cDNA insert, cut with *Nco*I and *Bam*HI, into the pET28 vector cut with the same restriction enzymes. The expressed DBAT-CT was purified by nickel affinity column chromatography to provide DBAT-CT at 70% purity, which was a modest improvement (65%) over purifying NT-DBAT through the same column matrix.

As done before to purify NDTBT, DBAT-CT was further purified by anion exchange which partitioned into 3 'Pools' eluting from the column (Figure 3.4.A). 'Pool' A was partitioned into three 5-mL fractions 21, 22, and 23, 'Pool' B into fractions 26, 27, and 28, and 'Pool' C into fractions 31, 32, and 33. 'Pool' A eluted in 260 – 300 mM salt were concentrated and desalted before testing positive for activity. 'Pools' B and C were not investigated further since protein bands observed by SDS-PAGE analysis with Coomassie Blue staining were not near the 50 kDa marker size (Figure 3.4.B).

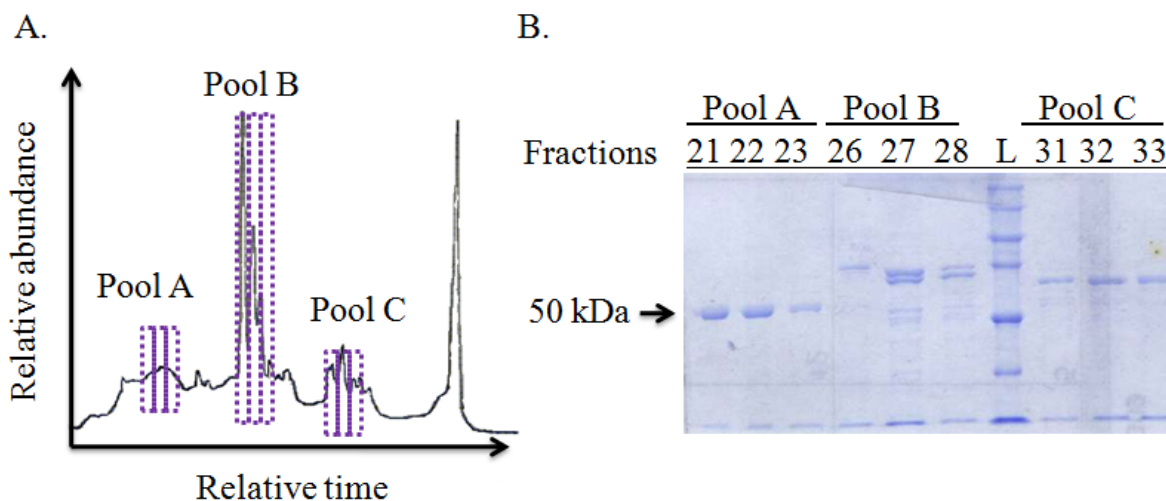


Figure 3.4 - DBAT-CT Purification from Q-Sepharose Anion Exchange Column.

A. Chromatogram of protein elution from FPLC with 5-mL fractions (5 mL/min) indicated in purple boxes. B. Stained SDS-PAGE of 10 µL of each fraction listed, and L is the protein ladder (225, 150, 100, 75, 50, 35, 25, 15, 10, 5 kDa). DBAT-CT at 50 kDa arrow.

The 'Pool' A fractions were combined and loaded onto a gel-filtration column of Superdex 200 prep from which the majority of DBAT-CT elution time coincided at that of a ~40 kDa standard (evaluated earlier), providing evidence that DBATT-CT was monomeric. After gel filtration chromatography, yielding functional protein was at 90-95% purity with an isolated yield from *E. coli* at about 1.2 mg/L culture.

3.3.1.3. Modified Taxane-2 α -O-benzoyltransferase (*mTBT*)

Similar to the purification methods previously described for the other transferases, a modified *tbt* cDNA (*mtbt*) was mutated to remove an internal *Nco*I restriction to allow directional ligation of the cDNA insert, cut with *Nco*I and *Bam*HI, into the pET28 vector cut with the same restriction enzymes. The resulting plasmid provided a C-terminal His₆-tag fusion of taxane-2 α -O-benzoyltransferase (*mTBT*), designated *mTBT*-CT and was expressed in BL21(DE3) *E. coli* cells.

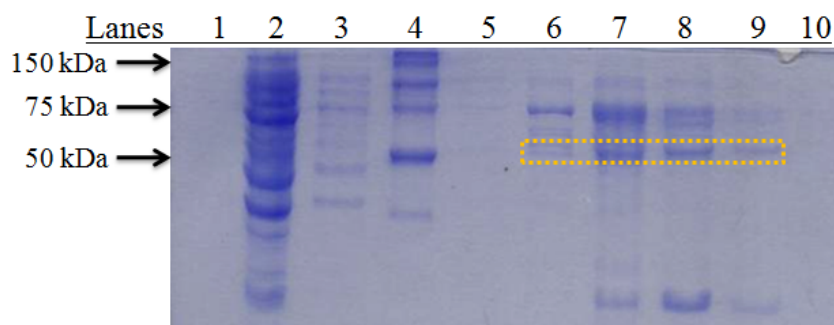


Figure 3.5 - SDS-PAGE of *mTBT*-CT Fractions from Nickel-Affinity Chromatography.

Protein bands corresponding to *mTBT* are boxed in yellow. Lane 1: empty, Lane 2: flow thru, Lane 3: wash, Lane 4: ladder, Lane 5: 10 mM imidazole, Lane 6: 50 mM imidazole, Lane 7: 100 mM imidazole, Lane 8: 150 mM imidazole, Lane 9: 200 mM imidazole, Lane 10: empty.

As described previously for the purification of NDTBT-CT and DBAT-CT, *m*TBT-CT was purified through a series of chromatography columns including nickel affinity, anion exchange, and gel filtration, to yield protein at 90-95% purity. The isolated yield of *m*TBT-CT from *E. coli* was at ~0.35 mg/L of culture. In comparison, *m*TBT-CT was isolated at 50% purity from the nickel affinity column, while the N-terminal His₆-tag fusion of *m*TBT, designated NT-*m*TBT, expressed from the same vector and isolated from the same host was obtained at 30% purity (Figure 3.5). The purified *m*TBT-CT was deemed functional in reactions containing 7,13-diacetyl-2-debenzoylbaccatin and benzoyl coenzyme A, and analyzed by LC-ESI/MS in positive-ion mode (Figure 3.6). The retention time ($R_t = 8.7$ min) and molecular ion ($[M + H]^+$ (m/z 671)) of the product 7,13-diacetylbaccatin III were identical to that of the authentic standard.

Figure 3.6 - Enzymatic Benzoylation of 7,13-*O,O*-diacetyl-2-*O*-debenzoylbaccatin III by Modified Taxane-2 α -*O*-benzoyltransferase (*m*TBT).

Crystal box screens were with NDTBT-CT (5 mg/mL) were incubated at room temperature (25 °C) and at 4 °C. Six 96-welled boxes were screened daily under a light microscope for the first two weeks, and no crystallization was observed. After ~6 weeks at 25

°C, one sample contained a precipitate that form a single-layer, but none formed clear, large crystals suitable for x-ray analysis, indicating that the precipitate was possibly salt instead of protein. The screening boxes were set up for a second round and incubated with benzoyl CoA (1 mM) added to the crystallization buffer to seed crystal growth, but to no avail.

3.3.3. Thrombin Digestions of NT-NDTBT

NT-NDTBT was purified following the same procedure used to isolate the NDTBT-CT, providing a smaller isolated yield from *E. coli* (~0.71 mg/L culture) at 95% purity. The pET28 vector contains a thrombin cleavage site between the multiple cloning sites and the N-terminal His₆-tag, whereas the NDTBT-CT does not. Thus, the purified NT-NDTBT fusion protein (1 mg) was used in small scaled digestions with biotinylated thrombin and the recovery of liberated NDTBT was 10% determined by Bradford assay, which was insufficient (0.1 mg) to stock-up for setting up crystal boxes.

3.4. Discussion

In Chapter 2, the N-terminal polyhistidine-tagged NDTBT (NT-NDTBT) was purified (70%) by nickel affinity column chromatography with imidazole elution. Based on immunoblot analysis, the tagged protein was co-eluting with other proteins that appeared as a smear underneath the target band of protein. This was attributed to premature termination of protein expression in the bacterial host or to nonspecific shearing of enzyme during isolation of the overexpressed protein. To circumvent this problem, *ndtbt* was sub-cloned to incorporate a C-terminal His₆-tag and ensure that only full-length protein was binding to the nickel column. Further anion exchange purification apparently separated NDTBT-CT from its complexes with

possible endogenous *E. coli* proteins (cf. Figure 3.1). Although it has not been verified by sequence analysis, the prominent unknown bands in 'Pools' B and C (cf. Figure 3.1) have retention factors on SDS-PAGE similar to those of DnaK (~67 kDa) and GroEL (~57 kDa), respectively. The latter are native proteins of *E. coli* known to co-elute on nickel-affinity resins with His₆-tagged proteins.²² Gel filtration confirmed NDTBT-CT as monomeric (~50 kDa). The series of purification steps employed for NDTBT-CT yielded protein of greater purity (95-98% purity) than any previous reports on the *Taxus* acyltransferase.

With the pure enzyme, crystal screening boxes were constructed for a sitting drop method. Only small or flat crystals were detected, but none was substantial for further optimization or x-ray analysis. To enhance the crystallization seeding, screens were repeated with NDTBT-CT and benzoyl CoA substrate, but no crystals were observed under these conditions. Hypothetically, the His₆-tag is likely affecting crystallization. The structures of vinorine synthase and anthocyanin malonyltransferase, belonging to the same superfamily as NDTBT, were solved when the histidine tag was removed before crystallization.^{10, 19} In addition, the structures of arginine methyltransferase 10 from *Arabidopsis thaliana* and the human arylamine *N*-acetyltransferases were recently solved when the histidine tag was removed before crystallization.^{23, 24} Therefore NT-NDTBT, which has a thrombin cleavage site between the N-terminal His₆-tag and NDTBT, was purified using the same purification protocol as NDTBT-CT. The current conditions for the thrombin cleavage setup with NT-NDTBT resulted in 10% cleaved protein (~0.1 mg), which was insufficient for crystal box screens. Since large amounts (~0.71 mg/L) of NT-NDTBT can be now be purified to >90% homogeneity, the

thrombin cleavage protocol remains to be optimized to access NDTBT without a His₆-epitope for crystal screening trials.

Prior to the work with NDTBT-CT, described herein, another lab member, Sean Sullivan, determined the kinetic parameters for NDTBT-CT in an independent study,²⁵ and these values were compared to those calculated in the present study. Since the protein amount was different between the data sets the only values that are comparable are the Michaelis-Menten constant (K_M) and the catalytic turnover (k_{cat}), the latter was ~25-fold increased for NDTBT-CT compared to NT-NDTBT (Table 3.3). Unfortunately, specific activity calculations of the purified protein at various stages of purification process were omitted. Only the final specific activity was reported while obtaining active protein at >90% purity for crystal screening.

Table 3.3 – Kinetic Parameters of N-terminal and C-terminal His₆-tagged NDTBT

<i>Parameters</i>	<i>NT-NDTBT</i>	<i>NDTBT-CT</i>
K_M	93 μ M	116 μ M
V_{max}	0.148 nmol/min	0.33 nmol/min
k_{cat}	0.07 min ⁻¹	1.7 min ⁻¹
Total Enzyme	100 μ g	10 μ g
Purity	65-70%	95-98%

Although both DBAT and *m*TBT were purified to about 90-95% purity, no crystal box screening was conducted due to limited time. However, since large amounts can be now be purified, crystallization studies can now be attempted by future researchers. Besides using these pure enzyme samples for x-ray crystallography, the two benzoyltransferases are also being used in a coupling assay with a benzoate ligase that recycles the CoA substrate (Figure 3.7).

Preliminary studies demonstrated an increase of product turnover from 2% to ~90% when coupled with NDTBT-CT.²⁵

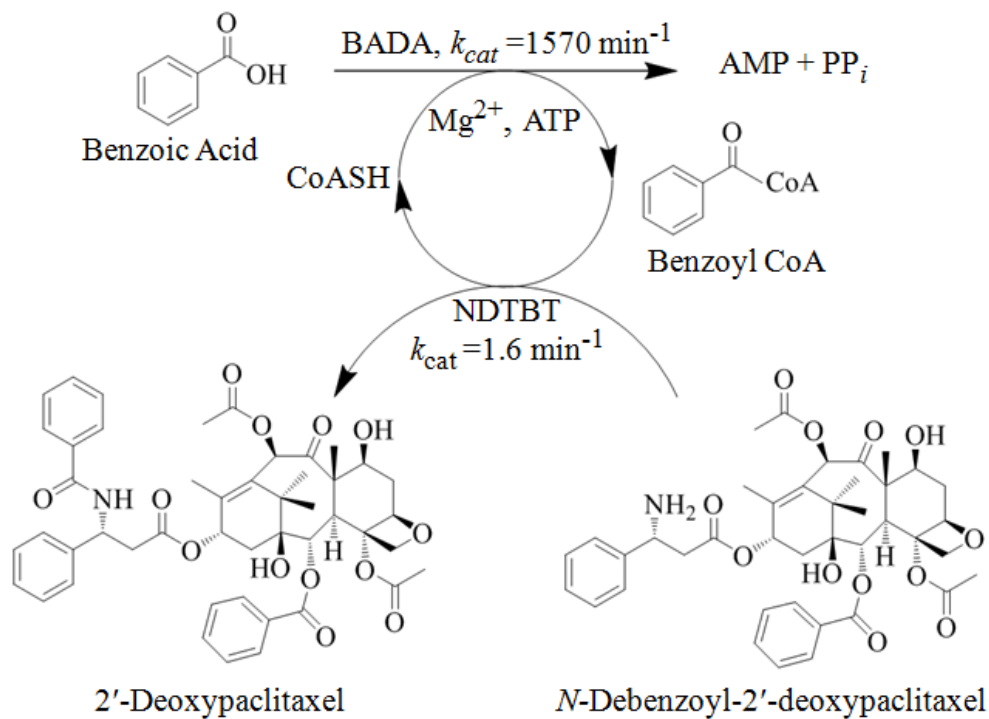


Figure 3.7 - Coupling Assay Scheme of Benzoate Ligase with *N*-Benzoyltransferase.
The k_{cat} values are based on the enzyme's natural substrate. Benzoate ligase (BADA) and *N*-benzoyltransferase (NDTBT).

REFERENCES

REFERENCES

1. St-Pierre, B., and De Luca, V. (2000) Evolution of acyltransferase genes: Origin and diversification of the BAHD superfamily of acyltransferases involved in secondary metabolism, *Recent Adv. Phytochem.* 34, 285-315.
2. Dudareva, N., Raguso, R. A., Wang, J., Ross, J. R., and Pichersky, E. (1998) Floral scent production in *Clarkia breweri*. III. Enzymatic synthesis and emission of benzenoid esters, *Plant Physiol.* 116, 599-604.
3. Suzuki, H., Sawada, S., Watanabe, K., Nagae, S., Yamaguchi, M. A., Nakayama, T., and Nishino, T. (2004) Identification and characterization of a novel anthocyanin malonyltransferase from scarlet sage (*Salvia splendens*) flowers: An enzyme that is phylogenetically separated from other anthocyanin acyltransferases, *Plant J.* 38, 994-1003.
4. Yang, Q., Reinhard, K., Schiltz, E., and Matern, U. (1997) Characterization and heterologous expression of hydroxycinnamoyl/benzoyl-CoA:anthranilate *N*-hydroxycinnamoyl/benzoyltransferase from elicited cell cultures of carnation, *Dianthus caryophyllus* L., *Plant Mol. Biol.* 35, 777-789.
5. Dudareva, N., D'Auria, J. C., Nam, K. H., Raguso, R. A., and Pichersky, E. (1998) Acetyl-CoA:benzylalcohol acetyltransferase--an enzyme involved in floral scent production in *Clarkia breweri*, *Plant J.* 14, 297-304.
6. Laflamme, P., St. Pierre, B., and De Luca, V. (2001) Molecular and biochemical analysis of a Madagascar periwinkle root-specific minovincinine-19-hydroxy-*O*-acetyltransferase, *Plant Physiol.* 125, 189-198.
7. Grothe, T., Lenz, R., and Kutchan, T. M. (2001) Molecular characterization of the salutaridinol 7-*O*-acetyltransferase involved in morphine biosynthesis in opium poppy *Papaver somniferum*, *J. Biol. Chem.* 276, 30717-30723.
8. St. Pierre, B., Laflamme, P., Alarco, A., and De Luca, V. (1998) The terminal *O*-acetyltransferase involved in vindoline biosynthesis defines a new class of proteins responsible for coenzyme A-dependent acyl transfer, *Plant J.* 14, 703-713.
9. D'Auria, J. C. (2006) Acyltransferases in plants: A good time to be BAHD, *Curr. Opin. Plant Biol.* 9, 331-340.
10. Unno, H., Ichimaida, F., Suzuki, H., Takahashi, S., Tanaka, Y., Saito, A., Nishino, T., Kusunoki, M., and Nakayama, T. (2007) Structural and mutational studies of anthocyanin malonyltransferases establish the features of BAHD enzyme catalysis, *J. Biol. Chem.* 282, 15812-15822.

11. Bayer, A., Ma, X., and Stockigt, J. (2004) Acetyltransfer in natural product biosynthesis--functional cloning and molecular analysis of vinorine synthase, *Bioorg. Med. Chem.* *12*, 2787-2795.
12. Suzuki, H., Nakayama, T., and Nishino, T. (2003) Proposed mechanism and functional amino acid residues of malonyl-CoA:anthocyanin 5-*O*-glucoside-6'''-*O*-malonyltransferase from flowers of *Salvia splendens*, a member of the versatile plant acyltransferase family, *Biochemistry* *42*, 1764-1771.
13. Tuominen, L. K., Johnson, V. E., and Tsai, C. J. (2011) Differential phylogenetic expansions in BAHD acyltransferases across five angiosperm taxa and evidence of divergent expression among *Populus* paralogues, *BMC Genomics* *12*, 236.
14. Nawarathne, I. N., and Walker, K. D. (2010) Point mutations (Q19P and N23K) increase the operational solubility of a 2 α -*O*-benzoyltransferase that conveys various acyl groups from CoA to a taxane acceptor, *J. Nat. Prod.* *73*, 151-159.
15. Nevarez, D. M., Mengistu, Y. A., Nawarathne, I. N., and Walker, K. D. (2009) An *N*-aroyltransferase of the BAHD superfamily has broad aroyl CoA specificity *in vitro* with analogues of *N*-dearoylpaclitaxel, *J. Am. Chem. Soc.* *131*, 5994-6002.
16. Walker, K., and Croteau, R. (2000) Molecular cloning of a 10-deacetylbaccatin III-10-*O*-acetyl transferase cDNA from *Taxus* and functional expression in *Escherichia coli*, *Proc. Natl. Acad. Sci. U. S. A.* *97*, 583-587.
17. Ondari, M. E., and Walker, K. D. (2008) The Taxol pathway 10-*O*-acetyltransferase shows regioselective promiscuity with the oxetane hydroxyl of 4-deacetyltaxanes, *J. Am. Chem. Soc.* *130*, 17187-17194.
18. Eswar, N., John, B., Mirkovic, N., Fiser, A., Ilyin, V. A., Pieper, U., Stuart, A. C., Marti-Renom, M. A., Madhusudhan, M. S., Yerkovich, B., and Sali, A. (2003) Tools for comparative protein structure modeling and analysis, *Nucleic Acids Res.* *31*, 3375-3380.
19. Ma, X. Y., Koepke, J., Panjikar, S., Fritzsche, G., and Stockigt, J. (2005) Crystal structure of vinorine synthase, the first representative of the BAHD superfamily, *J. Biol. Chem.* *280*, 13576-13583.
20. Geerlof, A., Brown, J., Coutard, B., Egloff, M. P., Enguita, F. J., Fogg, M. J., Gilbert, R. J., Groves, M. R., Haouz, A., Nettleship, J. E., Nordlund, P., Owens, R. J., Ruff, M., Sainsbury, S., Svergun, D. I., and Wilmanns, M. (2006) The impact of protein characterization in structural proteomics, *Acta Crystallogr. D* *62*, 1125-1136.
21. Sambrook, J. R., D. (2001) *Molecular Cloning: A Laboratory Manual*, Cold Spring Harbor Laboratory Press.

22. Edwards, A., Graslund, S., Nordlund, P., Weigelt, J., Bray, J., Hallberg, B. M., Gileadi, O., Knapp, S., Oppermann, U., Arrowsmith, C., Hui, R., Ming, J., Dhe-Paganon, S., Park, H. W., Savchenko, A., Yee, A., Vincentelli, R., Cambillau, C., Kim, R., Kim, S. H., Rao, Z., Shi, Y., Terwilliger, T. C., Kim, C. Y., Hung, L. W., Waldo, G. S., Peleg, Y., Albeck, S., Unger, T., Dym, O., Prilusky, J., Sussman, J. L., Stevens, R. C., Lesley, S. A., Wilson, I. A., Joachimiak, A., Collart, F., Dementieva, I., Donnelly, M. I., Eschenfeldt, W. H., Kim, Y., Stols, L., Wu, R., Zhou, M., Burley, S. K., Emtage, J. S., Sauder, J. M., Thompson, D., Bain, K., Luz, J., Gheyi, T., Zhang, F., Atwell, S., Almo, S. C., Bonanno, J. B., Fiser, A., Swaminathan, S., Studier, F. W., Chance, M. R., Sali, A., Acton, T. B., Xiao, R., Zhao, L., Ma, L. C., Hunt, J. F., Tong, L., Cunningham, K., Inouye, M., Anderson, S., Janjua, H., Shastry, R., Ho, C. K., Wang, D. Y., Wang, H., Jiang, M., Montelione, G. T., Stuart, D. I., Owens, R. J., Daenke, S., Schutz, A., Heinemann, U., Yokoyama, S., Bussow, K., Gunsalus, K. C., Consortium, S. G., Macromol, A. F., Ctr, B. S. G., Consortium, C. S. G., Function, I. C. S., Ctr, I. S. P., Genomics, J. C. S., Genomics, M. C. S., Ctr, N. Y. S. G. R., Consortium, N. S. G., Facility, O. P. P., Facility, P. S. P., Med, M. D. C. M., Proteomics, R. S. G., and Complexes, S. (2008) Protein production and purification, *Nature Methods* 5, 135-146.
23. Cheng, Y., Frazier, M., Lu, F., Cao, X., and Redinbo, M. (2011) Crystal structure of the plant epigenetic protein arginine methyltransferase 10, *J. Mol. Biol.* 414, 106-122.
24. Wu, H., Dombrovsky, L., Tempel, W., Martin, F., Loppnau, P., Goodfellow, G., Grant, D., and Plotnikov, A. (2007) Structural basis of substrate-binding specificity of human arylamine *N*-acetyltransferase, *J. Biol. Chem.* 282, 30189-30197.
25. Sullivan, S. A. (2010) A Broadly Specific Benzoate Coenzyme A Ligase Is Coupled With Taxus Acyltransferases *In Vitro* To Biosynthesize Paclitaxel Analogues (Master's Thesis), In *Chemistry*, Michigan State University, East Lansing.

CHAPTER 4

ACYLTRANSFERASE SELECTIVITY OF REGION-SWAPPED STRUCTURES

4.1. Introduction

Enzymes linked to secondary metabolic pathways diversify the pool of metabolites due to their relatively loose substrate specificity.¹ This is exemplified by the two *Taxus* acyltransferases on the paclitaxel biosynthetic pathway. The *N*-debenzoyl-2'-deoxypaclitaxel:*N*-benzoyltransferase (NDTBT) produced various analogues when incubated with acyl CoA donor substrates and three *N*-debenzoylpaclitaxel derivatives.^{2, 3} The taxane-2 α -*O*-benzoyltransferase (TBT) was genetically modified TBT (*m*TBT) to improve solubility, and the substrate specificity of *m*TBT was tested with several acyl CoA with one taxane acceptor substrate.³ Other BAHD family members such as the benzoyl CoA:benzylalcohol benzoyl transferase (*Clarkia breweri*), and alcohol acyltransferases from wild strawberry (*Fragaria vesca*), cultivated strawberry (*Fragaria* \times *ananassa*), and banana (*Musa sapientum*) have broad substrate specificity with varying donors and alcohol acceptor substrates.^{4, 5}

The rationale for the extensive substrate preference by these enzymes is based likely on the plasticity of the active site architecture and the broader tertiary and quaternary features of the acyltransferases. Therefore, a systematic mutagenesis study was conducted to evaluate regions of the enzyme responsible for substrate specificity. Currently, crystal structure data for the *Taxus* acyltransferases is so far unavailable. Thus, homology models of the *Taxus* acyltransferases were built on the two available crystal structures for BAHD family transferases, vinorine synthase and

anthocyanin malonyltransferase. These reasonable structure models guided the mutagenesis approaches to examine specific residues or domains that may be responsible for substrate specificity.^{6, 7}

Vinorine synthase (VS; EC 2.3.1.160) was the first crystallographically solved structure in the BAHD family. This acetyltransferase converts 16-epi-vellosimine to vinorine on the biosynthesis pathway of the antiarrhythmic agent ajmaline in *Rauvolfia serpentina*.⁶ The VS structure was not complexed with either 16-epi-vellosimine or acetyl CoA substrate, yet revealed N-terminal and C-terminal domains composed of 14 β -strands and 13 α -helices that are linked by a crossover loop (Figure 4.1). This structural arrangement was also observed in the structure of malonyl CoA:anthocyanidin 3-*O*-glucoside-6''-*O*-malonyltransferase (Dm3MaT3) from red chrysanthemum (*Dendratherm x morifolium*).⁷ The malonyltransferase structure was in complex with acyl CoA thioesters, which identified the CoA binding site as an internal tunnel space accessing the binding site of the acceptor substrate. Region swapping mutagenesis with the

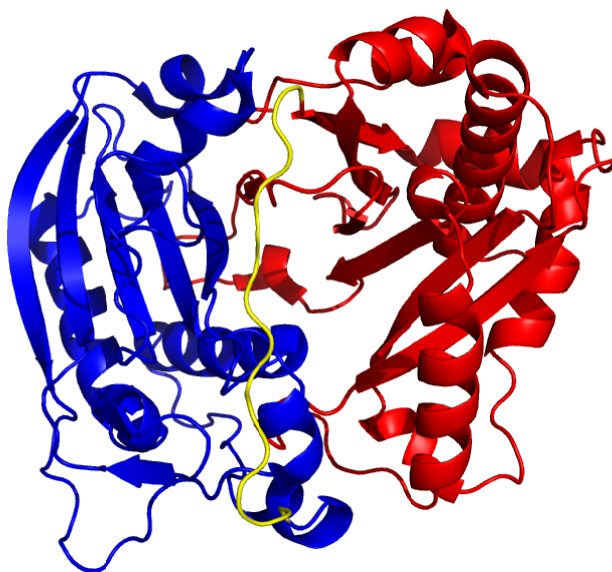


Figure 4.1 - Crystal Structure of Vinorine Synthase.

Blue is N-terminal Domain, yellow is loop region, and red is C-terminal Domain. Created using 2BGH on PyMOL.

malonyltransferases revealed key residues responsible for substrate specificity.⁷ This region swapping procedure identified 3 regions (designated A, B, and C) defined by natural endonuclease restriction sites shared between the cDNA (89% identical) encoding anthocyanidin 3-*O*-glucoside-6''-*O*-malonyltransferase (Dm3MaT1) and malonyl CoA:anthocyanidin 3-*O*-glucoside-3'',6''-*O*-dimalonyltransferase (Dm3MaT2) (Figure 4.2).⁷ The labeling scheme is concocted from the region number ascribed to Dm3MaT1 (designated as '1') and Dm3MaT2 (designated as '2'), and the first, second, or third positioning of the number corresponds to Region A, B, or C, respectively. For example, encoded protein of mutant '212' is comprised of N- to C-terminal amino acid sequence from Dm3MaT2 region A (2), Dm3MaT1 region B (1), and Dm3MaT2 region C (2).

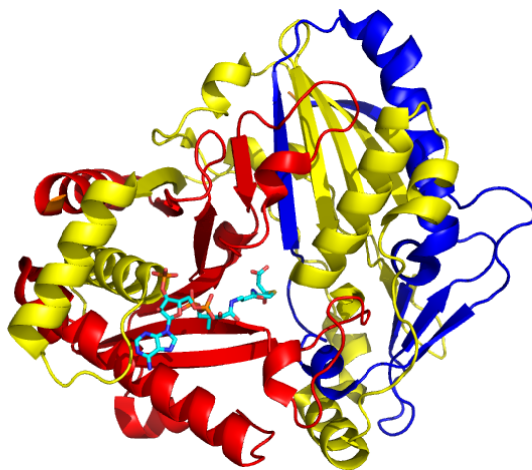


Figure 4.2 - Crystal Structure of the Anthocyanin Malonyltransferase.
Region A (blue), region B (yellow), and region C (red). Light blue coloring of the malonyl CoA substrate was created using 2E1T on PyMOL.

Fortuitously, during the evaluation of the 6 region-swapped mutants the substrate specificity of Dm3MaT2 with pelargonidin 3-*O*-glucoside and cyanidin 3-*O*-glucoside, the former was found to be the only productive substrate.⁷ Thus, this mutagenesis approach created chimeric enzymes with narrower substrate specificity than the parent enzyme. These region-swap

mutagenesis applications were applied to generate chimeric glycosyltransferases with expanded or exchangeable substrate specificity when compared to the parent enzymes by domain swapping.^{8, 9}

Based on the homology model of the anthocyanin malonyltransferase, chimeric mutants were constructed between NDTBT and the *Taxus* 10-deacetylbaaccatin III-10 β -O-acetyltransferase (DBAT), in an attempt to restrict the broad acyl CoA substrate specificity of NDTBT and expand the narrow alkyl CoA specificity of DBAT.^{10, 11} Besides switching the regions, domains were arbitrarily identified by the loop junction and swapped to evaluate if this exchange would affect acyl CoA and taxane selectivity. Differences in taxane substrates (*N*-debenzoyl-2'-deoxypaclitaxel and 10-deacetylbaaccatin III) of NDTBT and DBAT, respectively (Figure 4.3), and in the atom acylated (an amino group compared with a hydroxyl group, respectively),

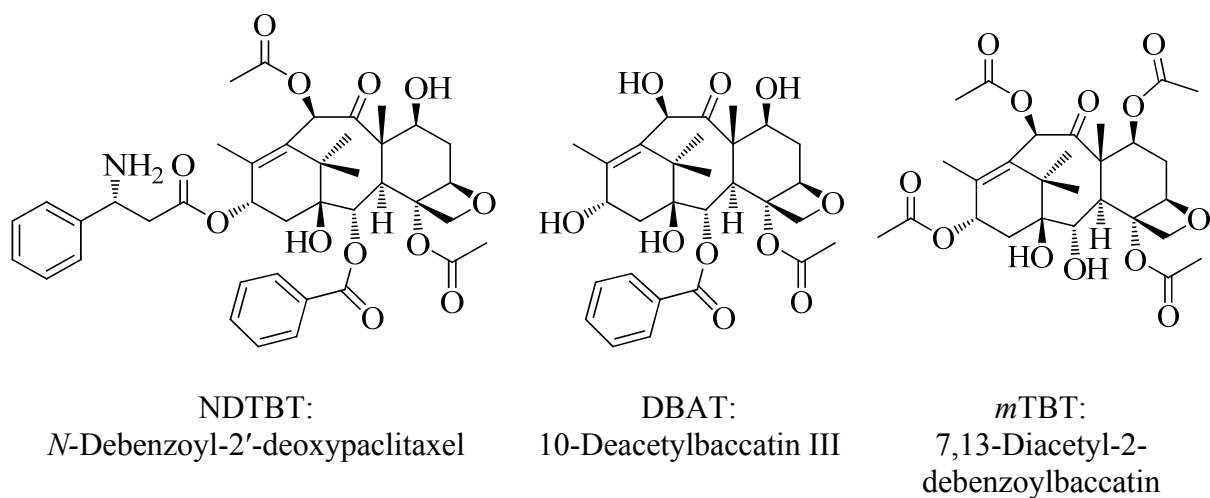


Figure 4.3 – Taxane Substrates Used by *Taxus* Acyltransferases.

however, encouraged building chimeric mutants between DBAT and *m*TBT. The wild-type enzymes of the latter use taxane substrates lacking the phenylpropanoid side chain (cf. Figure 4.3), and each enzyme similarly acylates a hydroxyl group. Thus, chimera made from DBAT and

*m*TBT may present fewer differences in substrate utility compared with those made from NDTBT and DBAT. All chimeric mutants were assayed with a mixture of the natural substrates used for the wild-type congeners, and the product mixtures were analyzed by LC-ESI/MS.

4.2. Materials and Methods

4.2.1. Reagents and Solvents

All substrates (*N*-debenzoyl-2'-deoxypaclitaxel; 10-deacetylbaccatin III; baccatin III; 7,13-diacetyl-2-debenzoylbaccatin III; 7,13-diacetylbaccatin) were obtained from laboratory stocks. Benzoyl CoA and acetyl CoA were obtained from Sigma (St. Louis, MO). The C-terminal histidine tagged *Taxus* acyltransferase plasmids were described in Chapter 3.

4.2.2. Genetic Manipulations

All protocols pertaining to genetic manipulation can be found in Chapter 2 Materials and Methods section. Any variations to previously described methods are listed in this section.

4.2.2.1. Customized Primers

Primers were ordered from the Macromolecular Structure, Sequencing and Synthesis Facility (MSSSF) (Michigan State University) using the Applied Biosystems 3948 DNA Synthesis and Purification System, Invitrogen, and Integrated DNA Technologies. The lyophilized primers were re-suspended in TE buffer (10 mM Tris-HCl, 1 mM EDTA, 7.5 pH) to 100 pmol/μL, and then a working solution was made to 20 pmol/μL in water. Both concentrations were stored at -20 °C. Sequencing primers for NDTBT, DBAT, and *m*TBT are listed in Chapter 3. All the primers used in this section are listed in Table 4.1.

4.2.2.2. Construction of Chimeric Mutants

4.2.2.2.1. *Construction of Regional Mutants Enzymes Between NDTBT and DBAT*

Plasmids separately containing cDNA encoding NDTBT or DBAT with an in-frame C-terminal histidine tag were used as templates to make the NDTBT/DBAT chimeras. In order to amplify Region A, of either NDTBT or DBAT, the T7 Promoter and Rev 10/6 AB primers were used in a PCR reaction; for Region B For 10/6 AB and Rev 10/6 BC primer; and for Region C For 10/6 BC and T7 terminator primer (Figure 4.4). The Region amplicons were individually extracted from an agarose gel using the Qiagen QIAquick Gel Extraction Kit. Different combinations of region inserts for Region A, Region B, and Region C derived from NDTBT (labeled as 1) or DBAT (labeled as 6) were added into another PCR reaction. These combinations produced 6 different chimeras (Figure 4.4).

Table 4.1. Custom Primer Sequences

Name	5' → 3' Sequence
For 10/6 AB	GGTGCTCTGTTTGTGGAAGC
Rev 10/6 AB	GCTTCCACAAACAGAGCACC
For 10/6 BC	GGCTCTTCAAATTCACATA
Rev 10/6 BC	TATGTGGAATTTGAAGTGCC
For 6/2 AB	GGTGCTGTCTTTGTGGAAGC
Rev 6/2 AB	GCTTCCACAAAGACAGCACC
For 6/2 BC	CCACCCAATGAGTATGTGAAAATT
Rev 6/2 BC	AATTTTCACATACTCATTGGGTGG
A-DiF2	CACTTTCAATTGATTTGCCACCGCTTAATCTTGAG
A-DiR2	CGAATGTTGACGGTGGGCAAATGAAATCAAAGTG
A-DiF6	CACTTTGAT TTCATTTGCCACCGTCAACATTCTG
A-DiR6	CTCAAGATTAAGCGGTGGGCAAATCAATTGAAAGTG
B-DiF2	CACTTTCAATTGATTCACCCACCTCTTAATCTTGAG
B-DiR2	CCGAATGTTGAAGGTGGGTGAATGAAATCAAAGTG
B-DiF6	CACTTTGATTTCAATTCACCCACCTTCAACATTCTCG
B-DiR6	CTCAAGATTAAGAGGTGGGTGAATCAATTG AAAGTG
C-DiF6	CAATTTGATTCGATTTGCCCGCCTTCAACATTCTG
C-DiR6	CAGCATTGGAGGCGGGCAAATCAATTGAAAGTG
C-DiF10	CACTTTCAATTGATTTGCCCGCCTCCAATGCTG
C-DiR10	CGAATGTTGAAGGCGGGCAAATCGAATCAAATTG
T7 promoter	TAATACGACTCACTATAGGG
T7 terminator	GCTAGTTATTGCTCAGCGG

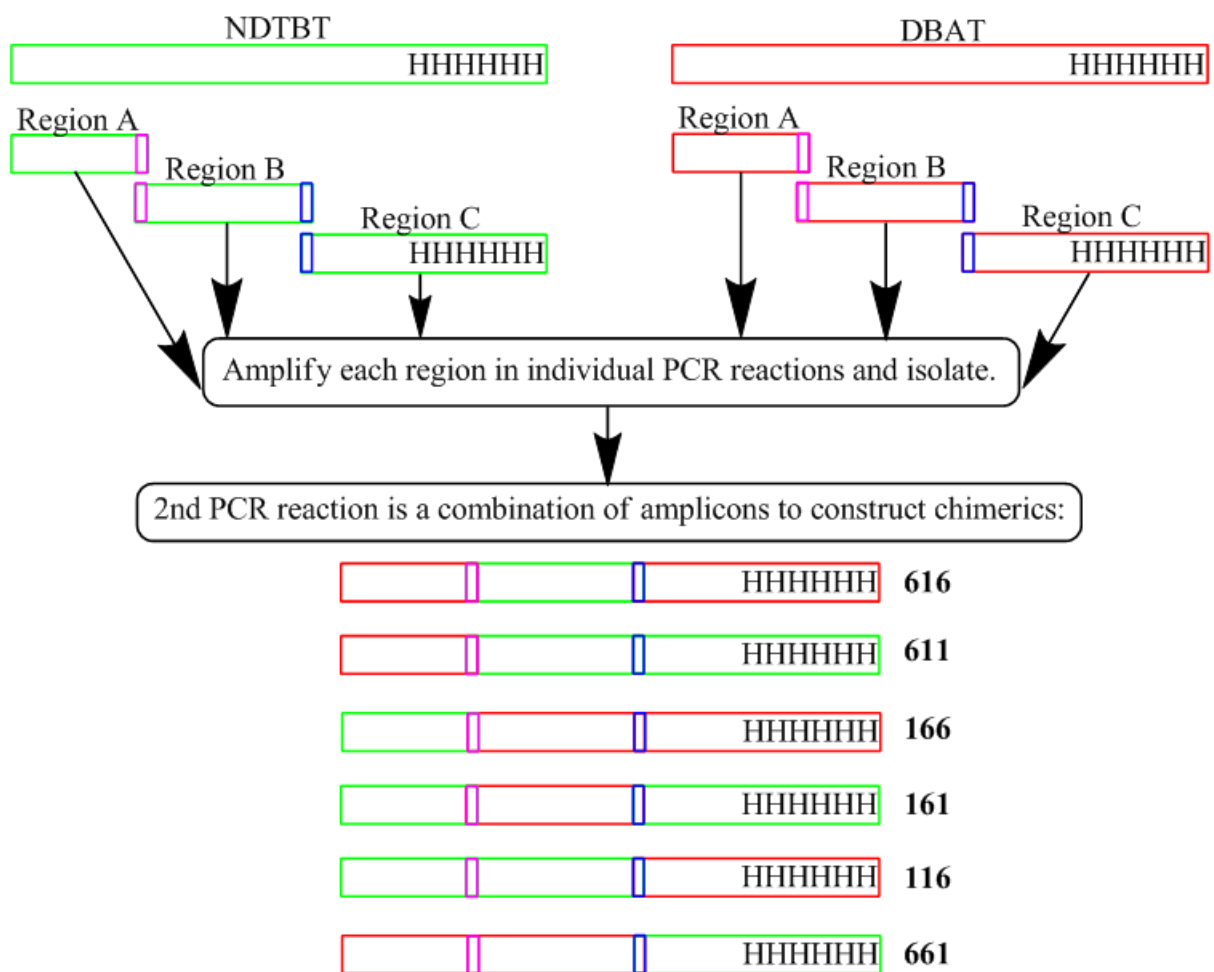


Figure 4.4 – Construction Scheme for Trimeric Mutants.

NDTBT cDNA (green) and DBAT cDNA (red) with a C-terminal poly-His₆-tag (HHHHHH).
10/6 AB primer (pink vertical rectangle); 10/6 BC primer (blue vertical rectangle).

4.2.2.2.2. Construction of Regional DBAT/*mTBT* Mutants

Plasmids separately containing cDNA encoding *mTBT* or DBAT with an in-frame C-terminal histidine tag were used as templates to make the *mTBT*/DBAT chimeras. In order to amplify Region A, of either *mTBT* or DBAT, the T7 Promoter and Rev 6/2 AB primers were used in a PCR reaction; for Region B For 6/2 AB and Rev 6/2 BC primer; and for Region C For 6/2 BC and T7 terminator primer. The Region amplicons were individually extracted from an agarose gel using the Qiagen QIAquick Gel Extraction Kit. Different combinations of region

inserts for Region A, Region B, and Region C derived from *mTBT* (labeled as 2) or *DBAT* (labeled as 6) were added into another PCR reaction. These combinations produced 6 different chimeras.

4.2.2.2.3. *Construction of Domain NDTBT/DBAT Mutants*

Plasmids separately containing cDNA encoding NDTBT or DBAT with an in-frame C-terminal histidine tag were used as templates to make the NDTBT/DBAT domain mutants. The N-terminal domain of NDTBT is amplified using T7 promoter and C-DiR10 primers, while the C-terminal domain is amplified by C-DiF10 and T7 terminator primers, separately. This is also respectively conducted using DBAT with T7 promoter and C-DiR6 primers for the N-terminal domain, and C-DiF6 and T7 terminator primers for the C-terminal domain (Figure 4.5).

The C-Di(R/F)(10/6) primers contained overlapping sequence to allow the 3'-end of the N-terminal domain of NDTBT to anneal to the 5'-end of the C-terminal domain of DBAT for elongation in a PCR reaction with T7 promoter and terminator primers. Amplicons are extracted from the agarose gel using Qiagen QIAquick Gel Extraction Kit.

4.2.2.2.4. *Construction of Domain DBAT/mTBT Mutants*

Plasmids separately containing cDNA encoding *mTBT* or DBAT with an in-frame C-terminal histidine tag were used as templates to make the *mTBT*/DBAT domain mutants. The N-terminal domain of *mTBT* is amplified using T7 promoter and A-DiR2 or B-DiR2 primers, while the C-terminal domain is amplified by A-DiF2 or B-DiF2 and T7 terminator primers, separately. This is also respectively conducted using DBAT with T7 promoter and A-DiR6 or B-DiR6

primers for the N-terminal domain, and A-DiF6 or B-DiF6 and T7 terminator primers for the C-terminal domain (Figure 4.5).

The A-Di(R/F)(2/6) primers contained overlapping sequence to allow the 3'-end of the N-terminal domain of *mTBT* to anneal to the 5'-end of the C-terminal domain of DBAT for elongation in a PCR reaction with T7 promoter and terminator primers. The B-Di(R/F)(2/6) primers do the same, but encodes a residue difference of a Histidine 211 found in *mTBT*, instead of a Cysteine 216 found in DBAT (Figure 4.5). Amplicons are extracted from the agarose gel using Qiagen QIAquick Gel Extraction Kit.



Figure 4.5 – Sequence Alignment for Domain Swapping Between *Taxus* Acyltransferases and Schematic of Dimeric Mutants.

4.2.3. Expression and Purification of Chimeric Mutants

4.2.3.1. Culture Medium and Solutions

All solutions were prepared in distilled, deionized water. Luria-Bertani (LB) liquid suspension medium (20 g of LB ‘Miller’ powder/850 mL water) was autoclaved, and the solid medium was prepared by adding 1.5% (w/v) Bacto agar to the LB medium before autoclaving.

The appropriate antibiotics were added to the solid medium after cooling and prior to pouring the media plates. Antibiotics were added to the following final concentrations unless noted otherwise: kanamycin, 50 $\mu\text{g}/\text{mL}$ and chloramphenicol 34 $\mu\text{g}/\text{mL}$. Stock solutions of antibiotics were prepared in water with the exceptions of chloramphenicol, which was prepared in 100% aqueous ethanol. Antibiotics and isopropyl β -D-thioglucoopyranoside (IPTG) stocks were sterilized through 0.22- μm membrane filters before storing at -20 °C.

4.2.3.2. *E. coli* Cell Culture

Recombinant chimeric mutants, regional and domain swaps, were expressed in the described bacterial expression system and harvested according to a previously reported protocol, with slight modifications.¹² Cultures were grown overnight at 37 °C in LB medium (5 mL) supplemented with kanamycin (50 $\mu\text{g}/\text{mL}$). Bacteria transformed with empty vector were processed analogously. The 5-mL inocula were added separately to LB medium (850 mL) supplemented with the appropriate antibiotics and grown at 37 °C to $\text{OD}_{600} = 0.5 - 0.7$. Gene expression was induced with isopropyl- β -D-1-thiogalactopyranoside (500 μM), and the cultures were incubated at 20 °C for 18 h. The cells were harvested by centrifugation (2000g, 20 min, 4 °C), the supernatant was discarded, and the pellets were transferred separately into pre-weighed 50 mL Corning Tubes for storage at -20 °C.

4.2.3.3. Protein Harvest

Generally, the pellets from two 850-mL cultures were re-suspended in lysis buffer (50 mM Tris-HCl, 300 mM sodium chloride, and 10% glycerol, pH 8.0 at 3 mL/g cells) and lysed at 4 °C by sonication (5 min \times 3 sec bursts at 60% power at 5 sec intervals) with a Misonix XL-

2020 sonicator (Misonix Inc., Farmingdale, NY). The cell-lysate was then clarified by ultracentrifugation at 46,000g for 1 h at 4 °C.

4.2.3.4. Protein Purification

Generally, the clarified supernatant of the lysed bacterial cells was loaded onto an Econo column (BioRad, 20 cm × 0.5 cm) with 0.5 mL of Ni-NTA Agarose (Qiagen, Valencia, CA). The resin was washed with an equivalent volume of lysis buffer (50 mM Tris-HCl and 300 mM sodium chloride, 10% glycerol, pH 8.0), and the column was eluted with 1-mL increments of elution buffer containing 10 mM, 50 mM, 100 mM, 150 mM, or 200 mM imidazole for each increment. SDS-PAGE analysis was used to identify fractions containing target protein that migrated to an R_f consistent with a 50 kDa standard. The fractions were combined and concentrated (30,000 MWCO, Amicon Ultra 0.5 mL, Millipore, Billerica, MA). The buffer was exchanged to storage buffer (20 mM Tris-HCl, 5% glycerol, pH 8.0) through concentration

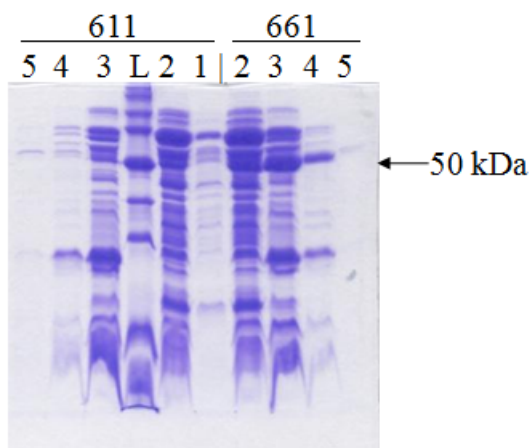


Figure 4.6 - SDS-PAGE Gel of Region Mutants 611 and 661.

10 μ L of 1 mL elutions from 10 mM (1), 50 mM (2), 100 mM (3), 150 mM (4), and 200 mM (5) imidazole fractions. L is molecular ladder. Region mutant 611 – composed of Region A from DBAT (labeled as 6), Region B and C from NDTBT (labeled as 1); and Region mutant 661 – composed of Region A and B from DBAT, Region C from NDTBT.

and dilution cycles to 2 mg/mL (Figure 4.6 and 4.7). Purity was determined by Bradford assay, as described previously, and aliquots (120 μ L) were flash frozen in liquid nitrogen and stored at -78 $^{\circ}$ C

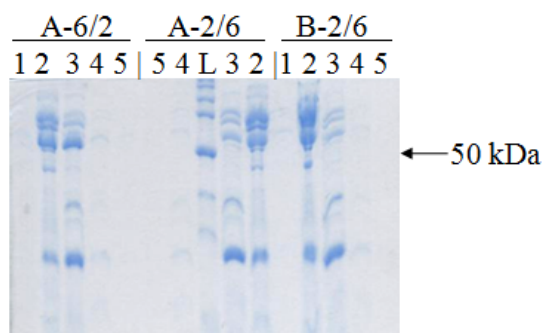


Figure 4.7 - SDS-PAGE Gel of Dimeric Mutants A-6/2, A2/6 and B-2/6.
10 μ L of 1 mL elutions from 10 mM (1), 50 mM (2), 100 mM (3), 150 mM (4), and 200 mM (5) imidazole fractions. L is molecular ladder. Dimeric mutants A-6/2 – composed of N-terminal from DBAT (labeled as 6), C-terminal from *m*TBT (labeled as 2), and vice versa. The ‘A’ label has a Cysteine instead of a Histidine found in ‘B’ Dimeric mutants

4.2.4. Enzymatic Assays and Analysis

4.2.4.1. Activity Assay

To verify functional expression of the chimeric mutants, total protein (100 μ g) isolated from the nickel column was assayed in both the forward- or reverse-catalyzed reaction, dictated by the relative amount of CoA or acyl CoA added to the assay buffer. The assay composition is listed in Table 4.2 and each assay was incubated at 31 $^{\circ}$ C for 1 h. The reactions were quenched and extracted with ethyl acetate (2 \times 1 mL), the respective organic fractions were combined, the solvents were evaporated, and the residues were redissolved in acetonitrile (100 μ L).

4.4.4.2. LC-ESI/MS Analysis

The compounds extracted from each sample were individually analyzed on a Waters 2795 Separations Module (fitted with a Betasil C18, 5 μ m, 150 \times 2.1 mm (Thermo-Fischer

Scientific Inc.) reversed-phase HPLC column) coupled to a QToF UltimaTM API (Walters Inc.)

mass spectrometer . A guard column was attached between the separations module and the mass

Table 4.2 – Activity Assay Composition for Chimeric Mutants

Type	Reaction	Taxane (1 mM)	Coenzyme A Substrate (1 mM)	Assay Volume & Buffer
NDTBT/DBAT	Forward	N-debenzoyl-2'- deoxypaclitaxel	Benzoyl CoA or Acetyl CoA	500 μL; 20 mM NaH ₂ PO ₄ , 5% glycerol, pH 7.6
		10-deacetylbaaccatin III		
DBAT/ <i>m</i> TBT	Forward	10-deacetylbaaccatin III	Benzoyl CoA or Acetyl CoA	1 mL; 20 mM MOPSO, 5% glycerol, pH 7.4
		7,13-diacetyl-2- debenzoylbaccatin		
	Reverse	Baccatin III	Free CoA	
		7,13-diacetylbaaccatin		

spectrometer. The column was eluted at 0.3 mL/min with a gradient of solvent A: 99.5% H₂O with 0.5% formic acid (v/v); 99.5% CH₃CN and solvent B: 0.5% formic acid (v/v) as follows: 0 - 1.5 min, held at 80% A; 1.5 - 3.3 min, decreased from 80 to 50% A; 3.3 - 6.3 min, decreased from 50 to 20% A; 6.3 - 6.9 min, decreased from 20 to 0% A; 6.9 - 7.5 min, held at 0% A; 7.5 - 7.6 min, increased from 0 to 80% A; 7.7 - 10 min, held at 80% A. Aliquots at 5-10 µL were injected for samples extracted from assays incubated with the parent (i.e. wild-type) enzyme. However, aliquots of 40-50 µL were injected for samples extracted from assays incubated with a chimeric mutant. The remaining substrate in the samples was diverted to waste prior to entering the QToF chamber to suppress its ionization signature compared to those of the small quantities of possible biosynthetic products. Controls assays and product standards were analyzed in parallel (cf. Figure 4.8 for an example).

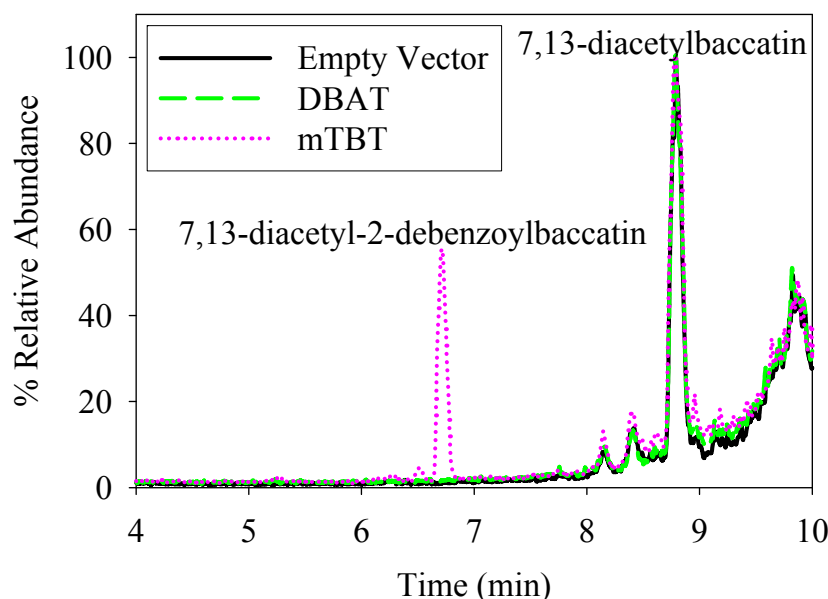


Figure 4.8 – Chromatogram from LC-ESI/MS of Controls from Reverse Reaction Assays with 7,13-Diacetyl-2-debenzoylbaccatin.

4.3. Results

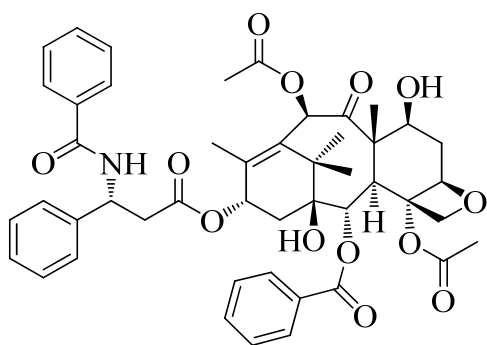
4.3.1. Regional Mutants Made by Recombination of NDTBT and DBAT

The splice sites of the model structure were estimated by the cut sites separating Regions A, B, and C identified in the bona fide structure of anthocyanin malonyltransferase (cf. Figure 4.2). The sites targeted in NDTBT were evaluated for stretches of amino acid sequences that were conserved in the modeled secondary structure of DBAT. As a first approach, that was later abandoned, the *Taxus* transferases were originally screened for the same restriction enzyme sites (*SphI*, *PmlI*, *SpeI*, and *SalI*) used to make the anthocyanin mutants.⁷ Equivalent sites were not found in the *Taxus* sequences. More importantly, if the Region B/C junction of the malonyltransferase was strictly applied to the *Taxus* mutants, the exchange site would introduce a frame shift and alter the amino acid sequence in domain C.

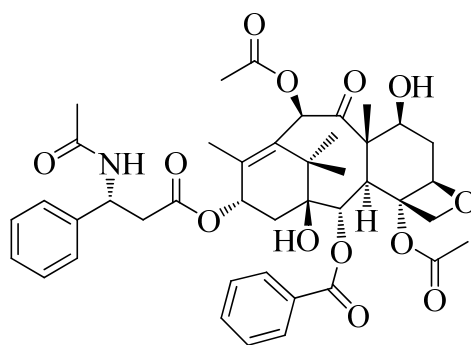
The nucleotide sequence between cDNA of *ndtbt* and *dbat* had consensus, but a few silent mutations were incorporated in the primer designed to allow amplification of each region with matching overhangs. These mutations did not change the amino acid sequence; they allowed annealing between the cDNA Region A, B, and C amplicons during the PCR reaction combining the precursor regions. By over-lap extension full-length chimeric mutants were constructed.

All six constructs for the NDTBT/DBAT chimeric mutants were subcloned and their sequences were verified. The labeling scheme is concocted from the region number ascribed to NDTBT (designated as '1') and DBAT (designated as '6'), and the first, second, or third positioning of the number corresponds to Region A, B, or C, respectively. For example, mutant '616' is comprised of N- to C-terminal amino acid sequence from DBAT region A (6), NDTBT region B (1), and DBAT region C (6). The chimeric mutants, ligated into a pET28 expression vector, were overexpressed in competent BL21 (DE3) *E. coli* cells. Generally, the isolated target protein was purified on nickel-affinity resin and eluted from the column with between 50 and 100 mM imidazole. The unaltered enzymes, NDTBT and DBAT, were purified with the same procedure and tested for activity under the same conditions as with the chimeric mutants.

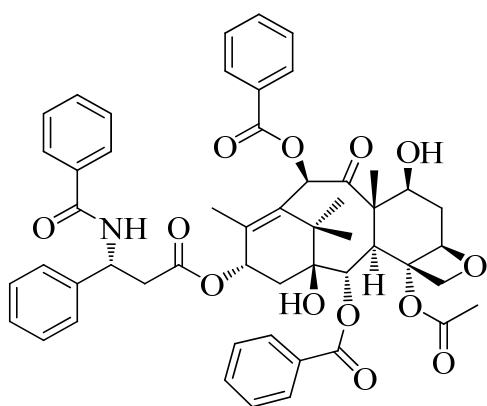
Activity assays were conducted with *N*-debenzoyl-2'-deoxypaclitaxel or 10-deacetylbaaccatin III and either benzoyl- or acetyl CoA for each regional chimeric and wild-type enzyme. The production of taxanes was monitored by LC-ESI/MS and the molecular ions ($M + H^+$) of each putative metabolite was searched (Figure 4.9). Wild-type NDTBT converted *N*-debenzoyl-2'-deoxypaclitaxel to 2'-deoxypaclitaxel ($[M + H]^+ = m/z$ 838.3), and to *N*-acetyl-*N*-debenzoyl-2'-deoxypaclitaxel when acetyl CoA ($[M + H]^+ = m/z$ 776.3) was used in place of benzoyl CoA, as shown previously.² No product was formed with 10-deacetylbaaccatin III and benzoyl- or acetyl



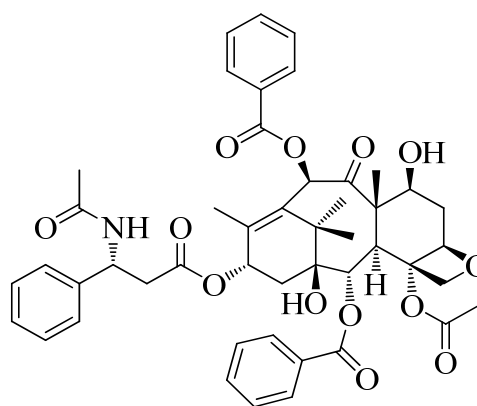
(1)
2'-Deoxypaclitaxel



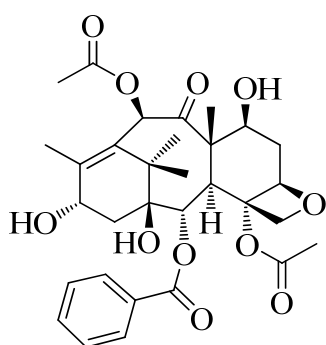
(2)
N-Acetyl-*N*-debenzoyl-2'-deoxypaclitaxel



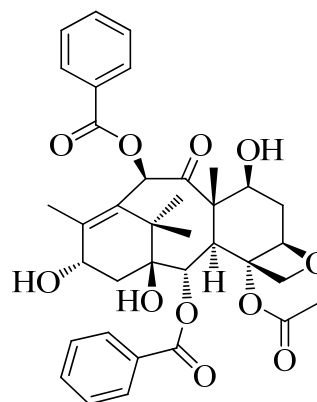
(3)
10-Benzoyl-10-deacetyl-2'-deoxypaclitaxel



(4)
N-Acetyl-*N*-debenzoyl-10-benzoyl-10-deacetyl-2'-deoxypaclitaxel



(5)
Baccatin III



(6)
10-Benzoyl-10-deacetylbaccatin

Figure 4.9 – Possible Products from NDTBT/DBAT Chimeric Mutants.

CoA substrate when incubated with wild-type NDTBT. Wild-type DBAT converted 10-deacetylbaccatin and acetyl CoA to baccatin III ($[M + H]^+ = m/z\ 587.2$), as shown previously.¹¹

Chimeric mutants 616 and 161 were isolated at the lowest protein yield 0.06 mg/L and no products were detected in any assay containing one of several combinations of taxane and CoA substrates. Mutants 611 and 661 had the highest yield of 0.18 mg/L, yet, no products were detected in any assay containing one of several combinations of taxane and CoA substrates. The other two mutants, 166 and 116 gave a yield of 0.12 mg/L and like the others; no products were detected in any assay containing one of several combinations of taxane and CoA substrates.

4.3.2. Regional DBAT/*m*TBT Mutants

DNA analysis of the *mtbt* and *dbat* sequences revealed that the junction sites used to construct the NDTBT/DBAT hybrid mutants were not applicable for constructing the DBAT/*m*TBT hybrids. Sites proximate to the junction sites for splicing *ndtbt* and *dbat* DNA were chosen for *mtbt* and *dbat*. The consensus sites shared between *mtbt* and *dbat* eliminated the need to make mutagenic primers to amplify the appropriate regions of the full-length cDNA. The hybrid cDNA was constructed similar to the technique described previously in this chapter (cf. Section 4.3.1). The labeling scheme is concocted from the 'Region number' ascribed to NDTBT (designated as '2') and DBAT (designated as '6'), and the first, second, or third positioning of the number corresponds to Region A, B, or C, respectively. Of the several possible *m*TBT/DBAT hybrid combinations, only two (226 and 266) were successfully sub-cloned and sequence verified. The other four cDNAs encoding hybrids 622, 662, 626, and 262 were successfully amplified by PCR, but were recalcitrant to restriction enzyme digestion and/or the ligation process.

During restriction enzyme digestions with *Nco*I and *Bam*HI, the cDNA seemed to degrade. The DNA band on an ethidium bromide-infused agarose gel appears as a smear when visualized under UV-light. Restriction sites were verified at the 5'- and 3'-ends by sequence analysis. The construction of these hybrids is pending, and they will likely be tested for function at a future date.

Generally, the isolated mutant protein was purified on nickel-affinity resin, similarly to the earlier process (cf. Section 4.3.1). The unaltered enzymes, DBAT and *m*TBT, were purified with the same procedure and tested for activity under the same conditions as with the hybrid mutants.

The first activity assays were conducted with baccatin III or 7,13-diacetylbaccatin and free CoA substrate, to conserve the acyl CoA substrates, for each hybrid mutant and wild-type enzyme. Since both DBAT and *m*TBT are able to catalyze their reverse reactions, that is, the acyltransferase can hydrolyze the acyl group off of the taxane product in the reverse reaction to liberate the deacylated taxanes. The productions of taxanes without an acyl group at the C2 or C10 position was monitored by LC-ESI/MS and the molecular ions ($M + H^+$) of each putative metabolite was searched. Wild-type DBAT converted baccatin III to 10-deacetylbaccatin ($[M + H]^+ = 545.3$) when free CoA was available. Wild-type *m*TBT converted 7,13-diacetylbaccatin to 7,13-diacetyl-2-debenzoylbaccatin ($[M + H]^+ = 567.3$) when free CoA was available. No products were formed when taxanes were switched in assays of the wild-type enzymes; for instance, 7,13-diacetyl-2-debenzoylbaccatin was not detectable when 7,13-diacetylbaccatin and free CoA substrate were incubated with wild-type DBAT.

To evaluate the chimeric mutants further, a forward reaction assay was performed using 10-deacetylbaccatin or 7,13-diacetyl-2-debenzoylbaccatin with benzoyl- and acetyl CoA separately. Each wild-type enzyme, DBAT and *m*TBT, converted their substrates to their proper products: 10-deacetylbaccatin to baccatin III ($[M + H]^+ = 587.3$), and 7,13-diacetyl-2-debenzoylbaccatin to either acetylated or benzoylated 7,13-diacetyl-2-debenzoylbaccatin ($[M + H]^+ = 609.3$ or 671.3), respectively. Chimeric mutants 226 and 266 were isolated at the lowest

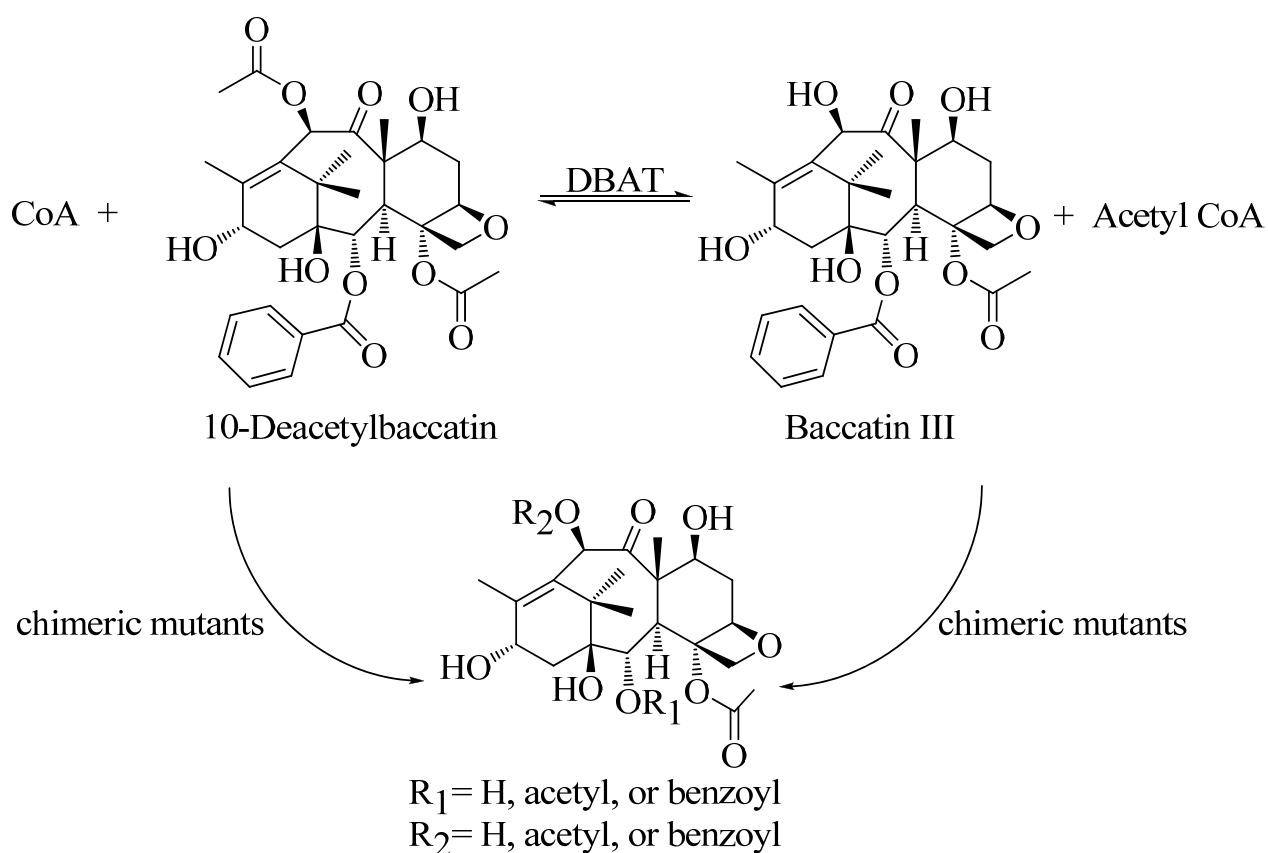


Figure 4.10 - Scheme for DBAT with Natural Substrates and Possible Products from Chimeric Mutants.

protein yield 0.06 mg/L and no semi-biosynthesized products were detected were detected in any assay containing one of several combinations of taxane and CoA substrates by LC-ESI/MS for individual $[M + H]^+$ ions (Figure 4.10 and Figure 4.11).

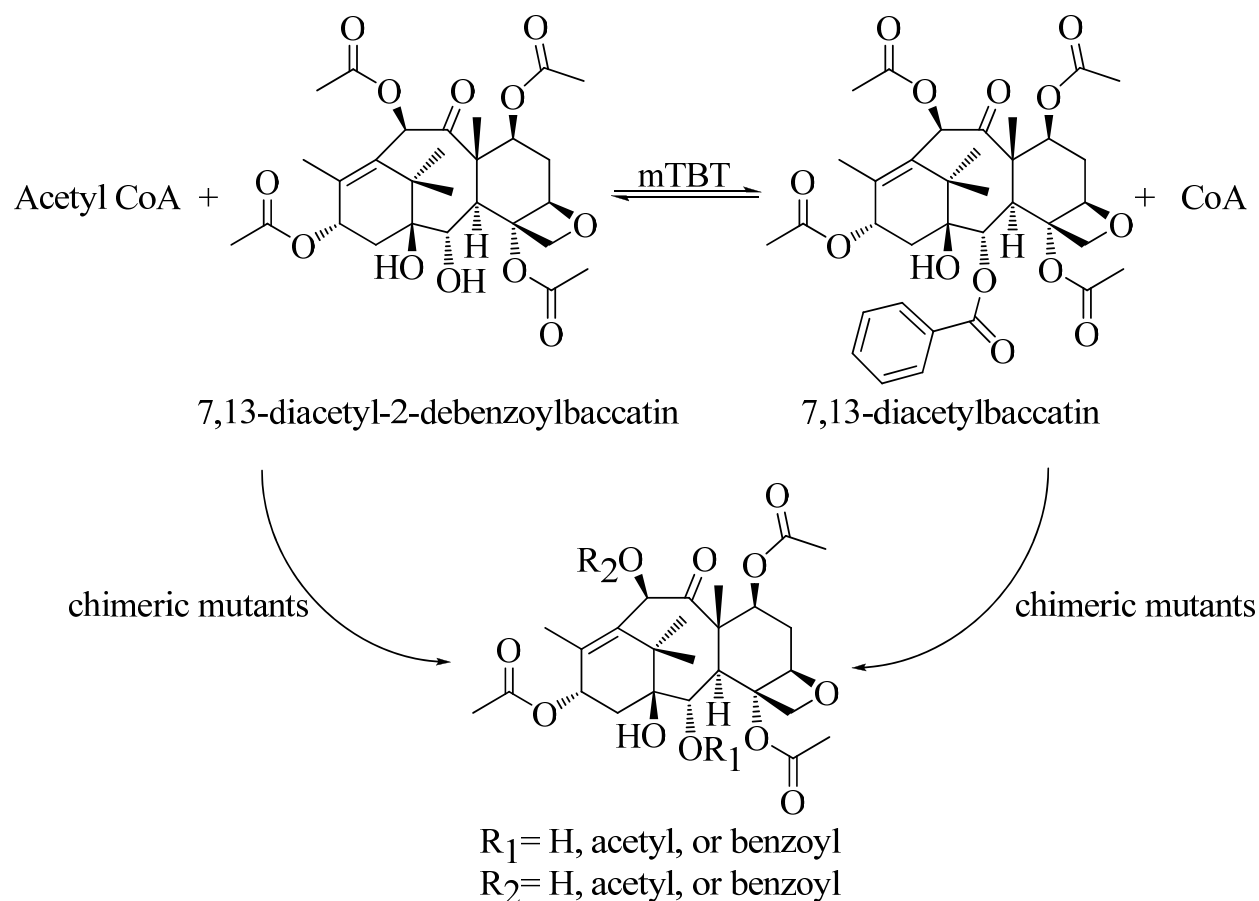


Figure 4.11 - Scheme for *mTBT* with Natural Substrates and Possible Products from Chimeric Mutants.

4.3.3. Domain Mutants

Comparison of the amino acid sequences of VS, Dm3MaT3, and three *Taxus* acyltransferases (NDTBT, DBAT, and *mTBT*, described herein) revealed a conserved loop region that was targeted as a junction point between two domains of this family. Oligonucleotide primers were designed to swap the domains between *ndtbt* and *dbat* as well as *dbat* and *mtbt* to make hybrid DNA. The resulting two hybrid cDNA made for each pair were sub-cloned and their DNA sequences were verified. The labeling scheme is concocted from the domain number ascribed to NDTBT (designated as '1'), DBAT (designated as '6') and *mTBT* (designated as '2'),

and the first and second positioning of the number corresponds to N-terminal Domain, or C-terminal domain, respectively.

Table 4.3 – Domain Mutants

Label	Domain	
	N-terminal	C-terminal
A-2/6	2	6
A-6/2	6	2
B-2/6	2	6
B-6/2	6	2
C-6/10	6	10
C-10/6	10	6

The cDNA of the domain mutants, ligated into a pET28 expression vector, were overexpressed in competent BL21 (DE3) *E. coli* cells. Generally, the isolated target protein was purified on nickel-affinity resin and eluted from the column with between 50 and 100 mM imidazole. The purity ranged between the mutants and had a slight improvement when compared to the regional swapped mutants, from 0.24-0.48 mg/L yield. The unaltered enzymes – NDTBT, *m*TBT and DBAT – were purified with the same procedure and tested for activity under the same conditions as with the domain mutants.

The difference between the A and B group of the DBAT/*m*TBT hybrid is the cysteine from DBAT or a histidine from *m*TBT is conserved in the loop region, respectively. These mutants were tested with substrates for the forward and reverse reactions in separate sets of assays and monitored by LC-ESI/MS and the molecular ions ($[M + H]^+$) of each putative metabolite was searched. Assay compositions were consistent with the previous conditions used for the NDTBT/DBAT and DBAT/*m*TBT chimeric Region mutants. Nothing was produced by the mutants when compared to their wild-type enzymes. Unfortunately, this observation was also seen when the NDTBT/DBAT dimeric mutants were screened for the forward reaction with *N*-

debenzoyl-2'-deoxypaclitaxel or 10-deacetylbaaccatin and either benzoyl CoA or acetyl CoA substrate.

4.4. Discussion

The earlier study on the anthocyanin malonyltransferase catalyst identified residues in Regions A and C responsible for activity and for honing the substrate selectivity. The study also showed that Region A was important for recognition of the acyl acceptor substrate, while regions B and C moderated the acyl CoA binding.⁷ Considering this information, two of the region-swapped hybrids (611 and 166) were projected to either transfer a larger than usual benzoyl group to the C10 position of 10-deacetylbaaccatin or a smaller than expected acetyl group to the amine of *N*-debenzoyl-2'-deoxypaclitaxel. Notably, the size of the taxane substrates assayed varied markedly; *N*-debenzoyl-2'-deoxypaclitaxel has a 3-amino phenylpropanoid side chain at C13 while 10-deacetylbaaccatin has a hydroxyl group at this position, This difference in sterics along with the acylation of a hydroxyl compared to an amine by the *N*-benzoyltransferase and the *O*-acetyltransferase, respectively, likely added challenges toward constructing a functional hybrid enzyme between NDTBT and *m*TBT. However, the similarities in the taxane substrates (i.e., baaccatin III analogues) used by the wild-type DBAT and *m*TBT coupled with both enzymes catalyzing the acylation of a hydroxyl group provided a reasonable chance that DBAT/*m*TBT hybrid mutants may be functional. Several technical difficulties (amplifying domains, combining domain precursors for PCR, and digesting full-length hybrid inserts for ligation) precluded progress towards constructing the desire three-region cDNA hybrids. Only the DBAT/*m*TBT 266 hybrid was constructed, and it did not catalyze any detectable product from a combination of a baaccatin III analogue and either benzoyl- or acetyl CoA.

The binding site for the taxane acceptor is comprised of residues from each of the three Regions that therefore add complexity to its reconstruction in the hybrid mutants. Despite the several identical residues shared between the wild-type NDTBT and DBAT (60% identity, 74% similarity), there is significant alteration at the taxane binding site when the domains are exchanged among the *Taxus* acyltransferases (Figure 4.12). Further, the homology models of NDTBT, DBAT, and *m*TBT used to identify the junction sites to make the Region-swaps were based on Dm3maT3 that was only 26% identical and 42% similar to the *Taxus* acyltransferases. These differences in the *Taxus* acyltransferases sequences may be too great, rendering hybrid enzymes with poor intramolecular interactions that affect their function, substrate selectivity and, occasionally, their heterologous expression. By contrast, the wild-type progenitor malonyltransferases used to make the cognate chimeras were 89% identical and 93% similar, and the thioester substrate malonyl CoA was used by both wild-type enzymes. These considerations

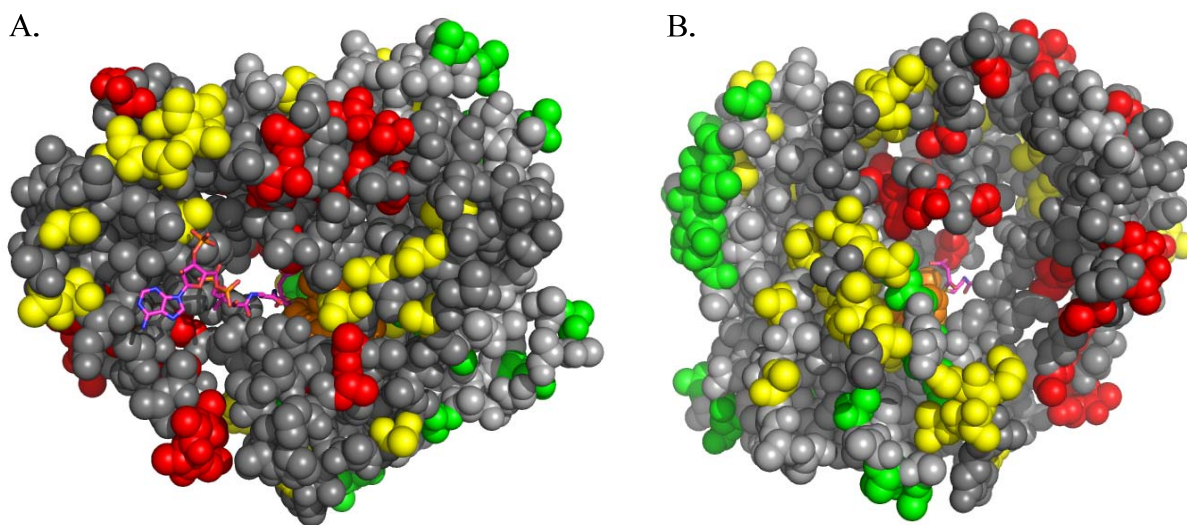


Figure 4.12 - Homology Model of NDTBT Based on Dm3MaT3 with Conserved Residues Between NDTBT and DBAT.

Region A (green), region B (yellow), and region C (red). All grey coloring represents conserved residues. Pink coloring of the malonyl CoA substrate with the catalytic diad (orange). A. View of CoA binding site. B. View of acceptor binding site. Created using PyMOL.

along with the wild-type malonyltransferases using structurally similar acyl acceptor substrates likely added to the construction of a functional malonyltransferase hybrid enzyme.

The junction sites between the domains of vinorine synthase and anthocyanin malonyltransferase raised concerns about whether the domain hybrids would fold correctly. The relatively modest sequence identity (~60%) among the *Taxus* acyltransferases used in this study may have contributed to the mismatches at the interface between the N-domain of one acyltransferase and C-domain of another. Proper alignment at this interface is needed to maintain the substrate-access tunnel through the middle of the enzyme (cf. Figure 4.12). It can be imagined that any slight disruption in this access tunnel would render nonfunctional enzyme. Intriguingly, the domain-swapped mutant proteins were obtained at two- to three-fold higher purity from the nickel-affinity column than were the region-swapped mutant protein yet they also did not produce detectable products from *in vitro* assays.

Even though the chimeric mutants – regional and domain swaps – between the two *Taxus* benzoyltransferases and acetyltransferase had no detectable activity with the native substrates of the wild-type enzymes, the future of engineering these enzymes to hone or expand substrate specificity could still be examined by this approach. There are four requirements that need to be investigated to continue this experiment – increase protein expression, improve the purification of the mutant enzymes, assay the enzymes with a wider range of substrates, construct mutants between NDTBT and *m*TBT (both use benzoyl CoA as a substrate), and obtain the crystal structure of a *Taxus* acyltransferase.

The benzoyltransferases, NDTBT and *m*TBT, were originally surveyed using purified protein from a nickel-affinity chromatography step providing a purity level of 70% and 30%, respectively, and demonstrating activity with their substrates.^{2, 3} Although these chimeric

proteins were assumed to have the same activity after this purification step, the yield of the target protein was extremely low as demonstrated by less the intense and indistinguishable bands from SDS-PAGE gel analysis. An empty vector control, which contained endogenous proteins that co-purified from the nickel-affinity column, was also tested to eliminate the background activity of the non-target protein. Although no activity was detected, it is unknown yet unlikely that these background enzymes sequester substrate from the chimeric mutants. In order to test this hypothesis the quantity of substrates incubated needs to be accounted for after an assay reaction with chimeric mutant and empty vector control, separately.

To evaluate whether the mutants folded correctly, first the purity of the chimeric mutants needs to be increased by additional purification steps using anion exchange and gel filtration, described previous herein for the wild-type enzymes. Then application of circular dichroism (CD) spectroscopy reveal whether the chimeric mutants share the same secondary structure conformation (α -helices and β -sheets) as the wild-type enzymes. Substrate binding evaluation can also be employed as a complement to CD to assess if the mutant proteins are misfolded. The binding site access can be monitored by measuring the levels of free substrate remaining in solution (i.e., the K_d) after incubating the substrate with an equal molar amount of mutant enzyme and comparing the results obtained with wild-type enzyme. If these experiments reveal no significant differences, then the activity of the chimeric mutants needs to be surveyed with a variety of functional substrates utilized by the wild-type enzymes. The changes imposed by the swapped regions could dramatically change the expected substrate specificity of the enzymes.

Chimeras were made between NDTBT and DBAT as well as between DBAT and *m*TBT to evaluate the effects of changing the secondary structure by screening with various substrates. The, hybrid enzymes constructed from two wild-type benzoyltransferases (NDTBT and *m*TBT)

could help identify residues or regions responsible for taxane selectivity, since both naturally use a common cosubstrate, benzoyl CoA. Most importantly, however, future mutagenesis studies to evaluate the catalytic mechanism and substrate selectivity would be greatly informed by the crystal structure of each *Taxus* acyltransferase. The structural data would likely show secondary structures that are substantially different than a model conceived from the Dm3MaT or VS structures.

APPENDICES

APPENDIX C

AMINO ACID SEQUENCE ALIGNMENTS OF *TAXUS* ACYLTRANSFERASES WITH ANTHOCYANIN MALONYLTRANSFERASE AND VINORINE SYNTHASE

Only sequences relating to Chapter 4 are listed in this appendix. Alignments were constructed by MultiAlin and viewed by ESPript 2.2.

	1	10	20	30
NDTBT	MEKAGSTD	FHVKKF	DPVMVAP	SLPSPKATVQL
DBAT	..MAGSTEF	VVRSLE	RVMVAP	SQPSPKAFLLQL
mTBTMGR	FNVDMI	ERVIVAP	CLPSPKKILLHL
consensus>70F.V...	#.V.VAP..	PSPK....L	

	40	50	60
NDTBT	SVDSLTICR.G	IFNTLLVFNA	PDNISADP
DBAT	STLDNLPGVREN	IFNTLLVYNAS	DRVSVDP
mTBT	SPIDNKR...G	LTNLSVYNAS	QRVSVSADP
consensus>70	S..D.....N.L.V	%NA.#.!S...	DP

	70	80	90
NDTBT	VKIIREALSKVLVYY	FPLAGRLRSKEI	GELEV
DBAT	AKVIRQALSKVLVYY	SPFAGRLRKKEN	GDLEV
mTBT	AKTIREALSKVLVYY	PPFAGRLRNTEN	GDLEV
consensus>70	.K.IR#ALSKVLVYY	.P.AGRLR..E.G	#LEV

	100	110	120
NDTBT	ECTGDGALFVEAMVE	DTISVLRLDLD	DLNPSFQ
DBAT	ECTGEGALFVEAMAD	TDLSVLGDLD	DYSPSLE
mTBT	ECTGEGAVFVEAMAD	NDLSVLQDFNE	YDPSFQ
consensus>70	ECTG#GA.FVEAM.#	...SVL.D.##	..PS.#

	130	140	150
NDTBT	QLVF	WHPLD	TAIEDLHLV
DBAT	QLLF	CLPPD	TDIEDIHPLV
mTBT	QLVF	NLRED	VNIEDLHLIT
consensus>70	QL.F....D..IED	.H...VQVTRFTCGG	..V

	160	170	180
NDTBT	GVTLP	HSVC	DGRGAQFVTALA
DBAT	GVSFCH	GICDGLGAGQFLIAM	EMARGEIKPS
mTBT	GTRFH	HSVS	DGKGIQQLKGM
consensus>70	G....H.!.DG.G..Q\$.EMARGE	.KPS

	190	200	210	220
NDTBT	LEPIWN	RELLNPED	PLH.LQLNQ	FDSICPPPM
DBAT	SEPIWK	RELKPED	PLYRFQYYHF	QLICPPST
mTBT	LEPIWN	REMVKPED	IMY.LQFDHF	DFIHPPLN
consensus>70	.EPIW.RE\$..PED	.\$...Q...F#	.I.PP..	

Figure C.1 – Sequence Alignment of *Taxus* Acyltransferases.

Figure C.1 (cont'd)

	230	240	250																													
NDTBT	LEELGQAS	FINVD	TEYMKQCVMEECN	EFCS																												
DBAT	FGKIVQGS	LVTSET	INC	IKQCLREESKEFCS																												
mTBT	LEKSIQAS	MVISFER	INYIKRCMMEEC	KEFFS																												
consensus>70Q.S.VI..#.	I#..K.C..EE..EF.S																														
	260	270	280																													
NDTBT	SFEVVAALV	WIARTKALQ	IPH	TENVKLLFAMD																												
DBAT	AFEVVSALAW	IARTRALQ	IPH	SEN	VKLIFAMD																											
mTBT	AFEVVALI	WLARTK	SFR	IP	NE	YVKIIF	PI	D																								
consensus>70	.FEVV.AL.W.ART....	IP..E.VK..F..D																														
	290	300	310																													
NDTBT	LRKLFN	PLPN	GYGN	AI	GTAY	AMD	NVQ	DL	LN																							
DBAT	MRKLFN	PLSK	GYGN	FE	VGTVC	AMD	NV	KD	LLS																							
mTBT	MRNS	FDS	PLPK	GYGN	AI	GNAC	AMD	NV	KD	LLN																						
consensus>70	\$R..F#.PL..	GYGN.!	G...AMD	NV.DLL.																												
	320	330	340																													
NDTBT	GSLLRA	IM	I	IKKAK	KAD	LK	D	NYSR	S	R	V	V	T	N	P	Y	S															
DBAT	GSLLRV	VR	I	IKKAK	KV	SL	N	E	H	F	T.	S	T	I	V	T	P	R	S	G												
mTBT	GSLLY	AL	M	L	IKKSK	F	A	L	N	E	N	F	K.	S	R	I	L	T	K	P	S	T										
consensus>70	GSLL.....	IKK.K..L.#.%..	S.!.T....																													
	350	360	370	380																												
NDTBT	LDV	N	K	K	S	D	N	I	L	A	L	S	D	W	R	R	L	G	F	Y	E	A	D	F	G	W	G	G	P	L		
DBAT	S	D	E	S	I	N	Y	E	N	I	V	G	F	G	D	R	R	R	L	G	F	D	E	V	D	F	G	W	G	H	A	D
mTBT	L	D	A	N	M	K	H	E	N	V	V	G	C	G	D	W	R	N	L	G	F	Y	E	A	D	F	G	W	G	N	A	V
consensus>70	.D.....#N!D.R.LGF.E.DFGWG...																														
	390	400	410																													
NDTBT	NVS	S	L	Q	R.	L	E	N	G	L	P	M	F	S	T	F	L	Y	L	L	P	A	K	N	K	S	D	G	I			
DBAT	NVS	L	V	Q	H	G	L	K	D	V	S	V	V	Q	S	Y	F	L	F	I	R	P	P	K	N	N	P	D	G	I		
mTBT	NVS	P	M	Q	Q	R	E	H	E	L	A	M	Q	N	Y	F	L	F	L	R	S	A	K	N	M	I	D	G	I			
consensus>70	NVS..Q.....	FL%....KN..DGI																														
	420	430	440																													
NDTBT	K	L	L	S	C	M	P	T	T	L	K	S	F	K	I	V	M	E	A	M	I	E	K	Y	V	S	K	V	..			
DBAT	K	I	L	.	S	F	M	P	S	I	V	K	S	F	K	F	E	M	E	T	M	T	N	K	Y	V	T	K	P	..		
mTBT	K	I	L	.	M	F	M	P	A	S	M	V	K	P	F	K	I	E	M	E	V	T	I	N	K	Y	V	A	K	I	C	N
consensus>70	K.L...MP....	K.FK..ME...#KYV.K...																														

Figure C.1 (cont'd)

NDTBT	...
DBAT	...
mTBT	SKL
<i>consensus</i> >70	...

	1	10	20																												
Dm3MaT3	..M	ASLPIL	T	VLEQSQVSP	PD	TLGDKS	..LQL																								
NDTBT	MEK	AGSTDF	H	VKKFDP	VMVAPS	LPSPKAT	VQL																								
DBAT	..M	AGSTEF	V	RSLE	RMVAPS	QPSPKAF	LQL																								
consensus>50	..m	Agstdf	.V	...d	.VmvaPs	.pspKa	.lQL																								
	30	40	50	60																											
Dm3MaT3	TFF	DF	..WL	RSP	PINN	LFFYELP	ITRSQFTET																								
NDTBT	SVV	DSL	TICR	.G	IFNT	LLVFNAP	...DNISAD																								
DBAT	STL	DN	LPGV	REN	IFNT	LLVYNAS	...DRVSVD																								
consensus>50	s..D	.l	...R	..ifNt	Llv%#ap	...dqis	.d																								
	70	80	90																												
Dm3MaT3	VVPN	IKHS	LSIT	LKH	FYP	FV	GKLV	VYP	APT	KK																					
NDTBT	PVKI	IREAL	SKVL	VYF	P	LAGRL	RSKE	I	GELE																						
DBAT	PAKV	IRQAL	SKVL	VYYS	P	FAGRL	R	K	EN	GDLE																					
consensus>50	pvki	Irea	Lskv	Lvy%	yPfa	GrLr	.ke	.gele																							
	100	110	120																												
Dm3MaT3	PEI	CYVEG	DSVA	VTFAE	C	NLD	.L	NEL	TGNH	PR																					
NDTBT	VE	.CTG	D	GALF	VEAM	VE	D	TISV	LRD	DDLN	PR																				
DBAT	VE	.CTG	E	GALF	VEAM	AD	T	DLSV	L	DDYS	P																				
consensus>50	vE	.Ctg	#Gal	fveama	#	.nlsv	L	.#Ldd	..P																						
	130	140	150																												
Dm3MaT3	NCD	KFYD	LVP	I	LGES	STR	LS	D	C	IK	IPL	F	S	VQVT																	
NDTBT	...	SFQQL	LVF	WHP	L	D	T	A	I	E	D	...	LHL	V	I	VQVT															
DBAT	...	SLEQL	LF	C	LP	D	T	I	E	D	...	IHPL	V	VQVT																	
consensus>50	...	sfq	#Lv	f	.lp	.dT	.ie	D	...	ihl	.i	VQVT																			
	160	170	180																												
Dm3MaT3	LFPNQ	GIA	GIT	NH	H	C	L	G	D	A	S	T	R	F	C	F	L	K	A	W	T	S									
NDTBT	RFTCG	GIA	V	GVT	L	P	H	S	V	C	D	G	R	G	A	Q	F	V	T	A	L	A	E								
DBAT	RFTCG	G	F	V	G	V	S	F	C	H	G	I	C	D	G	L	G	A	G	Q	F	L	I	A	M	G	E				
consensus>50	rFtcg	Gia	!G	!t	..H	.vc	Dg	.ga	.qF	l	.Al	.e																			
	190	200	210																												
Dm3MaT3	I	A	R	S	G	N	N	D	E	S	F	L	A	N	G	T	R	P	L	Y	D	R	I	K	Y	P	M	L	D	E	A
NDTBT	M	A	R	G	E	V	K	P	S	L	E	P	I	W	N	R	E	L	L	N	P	...	E	D						
DBAT	M	A	R	G	E	I	K	P	S	S	E	P	I	W	K	R	E	L	L	K	P	...	E	D						
consensus>50	mARge	vkps	.e	Piwd	Re	ll	.P	...	Ed																					

Figure C.2 – Sequence Alignment of NDTBT and DBAT with DmMaT3.

Figure C.2 (cont'd)

	220	230	240	250
Dm3Mat3	Y L K R A K V E S F N E D Y V T Q S L A G P S D K L R A T F I L			
NDTBT	P L H . L Q L N Q F D S I C P P P M L . . . E E L G Q A S F V I			
DBAT	P L Y R F Q Y Y H F Q L I C P P S T E . . . G K I V Q G S L V I			
consensus>50	p L . r . q . e . F # . i c p p . . l d . . q a s f ! i			
	260	270	280	
Dm3Mat3	T R A V I N Q L K D R V L A Q L P T L E Y V S S F T V A C A Y I			
NDTBT	N V D T I E Y M K Q C V M E E . . C N E F C S S F E V V A A L V			
DBAT	T S E T I N C I K Q C L R E E . . S K E F C S A F E V V S A L A			
consensus>50	t . d t I # . l K # c v l e # E % c S s F e V v . A l i			
	290	300	310	
Dm3Mat3	W S C I A K S R . . . N D K L Q L F G F P I D R R A R M K P P I			
NDTBT	W I A R T K A L Q I P H T E N V K L L F A M D L R K L F N P P L			
DBAT	W I A R T R A L Q I P H S E N V K L I F A M D M R K L F N P P L			
consensus>50	W i a r t k a l q i p h . e n v k l . F a m D l R k l f n P P l			
	320	330	340	
Dm3Mat3	P T A Y F G N C V G G C A A I A K T N L L I G K E G F I T A A K			
NDTBT	P N G Y Y G N A I G T A Y A M D N V Q D L L N G S . L L R A I M			
DBAT	S K G Y Y G N F V G T V C A M D N V K D L L S G S . L L R V V R			
consensus>50	p . g Y % G N . ! G t . . A m d n v n d L l . g s . l l r a i .			
	350	360	370	
Dm3Mat3	L I G E N I H K T L T D Y K D G V L K D D M E S F N D L V S E G			
NDTBT	I I K K A K A D L K D N Y S R S R V V T N P Y S L D V N K K S .			
DBAT	I I K K A K V S L N E H F T . S T I V T P R S G S D E S I N Y .			
consensus>50	i I k k a k . . l . d d % . . s . v v t d . . s . # d . v . .			
	380	390	400	
Dm3Mat3	M P T T M T W V S G T P K L R F Y D M D F G W G K P K K . . .			
NDTBT	. . D N I L A L S D W R R L G F Y E A D F G W G G P L N V S S L			
DBAT	. . E N I V G F G D R R R L G F D E V D F G W G H A D N V S L V			
consensus>50	. . d n i . . . s d . r r L g F y # . D F G W G . p . n v s . .			
	410	420	430	
Dm3Mat3	. . L E T V S I D H N G A I S I N S C K E S N E D L E I G . V			
NDTBT	Q R . L E N G L P M F S T F L Y L L P A K N K S D G I K L L S			
DBAT	Q H G L K D V S V V Q S Y F L F I R P P K N N P D G I K I L . S			
consensus>50	q . . L e n v s i . . s . f l y i . p . K # . . # g i k i l . s			

Figure C.2 (cont'd)

		440		450		
		.		.		
Dm3MaT3		CISATQ	MEDFVH	IFDDGL	KAYL..	
NDTBT		CMPPTT	LKSFKI	VMEAMI	EKYVSKV	
DBAT		FMPPSI	VKSFKF	EMETMT	NKYVTKP	
<i>consensus</i> >50		cmppt.mksFk.im#.m.ekYv.k.				

	1	10	20
VSMAPQMEKVSEELILPS	SP	PTPQSLKCYKI
DBAT	MAGSTE	FVVRSLERVMVAPS	QSPPKAF..LQL
mTBT	...MGR	FNVDMIERVIVAP	CLPSPPKKI..LHL
consensus>50f	qve.verv	l!aPs.PsPk....l.l
	30	40	50
VS	SHLDQL	L.LTCH	IPFILFY
DBAT	STLDNL	PGVREN	IFNTLLVYNASDRVSV..DP
mTBT	SPIDNK	T...RGLT	NILSVYNASQRVSVSADP
consensus>50	S.lD#li.ni	L.vyNas#rvsv.a#p
	60	70	80
VS	SQH	LKQSLSKVLTHFY	PLAGRI...NVNSSV
DBAT	AKV	IRQALSKVLVYY	SPFAGRLRKKENGDL
mTBT	AKT	IREALSKVLVYY	PPFAGRLRNTENGDL
consensus>50	ak.ir#a	LSKVLvy%	.PfAGRLr..eNg#leV
	90	100	110
VS	DCNDS	GV	FVEARVQAQLSQAIONVVELEKID
DBAT	ECTGE	GALFVEAMADTDLS	.VLGDLDDYSPS
mTBT	ECTGE	GAVFVEAMADNDLS	.VLQDFNEYDPS
consensus>50	#CtgeGa	.FVEAma#	.#LS.vlq#.d#yeps.
	120	130	140
VS	QYL	PSAAYPGGKIE	VNE
DBAT	EQLL	FCLPDPDIE	..DIHPLV
mTBT	QQL	VFNLR	EDVNIE..DLHLLT
consensus>50	#qL.f.l	.pd.dIE..#	.hpL.Vq!trFtCGG
	160	170	180
VS	TAIGV	NLS	HKIA
DBAT	FVVG	VSFCHGICDGLG	AGQFLI
mTBT	FVVG	TRFHHSVSDGKG	IGQLLK
consensus>50	fv!Gv.f.H.!	.Dglg.gqfL	.amgemaRGE.
	190	200	
VS	...	TEIVLP	NFDLAARHFP
DBAT	KPS	SEPIWKRELLKPED	P
mTBT	KPS	L	EP
consensus>50	kps.epiw	.rElvkP#d.\$y..q%.hf#.i.p	

Figure C.3 – Sequence Alignment of DBAT and *m*TBT with Vinorine Synthase.

Figure C.3 (cont'd)

	210	220	230																													
VS	P	ELVPD	ENVVMKRFVFDK	E	K	I	G	A	L	R	A	Q	A	S	S	A	S															
DBAT	P	STF..	GKIVQG	SLVITS	E	T	I	N	C	I	K	Q	C	L	R	E	E	S														
mTBT	P	LN..	EKSIQA	SMVISF	E	R	I	N	Y	I	K	R	C	M	E	E	E	C														
consensus>50	P	ekv!q.slVi..	E	.	I	n	.	i	k	.	c	l	.	e	e	s															
	240	250	260																													
VS	E	E	K	N	F	S	R	V	Q	L	V	V	A	Y	I	W	K	H	V	I	D	V	T	R	A	K	Y	G	A	K	N	K
DBAT	K	E	F	.	C	S	A	F	E	V	V	S	A	L	A	W	..	I	A	R	T	R	A	L	Q	I	P	H	S	E	N	
mTBT	K	E	F	.	F	S	A	F	E	V	V	A	L	I	W	..	L	A	R	T	K	S	F	R	I	P	N	E	Y			
consensus>50	k	E	f	.	f	S	a	f	#	v	V	v	A	l	i	W	..	v	a	r	t	...	i	p	..	#	.					
	270	280	290	300																												
VS	F	V	V	V	Q	A	V	N	L	R	S	R	M	N	P	P	L	P	H	Y	A	M	G	N	I	A	T	L	L	F	A	A
DBAT	V	K	L	I	F	A	M	D	M	R	K	L	F	N	P	P	L	S	K	G	Y	Y	G	N	F	V	G	T	V	.	C	A
mTBT	V	K	I	I	F	P	I	D	M	R	N	S	F	D	S	P	L	P	K	G	Y	Y	G	N	A	I	G	N	A	.	C	A
consensus>50	v	k	v	!	f	a	v	#	\$	R	..	f	#	p	P	L	p	k	g	y	y	G	N	.	v	g	...	c	a			
	310	320																														
VS	V	D	A	E	W	D	K	D	F	P	D	L	I	G	P	L	R	T	S	L	E	K	T	E	D	D	H	N		
DBAT	M	D	N	V	K	D	L	L	S	G	S	L	L	R	V	V	R	I	I	K	K	A	K	V	S	L	N	E	H	F	T	S
mTBT	M	D	N	V	K	D	L	L	N	G	S	L	L	Y	A	L	M	L	I	K	K	S	K	F	A	L	N	E	N	F	K	S
consensus>50	m	D	n	v	k	D	l	l	.	g	s	l	l	..	l	r	.	i	k	k	.	k	..	l	n	E	d	f	.	s		
	330	340	350	360																												
VS	H	E	L	L	K	G	M	T	C	L	Y	E	L	E	P	Q	E	L	L	S	F	T	S	W	C	R	L	G	F	Y	D	L
DBAT	T	I	V	T	P	R	S	G	S	D	E	S	I	N	Y	E	N	I	V	G	F	G	D	R	R	R	L	G	F	D	E	V
mTBT	R	I	L	T	K	P	S	T	L	D	A	N	M	K	H	E	N	V	G	C	G	D	W	R	N	L	G	F	Y	E	A	
consensus>50	.	i	l	t	k	.	s	t	.	d	.	e	l	e	.	#	#	i	v	g	f	g	d	w	r	r	L	G	F	y	#	.
	370	380																														
VS	D	F	G	W	G	K	P	L	S	A	C	T	T	T	F	P	K	R	N	A	A	L	L	M	D					
DBAT	D	F	G	W	G	H	A	D	N	V	S	L	V	Q	H	G	L	K	D	V	S	V	V	Q	S	Y	F	L	F	I	R	P
mTBT	D	F	G	W	G	N	A	V	N	V	S	P	M	Q	Q	R	E	H	E	L	A	M	Q	N	Y	F	L	F	L	R	S	
consensus>50	D	F	G	W	G	.	a	.	n	v	s	..	q	...	n	...	l	q	d	y	f	l	f	.	r							
	390	400	410																													
VS	.	T	R	S	G	D	G	V	E	A	W	L	P	M	A	E	D	E	M	A	M	L	P	V	E	L	L	S	L	V	D	S
DBAT	P	K	N	N	P	D	G	I	K	I	L	S	F	M	P	P	S	I	V	K	S	F	K	F	E	M	E	T	M	T	N	K
mTBT	A	K	N	M	I	D	G	I	K	I	L	M	F	M	P	A	S	M	V	K	P	F	K	I	E	M	E	V	T	I	N	K
consensus>50	.	k	n	..	D	G	!	k	i	l	l	f	M	p	.	s	.	v	k	.	f	k	v	E	\$	e	.	l	v	#	k	

Figure C.3 (cont'd)

	420	.	
VS	DE	S	K.....
DBAT	YV	T	KP.....
mTBT	YV	A	KICNSKL
<i>consensus</i> >50	yv	.	K.....

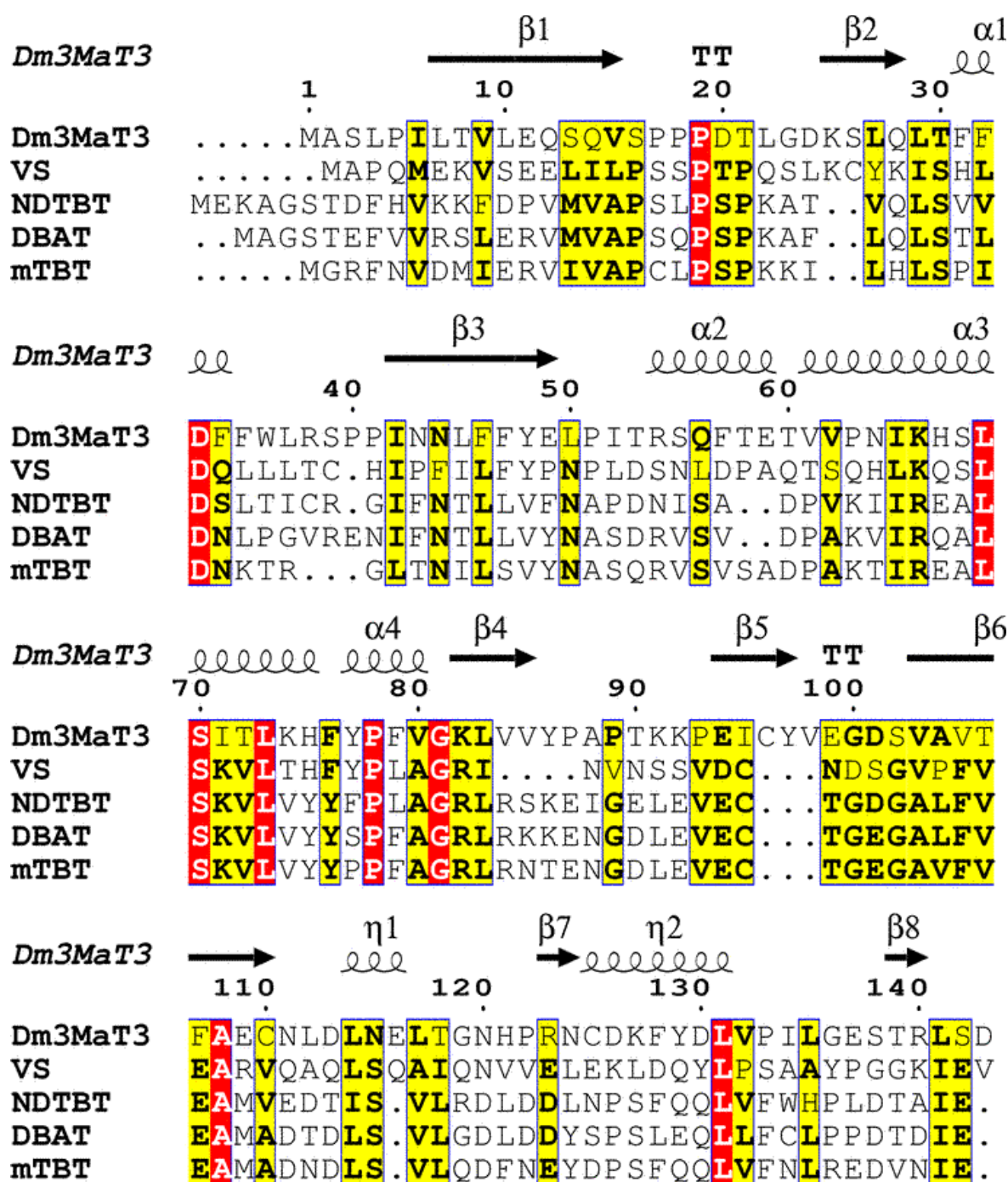


Figure C.4 – Sequence Alignment of Dm3MaT3 and Vinorine Synthase with *Taxus* Acyltransferases.

Figure C.4 (cont'd)

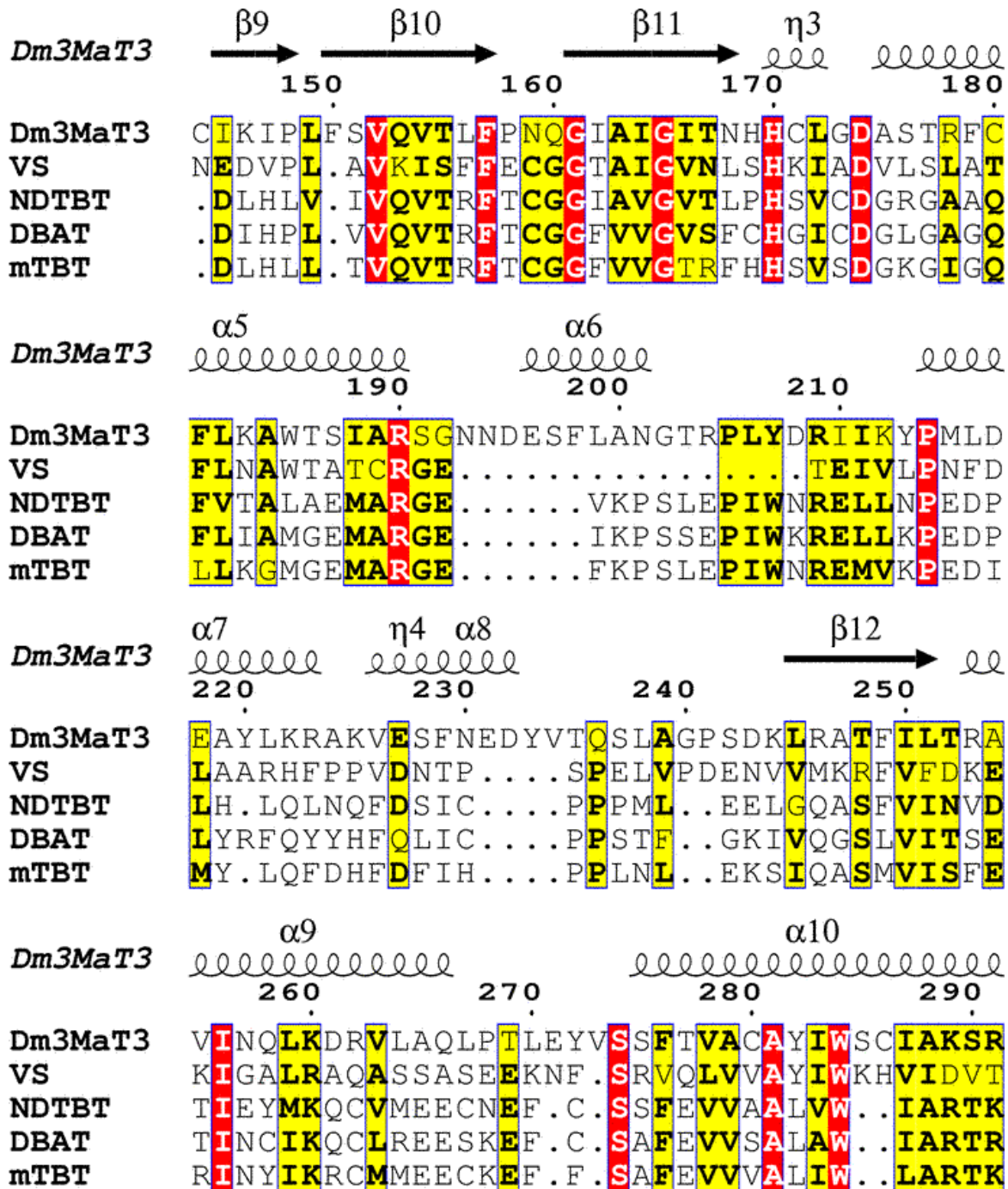


Figure C.4 (cont'd)

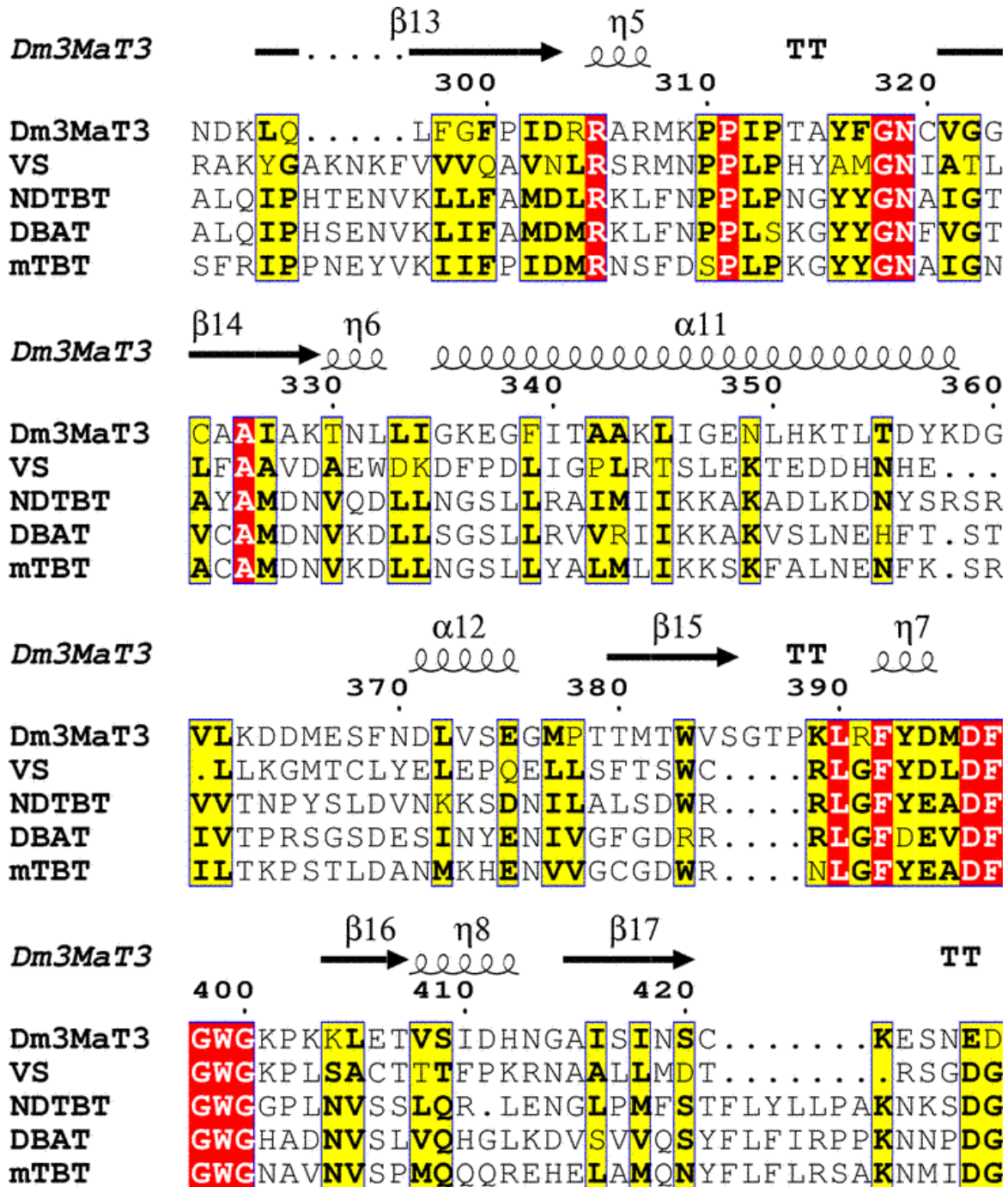
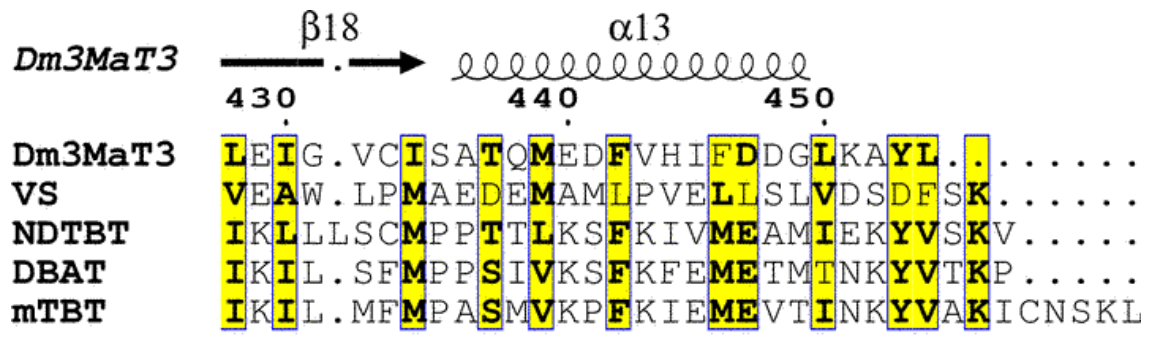


Figure C.4 (cont'd)



REFERENCES

REFERENCES

1. Firm, R. D., and Jones, C. G. (2003) Natural products - a simple model to explain chemical diversity, *Nat. Prod. Rep.* 20, 382-391.
2. Nevarez, D. M., Mengistu, Y. A., Nawarathne, I. N., and Walker, K. D. (2009) An *N*-aroyltransferase of the BAHD superfamily has broad aroyl CoA specificity *in vitro* with analogues of *N*-dearoylpaclitaxel, *J. Am. Chem. Soc.* 131, 5994-6002.
3. Nawarathne, I. N., and Walker, K. D. (2010) Point mutations (Q19P and N23K) increase the operational solubility of a 2 α -*O*-benzoyltransferase that conveys various acyl groups from CoA to a taxane acceptor, *J. Nat. Prod.* 73, 151-159.
4. D'Auria, J. C., Chen, F., and Pichersky, E. (2002) Characterization of an acyltransferase capable of synthesizing benzylbenzoate and other volatile esters in flowers and damaged leaves of *Clarkia breweri*, *Plant Physiol.* 130, 466-476.
5. Beekwilder, J., Alvarez-Huerta, M., Neef, E., Verstappen, F. W. A., Bouwmeester, H. J., and Aharoni, A. (2004) Functional characterization of enzymes forming volatile esters from strawberry and banana, *Plant Physiol.* 135, 1865-1878.
6. Ma, X. Y., Koepke, J., Panjikar, S., Fritzsche, G., and Stockigt, J. (2005) Crystal structure of vinorine synthase, the first representative of the BAHD superfamily, *J. Biol. Chem.* 280, 13576-13583.
7. Unno, H., Ichimaida, F., Suzuki, H., Takahashi, S., Tanaka, Y., Saito, A., Nishino, T., Kusunoki, M., and Nakayama, T. (2007) Structural and mutational studies of anthocyanin malonyltransferases establish the features of BAHD enzyme catalysis, *J. Biol. Chem.* 282, 15812-15822.
8. Truman, A. W., Dias, M. V., Wu, S., Blundell, T. L., Huang, F., and Spencer, J. B. (2009) Chimeric glycosyltransferases for the generation of hybrid glycopeptides, *Chem Biol* 16, 676-685.
9. Hansen, E. H., Osmani, S. A., Kristensen, C., Moller, B. L., and Hansen, J. (2009) Substrate specificities of family 1 UGTs gained by domain swapping, *Phytochemistry* 70, 473-482.
10. Loncaric, C., Merriweather, E., and Walker, K. D. (2006) Profiling a Taxol pathway 10 β -acetyltransferase: Assessment of the specificity and the production of baccatin III by *in vivo* acetylation in *E. coli*, *Chem. Biol.* 13, 1-9.
11. Walker, K., and Croteau, R. (2000) Molecular cloning of a 10-deacetylbaccatin III-10-*O*-acetyl transferase cDNA from *Taxus* and functional expression in *Escherichia coli*, *Proc. Natl. Acad. Sci. U. S. A.* 97, 583-587.

12. Sambrook, J. R., D. (2001) *Molecular Cloning: A Laboratory Manual*, Cold Spring Harbor Laboratory Press.

CHAPTER 5

CONCLUSIONS AND FUTURE PERSPECTIVES

5.1. Summary

5.1.1. Substrate Specificity of NDTBT

In Chapter 2, the extraordinarily broad substrate specificity of *Taxus* *N*-debenzoyl-2'-deoxypaclitaxel-*N*-benzoyltransferase (designated NDTBT), on the paclitaxel pathway, was elucidated by using a variety of aroyl CoA donors (benzoyl; *ortho*-, *meta*-, and *para*-substituted benzoyls; various heterole carbonyls; alkanoyls; and butenoyl) with *N*-debenzoylpaclitaxel derivatives (*N*-debenzoyl-2'-deoxypaclitaxel, *N*-debenzoylpaclitaxel, and 10-deacetyl-*N*-debenzoylpaclitaxel) by biocatalysis. Several unnatural *N*-aroyl-*N*-debenzoyl-2'-deoxypaclitaxel analogues were biocatalytically assembled with catalytic efficiencies (V_{\max}/K_M) ranging between 0.15 and 1.74 nmol · min⁻¹ · mM⁻¹. Although relative kinetics were calculated to conserve the limited supply of substrate, the results mostly demonstrated smaller turnover compared to natural substrates. The overall conclusion is that NDTBT has a wide substrate range.

Detection and verification of these bio-synthesized products were analyzed by LC-ESI/MS/MS and determined by typical diagnostic fragment ions of *m/z* 509, 569, and the C13 side chain fragment ion. Since the side groups tested were conserved in size, except for some of the larger substituents at the *ortho*-, *meta*-, and *para*-positions, the cavity that houses the benzoyl ring must be spacious enough to allow such a range of CoA substrates. To determine which residues to manipulate to alter the substrate specificity a crystal structure of NDTBT was sought by first improving protein purity levels.

5.1.2. Protein Purification for Crystal Structure

In Chapter 3, the purity level of C-terminal His₆-tagged NDTBT (CT-NDTBT) was shown to be at >95% after a series of nickel affinity, anion exchange, and gel filtration column chromatography. This represents an improvement over an original purification strategy employing only nickel affinity chromatography. This full length enzyme was active and was used to set up six 96-well plates by the sitting drop method for crystal screening; however, this effort did not provide substantial crystals for x-ray crystallography. Since the crystal structures of BAHD transferases vinorine synthase (VS) and anthocyanin malonyltransferase (Dm3MaT3) were obtained after removing the His-tag, the N-terminal His₆-tagged NDTBT (NT-NDTBT) was purified.^{1, 2} This fusion protein contained a thrombin cleavage site between the tag and NDTBT. Using the same purification protocol, the purity level was increased from 70% to >95% yield and the sample were used in a thrombin digestion experiment, which gave a 10% yield that was inadequate to set up crystallization. Also, taxane-2 α -*O*-benzoyltransferase (TBT) and 10-deacetylbaccatin III-10 β -*O*-acetyltransferase (DBAT) were purified to 90-95% purity, but remain to be screened for crystallization. However, while improving purification and screening for crystallization of the acyltransferases, an experiment to survey the sections of the enzyme responsible for substrate selectivity was conducted.

5.1.3. Mutagenesis Study to Analyze Substrate Selectivity

In Chapter 4, the mutagenesis screen was conducted among three *Taxus* acyltransferases *N*-debenzoyl-2'-deoxypaclitaxel:*N*-benzoyltransferase (NDTBT), 10-deacetylbaccatin III-10 β -*O*-acetyltransferase (DBAT), and taxane-2 α -*O*-benzoyltransferase (TBT) by domain and regional

swaps to create chimeric mutants. Namely, the objective was to convert aroyltransferases NDTBT or TBT into alkyl transferases, and vice versa with the alkyltransferase DBAT. Regional swapping sites were based on the homology model with an anthocyanin malonyltransferase (Dm3MaT3), which unfortunately had a low sequence identity (25-28%) to the *Taxus* acyltransferases.¹ Soluble protein extracts were assayed with parent substrates, but there was no detectable activity by LC-ESI/MS.

Even though the protein yield was below 20% for most of the regional mutants, the domain swapped constructs demonstrate an increase in soluble protein purified from a nickel-affinity column. This could indicate that the folding of the domain is dependent upon conserving the sequence from the parent transferase, or that the internal interaction between the domains is incompatible. If the former is true, then the regional swaps would cause such a disorder in each domain that purifying soluble protein would become non-existent.

5.2. Future Goals

5.2.1. Re-evaluate and Survey the Substrate Specificity of NDTBT

Since NT-NDTBT, at 70% purity, was assayed with benzoyl CoA and the previously proposed natural taxane substrate, *N*-debenzoyl-2'-deoxypaclitaxel, a re-evaluation is necessary with the reported natural substrate *N*-debenzoylpaclitaxel and purified NDTBT.³ Besides finding the kinetic parameters with benzoyl CoA, the activity of NDTBT should be surveyed with the same range of acyl CoA donors previously assessed in chapter 2, along with new substrates that increase the potency of the derivatives.

Besides using variants of the taxane acceptor substrate that have derivatives at the C2, C10, and C3' position, several types of CoA substrates with increased potency against cancer

should be surveyed. From structure-activity relationships (SARs) studies, paclitaxel analogues that have the phenyl group substituted with the following three ring structures – cyclopentyl, 1-cyclopentenyl, and 1-cyclohexenyl – have increased potency against non-small cell lung carcinoma and ovarian cancer.⁴ The likelihood that NDTBT uses the CoA versions of these side chains is probable since the other benzoyltransferase, taxane-2 α -O-benzoyltransferase (TBT), was tested with a cyclohexyl group and had a very low k_{cat} of 2.6×10^{-4} per min.⁵ Another SAR study also reported that various 3'-*N*-thiourea- and 3'-*N*-thiocarbamate-paclitaxel analogues had increased cytotoxicity against colon cancer cells.⁶ It may be premature to incubate the CoA versions of these groups with NDTBT due to the electron withdrawing effect of the sulfur or nitrogen on the carbonyl group. The more positively charged carbonyl group likely degrades rapidly in the basic assay buffer, because preliminary data shows no detectable products when NDTBT is assayed with *N*-debenzoyl derivatives and a CoA substrate with a tert-butyl group instead of a phenyl to make docetaxel (data not shown).

5.2.2. Improving Protein Yield for Crystallography

Although the improved protein purification scheme provides a 90-98% purity level, the actual amount of recombinant protein found in the soluble lysate is only a fraction of what is being expressed. A majority of these acyltransferases are found in the insoluble fraction when purified from *E. coli*. There are several approaches that can be utilized to overcome this bottleneck in final yield such as: codon optimization of the gene, sub-clone the genes into other expression vectors and their suitable *E. coli* type, mutagenesis studies to increase solubility, or change into a different expression system. If future applications are to produce paclitaxel

biosynthetically in bacteria, the first approach would be to codon optimize these *Taxus* transferases, because they are plant-derived enzymes containing several codons that are rarely expressed in the bacterial host. The translation of the NDTBT mRNA is hindered by the 30 rare codons that encode for arginine, proline, isoleucine, and leucine, whereas DBAT and *m*TBT have 38 and 40, respectively.

Once non-tagged, full length purified enzyme can be obtained, then another round of crystal screening can be performed. Should full length protein be difficult to crystallize, the transferases can be truncated to express the domain structures separately for isolation before the screening process. Molecular modeling of crystallized protein domains would be a guide for further mutational analysis.

5.3. Future Applications and Perspectives

5.3.1. Biocatalysis to Produce Paclitaxel

Biocatalysis-based synthesis of paclitaxel analogues is an alternative approach that eliminates or minimizes synthetic components, like organic solvent and heavy metal catalyst usage, which are not environmentally friendly. Although the ultimate goal is to pool all of the enzymes in the biosynthetic pathway into a one pot assay, there are several steps that are unknown and enzymes that have yet to be fully characterized, especially those responsible for constructing the CoA substrates. Currently, it could be possible to biocatalytically synthesize 2'-deoxypaclitaxel from 10-deacetylbaccatin using these three enzymes – 10-deacetylbaccatin III-10 β -*O*-acetyltransferase (DBAT), baccatin III:3-amino-3-phenylpropanoyltransferase (BAPT), and *N*-debenzoyl-2'-deoxypaclitaxel:*N*-benzoyltransferase (NDTBT) – with acetyl-, β -phenylalanine-, and benzoyl CoA substrates.

Besides semi-biosynthesis of paclitaxel analogues, these transferases can be coupled with coenzyme A ligases to optimize the turnover of acylated taxanes as well as to recycle the CoA by-product back into the reaction stream as an acyl CoA. Preliminary data have shown that the flux towards product formation is significantly increased from 2% to nearly 90% turnover when coupled with benzoate CoA ligase BadA (*Rhodopseudomonas palustris*).⁷

5.3.2. In vivo Studies

Over the last two decades, many of the genes in the paclitaxel pathway have been isolated from a cDNA library, and have been assayed in heterologous systems (e.g. *E. coli* and *Saccharomyces cerevisiae*) by analyzing their activity *in vitro* and *in vivo*.⁸⁻¹¹ A current goal is to bioengineer a recombinant organism to produce paclitaxel from primary metabolites to the final drug, through utility of the known *Taxus* enzymes and manipulation of the endogenous metabolic pathways.

There have been recent achievements in this endeavor pertaining to isoprenoids in microbes and taxadiene biosynthesis in yeast and *Arabidopsis thaliana*.¹²⁻¹⁴ Very recently, *E. coli* was successfully engineered to over-produce the building blocks of isoprenoid biosynthesis that served as a precursor for taxadiene biosynthesis. The hydrocarbon was subsequently converted to taxadiene-5-ol by the co-expression of a soluble P450 hydroxylase in this bacterial system.¹⁵ Besides constructing the complete paclitaxel pathway in another organism, a semi-biosynthesis approach was achieved when *E. coli*, engineered to express 10-deacetylbaaccatin III-10 β -O-acetyltransferase (DBAT) and a small/medium chain acid: CoA ligase, was fed 10-deacetylbaaccatin III and cosubstrates acetic-, propionic-, or butyric acid added to the media.

Baccatin III and its C10 analogues were produced and were partition by the *E. coli* into the media.^{16, 17}

It has been mentioned in articles that paclitaxel does not bind to FtsZ, a bacterial homolog to human β -tubulin, nor does it inhibit bacterial cell division, it is possible that *E. coli* could be engineered to produce paclitaxel.^{18, 19} Preliminary *in vivo* studies of NDTBT expressed in *E. coli* cultures were negative for detectable product in the cells or media (data not shown), which is likely due to the insolubility and bulkiness of the taxane substrate. Yet, this inconvenience may be overcome if the *Taxus* enzymes downstream of the DBAT can be concurrently expressed in the cells to synthesize the product, but ultimately be released from the cell during extraction and purification.

REFERENCES

REFERENCES

1. Unno, H., Ichimaida, F., Suzuki, H., Takahashi, S., Tanaka, Y., Saito, A., Nishino, T., Kusunoki, M., and Nakayama, T. (2007) Structural and mutational studies of anthocyanin malonyltransferases establish the features of BAHD enzyme catalysis, *J. Biol. Chem.* 282, 15812-15822.
2. Ma, X. Y., Koepke, J., Panjikar, S., Fritzsche, G., and Stockigt, J. (2005) Crystal structure of vinorine synthase, the first representative of the BAHD superfamily, *J. Biol. Chem.* 280, 13576-13583.
3. Long, R. M., Lagisetti, C., Coates, R. M., and Croteau, R. B. (2008) Specificity of the *N*-benzoyl transferase responsible for the last step of Taxol biosynthesis, *Arch. Biochem. Biophys.* 477, 384-389.
4. Roh, E. J., Song, C. E., Kim, D., Pae, H. O., Chung, H. T., Lee, K. S., Chai, K. B., Lee, C. O., and Choi, S. U. (1999) Synthesis and biology of 3'-*N*-acyl-*N*-debenzoylpaclitaxel analogues, *Bioorg. Med. Chem.* 7, 2115-2119.
5. Nawarathne, I. N., and Walker, K. D. (2010) Point mutations (Q19P and N23K) increase the operational solubility of a 2 α -*O*-benzoyltransferase that conveys various acyl groups from CoA to a taxane acceptor, *J. Nat. Prod.* 73, 151-159.
6. Xue, M., Long, B. H., Fairchild, C., Johnston, K., Rose, W. C., Kadow, J. F., Vyas, D. M., and Chen, S. H. (2000) Structure-activity relationships study at the 3'-*N* position of paclitaxel. Part 2: Synthesis and biological evaluation of 3'-*N*-thiourea- and 3'-*N*-thiocarbamate-bearing paclitaxel analogues, *Bioorg. Med. Chem. Lett.* 10, 1327-1331.
7. Sullivan, S. A. (2010) A Broadly Specific Benzoate Coenzyme A Ligase Is Coupled With *Taxus* Acyltransferases *In Vitro* To Biosynthesize Paclitaxel Analogues (Master's Thesis), In *Chemistry*, Michigan State University, East Lansing.
8. DeJong, J., Liu, Y., Bollon, A., Long, R., Jennewein, S., Williams, D., and Croteau, R. (2005) Genetic engineering of Taxol biosynthetic genes in *Saccharomyces cerevisiae*, *Biotechnol. Bioeng.* 93, 212-224.
9. Jennewein, S., Wildung, M. R., Chau, M., Walker, K., and Croteau, R. (2004) Random sequencing of an induced *Taxus* cell cDNA library for identification of clones involved in Taxol biosynthesis, *Proc. Natl. Acad. Sci. U. S. A.* 101, 9149-9154.
10. Loncaric, C., Ward, A. F., and Kevin D. Walker. (2007) Expression of an acetyl-CoA synthase and a CoA-transferase in *Escherichia coli* to produce modified taxanes *in vivo*, *Biotechnol. J.* 2, 266-274.

11. Jennewein, S., Park, H., DeJong, J. M., Long, R. M., Bollon, A. P., and Croteau, R. B. (2005) Coexpression in yeast of *Taxus* cytochrome P450 reductase with cytochrome P450 oxygenases involved in Taxol biosynthesis, *Biotechnol. Bioeng.* 89, 588-598.
12. Engels, B., Dahm, P., and Jennewein, S. (2008) Metabolic engineering of taxadiene biosynthesis in yeast as a first step towards Taxol (Paclitaxel) production, *Metab. Eng.* 10, 201-206.
13. Chang, M. C., and Keasling, J. D. (2006) Production of isoprenoid pharmaceuticals by engineered microbes, *Nat. Chem. Biol.* 2, 674-681.
14. Besumbes, O., Sauret-Gueto, S., Phillips, M. A., Imperial, S., Rodriguez-Concepcion, M., and Boronat, A. (2004) Metabolic engineering of isoprenoid biosynthesis in *Arabidopsis* for the production of taxadiene, the first committed precursor of Taxol, *Biotechnol. Bioeng.* 88, 168-175.
15. Ajikumar, P. K., Xiao, W. H., Tyo, K. E., Wang, Y., Simeon, F., Leonard, E., Mucha, O., Phon, T. H., Pfeifer, B., and Stephanopoulos, G. (2010) Isoprenoid pathway optimization for Taxol precursor overproduction in *Escherichia coli*, *Science* 330, 70-74.
16. Loncaric, C., Merriweather, E., and Walker, K. D. (2006) Profiling a Taxol pathway 10 β -acetyltransferase: Assessment of the specificity and the production of baccatin III by *in vivo* acetylation in *E. coli*, *Chem. Biol.* 13, 1-9.
17. Walker, K., and Croteau, R. (2000) Molecular cloning of a 10-deacetylbaccatin III-10-*O*-acetyl transferase cDNA from *Taxus* and functional expression in *Escherichia coli*, *Proc. Natl. Acad. Sci. U. S. A.* 97, 583-587.
18. Wang, J., Galgoci, A., Kodali, S., Herath, K. B., Jayasuriya, H., Dorso, K., Vicente, F., Gonzalez, A., Cully, D., Bramhill, D., and Singh, S. (2003) Discovery of a small molecule that inhibits cell division by blocking FtsZ, a novel therapeutic target of antibiotics, *J. Biol. Chem.* 278, 44424-44428.
19. Haydon, D. J., Stokes, N. R., Ure, R., Galbraith, G., Bennett, J. M., Brown, D. R., Baker, P. J., Barynin, V. V., Rice, D. W., Sedelnikova, S. E., Heal, J. R., Sheridan, J. M., Aiwale, S. T., Chauhan, P. K., Srivastava, A., Taneja, A., Collins, I., Errington, J., and Czaplewski, L. G. (2008) An inhibitor of FtsZ with potent and selective anti-staphylococcal activity, *Science* 321, 1673-1675.